ulm university universität
uulm

Universität Ulm
Institut für Stochastik

Spatial Stochastic Network Models

Scaling Limits and Monte–Carlo Methods

Dissertation

zur Erlangung des Doktorgrades Dr. rer. nat.
der Fakultät für Mathematik und Wirtschaftswissenschaften der
Universität Ulm

vorgelegt von

Florian Voß
aus
Seeheim-Jugenheim

Dezember 2009

Amtierender Dekan:	Prof. Dr. Werner Kratz
1. Gutachter:	Prof. Dr. Volker Schmidt
2. Gutachter:	Prof. Dr. Ulrich Stadtmüller
Tag der Promotion:	19. Februar 2010

Contents

Chapter 1

Introduction

1.1 Aims and motivation

The present thesis is motivated by a joint research project of the Institute of Stochastics at Ulm University and Orange Labs in Issy les Moulineaux, Paris, which deals with the analysis of telecommunication networks. During the last years the *Stochastic Subscriber Line Model* (SSLM) has been developed in this cooperation and it is still extended. The SSLM is a flexible model for telecommunication networks, especially designed for access networks in urban areas. It utilizes tools from Stochastic Geometry in order to represent the different parts of the network by spatial stochastic models which only depend on a small number of parameters. Real telecommunication networks are huge systems which are difficult to analyze due to their size and complexity. However, using spatial stochastic models it is possible to describe existing and future telecommunication networks by few parameters. Then the network can be analyzed based on a suitable model which leads to an alternative approach in comparison to traditional methods for cost measurement and strategic planning which are based on the direct analysis of network data.

Spatial stochastic modeling of telecommunication networks is a powerful approach in order to analyze huge networks globally since the variability and size of the network is used as an advantage to provide statistical properties of the whole system. Therefore, the main principles which control the behavior of the network have to be described by appropriate models from stochastic geometry. Such models have been shown to be useful e.g. in order to represent the locations of network components as well as the geometry of the underlying infrastructure. Since their first applications the number and diversity of spatial stochastic network models has been considerably extended using concepts from stochastic geometry like point processes and random geometric graphs, see e.g. [4, 39, 106] for recent surveys. Models which have been investigated include aggregated Poisson-Voronoi tessellations ([6, 28, 91]), modulated Poisson-Voronoi

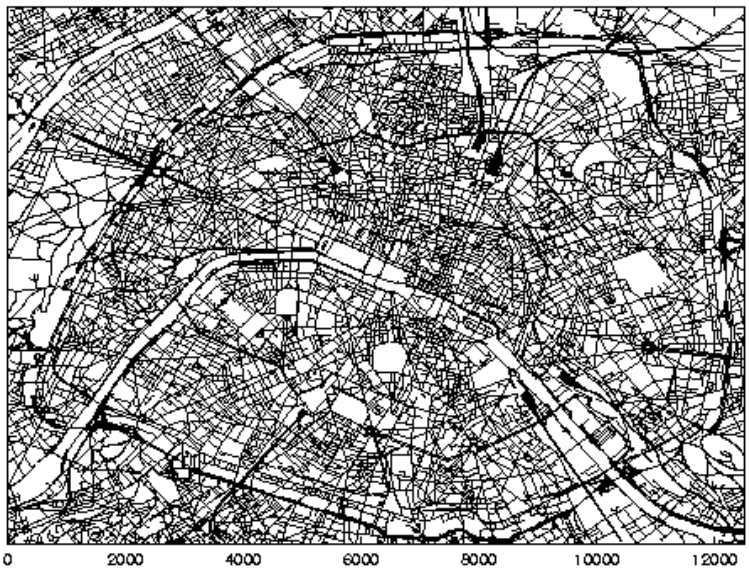

Figure 1.1: Street map in Paris

tessellations ([16, 17, 27]), coverage processes ([3]), spanning trees ([7, 9]), superpositions of Poisson-Voronoi tessellations ([5]) and point processes on the edges of random tessellations ([6, 30, 33]). In this thesis we focus on the latter approach which is described below in more detail.

Traditionally, planar Poisson processes have been applied to model locations of network components. The main reason for the use of Poisson processes is that the resulting network models can be analyzed analytically in many cases. However, such network models cannot take into account the underlying infrastructure of the network. For instance, in Figure 1.1 the street system of Paris is shown which can be regarded as the geometrical support of urban telecommunication networks, i.e., the cable system of such networks is deployed along the street system. From a macroscopic perspective, the street system exhibits a large variability which seems to be homogeneous in the plane. The SSLM takes advantage of this variability and models not only network components, but also the underlying infrastructure of the network by random processes which leads to a more realistic network model.

In particular, we consider two-level hierarchical models for access networks which consist of three distinct building blocks: The geometrical support of the network, the locations of network nodes and the connection topology, see Figure 1.2. In a first step the geometric support of the cable system is modeled. For this purpose we use planar random tessellations which are basic models from stochastic geometry in order to describe random segment systems, see Figure 1.3. Then, in the second step, network nodes of high and low hierarchy are modeled as random points on the edges of the tessellation. Suitable models are random point processes on the edges of random tessellations like Cox processes. In the

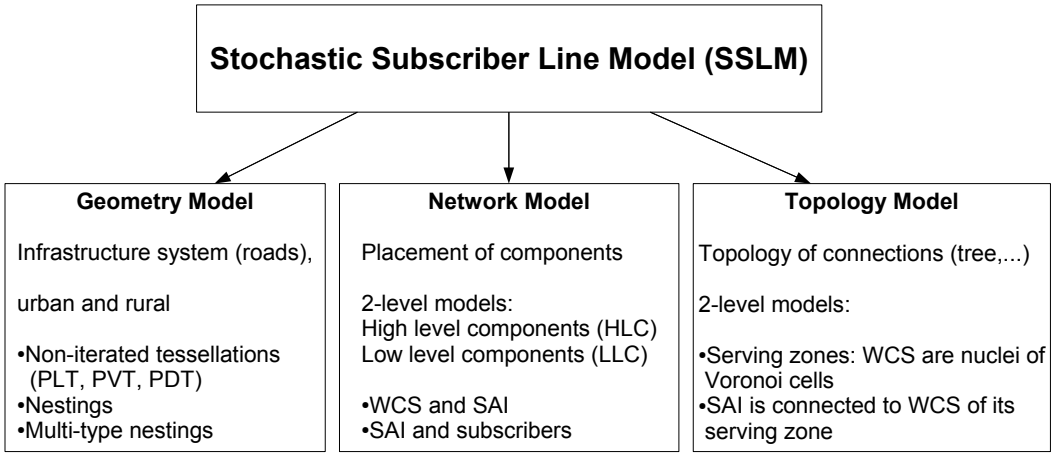

Figure 1.2: Basic components of the SSLM

final step, rules for the connections between network nodes have to be specified. We consider different scenarios here. One possibility is that network nodes of low hierarchy are connected to their nearest neighboring node of high hierarchy on the shortest path along the edges of the underlying tessellation, see Figure 1.4. Note that the network quality for single users is often not of interest, but the network operator is rather interested in the expected network quality averaged over all users in a large area. A mathematical tool in order to analyze spatial averages of stochastic processes is Palm calculus. In particular, we are interested in the average connection length of all network nodes of low hierarchy in a large telecommunication network. Using the terminology of Palm calculus, this average connection length can be described by the so–called typical connection length which is random variable defined via Palm distributions.

The aim of this thesis is to analyze typical connection lengths in various ways. One part of the thesis focuses on the estimation of their densities and distribution functions via Monte–Carlo simulation. The developed estimators are all based on samples of the so–called typical serving zone. Therefore, simulation algorithms for the typical serving zone are derived for various models. Another part of the thesis deals with limit theorems for the typical connection length. In particular, we show that the distribution of the typical connection length converges to well–known distributions if the parameters of the underlying model tend to extremal cases. On the one hand, we consider the case that the underlying cable system gets infinitely dense and, on the other hand, we regard infinitely sparse cable systems. In both cases the distribution of the typical connection length converges to simple parametric distributions. Both results, the estimated distributions and the asymptotic distributions, are used in order to obtain approximative parametric densities for the typical connection length. These parametric densities are finally compared to empirical distributions computed from huge databases

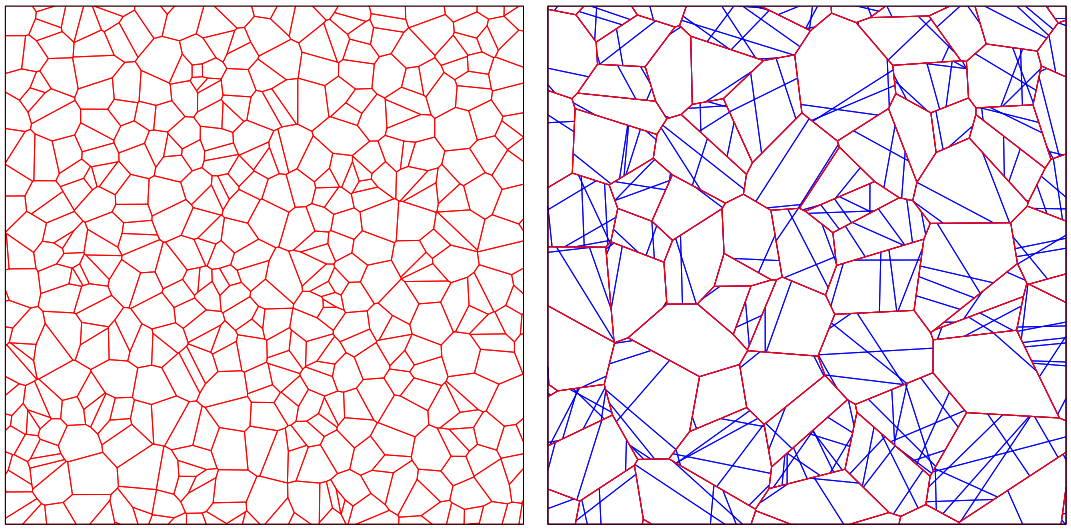

(a) Voronoi tessellation (b) Nested tessellation

Figure 1.3: Realizations of two different tessellation models

without using any spatial information. It is shown that the obtained parametric densities fit quite well to real network data. In the final part of the thesis, we go one step further and analyze required capacities at different locations of the network. First, the notion of typical capacity is introduced in the SSLM. Then, for different scenarios, estimators for the density and distribution function are developed which are again based on samples of the typical serving zone.

The results of this thesis can be directly applied for the analysis and planning of telecommunication networks. Now parametric distributions for connection lengths in large telecommunication networks are available, where the parameters can be determined based on the number of network components and characteristics of the underlying street system which can be estimated easily. Thus, the distributions of connection lengths are directly available for the analysis of urban telecommunication networks and time–consuming network reconstructions or simulation studies can be avoided. Furthermore, the obtained results can be applied for network planning. Using the techniques developed in this thesis, various scenarios for future (not yet existing) networks can be investigated before the network is built. In particular, the impact of new network technologies and architectures on connection lengths can be explored efficiently which is not possible with classical methods due to large computation times.

1.2 Outline

This thesis is organized as follows. In Chapter 2 basic concepts of stochastic geometry are introduced. We start with the definition of point processes and marked

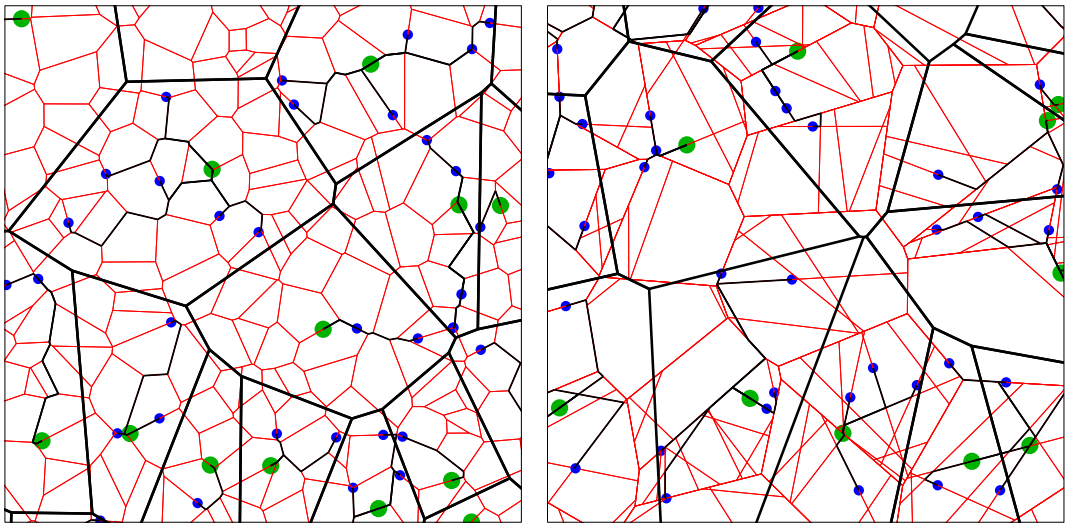

(a) Voronoi tessellation as street model (b) Nested tessellation as street model

Figure 1.4: Network nodes with shortest path connections

point processes and summarize some basic properties and notions. In particular, Palm distributions and the typical mark of stationary marked point processes are discussed and the relationship between spatial averages of ergodic marked point processes and their typical marks is explained. Furthermore, Neveu's exchange formula for the Palm distributions of two jointly stationary marked point processes is discussed which is used frequently throughout this thesis. Finally, at the end of Chapter 2, random closed sets and random measures are introduced.

Subsequently, deterministic and random tessellations are discussed in Chapter 3. Random tessellations are flexible models from stochastic geometry which serve as a basis for all spatial stochastic models investigated in this thesis. It is shown that random tessellations can be regarded as random segment systems, random measures and various types of marked point processes. Finally, we introduce point processes on random segment systems induced by random tessellations, where we focus on two specific models. On the one hand, we consider Cox processes on the edges of random tessellations and, on the other hand, we regard thinnings of the vertices of random tessellations. For both considered models, we discuss some basic properties.

Chapter 4 is dedicated to simulation algorithms for the typical Voronoi cell of point processes on the edges of random tessellations. First, well–known simulation algorithms for the typical Voronoi cell of Poisson processes and Cox processes on the edges of Poisson line tessellations are reviewed. Afterwards, new simulation algorithms for the typical Voronoi cell of various point process models are developed. In particular, Cox processes on Poisson–Voronoi tessellations and Poisson–Delaunay tessellations as well as thinnings of the vertices of Poisson–Delaunay tessellations, Poisson line tessellations and Poisson–Voronoi tessella-

tions are considered. For each model new simulation algorithms for the typical Voronoi cell are derived and some results obtained from a numerical study are presented.

In Chapter 5 spatial stochastic models for two-level hierarchical networks are introduced. As described above, the geometrical support of the network is modeled by the edges of a random tessellation and network components of low and high hierarchy levels are represented by point processes on this edge set. Based on this modeling approach, it is possible to define cost functionals for the connection between components of low and high hierarchy levels. In particular, we consider the direct Euclidean connection distance and the shortest path length from the typical low–level component to its associated high–level component which we call the typical Euclidean distance and the typical shortest path length, respectively. For both cases it is shown how the distribution can be estimated based on samples of the typical serving zone and its inner structure. Thus, the developed estimators can be computed based on samples generated with the simulation algorithms introduced in Chapter 4. Moreover, statistical properties of the considered estimators are investigated and some numerical results are presented.

The subject of Chapter 6 are scaling limits for the typical Euclidean distance and the typical shortest path length. We consider the network model introduced in Chapter 5 which is subsequently rescaled and network components are added and deleted in order to get infinitely sparse and dense networks, respectively. Then it is possible to prove that the considered cost functionals converge in distribution to known parametric distributions. First it is shown that the distribution of the typical shortest path length converges to an exponential distribution for infinitely sparse networks. Afterwards, we prove for infinitely dense networks that the distribution of the typical Euclidean distance converges to the distribution of the distance from the origin to the nearest point of a stationary Poisson process, which is known to be a Weibull distribution. This result is then used in order to derive the main theorem of Chapter 6, that is to show that the typical shortest path length converges in distribution to some constant $\xi \geq 1$ multiplied with the Weibull–distributed random variable mentioned above. Here, the constant ξ depends on the random tessellation which models the infrastructure of the network. For some cases we can even compute ξ explicitly. In order to make the proof more transparent, we first state the main theorem in Section 6.3 and then split the proof into different parts which are provided in Sections 6.4 and 6.5. Then, in Section 6.6 it is shown that the conditions of the main theorem are fulfilled by many models considered in the literature.

In Chapter 7 the results obtained in Chapters 4 – 6 are applied to real data. First, we compute empirical densities of the typical shortest path lengths as well as means and variances for various models using the estimators introduced in Chapter 5 and the simulation algorithms developed in Chapter 4. In particular, it is shown that the distribution strongly depends on the considered model type. Afterwards, we use the limit theorems of Chapter 6 in order to choose parametric

densities which can be fitted to the estimated ones. In this way, we obtain a library of parametric distributions for connection lengths, where the parameters are known and depend on the considered model. These parametric densities are then compared to real data which reveals a very good fit between distributions for connection lengths estimated from real data and parametric distributions chosen from the library.

Finally, in Chapter 8 we define the notion of capacities in the framework of the SSLM. In particular, we are interested in the capacity required at given locations of the network which are modeled by various point processes. We show that the capacity at the typical point of these point processes depends only on the length of some subtree of the network. Thus, we analyze this subtree length and show for different scenarios how its distribution can be estimated based on samples of the typical serving zone. Again, some statistical properties of this estimator are discussed.

In the final Chapter 9 the results of the thesis are summarized. Furthermore, interesting questions and possible extensions for future research are given. At the end of the thesis an appendix summarizes some results which are used in the proofs of the thesis. In particular, different modes of convergence of random variables, measurable functions and measures are reviewed and relationships between them are discussed. Furthermore, Kingman's ergodic theorem for subadditive processes and some basic concepts from geometric measure theory like the generalized Blaschke-Petkantschin formula for Hausdorff measures are reviewed which are used e.g. in the proofs of Chapter 6.

1.3 The Geostoch library

The software which was developed during this thesis is embedded in the Geostoch library of the Institute of Stochastics at Ulm University. This library is JAVA-based and comprises methods from spatial statistics, stochastic geometry and image analysis ([59, 61]).

The main idea of the Geostoch library is to provide basic methods in order to analyze spatial data and to simulate stochastic models for various research projects. In particular, methods in order to analyze and simulate random tessellations and point processes are implemented. These implementations were used as a basis for the implementations of the simulation algorithms and estimators developed during this thesis. The Geostoch library is continuously extended, for further information, see *http://www.geostoch.de*.

Chapter 2

Preliminaries from stochastic geometry

This chapter introduces the basic notation and mathematical background used in this thesis. In particular, we briefly summarize basic notions and principles from stochastic geometry like random (marked) point processes, random closed sets and random measures. For more details and further information about these topics and stochastic geometry in general, see for example [10, 21, 44, 48, 56, 70, 79, 86, 87, 90].

In the following, we only regard the planar case, although most of the results presented in this thesis can be generalized easily to $\mathbb{R}^d$ for $d \geq 2$. First, in Section 2.1, some basic notation is summarized. Subsequently, simple and marked point processes are introduced in Sections 2.2 and 2.3, respectively, and notions like stationarity and ergodicity are defined. In particular, basic concepts of Palm calculus for stationary (marked) point processes are reviewed and the notion of the typical mark is introduced. Finally, random closed sets and random measures are discussed in Sections 2.4 and 2.5.

2.1 Basic notation and definitions

In the following, let $\mathbb{R}$ and $\mathbb{N}_0$ denote the set of real numbers and non–negative integers, respectively. We use the notation $\mathring{B}, \partial B$, and B^c for the interior, the boundary, and the complement of a set $B \subset \mathbb{R}^2$, respectively. Here, $\mathbb{R}^2$ denotes the 2–dimensional Euclidean plane and we use the notation $\langle \cdot, \cdot \rangle$ for the Euclidean scalar product on $\mathbb{R}^2$. Below, $|\,.\,| : \mathbb{R}^2 \to [0, \infty)$ denotes the Euclidean norm defined by

$$|x| = \sqrt{x_1^2 + x_2^2} = \sqrt{\langle x, x \rangle} \tag{2.1}$$

for each $x = (x_1, x_2) \in \mathbb{R}^2$. Furthermore, we denote by $B(x, r)$ and $B^{\neq}(x, r)$ the 2–dimensional closed and open ball centered at $x \in \mathbb{R}^2$ with radius $r > 0$, i.e.,

$B(x,r) = \{y \in \mathbb{R}^2 : |x-y| \leq r\}$ and $B_r^{\neq}(x) = \{y \in \mathbb{R}^2 : |x-y| < r\}$.

On $\mathbb{R}^2$ we define the group $t_x : y \mapsto y + x$ of translations by a vector $x \in \mathbb{R}^2$ and the group $\vartheta_R : y \mapsto Ry$ of rotations around the origin o, where R denotes a 2×2–matrix which is orthogonal with $\det R = 1$. Note that translations and rotations can also be defined for a set $B \subset \mathbb{R}^2$ by $t_x B = \{y + x : y \in B\}$ for $x \in \mathbb{R}^2$ and $\vartheta_R B = \{\vartheta_R x : x \in B\}$ for rotations ϑ_R around the origin.

Let $\mathcal{B}(\mathbb{R}^2)$ denote the family of Borel sets of $\mathbb{R}^2$ and let $\mathcal{B}_0(\mathbb{R}^2)$ denote the family of those Borel sets in $\mathbb{R}^2$ which are in addition bounded. An important measure acting on the measurable space $(\mathbb{R}^2, \mathcal{B}(\mathbb{R}^2))$ is the (2–dimensional) Lebesgue measure $\nu_2 : \mathcal{B}(\mathbb{R}^2) \to [0, \infty]$. For any Borel set $B \in \mathcal{B}(\mathbb{R}^2)$ we can interpret $\nu_2(B)$ as the area of B. Note that each locally finite and translation-invariant measure μ on $\mathcal{B}(\mathbb{R}^2)$ is a multiple of the Lebesgue measure ν_2, i.e., $\mu(B) = \lambda \nu_2(B)$ for all $B \in \mathcal{B}(\mathbb{R}^2)$ and some $\lambda \geq 0$ if $\mu(B) < \infty$ for all $B \in \mathcal{B}_0(\mathbb{R}^2)$ and $\mu(t_x B) = \mu(B)$ for all $B \in \mathcal{B}(\mathbb{R}^2), x \in \mathbb{R}^2$, see e.g. [11], Theorem 1.8.1. Thus, up to a normalizing constant, ν_2 is the only translation-invariant measure on $\mathcal{B}(\mathbb{R}^2)$.

Furthermore, we use the notation ν_1 for the 1–dimensional Hausdorff measure on $\mathcal{B}(\mathbb{R}^2)$. For $B \subset \mathbb{R}^2$ it is defined via

$$\nu_1(B) = \sup_{\varepsilon > 0} \inf \Big\{ \sum_{j \in \mathbb{N}} D(A_j) : B \subset \cup_{j \in \mathbb{N}} A_j, D(A_j) \leq \varepsilon \Big\},$$

where $D(A_j) = \sup\{\| x - y \| : x, y \in A_j\}$ is the diameter of A_j. Note that for any Borel set B we can interpret $\nu_1(B)$ as the length of B. In particular, if $0 < \nu_1(B) < \infty$ for $B \in \mathcal{B}_0(\mathbb{R}^2)$, we say that B has dimension 1.

2.2 Point processes

In this section we introduce the notion of random point processes in $\mathbb{R}^2$. Some realizations of different point process models in $\mathbb{R}^2$ are displayed in Figure 2.1. Point processes are models from stochastic geometry which can describe random point configurations, i.e., sets of points which are randomly scattered in the Euclidean plane. In the following, we mainly focus on so–called simple point processes, i.e., multiple points at the same location cannot be observed. Spatial point processes are important stochastic models which are applied in many fields of science like biology, medicine and telecommunication ([23, 31, 57]).

2.2.1 Point processes as random counting measures

A single point $x \in \mathbb{R}^2$ can be identified with the Dirac measures $\delta_x : \mathcal{B}(\mathbb{R}^2) \to \mathbb{N}_0$ on $\mathcal{B}(\mathbb{R}^2)$ defined by

$$\delta_x(B) = \mathbb{1}_B(x),$$

where $\mathbb{1}_B$ denotes the indicator function of the set B. Similarly, a finite or (countably) infinite set of points $\{x_1, \ldots, x_k\}$, $k \in \mathbb{N}_0$, or $\{x_1, x_2, \ldots\}$ can be identified

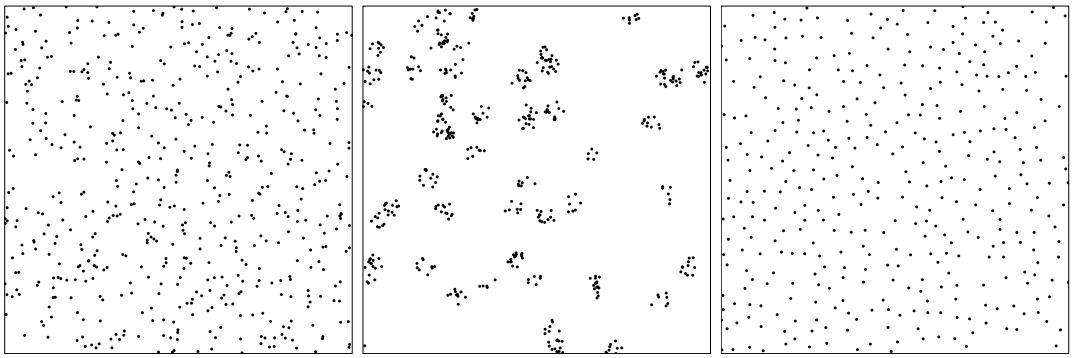

(a) Poisson process (b) Cluster process (c) Hardcore process

Figure 2.1: Realizations of different point process models

with a counting measure. Let $\varphi : \mathcal{B}(\mathbb{R}^2) \to \mathbb{N}_0$ denote a counting measure on $\mathcal{B}(\mathbb{R}^2)$, then φ can be expressed by a (countable) sum of Dirac measures, i.e.,

$$\varphi = \sum_{n=1}^{k} \delta_{x_n} ,$$

where $k \in \mathbb{N}_0 \cup \{\infty\}$. In the context of counting measures we call $x \in \mathbb{R}^2$ an *atom* of φ if $\varphi(\{x\}) > 0$. The *support* of φ is defined as the set $\mathrm{supp}(\varphi) = \{x \in \mathbb{R}^2 : \varphi(\{x\}) > 0\}$. We say that φ is simple if $\varphi(\{x\}) \in \{0, 1\}$ for all $x \in \mathbb{R}^2$ and locally finite if $\varphi(B) < \infty$ for any set $B \in \mathcal{B}_0(\mathbb{R}^2)$. Note that $\mathrm{supp}(\varphi)$ is locally finite if φ is locally finite. In the following only simple and locally finite counting measures are considered. If a counting measure φ is simple, then we can identify φ with its support, i.e., the set of its atoms, and we also write $\varphi = \mathrm{supp}(\varphi)$. Let $\mathsf{N} = \mathsf{N}(\mathbb{R}^2)$ denote the family of simple and locally finite counting measures on $\mathcal{B}(\mathbb{R}^2)$. Then we define the σ–algebra $\mathcal{N} = \mathcal{N}(\mathbb{R}^2)$ on N as the smallest σ–algebra containing all sets of the form $\{\varphi \in \mathsf{N} : \varphi(B) = j\}$ with $j \in \mathbb{N}_0$ and $B \in \mathcal{B}_0(\mathbb{R}^2)$.

Now we introduce shifts and rotations of counting measures which are important operations on N. In the following, $t_x : \mathsf{N} \to \mathsf{N}$ denotes the shift operator defined by $t_x\varphi(B) = \varphi(B+x)$ for all $x \in \mathbb{R}^2$ and $\vartheta_R : \mathsf{N} \to \mathsf{N}$ denotes the rotation operator defined by $\vartheta_R\varphi(B) = \varphi(\vartheta_R^{-1}B) = \varphi(\vartheta_{R^{-1}}B)$ for all rotations R around the origin o. Thus, t_x translates all atoms of φ by $-x$ for $x \in \mathbb{R}^2$ and ϑ_R rotates all atoms by ϑ_R for any rotation ϑ_R.

A measurable mapping $X : \Omega \to \mathsf{N}$ from some probability space $(\Omega, \mathcal{A}, \mathbb{P})$ into the measurable space $(\mathsf{N}, \mathcal{N})$ is called a *random point process* in $\mathbb{R}^2$. There are different ways to look at point processes. One possibility is to regard them as random counting measures $\sum_{x \in \mathrm{supp}(X)} \delta_x$. Then $X(B)$ can be interpreted as the (random) number of atoms of X in $B \in \mathcal{B}(\mathbb{R}^2)$. Another possibility is to identify a point process X with its atoms $X = \{X_n\} = \{X_n, n = 1, \ldots, k\}$, where

$k : \Omega \to \mathbb{N}_0 \cup \{\infty\}$ is the random (total) number of atoms. From this point of view, X can be regarded as a sequence of (2–dimensional) random vectors $X_n : \Omega \to \mathbb{R}^2$.

In the following, we use the notation $X = \{X_n\}$ and it will be clear from the context if X is regarded as a random counting measure or a random sequence of points in $\mathbb{R}^2$.

2.2.2 Fundamental properties

Now we regard some important properties of random point processes.

Stationarity, isotropy and the intensity measure

Let X be any point process in $\mathbb{R}^2$. The probability measure P_X defined on $\mathcal{N}$ by $P_X(A) = \mathbb{P}(X \in A)$ for $A \in \mathcal{N}$ is called the *distribution* of X. A point process X is called

- *stationary* if its distribution is translation invariant, i.e. if $P_X = P_{t_x X}$ for any $x \in \mathbb{R}^2$,
- *isotropic* if its distribution is rotation invariant, i.e. if $P_X = P_{\vartheta_R X}$ for all rotations ϑ_R around the origin, and
- *motion-invariant* if X is both stationary and isotropic.

If X is a stationary point process, then we always assume that $\mathbb{P}(X(\mathbb{R}^2)=\infty) = 1$ and $\mathbb{P}(X(\mathbb{R}^2) = 0) = 0$. We define the *intensity measure* $\mu : \mathcal{B}(\mathbb{R}^2) \to [0, \infty]$ of a point process X by

$$\mu(B) = \mathbb{E}X(B)\,, \quad B \in \mathcal{B}(\mathbb{R}^2)\,. \tag{2.2}$$

That means $\mu(B)$ is the expected number of points of X in the Borel set B. In the following, we always assume that μ is locally finite and not equal to the zero measure, i.e., $\mu(B) < \infty$ for all $B \in \mathcal{B}_0(\mathbb{R}^2)$ and $\mu(\mathbb{R}^2) > 0$. Furthermore, we always assume that μ is diffuse. If X is stationary with intensity measure μ, then

$$\mu(B) = \mathbb{E}X(B) = \mathbb{E}X(B + x) = \mu(B + x)$$

for any $x \in \mathbb{R}^2$ and $B \in \mathcal{B}(\mathbb{R}^2)$. Since every translation-invariant and locally finite measure on $\mathcal{B}(\mathbb{R}^2)$ is proportional to the Lebesgue measure we get that $\mu(B) = \lambda\nu_2(B)$ for some constant $\lambda > 0$. We call λ the *intensity* of the stationary point process X. It can be regarded as the mean number of points per unit area since $\lambda = \mathbb{E}X(B)$ for each $B \in \mathcal{B}(\mathbb{R}^2)$ with $\nu_2(B) = 1$.

An important result in the theory of point processes is Campbell's theorem which is stated below. It can be seen as a version of Fubini's theorem for point processes. There are various modifications of Campbell's theorem, e.g. for marked point processes and random measures which will be discussed later on. For a proof see e.g. [87].

Theorem 2.1 (Campbell's theorem) *Let $X = \{X_n\}$ be a point process and let $f : \mathbb{R}^2 \to [0, \infty)$ be a measurable function. Then $\sum_{X_n \in X} f(X_n) : \Omega \to [0, \infty]$ is measurable and*

$$\mathbb{E} \sum_{X_n \in X} f(X_n) = \mathbb{E} \int_{\mathbb{R}^2} f(x) X(dx) = \int_{\mathbb{R}^2} f(x)\, \mu(dx)\,.$$

If X is stationary with intensity λ, then

$$\mathbb{E} \sum_{X_n \in X} f(X_n) = \lambda \int_{\mathbb{R}^2} f(x)\, \nu_2(dx)\,.$$

Finite-dimensional distributions

The family of *finite–dimensional distributions*

$$\{\mathbb{P}_{B_1,\ldots,B_n}(k_1, \ldots, k_n) : n \geq 1, k_1, \ldots, k_n \geq 0, B_1, \ldots, B_n \in \mathcal{B}_0(\mathbb{R}^2)\}$$

of a point process X is defined by

$$\mathbb{P}_{B_1,\ldots,B_n}(k_1, \ldots, k_n) = \mathbb{P}(X(B_1) = k_1, \ldots, X(B_n) = k_n)\,. \tag{2.3}$$

Note that a point process X can be regarded as a stochastic process $\{X(B), B \in \mathcal{B}(\mathbb{R}^2)\}$ indexed by the Borel sets of $\mathbb{R}^2$. Thus, the theory of stochastic processes can be applied which yields that the finite–dimensional distributions characterize the distribution of a point process, see e.g. [21], Corollary 9.2.IV.

Theorem 2.2 *Let X be an arbitrary point process. Then the distribution of X is uniquely determined by its finite–dimensional distributions.*

Furthermore, Kolmogorov's existence theorem can be formulated for point processes in the following way, see [21], Theorem 9.2.X.

Theorem 2.3 *Let $\{\mathbb{P}_{B_1,\ldots,B_n}(k_1, \ldots, k_n) : n \geq 1, k_1, \ldots, k_n \geq 0, B_1, \ldots, B_n \in \mathcal{B}_0(\mathbb{R}^2)\}$ be a family of probabilities with*

$$\mathbb{P}_{B_1,\ldots,B_n}(k_1, \ldots, k_n) = \mathbb{P}_{B_{\pi(1)},\ldots,B_{\pi(n)}}(k_{\pi(1)}, \ldots, k_{\pi(n)})$$

and

$$\sum_{i=1}^{\infty} \mathbb{P}_{B_1,\ldots,B_n,B_{n+1}}(k_1, \ldots, k_n, i) = \mathbb{P}_{B_1,\ldots,B_n}(k_1, \ldots, k_n)$$

for any permutation π of $\{1, \ldots, n\}$, for any $k_1, \ldots, k_n \in \mathbb{N}_0$ and for any bounded Borel sets $B_1, \ldots, B_{n+1}$. Moreover, assume that

$$\sum_{k_j + \cdots + k_n = k, k_j, \ldots, k_n \geq 0} \mathbb{P}_{B_1,\ldots,B_n}(k_1, \ldots, k_n) = \mathbb{P}_{B_1,\ldots,B_{j-1},\cup_{i=j}^n B_i}(k_1, \ldots, k_{j-1}, k)$$

for any $j, n \in \mathbb{N}$ *with* $j \leq n$, $k_1, \ldots, k_{j-1}, k \in \mathbb{N}_0$ *and pairwise disjoint sets* $B_1, \ldots, B_n \in \mathcal{B}_0(\mathbb{R}^2)$ *and assume that*

$$\lim_{n\to\infty} \mathbb{P}_{[x_1-\frac{1}{n},x_1)\times[x_2-\frac{1}{n},x_2)}(0) = 1$$

for any $x = (x_1, x_2) \in \mathbb{R}^2$. *Then there exists a probability space* $(\Omega, \mathcal{A}, \mathbb{P})$ *and a point process* X *defined on* $(\Omega, \mathcal{A}, \mathbb{P})$ *such that the finite–dimensional distributions of* X *are equal to* $\{\mathbb{P}_{B_1,\ldots,B_n}(k_1, \ldots, k_n) : n \geq 1, k_1, \ldots, k_n \geq 0, B_1, \ldots, B_n \in \mathcal{B}_0(\mathbb{R}^2)\}$.

Note that it is even possible to consider the finite–dimensional distributions only for bounded, half open rectangles. Then the theorems above remain valid.

2.2.3 Ergodicity and mixing

Another important property of point processes is ergodicity. Let $\mathcal{I}$ denote the σ-algebra of shift invariant sets of $\mathcal{N}$, i.e.,

$$\mathcal{I} = \{A \in \mathcal{N} : A = t_x A \text{ for all } x \in \mathbb{R}^2\}, \tag{2.4}$$

where $t_x A = \{t_x\varphi : \varphi \in A\}$. Then a stationary point process X is said to be *ergodic* if $\mathbb{P}(X \in A) \in \{0, 1\}$ for all $A \in \mathcal{I}$. Moreover, a stationary point process X is called *mixing* if

$$\lim_{|x|\to\infty} \mathbb{P}(X \in A, X \in t_x B) = \mathbb{P}(X \in A)\mathbb{P}(X \in B) \tag{2.5}$$

for all $A, B \in \mathcal{N}$. The following result connects the notions of mixing and ergodic point processes.

Theorem 2.4 *Let* X *be an arbitrary stationary point process. If* X *is mixing, then* X *is ergodic.*

Proof Let $A \in \mathcal{I}$, then $A = t_x A$ for each $x \in \mathbb{R}^2$ and

$$\begin{aligned} \mathbb{P}(X \in A) &= \lim_{|x|\to\infty} \mathbb{P}(X \in A, X \in t_x A) \\ &= \mathbb{P}(X \in A)\mathbb{P}(X \in A) = \mathbb{P}(X \in A)^2, \end{aligned}$$

provided that X is mixing. Thus $\mathbb{P}(X \in A) \in \{0, 1\}$. □

Note that there are point processes which are ergodic, but do not fulfill the mixing condition (2.5). If a point process X is ergodic, then, loosely speaking, statistical averages can be expressed as spatial averages over single realizations of X. Mathematically, this statement can be formulated in the following way using sequences of unboundedly increasing sampling windows. A sequence $\{W_n\} \subset \mathcal{B}_0(\mathbb{R}^2)$ of sampling windows is said to be a *convex averaging sequence* if

- W_n is convex for all $n \in \mathbb{N}$,
- $W_n \subset W_{n+1}$ for all $n \in \mathbb{N}$, and
- $\rho(W_n) \to \infty$ for $n \to \infty$, where $\rho(W_n)$ is the radius of the largest ball contained in W_n, i.e., $\rho(W_n) = \sup\{r > 0 : B(x, r) \subset W_n \text{ for some } x \in \mathbb{R}^2\}$.

Using this definition we can state the so–called individual and statistical ergodic theorem for point processes, see e.g. [78] and [21], Theorem 12.2.IV.

Theorem 2.5 *Let X be a stationary and ergodic point process with intensity λ and let $\{W_n\}$ be a convex averaging sequence. Then*

$$\lim_{n\to\infty} \frac{X(W_n)}{\nu_2(W_n)} = \lambda \tag{2.6}$$

almost surely and in L^1.

2.2.4 Palm distribution

Often it is convenient to regard the distribution of a stationary point process X conditioned to the event that there is one point of the process located at the origin $o \in \mathbb{R}^2$. Since $\mathbb{P}(o \in X) = 0$, this conditional distribution cannot be calculated in the usual sense. An alternative approach leading to probability measures on $\mathcal{N}$ which can be interpreted as the conditional distributions of stationary point processes X conditioned on the event $\{o \in X\}$ are Palm distributions.

The *Palm distribution* P_X^* of a stationary point process X is defined by

$$P_X^*(A) = \frac{1}{\lambda \nu_2(B)} \mathbb{E}\#\{n \in \mathbb{N} : X_n \in B, t_{X_n} X \in A\}, \quad A \in \mathcal{N}, \tag{2.7}$$

where $B \in \mathcal{B}_0(\mathbb{R}^2)$ with $0 < \nu_2(B) < \infty$ and $\lambda > 0$ is the intensity of X. It is easy to see that P_X^* does not depend on the specific choice of B, thus we can choose $B = [0, 1)^2$. The Palm distribution P_X^* can be interpreted as the conditional distribution of the point process under the condition that one point is located at the origin o. Note that $o \in X^*$ almost surely if X^* is distributed according to P_X^*. In the following, we frequently use the notation X^* for a point process distributed according to P_X^* and also speak of the *Palm version* X^* of the stationary point process X. If X is ergodic, then we get for $A \in \mathcal{N}$ that

$$P_X^*(A) = \lim_{m\to\infty} \frac{\#\{n \in \mathbb{N} : X_n \in [-m, m]^2, t_{X_n} X \in A\}}{X([-m, m]^2)} \tag{2.8}$$

with probability 1. This is a consequence of Theorem 2.5 since the point process $X_A = \{X_n : t_{X_n} X \in A\}$ is ergodic for any $A \in \mathcal{N}$ if X is ergodic. Thus, the Palm distribution can be regarded as the distribution of the point process X seen from a point of X which is chosen at random. Therefore, we also speak of the typical point of X in the following meaning the point at the origin o of the Palm version X^* of X.

2.2.5 Poisson point processes

In this section we introduce the notion of Poisson (point) processes which is the most frequently studied point process model. There are several reasons for that. First, the Poisson process is analytically tractable, i.e., many theoretical results can be derived for Poisson processes. In addition, many point process models are constructed based on Poisson processes like Poisson cluster processes, specific hardcore processes and Cox processes. Furthermore, it is a model for complete spatial randomness, i.e., there is no interaction between the points. This is the reason why the Poisson process is often used as a reference model in order to analyze clustering or repulsion effects between points. In Figure 2.1 a realization of a Poisson process is shown together with realizations of point processes that possess clustering and hardcore effects, respectively.

Let $\mu : \mathcal{B}(\mathbb{R}^2) \to [0, \infty]$ be a diffuse and locally finite measure om $\mathcal{B}(\mathbb{R}^2)$. Then a point process X is called *Poisson point process* with intensity measure μ if

- the random variables $X(B_1), \ldots, X(B_n)$ are independent for any pairwise disjoint sets $B_1, \ldots, B_n \in \mathcal{B}_0(\mathbb{R}^2)$, and if
- it holds that $X(B) \sim Poi(\mu(B))$ for any $B \in \mathcal{B}_0(\mathbb{R}^2)$, i.e.,

$$\mathbb{P}(X(B) = k) = e^{-\mu(B)} \frac{\mu(B)^k}{k!}, \quad B \in \mathcal{B}_0(\mathbb{R}^2), k \in \mathbb{N}_0 . \tag{2.9}$$

If $\mu(B) = \lambda \nu_2(B)$ for $B \in \mathcal{B}(\mathbb{R}^2)$, then the Poisson process X is stationary and isotropic. Furthermore, the Palm distribution of a stationary Poisson process X can be obtained by just adding the origin to the original Poisson process X. This result is called Slivnyak's theorem ([88]).

Theorem 2.6 (Slivnyak's theorem) *Let X be a stationary Poisson process with Palm distribution P_X^*. Then*

$$P_X^*(A) = \mathbb{P}(X \cup \{o\} \in A), \quad A \in \mathcal{N} . \tag{2.10}$$

2.3 Marked point processes

Point processes can be generalized by adding a (random) mark from some mark space $\mathbb{M}$ to each point. Such generalizations are called marked point processes.

2.3.1 Definitions and basic properties

In the following, the *mark space* $\mathbb{M}$ is assumed to be a Polish space which is equipped with the Borel–σ–algebra $\mathcal{B}(\mathbb{M})$ on $\mathbb{M}$. Let $\mathsf{N}_{\mathbb{M}} = \mathsf{N}(\mathbb{R}^2 \times \mathbb{M})$ denote

the set of all counting measures $\psi : \mathcal{B}(\mathbb{R}^2) \otimes \mathcal{B}(\mathbb{M}) \to \mathbb{N}_0 \cup \{\infty\}$ that are simple and additionally locally finite in the first component, i.e., $\psi(B \times \mathbb{M}) < \infty$ for all $B \in \mathcal{B}_0(\mathbb{R}^2)$ and $\psi(\{x\} \times \mathbb{M}) \in \{0, 1\}$ for all $x \in \mathbb{R}^2$. The support of ψ is then defined as the (countable) set $\mathrm{supp}(\psi) = \{(x, m) \in \mathbb{R}^2 \times \mathbb{M} : \psi(\{(x, m)\}) > 0\}$ and each $\psi \in \mathsf{N}_{\mathbb{M}}$ can be written as

$$\psi(B \times G) = \sum_{(x,m) \in \mathrm{supp}(\psi)} \delta_{(x,m)}(B \times G)\,, \quad B \in \mathcal{B}(\mathbb{R}^2),\, G \in \mathcal{B}(\mathbb{M})\,. \tag{2.11}$$

Thus, we can identify each $\psi \in \mathsf{N}_{\mathbb{M}}$ with its support and therefore also write $\psi = \{(x_n, m_n)\}$ if $\mathrm{supp}(\psi) = \{(x_n, m_n)\} = \{(x_n, m_n)\}$. Now let $\mathcal{N}_{\mathbb{M}}$ be the σ–algebra generated by the subsets of $\mathsf{N}_{\mathbb{M}}$ of the form $\{\psi \in \mathsf{N}_{\mathbb{M}} : \psi(B \times G) = j\}$ for $B \in \mathcal{B}_0(\mathbb{R}^2)$, $G \in \mathcal{B}(\mathbb{M})$ and $j \in \mathbb{N}_0$. We then call a measurable mapping $X_M : \Omega \to \mathsf{N}_{\mathbb{M}}$ from some probability space $(\Omega, \mathcal{A}, \mathbb{P})$ into the measurable space $(\mathsf{N}_{\mathbb{M}}, \mathcal{N}_{\mathbb{M}})$ *random marked point process* in $\mathbb{R}^2$ with mark space $(\mathbb{M}, \mathcal{B}(\mathbb{M}))$. Again, often alternative representations of X_M are convenient. For instance, X_M can be represented as a sequence of random marked points written as $X_M = \{(X_n, M_n)\}$. Here both $X_n : \Omega \to \mathbb{R}^2$ and $M_n : \Omega \to \mathbb{M}$ are measurable mappings. The marked point process X_M is called *independently marked* if the points $\{X_n\}$ and the marks $\{M_n\}$ are independent and furthermore the marks $\{M_n\}$ are independent and identically distributed random variables. In the following, we use the notation $X_M = \{(X_n, M_n)\}$ and, depending on the context, we regard X_M as a random sequence of marked points or a random element of $\mathcal{N}_{\mathbb{M}}$. Note that we obtain a simple point process $\{X_n\}$ by regarding the projection of the marked point process $X_M = \{(X_n, M_n)\}$ on N. This point process is called the unmarked point process of X_M in the following.

Like for point processes we define the *distribution* P_{X_M} of X_M by $P_{X_M}(A) = \mathbb{P}(X_M \in A)$ for $A \in \mathcal{N}_{\mathbb{M}}$. Stationarity and isotropy are now defined with respect to the first component of X_M. Let $\psi = \{(x_n, m_n)\} \in \mathsf{N}_{\mathbb{M}}$, then we define the shift operator $t_x : \mathsf{N}_{\mathbb{M}} \to \mathsf{N}_{\mathbb{M}}$ by $t_x\psi = \{(x_n - x, m_n)\}$ and the rotation operator $\vartheta_R : \mathsf{N}_{\mathbb{M}} \to \mathsf{N}_{\mathbb{M}}$ by $\vartheta_R\psi = \{(\vartheta_R x_n, m_n)\}$. A marked point process X_M is called

- *stationary* if the distribution of X_M is translation invariant in the first component, i.e. if $X_M \stackrel{\mathrm{d}}{=} t_x X_M$ for all $x \in \mathbb{R}^2$,
- *isotropic* if its distribution is rotation invariant in the first component, i.e. if $X_M \stackrel{\mathrm{d}}{=} \vartheta_R X_M$ for all rotations ϑ_R around the origin, and
- *motion-invariant* if X_M is both stationary and isotropic.

2.3.2 Intensity measure and Palm distribution

For a marked point process X_M its *intensity measure* $\mu_M : \mathcal{B}(\mathbb{R}^2) \otimes \mathcal{B}(\mathbb{M}) \to [0, \infty]$ is defined by

$$\mu_M(B \times G) = \mathbb{E}X_M(B \times G)\,, \quad B \in \mathcal{B}(\mathbb{R}^2)\,, G \in \mathcal{B}(\mathbb{M})\,. \tag{2.12}$$

Here $\mu_M(B \times G)$ is the expected number of points of the marked point process X_M in B with mark in G. For a stationary marked point processes X_M with $0 < \lambda = \mathbb{E}X_M([0,1)^2 \times \mathbb{M}) < \infty$, the intensity measure μ_M can be written in a similar way as for stationary non–marked point processes. In particular,

$$\mu_M(B \times G) = \lambda\, \nu_2(B)\, P^o_{X_M}(G)\,, \quad B \in \mathcal{B}(\mathbb{R}^2), G \in \mathcal{B}(\mathbb{M})\,, \tag{2.13}$$

see [87], Theorem 3.5.1. The constant λ is again called the *intensity* of X_M and the probability measure $P^o_{X_M} : \mathcal{B}(\mathbb{M}) \to [0,1]$ is called the *Palm mark distribution* of X_M which is defined by

$$P^o_{X_M}(G) = \frac{1}{\lambda \nu_2(B)}\, \mathbb{E}\#\{n \in \mathbb{N} \,:\, X_n \in B\,,\, D_n \in G\} \tag{2.14}$$

for $G \in \mathcal{B}(\mathbb{M})$, where $B \in \mathcal{B}_0(\mathbb{R}^2)$ with $0 < \nu_2(B) < \infty$ is arbitrary and can be chosen e.g. as $[0,1)^2$. A random variable $M^* : \Omega \to \mathbb{M}$ distributed according to $P^o_{X_M}$ is called the *typical mark* of X_M. It can be interpreted as the mark at the origin o given that there is a point of X_M located at the origin. Therefore, we sometimes also say that the typical mark is the mark at a typical point of the unmarked point process $\{X_n\}$ of X_M.

Moreover, for stationary marked point processes the *Palm distribution* $P^*_{X_M}$ is defined on $\mathcal{N}_{\mathbb{M}} \otimes \mathcal{B}(\mathbb{M})$ by

$$P^*_{X_M}(A \times G) = \frac{1}{\lambda \nu_2(B)} \mathbb{E}\#\{n \in \mathbb{N} : X_n \in B, M_n \in G, t_{X_n} X_{\mathbb{M}} \in A\} \tag{2.15}$$

for $A \in \mathcal{N}_{\mathbb{M}}$ and $G \in \mathcal{B}(\mathbb{M})$, where $B \in \mathcal{B}(\mathbb{R}^2)$ with $0 < \nu_2(B) < \infty$. Again, the definition is independent of B which can be chosen as $[0,1)^2$. The Palm distribution $P^*_{X_M}$ can be interpreted as the conditional distribution of X_M under the condition that there is a point located at o.

For stationary marked point processes we can modify Campbell's theorem in the following way, see e.g. Theorem 3.5.3 in [87].

Theorem 2.7 (Refined Campbell theorem) *Let X_M be a stationary marked point process in $\mathbb{R}^2$ with mark space $\mathbb{M}$ and intensity $\lambda > 0$. Furthermore, let $f : \mathbb{R}^2 \times \mathbb{M} \times \mathsf{N}_{\mathbb{M}} \to [0,\infty)$ be measurable. Then $\sum_{(x,m)\in X_M} f(x, m, t_x X_M)$ is measurable and*

$$\mathbb{E} \sum_{(x,m)\in X_M} f(x, m, t_x X_M) = \lambda \int_{\mathbb{R}^2} \int_{\mathsf{N}_{\mathbb{M}}\times\mathbb{M}} f(x, m, \psi)\, P^*_{X_M}(d(\psi, m))\, \nu_2(dx)\,. \tag{2.16}$$

It is easy to see that the preceding theorem reduces to Campbell's theorem for unmarked point processes if we only consider functions $f : \mathbb{R}^2 \times \mathbb{M} \times \mathsf{N}_{\mathbb{M}} \to [0,\infty)$ with $f(x, m, \psi) = g(x)$ for all $x \in \mathbb{R}^2, m \in \mathbb{M}, \psi \in \mathsf{N}_{\mathbb{M}}$ and some function $g : \mathbb{R}^2 \to [0,\infty)$.

2.3.3 Ergodic theorem

Ergodic and mixing marked point processes can be defined in a similar way as ergodic and mixing unmarked point processes. We define a shift $t_x A$ of a set $A \in \mathcal{N}_{\mathbb{M}}$ by $t_x A = \{t_x \psi : \psi \in A\}$ for all $x \in \mathbb{R}^2$. Let $\mathcal{I}$ denote the σ-algebra of shift invariant sets of $\mathcal{N}_{\mathbb{M}}$, i.e.,

$$\mathcal{I} = \{A \in \mathcal{N}_{\mathbb{M}} : A = t_x A \text{ for all } x \in \mathbb{R}^2\}. \tag{2.17}$$

Then a stationary marked point process X_M is called *ergodic* if $\mathbb{P}(X_M \in A) \in \{0, 1\}$ for all $A \in \mathcal{I}$. Furthermore, a stationary marked point process X_M is said to be *mixing* if for all $A, B \in \mathcal{N}_{\mathbb{M}}$ it holds that

$$\lim_{|x| \to \infty} \mathbb{P}(X_M \in A, X_M \in t_x B) = \mathbb{P}(X_M \in A)\mathbb{P}(X_M \in B). \tag{2.18}$$

In the same way as for unmarked point processes it can be shown that a marked point process is ergodic if it is mixing.

We now state a theorem which is a version of the individual and statistical ergodic theorem applied to ergodic marked point processes, see Theorem 12.2.IV and Corollary 12.2.V in [21]. This theorem connects spatial averages of the marks of a marked point process with statistical averages of the typical mark.

Theorem 2.8 *Let $\{W_n\}$ be a convex averaging sequence and let X_M be a stationary and ergodic marked point process with intensity λ and mark space $\mathbb{M}$. Moreover, let $h : \mathbb{M} \to [0, \infty)$ be a measurable function and M^* the typical mark of X_M. Then*

$$\mathbb{E}h(M^*) = \lim_{n \to \infty} \frac{1}{\lambda \nu_2(W_n)} \sum_{i=1}^{\infty} \mathbb{1}_{W_n}(X_i) h(M_i) \tag{2.19}$$

almost surely and in L^1. Furthermore,

$$\mathbb{E}h(M^*) = \lim_{n \to \infty} \frac{1}{\#\{i : X_i \in W_n\}} \sum_{i=1}^{\infty} \mathbb{1}_{W_n}(X_i) h(M_i) \tag{2.20}$$

with probability 1.

The preceding theorem is the reason why we are especially interested in the typical mark of ergodic marked point processes in this thesis. In particular, we get for $h = \mathbb{1}_G$ that

$$P^o_{X_M}(G) = \lim_{n \to \infty} \frac{\#\{n \in \mathbb{N}_0 : X_n \in [-n, n]^2, M_n \in G\}}{X_M([-n, n]^2 \times \mathbb{M})} \tag{2.21}$$

with probability 1. So the typical mark can be regarded as the mark at a point chosen at random among all points, i.e., at a typical point of the unmarked point process $\{X_n\}$ of X_M.

2.3.4 Jointly stationary point processes and Neveu's exchange formula

In the proofs of this thesis we frequently utilize a version of Neveu's exchange formula (see e.g. [76]) for two jointly stationary marked point processes $X^{(1)} = \{(X_n^{(1)}, M_n^{(1)})\}$ and $X^{(2)} = \{(X_n^{(2)}, M_n^{(2)})\}$ with mark spaces $\mathbb{M}_1$ and $\mathbb{M}_2$, respectively. This formula allows to represent the distribution of functionals of $X^{(1)}$ and $X^{(2)}$ distributed according to the Palm distribution $P^*_{X^{(1)}}$ by functionals distributed according to $P^*_{X^{(2)}}$. Thus, we can switch from the joint distribution of $X^{(1)}$ and $X^{(2)}$ conditioned on $o \in \{X_n^{(1)}\}$ to the joint distribution of $X^{(1)}$ and $X^{(2)}$ conditioned on $o \in \{X_n^{(2)}\}$. In order to make this precise we first have to define $X^{(1)}$ and $X^{(2)}$ as a random element of a common probability space.

Let $\mathsf{N}_{\mathbb{M}_i}$ denote the family of all counting measures in $\mathcal{B}(\mathbb{R}^2) \otimes \mathcal{B}(\mathbb{M}_i)$ which are simple and locally finite in the first component, equipped with the usual σ–algebra $\mathcal{N}_{\mathbb{M}_i}$ for $i = 1, 2$. We then define $Y = (X^{(1)}, X^{(2)})$ which can be regarded as a random element of the product space $\mathsf{N}_{\mathbb{M}_1,\mathbb{M}_2} = \mathsf{N}_{\mathbb{M}_1} \times \mathsf{N}_{\mathbb{M}_2}$. Let λ_1 and λ_2 denote the intensities of $X^{(1)}$ and $X^{(2)}$, respectively, and define the shift operator t_x by $t_x Y = (t_x X^{(1)}, t_x X^{(2)})$ for $x \in \mathbb{R}^2$. Thus, $t_x Y$ is obtained if the points of both $X^{(1)}$ and $X^{(2)}$ are shifted by $-x \in \mathbb{R}^2$. Now assume that Y and $t_x Y$ have the same distribution for all $x \in \mathbb{R}^2$. Then the *Palm distributions* $P_Y^{(i)}, i = 1, 2$ on $\mathcal{N}_{\mathbb{M}_1} \otimes \mathcal{N}_{\mathbb{M}_2} \otimes \mathcal{B}(\mathbb{M}_i)$ with respect to the i-th component of Y are defined by

$$P_Y^{(i)}(A \times G) = \frac{1}{\lambda_i} \, \mathbb{E}\#\{n : X_n^{(i)} \in [0,1)^2, M_n^{(i)} \in G, t_{X_n^{(i)}} Y \in A\} \tag{2.22}$$

for any $A \in \mathcal{N}_{\mathbb{M}_1} \otimes \mathcal{N}_{\mathbb{M}_2}, G \in \mathcal{B}(\mathbb{M}_i)$. Note that for $A \in \mathcal{N}_{\mathbb{M}_i}, G \in \mathcal{B}(\mathbb{M}_i)$ we get

$$P_Y^{(1)}(A \times \mathsf{N}_{\mathbb{M}_2} \times G) = P^*_{X^{(1)}}(A \times G)$$

for $i = 1$ and

$$P_Y^{(2)}(\mathsf{N}_{\mathbb{M}_1} \times A \times G) = P^*_{X^{(2)}}(A \times G)\,,$$

for $i = 2$, where $P^*_{X^{(1)}}$ and $P^*_{X^{(2)}}$ are the ordinary Palm distributions of the marked point processes $X^{(1)}$ and $X^{(2)}$, respectively. In the following we also write $P^*_{X^{(i)}}$ for the Palm distribution $P_Y^{(i)}$ of the vector $(X^{(1)}, X^{(2)})$ in order to emphasize the dependence on $X^{(i)}$ for $i = 1, 2$. Using the notation introduced above, and $\psi = (\psi^{(1)}, \psi^{(2)})$ for the elements of $\mathsf{N}_{\mathbb{M}_1,\mathbb{M}_2}$, Neveu's exchange formula can be stated in the following way, see e.g. [53, 54].

Theorem 2.9 (Neveu's exchange formula) *For any measurable mapping $f : \mathbb{R}^2 \times \mathbb{M}_1 \times \mathbb{M}_2 \times \mathsf{N}_{\mathbb{M}_1,\mathbb{M}_2} \to [0, \infty)$, it holds that*

$$\begin{aligned}
&\lambda_1 \int_{\mathsf{N}_{\mathbb{M}_1,\mathbb{M}_2} \times \mathbb{M}_1} \int_{\mathbb{R}^2 \times \mathbb{M}_2} f(x, m^{(1)}, m^{(2)}, t_x\psi) \; \psi^{(2)}(d(x, m^{(2)})) \, P_Y^{(1)}(d(\psi, m^{(1)})) \\
&\quad = \lambda_2 \int_{\mathsf{N}_{\mathbb{M}_1,\mathbb{M}_2} \times \mathbb{M}_2} \int_{\mathbb{R}^2 \times \mathbb{M}_1} f(-x, m^{(1)}, m^{(2)}, \psi) \; \psi^{(1)}(d(x, m^{(1)})) \, P_Y^{(2)}(d(\psi, m^{(2)}))\,.
\end{aligned} \tag{2.23}$$

Let $X^{(1)}$ and $X^{(2)}$ be two jointly stationary point processes which are independent. Furthermore, assume that $Y = (X^{(1)*}, \widetilde{X}^{(2)})$ is distributed according to the Palm distribution $P_Y^{(1)}$ with respect to $X^{(1)}$. Then, using the definition of the Palm distribution $P_Y^{(1)}$, we get for all $A \in \mathcal{N}_{\mathbb{M}_1}$ and $B \in \mathcal{N}_{\mathbb{M}_2}$ that

$$\begin{aligned}
\mathbb{P}(X^{(1)*} \in A, \widetilde{X}^{(2)} \in B) &= \mathbb{E}\mathbb{1}_A(X^{(1)*})\mathbb{1}_B(\widetilde{X}^{(2)}) \\
&= \frac{1}{\lambda_1}\mathbb{E}\sum_{X_n^{(1)} \in [0,1)^2} \mathbb{1}_A(t_{X_n^{(1)}}X^{(1)})\mathbb{1}_B(t_{X_n^{(1)}}X^{(2)}) \\
&= \frac{1}{\lambda_1}\mathbb{E}\sum_{X_n^{(1)} \in [0,1)^2} \mathbb{1}_A(t_{X_n^{(1)}}X^{(1)})\mathbb{E}[\mathbb{1}_B(t_{X_n^{(1)}}X^{(2)}) \mid X^{(1)}] \\
&= \mathbb{P}(X^{(1)*} \in A)\mathbb{P}(X^{(2)} \in B)\,,
\end{aligned}$$

where we used in the last equality that $X^{(2)}$ is stationary and independent of $X^{(1)}$. Thus, we have shown that $X^{(1)*}$ is independent of $\widetilde{X}^{(2)}$ and $\widetilde{X}^{(2)} \stackrel{\mathrm{d}}{=} X^{(2)}$. This observation is used later on in the proofs of this thesis.

2.4 Random closed sets

In this section we define the notion of a random closed set. Examples of random closed sets are random point patterns, unions of balls with random centers and radii or unions of line segments.

2.4.1 Definitions and basic properties

A *random closed set* is a random element of the family of closed subsets of $\mathbb{R}^2$ which we denote with $\mathcal{F}$. Let $\mathcal{C}$ and $\mathcal{K}$ denote the families of compact sets and convex bodies (compact and convex sets), respectively, and define

$$\mathcal{F}_B = \{F \in \mathcal{F} : F \cap B \neq \emptyset\} \quad \text{and} \quad \mathcal{F}^B = \{F \in \mathcal{F} : F \cap B = \emptyset\}$$

for $B \subset \mathbb{R}^2$ as well as

$$\mathcal{F}^B_{B_1,\ldots,B_n} = \mathcal{F}^B \cap \mathcal{F}_{B_1} \cdots \cap \mathcal{F}_{B_n}$$

for $B, B_1, \ldots, B_n \subset \mathbb{R}^2$. We define the σ–algebra $\mathcal{B}(\mathcal{F})$ on $\mathcal{F}$ as the σ-algebra generated by the family $\{\mathcal{F}_C : C \in \mathcal{C}\}$. Note that the family $\{\mathcal{F}^G : G \subset \mathbb{R}^2 \text{ open}\}$ also generates $\mathcal{B}(\mathcal{F})$ and it can be shown that $\mathcal{C} \in \mathcal{B}(\mathcal{F})$ and $\mathcal{K} \in \mathcal{B}(\mathcal{F})$. A measurable mapping $\Xi : \Omega \to \mathcal{F}$ from some probability space $(\Omega, \mathcal{A}, \mathbb{P})$ into the measurable space $(\mathcal{F}, \mathcal{B}(\mathcal{F}))$ is called a random closed set. If $\mathbb{P}(\Xi \in \mathcal{C}) = 1$ and $\mathbb{P}(\Xi \in \mathcal{K}) = 1$, then we call Ξ a *random compact set* or a *random convex body*,

respectively. The *distribution* P_Ξ of Ξ is the probability measure on $\mathcal{B}(\mathcal{F})$ defined by

$$P_\Xi(B) = \mathbb{P}(\Xi \in B) \quad \text{for } B \in \mathcal{B}(\mathcal{F}).$$

We call a random closed set Ξ

- *stationary* if $\Xi \stackrel{\mathrm{d}}{=} t_x\Xi$ for all $x \in \mathbb{R}^2$, i.e., $P_\Xi = P_{t_x\Xi}$ for all $x \in \mathbb{R}^2$,
- *isotropic* if $\Xi \stackrel{\mathrm{d}}{=} \vartheta_R\Xi$, i.e., $P_\Xi = P_{\vartheta_R\Xi}$, for all rotations ϑ_R around the origin o, and
- *motion-invariant* if Ξ is both stationary and isotropic.

An important characteristic of a stationary random closed set Ξ is its *area fraction* p which is defined by $p = \mathbb{E}\nu_2(\Xi \cap [0,1)^2)$. Thus, p is the expected area of Ξ per unit area. The capacity functional $T_\Xi : \mathcal{C} \to [0,1]$ of a random closed set Ξ is defined by

$$T_\Xi(C) = P_\Xi(\mathcal{F}_C) = \mathbb{P}(\Xi \cap C \neq \emptyset) \quad \text{for} \quad C \in \mathcal{C}.$$

Note that the capacity functional can be regarded as the analogon of the distribution function of a random variable in $\mathbb{R}$. In particular, it determines the distribution of Ξ uniquely since the family $\{F^C : C \in \mathcal{C}\}$ generates $\mathcal{B}(\mathcal{F})$ and $F^{C_1} \cap F^{C_2} = F^{C_1 \cup C_2}$.

Theorem 2.10 *Let Ξ and Ξ' be two random closed sets with $T_\Xi = T_{\Xi'}$, then $\Xi \stackrel{\mathrm{d}}{=} \Xi'$.*

Note that given a so–called alternating Choquet capacity T of infinite order it is also possible to prove that there exists a random closed set Ξ with $T_\Xi = T$, see e.g. [70], Theorem 1.13.

2.4.2 Examples

In this section some examples of random closed sets are briefly introduced.

Point processes

A point process $X = \{X_n\}$ can be regarded as a random set of points $\{X_n\}$ which is locally finite almost surely. Thus, a point process can be interpreted as a random closed set. The capacity functional of $\Xi = \{X_n\}$ is given by $T_\Xi(C) = \mathbb{P}(X(C) > 0) = 1 - \mathbb{P}(X(C) = 0)$ for $C \in \mathcal{C}$. Since the capacity functional determines the distribution of X, we immediately get that the distribution of a point process is already determined by its *void probabilities* $\mathbb{P}(X(C) = 0)$ for $C \in \mathcal{C}$ which is a much smaller class of probabilities than the finite–dimensional probabilities considered in Section 2.2.2.

Boolean model

Another example of a random closed set is the Boolean model. Let $\Xi_1, \Xi_2, \ldots$ be a sequence of independent copies of a random compact set Ξ_0 which are called *grains* and let $X = \{X_n\}$ be an independent and stationary Poisson process with intensity λ. We assume that $\mathbb{E}R(\Xi_0)^2 < \infty$, where $R(\Xi_0)$ denotes the radius of the smallest ball which contains Ξ_0. Then the *Boolean model* Ξ is defined via $\Xi = \cup_{n=1}^{\infty}(\Xi_n + X_n)$. Here, Ξ_0 can be e.g. a ball $B(o, R)$ with random radius R or a line segment with random length and orientation, see Figure 2.2. The condition $\mathbb{E}R(\Xi_0)^2 < \infty$ ensures that the resulting random set is closed with probability 1.

It is easy to see that Ξ is stationary since X is stationary. If Ξ is a Boolean model, then it is known that its area fraction p is given by $p = 1 - \exp(-\lambda \mathbb{E}\nu_2(\Xi_0))$, see [90], p. 67.

Fiber processes

Later on, we are especially interested in random closed sets Ξ which are locally finite segment systems with probability 1. For instance, Ξ can be a Boolean model with random line segments as grains, see Figure 2.2. Such random closed sets can be generalized to so–called *fiber processes*. A fiber process is a random closed set Ξ such that for any $B \in \mathcal{B}_0(\mathbb{R}^2)$ the intersection $\Xi \cap B$ is almost surely a union of piecewise smooth curves, see e.g. [63] and [90], Chapter 9. If Ξ is a stationary fiber process, then $\mathbb{E}\nu_1(\Xi \cap B) = \gamma\nu_2(B)$ for all $B \in \mathcal{B}_0(\mathbb{R}^2)$ and some constant $\gamma > 0$, where ν_1 denotes the 1–dimensional Hausdorff measure. We call γ the (length) intensity of Ξ which can be interpreted as the mean length of Ξ per unit area. In this thesis, we are especially interested in fiber processes obtained from the edges of random tessellations which are locally finite unions of line segments, see Chapter 3 for details.

2.4.3 Ergodicity and mixing

An important property apart from stationarity and isotropy is ergodicity which can be defined in the same way as for (marked) point processes. For any $x \in \mathbb{R}^2$, we define the shift $t_x A$ of a set $A \in \mathcal{B}(\mathcal{F})$ by $t_x A = \{t_x F : F \in A\}$. Let $\mathcal{I}$ denote the σ-algebra of shift invariant sets of $\mathcal{B}(\mathcal{F})$, i.e.,

$$\mathcal{I} = \{F \in \mathcal{B}(\mathcal{F}) : F = t_x F \text{ for all } x \in \mathbb{R}^2\}. \tag{2.24}$$

Then a stationary random closed set Ξ is called *ergodic*, if $\mathbb{P}(\Xi \in A) \in \{0, 1\}$ for all $A \in \mathcal{I}$. There is also an (individual and statistical) ergodic theorem for random closed sets which expresses statistical averages by spatial averages, see [90], Theorem 6.2.

Theorem 2.11 *Let Ξ be a stationary ergodic random closed set and $\{W_n\}$ be a convex averaging sequence. Moreover, let $h : \mathcal{B}(\mathbb{R}^2) \to [0, \infty)$ be a translation*

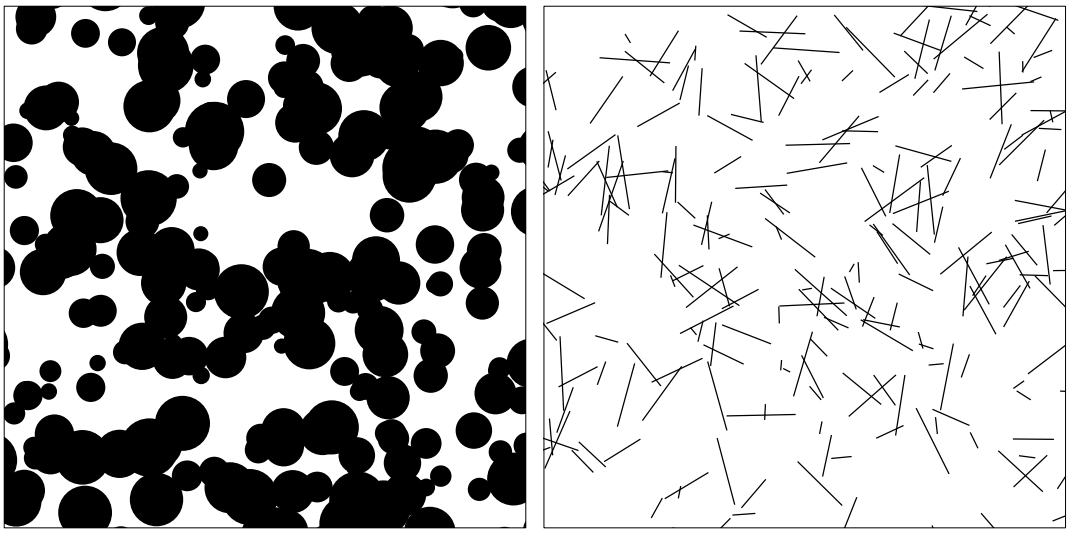

(a) Boolean model with random balls (b) Boolean model with random line segments

Figure 2.2: Realizations of the Boolean model with different types of grains

invariant function with $h(B_1 \cup B_2) = h(B_1) + h(B_2)$ *for all disjoint* $B_1, B_2 \in \mathcal{B}(\mathbb{R}^2)$*. If there exists a non–negative random variable* Z *such that* $h(\Xi \cap B) \leq Z$ *for all* $B \in \mathcal{B}([0,1)^2)$ *and* $\mathbb{E}Z < \infty$*, then*

$$\lim_{n\to\infty} \frac{h(\Xi \cap W_n)}{\nu_2(W_n)} = \mathbb{E}h(\Xi \cap [0,1)^2)$$

almost surely and in L^1*.*

Now suppose that Ξ is a stationary and ergodic fiber process of length intensity $\gamma \in (0,\infty)$, then we can consider the translation invariant function $h(B) = \nu_1(B)$ for $B \in \mathcal{B}(\mathbb{R}^2)$. Note that $\nu_1(\Xi \cap B) \leq \nu_1(\Xi \cap [0,1)^2)$ for all $B \in \mathcal{B}([0,1)^2)$ and $\mathbb{E}\nu_1(\Xi \cap [0,1)^2) = \gamma < \infty$. Thus, Theorem 2.11 yields

$$\lim_{n\to\infty} \frac{\nu_1(\Xi \cap W_n)}{\nu_2(W_n)} = \gamma \tag{2.25}$$

almost surely and in L^1.

A stationary random closed set Ξ is called *mixing* if for all $A, B \in \mathcal{B}(\mathcal{F})$ it holds that

$$\lim_{|x|\to\infty} \mathbb{P}(\Xi \in A, \Xi \in t_x B) = \mathbb{P}(\Xi \in A)\, \mathbb{P}(\Xi \in B)\,. \tag{2.26}$$

Note that a mixing random closed set is ergodic which can be shown in the same way as for (marked) point processes, see Theorem 2.4. It is often convenient to use the capacity functional in order to characterize mixing random closed sets.

Theorem 2.12 *A stationary random closed set Ξ is mixing if and only if for all $C_1, C_2 \in \mathcal{C}$ it holds that*

$$\lim_{|x|\to\infty} (1 - T_\Xi(C_1 \cup t_x C_2)) = (1 - T_\Xi(C_1))(1 - T_\Xi(C_2)) \,,$$

or, equivalently,

$$\lim_{|x|\to\infty} \mathbb{P}(\Xi \cap (C_1 \cup t_x C_2) = \emptyset) = \mathbb{P}(\Xi \cap C_1 = \emptyset)\mathbb{P}(\Xi \cap C_2 = \emptyset) \,.$$

A proof of Theorem 2.12 can be found in [40] and in [87], p. 408.

2.5 Random measures

Point processes in $\mathbb{R}^2$ can be regarded as random counting measures on $\mathcal{B}(\mathbb{R}^2)$. The concept of random counting measures can be generalized in a straightforward way to random measures on $\mathcal{B}(\mathbb{R}^2)$ since locally finite counting measures are a special case of locally finite measures on $\mathcal{B}(\mathbb{R}^2)$.

2.5.1 Definitions and basic properties

Let $\mathsf{M} = \mathsf{M}(\mathbb{R}^2)$ denote the set of all locally finite measures on $\mathcal{B}(\mathbb{R}^2)$. If we equip M with the smallest σ–algebra $\mathcal{M}$ such that the mappings $\eta \longmapsto \eta(B)$ are $(\mathcal{M}, \mathcal{B}(\mathbb{R}^2))$–measurable for all $\eta \in \mathsf{M}$ and $B \in \mathcal{B}_0(\mathbb{R}^2)$, then we obtain the measurable space $(\mathsf{M}, \mathcal{M})$. The shift operator $t_x : \mathsf{M} \to \mathsf{M}$ on M can be defined in the same way as for counting measures, i.e. $t_x\eta(B) = \eta(B + x)$ for all $x \in \mathbb{R}^2$. Similarly, we define the rotation operator $\vartheta_R : \mathsf{M} \to \mathsf{M}$ by $\vartheta_R\eta(B) = \eta(\vartheta_R^{-1}B) = \eta(\vartheta_{R^{-1}}B)$ for all rotations ϑ_R around the origin.

A measurable mapping $\Lambda : \Omega \to \mathsf{M}$ from some probability space $(\Omega, \mathcal{A}, \mathbb{P})$ into the measurable space $(\mathsf{M}, \mathcal{M})$ is called a *random measure* on $\mathcal{B}(\mathbb{R}^2)$. As for (marked) point processes we define the *distribution* P_Λ of Λ by $P_\Lambda(A) = \mathbb{P}(\Lambda \in A)$ for $A \in \mathcal{M}$. A random measure Λ with distribution P_Λ is then called

- *stationary* if $\Lambda \stackrel{\mathrm{d}}{=} t_x\Lambda$ for all $x \in \mathbb{R}^2$,
- *isotropic* if $\Lambda \stackrel{\mathrm{d}}{=} \vartheta_R\Lambda$ for all rotations ϑ_R around the origin, and
- *motion-invariant* if Λ is stationary and isotropic.

We say that a stationary random measure Λ is *ergodic* if $\mathbb{P}(\Lambda \in A) \in \{0, 1\}$ for all $A \in \mathcal{I} = \{A \in \mathcal{M} : A = t_x A \ \text{ for all}\, x \in \mathbb{R}^2\}$, where $t_x A = \{t_x\eta : \eta \in A\}$. Moreover, a stationary random measure is called *mixing* if

$$\lim_{|x|\to\infty} \mathbb{P}(\Lambda \in A, \Lambda \in t_x B) = \mathbb{P}(\Lambda \in A)\mathbb{P}(\Lambda \in B)$$

for all $A, B \in \mathcal{M}$. Again, it can be shown that Λ is ergodic if it is mixing.

2.5.2 Intensity measure and Palm distribution

The *intensity measure* $\mu : \mathcal{B}(\mathbb{R}^2) \to [0, \infty]$ of a random measure Λ is defined by

$$\mu(B) = \mathbb{E}\Lambda(B) \quad \text{for } B \in \mathcal{B}(\mathbb{R}^2)\,,$$

where we always assume that the measure μ is locally finite with $\mu(\mathbb{R}^2) > 0$. Let Λ be a stationary random measure, then $\mathbb{E}\Lambda(B) = \lambda\nu_2(B)$ for $B \in \mathcal{B}(\mathbb{R}^2)$, where $\lambda \in (0, \infty)$ is some constant which we call the *intensity* of Λ. Note that $\lambda = \mathbb{E}\Lambda([0,1]^2)$. The probability measure $P^*_\Lambda : \mathcal{M} \to [0,1]$ defined by

$$P^*_\Lambda(A) = \frac{1}{\lambda}\,\mathbb{E}\left[\int_{[0,1]^2} \mathbb{1}_A(t_x\Lambda)\,\Lambda(dx)\right], \quad A \in \mathcal{M} \tag{2.27}$$

is called the *Palm distribution* of the stationary random measure Λ. Again, there is a Campbell–type theorem for stationary random measures Λ which generalizes Campbell's theorem for point processes, see [62] and Theorem 7.1 in [90].

Theorem 2.13 (Campbell's theorem) *Let Λ be a stationary random measure in $\mathbb{R}^2$ with intensity λ. Furthermore, let $f : \mathbb{R}^2 \times \mathsf{M} \to [0, \infty)$ be measurable. Then $\int_{\mathbb{R}^2} f(x, t_x\Lambda)\,\Lambda(dx)$ is measurable and*

$$\mathbb{E}\left(\int_{\mathbb{R}^2} f(x, t_x\Lambda)\Lambda(dx)\right) = \lambda \int_{\mathbb{R}^2}\int_{\mathsf{M}} f(x,\eta)P^*_\Lambda(d\eta)\nu_2(dx) \tag{2.28}$$

2.5.3 Random measures associated with random closed sets

Every point process X can be regarded as a random counting measure and thus a random measure Λ. Furthermore, let $\{\lambda(x), x \in \mathbb{R}^2\}$ be a (measurable) random field such that almost surely $\lambda(x) \geq 0$, $\int_{\mathbb{R}^2} \lambda(x)\,\nu_2(dx) > 0$ and $\int_B \lambda(x)\,\nu_2(dx) < \infty$ for each $B \in \mathcal{B}_0(\mathbb{R}^2)$. Then Λ defined by

$$\Lambda(B) = \int_B \lambda(x)\,\nu_2(dx)\,, \quad B \in \mathcal{B}(\mathbb{R}^2) \tag{2.29}$$

is a random measure. For instance, assume that Ξ is a stationary random closed set with volume fraction $p = \mathbb{E}\nu_2(\Xi \cap [0,1)^2) > 0$ and define the stationary random field $\{\lambda(x), x \in \mathbb{R}^2\}$ by

$$\lambda(x) = \begin{cases} \lambda_1 & \text{if } x \in \Xi\,, \\ \lambda_2 & \text{if } x \notin \Xi\,. \end{cases}$$

Then the random measure Λ defined in (2.29) is given by

$$\Lambda(B) = \int_B \lambda(x)\,\nu_2(dx) = \lambda_1\nu_2(B \cap \Xi) + \lambda_2\nu_2(B^c \cap \Xi) \quad \text{for} \quad B \in \mathcal{B}(\mathbb{R}^2)\,.$$

Since Ξ is stationary and

$$t_y\Lambda(B) = \int_{B+y} \lambda(x)\,\nu_2(dx) = \int_B \lambda(x-y)\,\nu_2(dx) \quad \text{for} \quad B \in \mathcal{B}(\mathbb{R}^2)$$

we immediately get that Λ is stationary. Furthermore, the intensity λ of Λ is given by

$$\begin{aligned} \lambda &= \mathbb{E}\int_{[0,1)^2} \lambda(x)\,\nu_2(dx) \\ &= \lambda_1 \mathbb{E}\nu_2(\Xi \cap [0,1)^2) + \lambda_1 \mathbb{E}\nu_2(\Xi^c \cap [0,1)^2) = \lambda_1 p + \lambda_2(1-p)\,. \end{aligned}$$

In a similar way we can define random measures based on fiber processes. Assume that Ξ is a stationary fiber process, i.e., $\Xi \cap B$ is almost surely a union of piecewise smooth curves for any $B \in \mathcal{B}_0(\mathbb{R}^2)$. Then we can consider the 1-dimensional Hausdorff measure on Ξ and define the random measure Λ by $\Lambda(B) = \lambda_\ell \nu_1(B \cap \Xi)$ for $B \in \mathcal{B}(\mathbb{R}^2)$ and some constant $\lambda_\ell > 0$. Similarly as above, we get that Λ is stationary and its intensity can be calculated as $\lambda = \lambda_\ell \mathbb{E}\nu_1(\Xi \cap [0,1)^2) = \lambda_\ell \gamma$, where γ is the length intensity of Ξ. Random measures of this kind are frequently utilized in this thesis. In particular, we consider random Hausdorff measures on the edge sets of random tessellations, see Chapter 3.

Chapter 3

Random tessellations and point processes on their edges

In this chapter we define the notion of random tessellations in the Euclidean plane $\mathbb{R}^2$. Roughly speaking, a tessellation is a subdivision of $\mathbb{R}^2$ into convex polygons. Thus, a tessellation can be regarded as a sequence of convex polygons. However, a tessellation can also be identified with the segment system consisting of the boundaries of these polygons. Because of these different viewpoints, random tessellations are flexible models which are used in different fields of science. For instance, (random) tessellations are applied in astrophysics ([41, 95]), biology ([14, 25]), telecommunication ([3, 6, 32, 34]), material sciences ([51, 92, 93]) and even linguistics ([83]). Furthermore, all spatial stochastic models investigated later on in this thesis are based on random tessellations. On the one hand, we use random tessellations in order to model the street system underlying the considered telecommunication network, but we also use so–called Voronoi tessellations in order to represent serving zones of network components. This chapter introduces random tessellations and summarizes some of their basic properties. Furthermore, two classes of point processes on the edges of random tessellations are introduced which serve as a basis for the stochastic models investigated e.g. in Chapter 5.

The present chapter is organized as follows. First deterministic tessellations are introduced in Section 3.1. In addition, some basic principles in order to construct deterministic tessellations based on point and line systems are discussed. These concepts are used afterwards to introduce random tessellations. In particular, random tessellations are defined in Section 3.2 and it is shown that there are various ways to represent random tessellations. For instance, they can be regarded as marked point processes with appropriate mark spaces, but also as random closed sets and random measures. This leads to different characteristics of stationary random tessellations which are briefly analyzed in Section 3.3. Subsequently, in Section 3.4, some particular models of random tessellations like Poisson–Delaunay tessellations (PDT), Poisson line tessellations (PLT) and Poisson–Voronoi tessellations (PVT) are introduced. Finally, point processes on

the edges of random tessellations are considered in Section 3.5 which are used to model the locations of network components later on. In particular, we define Cox processes on the edges and thinnings of the vertices of random tessellations. Further details on (random) tessellations can be found e.g. in [72, 79, 87, 90].

3.1 Deterministic tessellations

We start with the definition of deterministic planar tessellations. A *tessellation* τ in $\mathbb{R}^2$ is a countable family $\{\xi_n\}_{n\geq 1}$ of convex bodies ξ_n fulfilling the conditions

- $\mathring{\xi}_n \neq \emptyset$ for all n, i.e., the convex bodies have non-empty interior,
- $\mathring{\xi}_n \cap \mathring{\xi}_m = \emptyset$ for all $n \neq m$, i.e., two convex bodies can only intersect at their boundaries,
- $\bigcup_{n\geq 1} \xi_n = \mathbb{R}^2$, i.e., the union of the convex bodies covers the whole $\mathbb{R}^2$, and
- $\sum_{n\geq 1} \mathbb{1}_{\{\xi_n \cap C \neq \emptyset\}} < \infty$ for any $C \in \mathcal{C}$, i.e., τ is locally finite.

The sets ξ_n are called the *cells* of the tessellation τ and are polygons in $\mathbb{R}^2$. We use the notation $\mathbb{T}$ for the family of all tessellations in $\mathbb{R}^2$. Note that we can identify a tessellation τ with the segment system $\tau^{(1)} = \cup_{n=1}^{\infty} \partial\xi_n$ constructed from the boundaries of the cells of τ. Thus, a tessellation can be identified with a closed subset of $\mathbb{R}^2$ and hence we can regard $\mathbb{T}$ as a subset of $\mathcal{F}$. This connection can be used in order to define the σ–algebra $\mathcal{T}$ on $\mathbb{T}$ as the trace–σ–algebra of $\mathcal{B}(\mathcal{F})$ in $\mathbb{T}$.

We can associate with each cell ξ_n of τ a "marker point" in the following way. Consider a mapping $\alpha : \mathcal{C}\backslash\{\emptyset\} \to \mathbb{R}^2$ which satisfies

- $\alpha(\xi) \in \xi$ and
- $\alpha(\xi + x) = \alpha(\xi) + x$

for all $\xi \in \mathcal{C}$, $\xi \neq \emptyset$ and $x \in \mathbb{R}^2$. Then the point $\alpha(\xi) \in \mathbb{R}^2$ is called the *nucleus* of ξ and it can be chosen e.g. as the lexicographically smallest point of ξ or its center of gravity. This approach is important later on when we consider random tessellations. Note that the condition $\alpha(\xi) \in \xi$ is not really necessary. Sometimes we relax this assumption and allow that $\alpha(\xi) \notin \xi$. However, if we speak of the nucleus, then it is natural to assume that $\alpha(\xi) \in \xi$.

There are various ways to construct tessellations e.g. based on sets of points and lines. Particular models are Voronoi tessellations and Delaunay tessellations as well as line tessellations which are introduced in the following.

Voronoi tessellation

Let $\mathbf{x} = \{x_1, x_2, \ldots\} \subset \mathbb{R}^2$ be a locally finite set of points such that $conv(\mathbf{x}) = \mathbb{R}^2$, where $conv(\mathbf{x})$ denotes the convex hull of $\mathbf{x}$. Then the *Voronoi tessellation* τ induced by $\mathbf{x}$ is defined by the nearest–neighbor principle, i.e., the cells of τ are defined by the sets

$$\xi_n = \{x \in \mathbb{R}^2 : |x - x_n| \leq |x - x_m| \text{ for all } m \neq n\}\,.$$

Note that ξ_n can be written as the intersection of the halfplanes $H(x_n, x_m) = \{x \in \mathbb{R}^2 : |x - x_n| \leq |x - x_m|\}$ for all $m \neq n$, i.e.,

$$\xi_n = \bigcap_{m \neq n} H(x_n, x_m)\,.$$

The halfplanes $H(x_n, x_m)$ are also called bisectors. Since $\mathbf{x}$ is locally finite it is immediately clear that the cells of τ have non–empty interior and are locally finite. Furthermore, they cover the whole Euclidean plane and two different cells can only intersect at their boundaries. Using that $conv(\mathbf{x}) = \mathbb{R}^2$, it can be shown that the cells are convex polygons which are bounded. Thus, $\tau = \{\xi_n\}$ constructed in this way is indeed a tessellation. A Voronoi tessellation together with the generating point set is displayed in Figure 3.1(a).

Delaunay tessellation

Let $\mathbf{x} = \{x_1, x_2, \ldots\} \subset \mathbb{R}^2$ be again a locally finite set of points with $conv(\mathbf{x}) = \mathbb{R}^2$. Furthermore, we assume that four cocircular points do not exist, i.e., there are no pairwise different points $x_i, x_j, x_k, x_l \in \mathbf{x}$ which are located on a circle. Then the *Delaunay tessellation* τ' induced by $\mathbf{x}$ can be defined uniquely as the dual tessellation of the Voronoi tessellation τ induced by $\mathbf{x}$. The cells of τ' are all triangles which are generated in the following way. Three points $x_i, x_j, x_k \in \mathbf{x}$ form a triangle of τ' if the Voronoi cells ξ_i, ξ_j and ξ_k induced by $\mathbf{x}$ have a common intersection point. This construction rule is equivalent to the empty circle criterion: three points of $\mathbf{x}$ are the vertices of a triangle of τ' if and only if the circumcircle of these three points does not contain other points of $\mathbf{x}$. Then it can be shown that the resulting sequence of triangles forms a tessellation in $\mathbb{R}^2$. In Figure 3.1(b) a Delaunay tessellation is shown together with its generating points and the dual Voronoi tessellation.

Tessellations induced by line systems

Let $\boldsymbol{\ell} = \{\ell_1, \ell_2, \ldots\}$ be a set of lines in $\mathbb{R}^2$ and let $p_i \in \mathbb{R}^2$ denote the orthogonal projection of o onto ℓ_i, where we assume that $conv(\{p_1, p_2, \ldots\}) = \mathbb{R}^2$. Furthermore, we assume that $\#\{i : \ell_i \cap B \neq \emptyset\} < \infty$ for all $B \in \mathcal{C}$. Then we can construct a tessellation with respect to $\boldsymbol{\ell}$ in a natural way. Recall that we can identify a

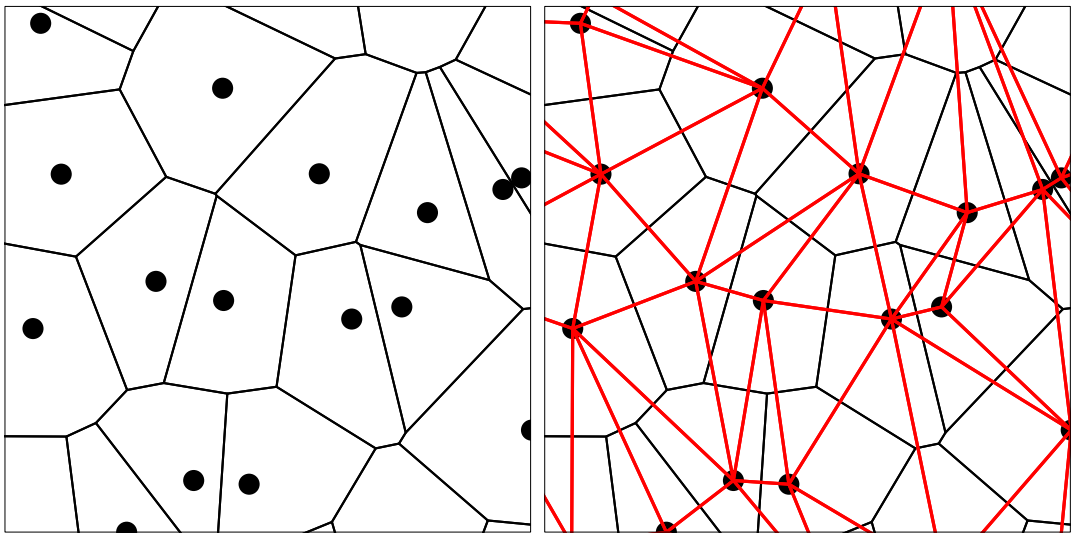

(a) PVT with nuclei (b) PDT (red) together with PVT (black)

Figure 3.1: Realizations of different tessellation models

tessellation τ with the segment system $\tau^{(1)} = \cup_{n=1}^{\infty} \partial\xi_n$ formed by the union of the cell boundaries. Thus, we define the line tessellation τ induced by $\boldsymbol{\ell}$ as the tessellation which corresponds to the segment system $\tau^{(1)} = \cup_{i=1}^{\infty} \ell_i$ formed by the union of the lines $\ell_1, \ell_2, \ldots$. If $\boldsymbol{\ell}$ fulfills the assumptions mentioned above, then it is ensured that the resulting cells form a tessellation in $\mathbb{R}^2$. A line tessellation is displayed e.g. in Figure 3.3(c).

3.2 Random tessellations

Now we are able to define random tessellations. A *random tessellation* $T = \{\Xi_n\}$ in $\mathbb{R}^2$ is defined as a sequence of random convex bodies Ξ_n such that $\mathbb{P}(\{\Xi_n\} \in \mathbb{T}) = 1$. It is called stationary and isotropic if $t_x T = \{t_x \Xi_n\} \stackrel{\mathrm{d}}{=} T$ for all $x \in \mathbb{R}^2$ and $\vartheta_R T = \{\vartheta_R \Xi_n\} \stackrel{\mathrm{d}}{=} T$ for all rotations ϑ_R around the origin, respectively. Note that there are various ways to look at random tessellations. In particular, they can be regarded as marked point processes, random closed sets and random measures. Each different point of view leads to different characteristics which can be associated with random tessellations.

3.2.1 Random tessellations as marked point processes

In many applications it is convenient to represent a random tessellation $T = \{\Xi_n\}$ as a marked point process. Note that we can associate various point processes with T, e.g. the point processes of vertices, edge midpoints and cell nuclei. If we

mark these point processes with suitable marks, then we can represent T by the resulting marked point processes.

Cell nuclei marked with cells

Let the mapping $\alpha : \mathcal{C}\backslash\{\emptyset\} \to \mathbb{R}^2$ define the nuclei of the cells of the random tessellation T and let $\mathcal{P}^o$ denote the family of all convex and compact polygons ξ with their nucleus $\alpha(\xi)$ at the origin. Then $\mathcal{P}^o \subset \mathcal{F}$ is an element of $\mathcal{B}(\mathcal{F})$ and we define the σ-algebra $\mathcal{B}(\mathcal{P}^o) = \mathcal{B}(\mathcal{F}) \cap \mathcal{P}^o$ on $\mathcal{P}^o$. With the definitions of α and $\mathcal{P}^o$ above we can then identify the random tessellation $T = \{\Xi_n\}$ with the marked point process $\{(\alpha(\Xi_n), \Xi_n^o)\}$ with mark space $\mathcal{P}^o$, where $\Xi_n^o = \Xi_n - \alpha(\Xi_n)$ is the n-th cell shifted to the origin. If T is stationary, then the marked point process $\{(\alpha(\Xi_n), \Xi_n^o)\}$ is stationary and we denote its intensity by $\lambda^{(2)}$. In the following, we always assume that $0 < \lambda^{(2)} < \infty$.

Now suppose that $\{(\alpha(\Xi_n), \Xi_n^o)\}$ is stationary. Then the typical mark $\Xi^* : \Omega \to \mathcal{P}^o$ of $\{(\alpha(\Xi_n), \Xi_n^o)\}$ is a random polygon which is distributed according to the Palm mark distribution of $\{(\alpha(\Xi_n), \Xi_n^o)\}$ as defined in (2.14) for stationary marked point processes with arbitrary mark space. The random polygon Ξ^* is called the *typical cell* of the tessellation T.

Vertices marked with edge stars

Another possibility to construct a marked point process which can be identified with T is the following. First consider the point process of vertices $V = \{V_n\}$ of T. For each vertex V_n we define the *edge star* E_n as the union of all edges of T emanating from V_n. Thus, $E_n^o = E_n - V_n$ is an element of the family of finite segment systems containing the origin which is denoted by $\mathcal{L}^o$. Since $\mathcal{L}^o \in \mathcal{B}(\mathcal{F})$ we define the σ–algebra $\mathcal{B}(\mathcal{L}^o) = \mathcal{B}(\mathcal{F}) \cap \mathcal{L}^o$ on $\mathcal{L}^o$. Hence, we can identify the random tessellation T with the marked point process $\{(V_n, E_n^o)\}$ with mark space $\mathcal{L}^o$. If T is stationary, then $\{(V_n, E_n^o)\}$ is stationary and we denote its intensity by $\lambda^{(0)}$, where we always assume that $0 < \lambda^{(0)} < \infty$.

For stationary $\{(V_n, E_n^o)\}$, the *typical edge star* $E^* : \Omega \to \mathcal{L}^o$ of T is defined as a random segment system which is distributed according to the Palm mark distribution of $\{(V_n, E_n^o)\}$. In the following, we also use the notation $T^{(0)} = \{V_n\}$ for the point process V of the vertices of a random tessellation T in order to emphasize the dependence on T.

Edge midpoints marked with segments

Let $\{Y_n\}$ denote the point process of edge midpoints of the random tessellation T, where an edge is defined as a segment of $T^{(1)}$ which does not contain a vertex in its relative interior. Then each point Y_n can be marked with the corresponding centered edge $S_n^o = S_n - Y_n$ which yields another marked point process. Note that $S_n^o \in \mathcal{L}^o$, thus we define the marked point process $\{(Y_n, S_n^o)\}$ with mark space $\mathcal{L}^o$.

If T is stationary, then it is easy to see that $\{(Y_n, S_n^o)\}$ is stationary and we use the notation $\lambda^{(1)}$ for its intensity. Again, the intensity $\lambda^{(1)}$ is always assumed to be positive and finite.

The *typical edge* $S^* : \Omega \to \mathcal{L}^o$ is defined for stationary T as the typical mark of the stationary marked point process $\{(Y_n, S_n^o)\}$.

3.2.2 Random tessellations as random closed sets and random measures

In the preceding section random tessellations have been represented as marked point processes with different mark spaces. Alternatively, a random tessellation T can be regarded as a random closed set. Recall that a deterministic tessellation can be identified with its edge set. Thus, in the random setting, we can identify a random tessellation $T = \{\Xi_n\}$ with the random closed set of its edges defined by $T^{(1)} = \cup_{n=1}^{\infty} \partial \Xi_n$. If T is stationary, then the random closed set $T^{(1)}$ is stationary and we say that T is ergodic and mixing if $T^{(1)}$ is ergodic and mixing, respectively. Note that $T^{(1)}$ is almost surely a locally finite system of line segments. Thus, we can regard the 1–dimensional Hausdorff measure ν_1 on $T^{(1)}$. If T is a stationary random tessellation, then we get that $\mathbb{E}\nu_1(B \cap T^{(1)}) = \gamma \nu_2(B)$ for any $B \in \mathcal{B}(\mathbb{R}^2)$ and some constant γ which we call the length intensity of $T^{(1)}$, compare also Section 2.4.2. Like for the intensities $\lambda^{(0)}, \lambda^{(1)}$ and $\lambda^{(2)}$ defined above, we always assume that $0 < \gamma < \infty$.

This point of view also leads to a random measure Λ associated with the random tessellation T. In particular, we regard the random Hausdorff measure Λ on $T^{(1)}$, i.e., Λ is defined by

$$\Lambda(B) = \nu_1(B \cap T^{(1)}) \qquad \text{for} \quad B \in \mathcal{B}(\mathbb{R}^2)\,.$$

Hence, another alternative representation of a random tessellation T is the random Hausdorff measure Λ on its edges. If T is stationary, then the random measure Λ is stationary and its intensity is given by γ. Moreover, we can regard the Palm version Λ^* of Λ, i.e., a random measure Λ^* distributed according to the Palm distribution P_Λ^* of Λ. For brevity, we also write $P_{T^{(1)}}^*$ for the Palm distribution P_Λ^* to emphasize the dependence on $T^{(1)}$. It is not difficult to see that Λ^* can be regarded as the Hausdorff measure ν_1 on the edges of a random tessellation $\widetilde{T}$ with $o \in \widetilde{T}^{(1)}$ almost surely, see also Lemma 3.4. Note that $\widetilde{T}$ can be regarded as the conditional variant of the random tessellation T under the condition that $o \in T^{(1)}$. Thus, under $P_{T^{(1)}}^*$ there is an edge $\widetilde{S}$ of $\widetilde{T}$ through o with probability 1. However, notice that $\widetilde{S}$ and the typical edge S^* do not have the same distribution. Let $h : \mathcal{L}^o \to [0, \infty)$ be a translation-invariant measurable

function and let $S(x)$ denote the segment of $T^{(1)}$ through $x \in T^{(1)}$, then

$$\begin{aligned}\mathbb{E}h(\widetilde{S}) &= \frac{1}{\gamma}\,\mathbb{E}\int_{T^{(1)}\cap[0,1)^2} h(S(x)-x)\,\nu_1(dx)\\ &= \frac{1}{\gamma}\,\mathbb{E}\sum_{(Y_i,S_i^o)\in T} h(S_i^o)\int_{S_i}\mathbb{1}_{[0,1)^2}(x)\,\nu_1(dx)\\ &= \frac{\lambda^{(1)}}{\gamma}\,\mathbb{E}h(S^*)\int_{\mathbb{R}^2}\int_{S^*}\mathbb{1}_{[0,1)^2-y}(x)\,\nu_1(dx)\,\nu_2(dy) = \frac{1}{\mathbb{E}\nu_1(S^*)}\,\mathbb{E}\,\nu_1(S^*)h(S^*)\,,\end{aligned}$$

where the last line is a consequence of the refined Campbell theorem (see Theorem 2.7) and the mean value formulae given in Theorem 3.1 below. Thus, the distribution of $\widetilde{S}$ can be regarded as the length–weighted distribution of the typical edge S^*. Similar weighted distributions appear frequently in this thesis.

3.3 Mean value formulae

In the preceding section we have demonstrated that random tessellations can be regarded as several marked point processes, random closed sets and random measures. Each of these representations leads to new characteristics which can be associated with a stationary random tessellation. In particular, we define

- the intensities of vertices $\lambda^{(0)}$, edge midpoints $\lambda^{(1)}$ and cell nuclei $\lambda^{(2)}$,
- the length intensity $\gamma = \mathbb{E}\nu_1(T^{(1)} \cap [0,1)^2)$,
- the expected area $\mathbb{E}\nu_2(\Xi^*)$, perimeter $\mathbb{E}\nu_1(\partial\Xi^*)$ and number of vertices $\mathbb{E}\nu_0(\Xi^*)$ of the typical cell Ξ^*,
- the expected length of the typical edge $\mathbb{E}\nu_1(S^*)$,
- the expected length $\mathbb{E}\nu_1(E^*)$ and number of edges $\mathbb{E}\nu_0(E^*)$ of the typical edge star E^*.

However, all these characteristics can be expressed e.g. by the three parameters $\lambda^{(0)}, \lambda^{(2)}$ and γ. Note that $\nu_0(\Xi^*)$ is only defined as the number of vertices of the polygon Ξ^* if T is face-to-face ([87]). If T is not face-to-face, then we define $\nu_0(\Xi^*)$ as the number of cells touching the typical cell Ξ^*.

Theorem 3.1 *It holds that*

$$\begin{aligned}
\lambda^{(1)} &= \lambda^{(0)} + \lambda^{(2)}, \\
\gamma &= \lambda^{(1)}\mathbb{E}\nu_1(S^*) = \frac{\lambda^{(2)}}{2}\mathbb{E}\nu_1(\partial\Xi^*)\,, \\
\mathbb{E}\nu_0(E^*) &= 2 + 2\frac{\lambda^{(2)}}{\lambda^{(0)}}\,, \\
\mathbb{E}\nu_1(E^*) &= 2\frac{\lambda^{(1)}}{\lambda^{(0)}}\mathbb{E}\nu_1(S^*)\,, \\
\mathbb{E}\nu_0(\Xi^*) &= 2 + 2\frac{\lambda^{(0)}}{\lambda^{(2)}}\,, \\
\mathbb{E}\nu_2(\Xi^*) &= \frac{1}{\lambda^{(2)}}\,, \\
\mathbb{E}\nu_1(\partial\Xi^*) &= 2\frac{\lambda^{(1)}}{\lambda^{(2)}}\mathbb{E}\nu_1(S^*)\,.
\end{aligned}$$

Furthermore, $3 \leq \mathbb{E}\nu_0(\Xi^*), \mathbb{E}\nu_0(E^*) \leq 6$.

For a proof of Theorem 3.1, see e.g. [20, 64].

Thus, local characteristics of random tessellations like the typical cell and edge star provide information about spatial averages of the whole tessellation. However, note that the typical cell does not determine the distribution of a random tessellation. It is possible to define various tessellation models which are not identically distributed, but have the same typical cell, see e.g. [67, 68].

3.4 Random tessellation models

In this section we introduce some random tessellation models which are frequently considered in this thesis. They are all based on Poisson processes.

3.4.1 Poisson–Voronoi tessellation

In Section 3.1 the notion of a deterministic Voronoi tessellation has been defined for locally finite point sets. Since the realizations of a stationary point process $X = \{X_n\}$ with $\mathbb{P}(X(\mathbb{R}^2) = 0) = 0$ are almost surely locally finite point sets with $conv(X) = \mathbb{R}^2$, we can define random Voronoi tessellations $\{\Xi_n\}$ with respect to such point processes. Then, the cells Ξ_n are given by the random closed sets

$$\Xi_n = \{x \in \mathbb{R}^2 : |x - X_n| \leq |x - X_m| \text{ for all } m \neq n\}.$$

We call $T = \{\Xi_n\}$ the Voronoi tessellation induced by X. Note that we can use the atom X_n of X as nucleus of the cell Ξ_n.

If the underlying point process X is a Poisson process, then we call the induced Voronoi tessellation a *Poisson–Voronoi tessellation* (PVT). Realizations of a PVT

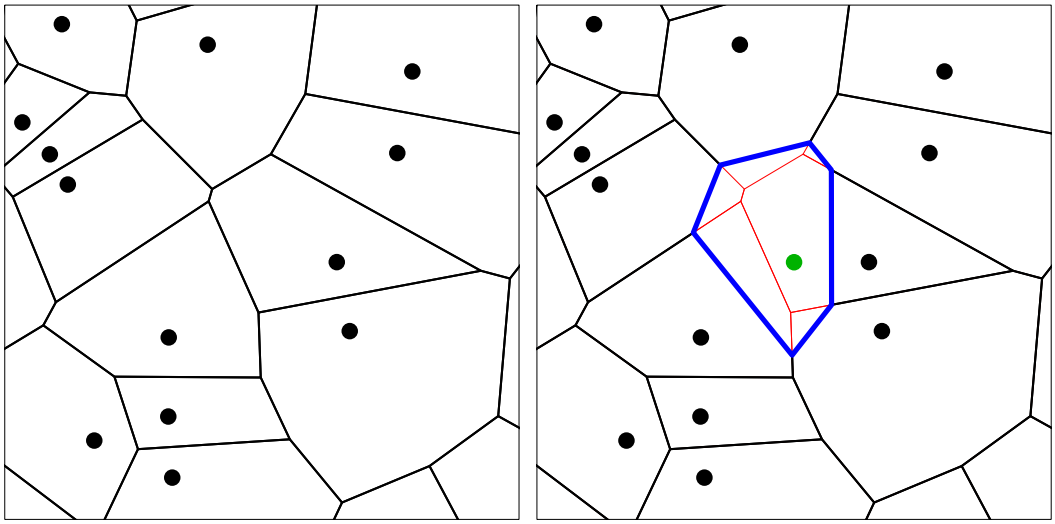

(a) Realization of a PVT (b) Typical cell of PVT

Figure 3.2: Realization of a PVT and its typical cell

are shown in Figures 3.2(a) and 3.3(a). If the Poisson process X is stationary with intensity λ, then the induced PVT is stationary and isotropic. Furthermore, it can be shown that

$$\lambda^{(0)} = 2\lambda, \qquad \lambda^{(1)} = 3\lambda, \qquad \lambda^{(2)} = \lambda, \qquad \gamma = 2\sqrt{\lambda}\,,$$

see e.g. [87], Chapter 10. Note that for a random Voronoi tessellation T induced by a stationary point process X, the distribution of the typical cell coincides with the distribution of the Voronoi cell at o with respect to the Palm version X^* of X. Since the point process of nuclei of a PVT is a Poisson process, we get that the Palm distribution of a stationary PVT with respect to its cell nuclei is obtained by generating the Voronoi tessellation induced by $X^* = X \cup \{o\}$, see Theorem 2.6. The cell centered at o can then be regarded as the typical cell of the PVT, see Figure 3.2(b).

3.4.2 Poisson–Delaunay tessellation

In the preceding section we introduced Voronoi tessellations induced by random point processes. In the same way as for deterministic Voronoi tessellations, we can construct the dual Delaunay tessellation induced by random point processes and in particular by Poisson processes. Let $X = \{X_n\}$ be a stationary Poisson process with intensity $\lambda > 0$. Then, almost surely, X is locally finite, $conv(X) = \mathbb{R}^2$ and four points of X are not cocircular. Thus, we can construct almost surely the Delaunay tessellation $T = \{\Xi_n\}$ of X which is the dual tessellation of the PVT induced by X, see Section 3.1. The resulting random tessellation T is then called *Poisson–Delaunay tessellation* (PDT). In Figure 3.3(b) a realization of a PDT is

displayed. Since X is stationary, we get that T is also stationary. Furthermore, it can be shown that

$$\lambda^{(0)} = \lambda, \qquad \lambda^{(1)} = 3\lambda, \qquad \lambda^{(2)} = 2\lambda, \qquad \gamma = \frac{32}{3\pi}\sqrt{\lambda}\,,$$

see e.g. [87], Chapter 10. If $T = \{\Xi_n\}$ is a PDT induced by X, then the point process of vertices is given by X. Thus, using Theorem 2.6, the Palm version T^* of T with respect to the point process of vertices can be constructed as the Delaunay tessellation with respect to $X^* = X \cup \{o\}$. Note that the union of edges of T^* emanating from o can then be regarded as the typical edge star E^* of T.

3.4.3 Poisson line tessellation

Now we construct a tessellation based on Poisson line processes. A *Poisson line process* can be defined in the following way. Consider a stationary Poisson process $\{R_n\}$ on $\mathbb{R}$ of intensity γ, where each point R_n is independently marked with a random angle $\Phi_n \sim U[0, \pi)$. Then we can identify each pair (R_n, Φ_n) with a line $\ell_{(R_n,\Phi_n)} = \{(x, y) \in \mathbb{R}^2 : x \cos\Phi_n + y \sin\Phi_n = R_n\}$ defined by the Hessian normal form. The stationary random closed set $\bigcup_{n\geq 1} \ell_{(R_n,\Phi_n)}$ is called Poisson line process. It can be regarded as the edge set of a random tessellation T which we call *Poisson line tessellation* (PLT). Thus, $T^{(1)} = \bigcup_{n\geq 1} \ell_{(R_n,\Phi_n)}$ and T is stationary with length intensity γ. Furthermore, it holds that

$$\lambda^{(0)} = \frac{1}{\pi}\gamma^2, \qquad \lambda^{(1)} = \frac{2}{\pi}\gamma^2, \qquad \lambda^{(2)} = \frac{1}{\pi}\gamma^2\,,$$

see [87], Chapter 10. A realization of T is displayed in Figure 3.3(c). Using Slivnyak's theorem (see Theorem 2.6), it can be shown that the Palm distribution of T with respect to the Hausdorff measure on $T^{(1)}$ is obtained by the tessellation induced by the edge set $T^{(1)} \cup \ell_{(0,\Phi)}$, where $\Phi \sim U[0, \pi)$ is independent of T.

3.4.4 Iterated tessellations

From the three basic tessellation models introduced above more complex models can be generated like iterated tessellations ([55]). Two major principles can be used in order to construct these flexible tessellation models. On the one hand, we can superpose (basic) random tessellations and, on the other hand, we can nest them, see Figure 3.4. In particular, nested random tessellations are used in order to model telecommunication networks since the construction principle is similar to the evolution of street (and hence cable) systems. More precisely, the edges of a so–called initial tessellation are used to model main roads, whereas each cell of the initial tessellation is subdivided by a component tessellation whose edges represent side streets between main roads, see e.g. [32, 53].

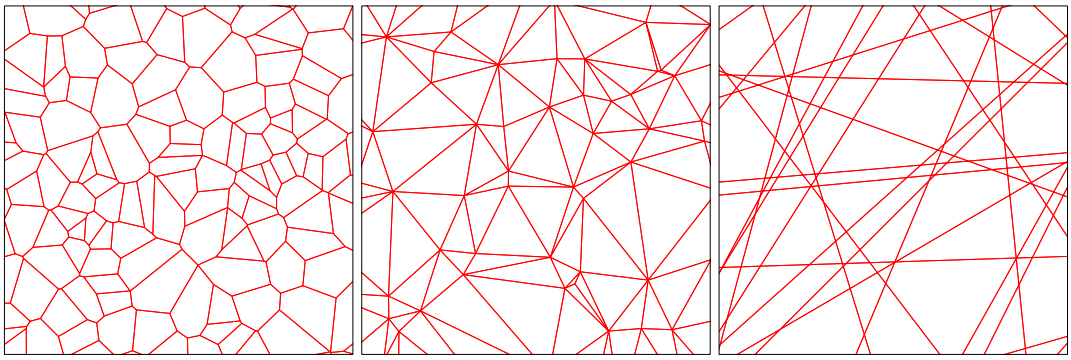

(a) PVT (b) PDT (c) PLT

Figure 3.3: Realizations of different tessellation models

Recall that a random tessellation T can be identified with its edge set $T^{(1)} = \bigcup_{n=1}^{\infty} \partial\Xi_n$. We now regard some initial tessellation T_0 and in addition a sequence $T_1, T_2, \ldots$ of so–called component tessellations, which are independent of T_0. For each $n \geq 1$, we consider the n-th cell Ξ_{0n} of T_0 and divide it by the cells of the random tessellation T_n. Thus, we consider Ξ_{0n} and $\Xi_{0n} \cap T_n^{(1)}$ which is the part of the segment system $T_n^{(1)}$ inside Ξ_{0n}. Then the edge set of the *iterated tessellation* T, and hence the tessellation itself, is defined by $T^{(1)} = \bigcup_{n=1}^{\infty}(\partial\Xi_{0n} \cup (\Xi_{0n} \cap T_n^{(1)}))$. The construction of an iterated tessellation which has been explained so far is very general, but we focus on two distinct cases. On the one hand, we consider the case that $T_1, T_2, \ldots$ is a sequence of independent copies of a random tessellation T_1 which are independent of T_0. In this case, we call T a T_0/T_1 *nesting*, see Figure 3.4(a). On the other hand, we regard the case that $T_1 = T_2 = \ldots$, i.e., $T_1, T_2, \ldots$ are all identical with probability 1. Then we call T a T_0/T_1 *superposition*, see Figure 3.4(b).

Now let T be either a nesting or a superposition. If T_0 as well as $T_1, T_2, \ldots$ are stationary with length intensities γ_0 and γ_1, respectively, then T is stationary as well and its length intensity γ is given by $\gamma = \gamma_0 + \gamma_1$. Furthermore, if T_0 and T_1 are stationary, it is possible to express further intensities of T like the intensity of nuclei, vertices and edge midpoints by the intensities of T_0 and T_1, see e.g. [53, 55].

3.5 Point processes on the edges of random tessellations

Later on, we study spatial stochastic models which are based on a random tessellation T and point processes X on the edges of T, i.e., we assume that $\mathbb{P}(X_n \in T^{(1)} \text{ for all } n \in \mathbb{N}) = 1$. In this section we introduce two specific types of point processes concentrated on the edges of random tessellations. More pre-

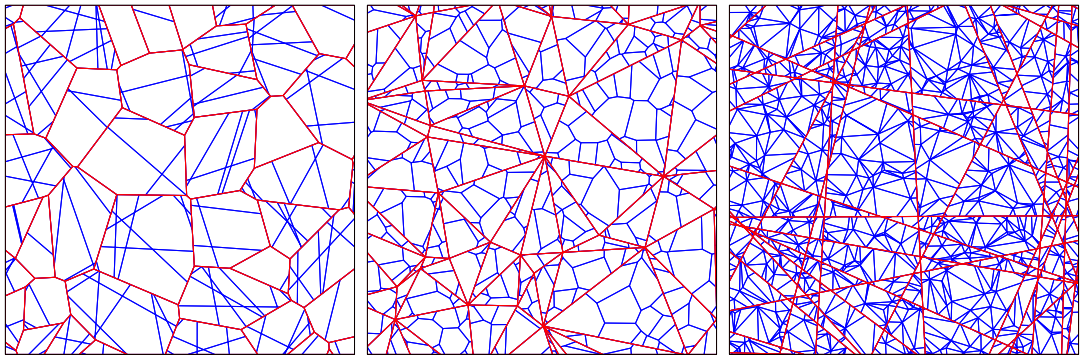

(a) Nested tessellations

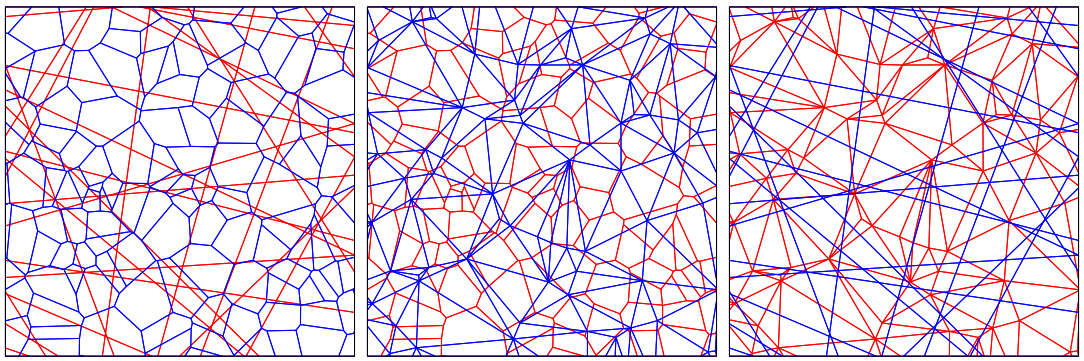

(b) Superposed tessellations

Figure 3.4: Iterated tessellations

cisely, we define Cox processes on the edge set $T^{(1)}$ and independent thinnings of the vertex set $T^{(0)}$ of T.

First, in Section 3.5.1, we start with the definition of Cox processes in the Euclidean plane $\mathbb{R}^2$ and discuss some basic properties. Afterwards, Cox processes on the edges of random tessellations are introduced in Section 3.5.2, whereas in Section 3.5.3 thinnings of the vertex set $T^{(0)}$ of T are considered. Finally, in Section 3.5.4, Voronoi tessellations induced by point processes on the edges of random tessellations are briefly discussed which are the fundamental components of the hierarchical network models considered in Chapters 5 to 8.

3.5.1 Cox processes

Definition and basic properties

Cox processes are generalizations of Poisson processes. The difference is that we now use a *random intensity measure* Λ instead of the deterministic intensity measure μ used for Poisson processes. Then, conditioned on $\Lambda = \eta$, the *Cox process* X is a Poisson process with intensity measure η, i.e., the finite-dimensional

distributions of X for pairwise disjoint sets $B_1, \dots, B_n \in \mathcal{B}_0(\mathbb{R}^2)$ are given by

$$\mathbb{P}(X(B_1) = k_1, \dots, X(B_n) = k_n) = \mathbb{E}\left(\prod_{i=1}^{n} \frac{\Lambda(B_i)^{k_i} e^{-\Lambda(B_i)}}{k_i!}\right) \tag{3.1}$$

for $k_1, \dots, k_n \in \mathbb{N}_0$. Thus, the distribution of a Cox process can be regarded as a mixture of the distributions of (in general non-stationary) Poisson processes. This is the reason why Cox processes are sometimes called doubly–stochastic Poisson processes. The definition of a Cox process directly leads to a simulation method based on a two–step procedure. First, a realization η is sampled from the random intensity measure Λ. Then, in the second step, a Poisson process with intensity measure η is simulated. We now summarize some basic properties of Cox processes.

Lemma 3.2 *Let X be a Cox process with random intensity measure Λ. Then the intensity measure μ of X is given by*

$$\mu(B) = \mathbb{E}\Lambda(B), \quad B \in \mathcal{B}(\mathbb{R}^2)\,. \tag{3.2}$$

Furthermore, X is stationary, isotropic and ergodic if and only if Λ is stationary, isotropic and ergodic, respectively. If X is stationary, then its intensity is the intensity λ of its stationary intensity measure Λ.

Proof Equation (3.2) easily follows from $\mathbb{E}(X(B) \mid \Lambda) = \Lambda(B)$ for $B \in \mathcal{B}_0(\mathbb{R}^2)$. From (3.1) we immediately get that X is stationary and isotropic if and only if Λ is stationary and isotropic, respectively, and for a proof that X is ergodic if and only if Λ is ergodic, we refer to [21], p. 212. □

Of course, Poisson processes are Cox processes, but there are many other point process models which are Cox processes. Examples are Neyman-Scott processes ([77]) and modulated Poisson processes ([26]). Recall that the Palm version X^* of a stationary Poisson process X is obtained due to Slivnyak's theorem by adding the origin o to the original Poisson process X, see Theorem 2.6. Similarly, the Palm distribution P_X^* of a stationary Cox process X with random driving measure Λ can be characterized as follows, see e.g. [90], p. 156, and Theorem 5.3.3 in [48].

Theorem 3.3 (Slivnyak's theorem for Cox processes) *Let X be a stationary Cox process with random intensity measure Λ. Then*

$$P_X^*(A) = \mathbb{P}(\widetilde{X} \cup \{o\} \in A), \quad A \in \mathcal{N}\,, \tag{3.3}$$

where $\widetilde{X}$ is a Cox process with random intensity measure Λ^* distributed according to the Palm distribution P_Λ^* of Λ.

So if we want to simulate the Palm version X^* of X, we can again use a two–step procedure. But this time we first have to generate a realization η^* of Λ^* and then, in the second step, we have to place a point at the origin o and simulate a Poisson process $\widetilde{X}$ with intensity measure η^*. In this way, we get a realization of the Palm version $X^* = \widetilde{X} \cup \{o\}$ of the Cox process X.

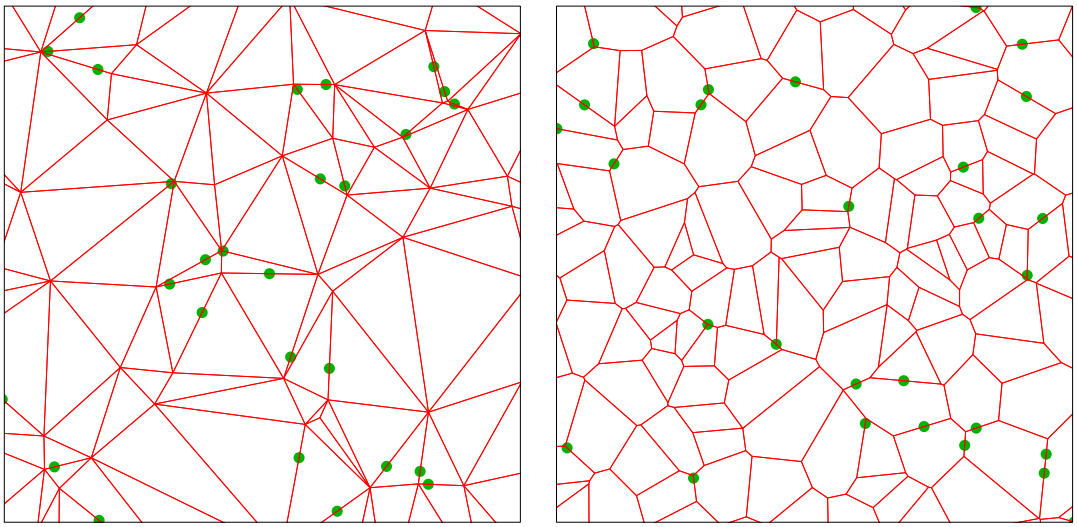

(a) PDT (b) PVT

Figure 3.5: Realizations of Cox processes on PDT and PVT.

3.5.2 Cox processes on the edges of random tessellations

In this thesis, we frequently consider point processes X which are located along segment systems in the Euclidean plane. These segment systems are represented by the edge sets of random tessellations, i.e., the points of X are located with probability 1 on the random closed set $T^{(1)}$ of some random tessellation T. For given T, define the random measure $\Lambda : \mathcal{B}(\mathbb{R}^2) \to [0, \infty]$ by

$$\Lambda(B) = \lambda_\ell \nu_1(B \cap T^{(1)}) \tag{3.4}$$

for each $B \in \mathcal{B}(\mathbb{R}^2)$ and some $\lambda_\ell > 0$. Then we call a Cox process X with random intensity measure Λ a *Cox process on (the edges $T^{(1)}$ of) T* with *linear intensity* λ_ℓ. If T is stationary and its length intensity is given by γ, then Λ is stationary and its intensity can be calculated as $\lambda = \lambda_\ell \mathbb{E}\nu_1([0,1)^2 \cap T^{(1)}) = \lambda_\ell \gamma$. Thus, X is stationary with intensity λ. Furthermore, if T is isotropic resp. ergodic, then it is not difficult to see that Λ is isotropic resp. ergodic as well and a direct application of Lemma 3.2 yields that X is isotropic resp. ergodic.

A realization of X can be constructed in the following way. For a given realization of $T^{(1)}$, linear Poisson processes with (linear) intensity $\lambda_\ell > 0$ are placed on each segment of $T^{(1)}$. In Figure 3.5 realizations of Cox processes on T are shown for PDT and PVT as underlying tessellation T. Recall that in Theorem 3.3 the Palm distribution of stationary Cox processes is characterized and it is shown that it is uniquely determined by the Palm distribution of the random intensity measure. For Cox processes on random tessellations this can be specified in the following way.

Lemma 3.4 *Let T be a stationary tessellation and let Λ be the stationary random measure given by $\lambda_\ell \nu_1(B \cap T^{(1)})$ for $B \in \mathcal{B}(\mathbb{R}^2)$ for some $\lambda_\ell > 0$. Then*

$$\Lambda^*(B) = \lambda_\ell \nu_1(B \cap \widetilde{T}^{(1)}), \qquad B \in \mathcal{B}(\mathbb{R}^2)\,,$$

where the tessellation $\widetilde{T}$ is distributed according to the Palm distribution $P^*_{T^{(1)}}$ with respect to the 1-dimensional Hausdorff measure on $T^{(1)}$.

Proof Let τ denote a deterministic tessellation, then we can identify the measure given by $\eta(\,\cdot\,) = \lambda_\ell \nu_1(\,\cdot \cap \tau^{(1)})$ with τ and also write $\eta(\tau)$. It holds that $\eta(t_x\tau) = t_x\eta(\tau)$ for all $x \in \mathbb{R}^2$. We can use the definition of the Palm distribution P^*_Λ of stationary random measures given in (2.27) in order to get for each $A \in \mathcal{M}$ that

$$\begin{aligned} P^*_\Lambda(A) &= \frac{1}{\lambda} \int_{\mathsf{M}} \int_{[0,1]^2} \mathbb{1}_A(t_x\eta)\, \eta(dx)\, P_\Lambda(d\eta) \\ &= \frac{1}{\gamma} \int_{\mathbb{T}} \int_{[0,1]^2 \cap \tau^{(1)}} \mathbb{1}_A(t_x\eta(\tau))\, \nu_1(dx)\, P_T(d\tau) \\ &= P^*_{T^{(1)}}(\{\tau \in \mathbb{T} : \eta(\tau) \in A\})\,, \end{aligned}$$

where the last equality is a direct consequence of the definition of the Palm distribution $P^*_{T^{(1)}}$ bearing in mind that $\gamma = \mathbb{E}\nu_1(T^{(1)} \cap [0,1)^2)$. Thus we get that $\eta(\widetilde{T})(\,\cdot\,) = \lambda_\ell \nu_1(\,\cdot \cap \widetilde{T}^{(1)})$ and Λ^* have the same distribution. □

Note that a scaling invariance can be observed for Cox processes on the edges of random tessellations. Let T be a stationary random tessellation with length intensity 1 and define the scaled tessellation T_γ as the random tessellation with the scaled edge set $T^{(1)}_\gamma = \frac{1}{\gamma} T^{(1)}$. Then the length intensity of T_γ is given by γ since $\mathbb{E}\nu_1(T^{(1)}_\gamma \cap [0,1)^2) = \mathbb{E}\nu_1(T^{(1)} \cap [0,\gamma)^2)/\gamma = \gamma$ due to the homogeneity of the Hausdorff measure ν_1. Now let X be a Cox process on T_γ with linear intensity λ_ℓ and let X' be a Cox process on $T_{\gamma'}$ with linear intensity λ'_ℓ. Furthermore, assume that the intensity quotients $\kappa = \gamma/\lambda_\ell$ and $\kappa' = \gamma'/\lambda'_\ell$ are equal, i.e., $\kappa = \kappa'$. Then, for any $C \in \mathcal{C}$, it holds that

$$\begin{aligned} \mathbb{P}(X(C) = 0) &= \mathbb{E} \exp\big(\lambda_\ell \nu_1(C \cap T^{(1)}_\gamma)\big) \\ &= \mathbb{E} \exp\Big(\frac{\lambda_\ell \gamma'}{\gamma} \nu_1\big(\frac{\gamma}{\gamma'} C \cap T^{(1)}_{\gamma'}\big)\Big) \\ &= \mathbb{P}\Big(X'\big(\frac{\gamma}{\gamma'} C\big) = 0\Big) = \mathbb{P}\Big(\big(\frac{\gamma'}{\gamma} X'\big)(C) = 0\Big)\,, \end{aligned}$$

where the scaled point process $\frac{\gamma'}{\gamma} X'$ is defined by $\frac{\gamma'}{\gamma} X' = \{\frac{\gamma'}{\gamma} X'_n\}$ for $X' = \{X'_n\}$. Since the distribution of a point process X is uniquely determined by its void probabilities $\mathbb{P}(X(C) = 0), C \in \mathcal{C}$, we get that $X \stackrel{\mathrm{d}}{=} \frac{\gamma'}{\gamma} X'$. Thus, for a given tessellation model T, the intensity quotient κ defines the Cox process X on T_γ

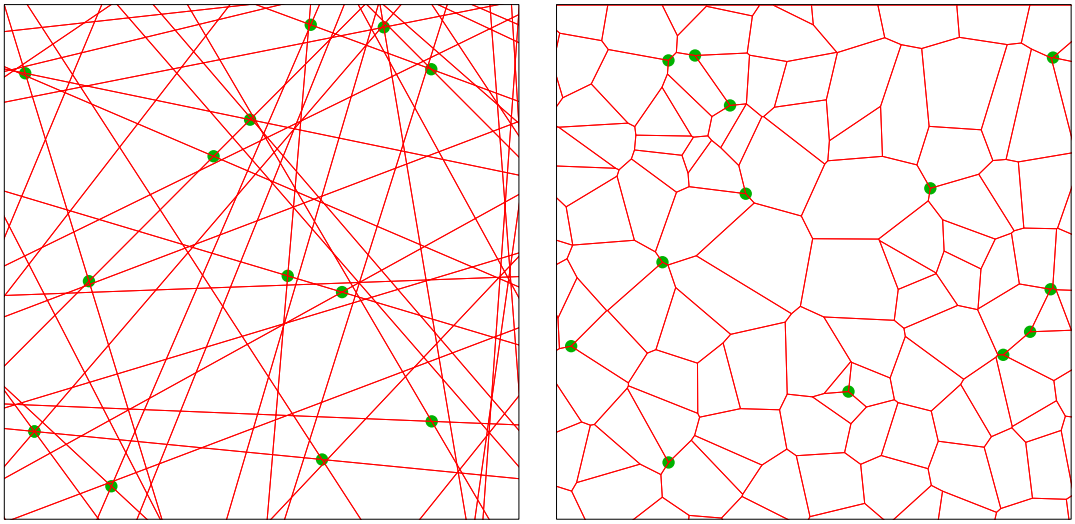

(a) PLT (b) PVT

Figure 3.6: Realizations of p-thinnings on PLT and PVT.

with linear intensity λ_ℓ uniquely up to a scaling and we therefore call κ the *scaling factor* of X. For the numerical results considered later on, we only focus on single parameter pairs γ and λ_ℓ for each value of κ. The corresponding results for other parameters with the same scaling factor κ can then be obtained by an appropriate scaling.

3.5.3 Thinnings of the vertices

In the preceding section a specific class of Cox processes on the edges of random tessellations has been defined. If X is such a Cox process on the random tessellation T, then almost surely no point of X is located at a vertex of T since its random intensity measure is diffuse. However, for some applications it is of interest that points are also located at vertices $T^{(0)}$ of T. One possibility to construct point processes with this property are independent thinnings of the point process $T^{(0)}$.

Let T be a random tessellation. Like in Section 3.2.1, we also use the notation $V = \{V_n\}$ for the point process $T^{(0)}$ of the vertices of T. Furthermore, consider the independently marked point process $\{(V_n, U_n)\}$, where $U_1, U_2, \ldots$ are $U[0,1)$-distributed. For some constant $p \in (0,1)$, we then construct the point process X as the subset of those points V_i in $\{V_n\}$ with $U_i \leq p$. The point process X is then called a (independent) *p-thinning of V*, where we call p the *survival probability* and also write $X = V_p$. Realizations of p-thinnings of the vertices of PLT and PVT are shown in Figure 3.6.

If $\{V_n\}$ is stationary with intensity $\lambda^{(0)}$ and isotropic, then it is easy to see that X is stationary with intensity $\lambda_p^{(0)} = p\lambda^{(0)}$ and isotropic, respectively. Fur-

thermore, for stationary V the Palm version X^* of X can be obtained from the Palm version V^* of $V = \{V_n\}$ by an independent thinning of all points in $\mathbb{R}^2\backslash\{o\}$ with survival probability p since for each $A \in \mathcal{N}$ we have

$$\begin{aligned}\mathbb{P}(X^* \in A) &= \frac{1}{p\lambda^{(0)}}\mathbb{E}\sum_{X_n\in[0,1)^2}\mathbb{1}_A(t_{X_n}X)\\ &= \frac{1}{p\lambda^{(0)}}\mathbb{E}\sum_{V_n\in[0,1)^2}\mathbb{1}_{[0,p]}(U_n)\mathbb{1}_A(t_{V_n}V_p)\\ &= \frac{1}{p}\mathbb{E}\mathbb{1}_{[0,p]}(U_1)\mathbb{1}_A(V_p^*) = \mathbb{P}(V_p^*\cup\{o\}\in A)\,.\end{aligned}$$

Similarly as for Cox processes on T, a scaling invariance can be observed for p-thinnings of V. Let T be a stationary random tessellation with length intensity 1 and let $\lambda^{(0)}$ denote the intensity of its vertex set. Furthermore, let $T_\gamma = T/\gamma$ be the scaled version of T such that $\mathbb{E}\nu_1(T_\gamma^{(1)} \cap [0,1)^2) = \gamma$. Then the intensity of the vertices $T_\gamma^{(0)}$ of T_γ is given by $\lambda^{(0)}\gamma^2$. If X and X' are p-thinnings of $T_\gamma^{(0)}$ and $T_{\gamma'}^{(0)}$, respectively, it is easy to see that $X \stackrel{\mathrm{d}}{=} \frac{\gamma'}{\gamma}X'$ since $T_\gamma = \frac{1}{\gamma}T = \frac{\gamma'}{\gamma}T_{\gamma'}$.

Note that for Cox processes X the linear intensity λ_ℓ is given by λ/γ, where λ is the spatial intensity of X, and the *scaling factor* κ is defined by $\kappa = \gamma/\lambda_\ell$. For p-thinnings X of $T_\gamma^{(0)}$, we define λ_ℓ and κ in the same way, i.e., $\lambda_\ell = p\lambda^{(0)}\gamma^2/\gamma = p\lambda^{(0)}\gamma$ is defined as the spatial intensity of X divided by the length intensity of T and κ is defined by $\kappa = \gamma/\lambda_\ell$. Let X and X' be two thinnings of $T^{(0)}$ with survival probabilities p and p', respectively. Then $\kappa = 1/(\lambda^{(0)}p)$ and $\kappa' = 1/(\lambda^{(0)}p')$ are equal if and only if $p = p'$. Thus, we can consider the same scaling factor κ both for p-thinnings of $T^{(0)}$ and Cox processes on T.

3.5.4 Voronoi tessellations of point processes on random tessellations

Assume that $X = \{X_n\}$ is a stationary point process on the edges of a stationary random tessellation T such that $\mathbb{P}(X(\mathbb{R}^2) = \infty) = 1$. Then the Voronoi tessellation $T_X = \{\Xi_{X_n}\}$ induced by X can be considered. Note that T_X is a stationary random tessellation which can be identified with the marked point process $\{(X_n, \Xi^o_{X_n})\}$, where $\Xi^o_{X,n} = \Xi_{X_n} - X_n$ denotes the centered Voronoi cell at X_n with respect to X. If the point process X models locations of network components in telecommunication networks, then $\Xi_{X,n}$ can be regarded as the influence zone of the network component at X_n. In this context, we call $\Xi_{X,n}$ also the *serving zone* of X_n, see Chapter 5 for a more detailed discussion. The typical cell of T_X is denoted by Ξ^*_X which is an important characteristic in the analysis of telecommunication networks.

In the context of telecommunication networks, we assume that network components of two hierarchy levels are located along the infrastructure of the network,

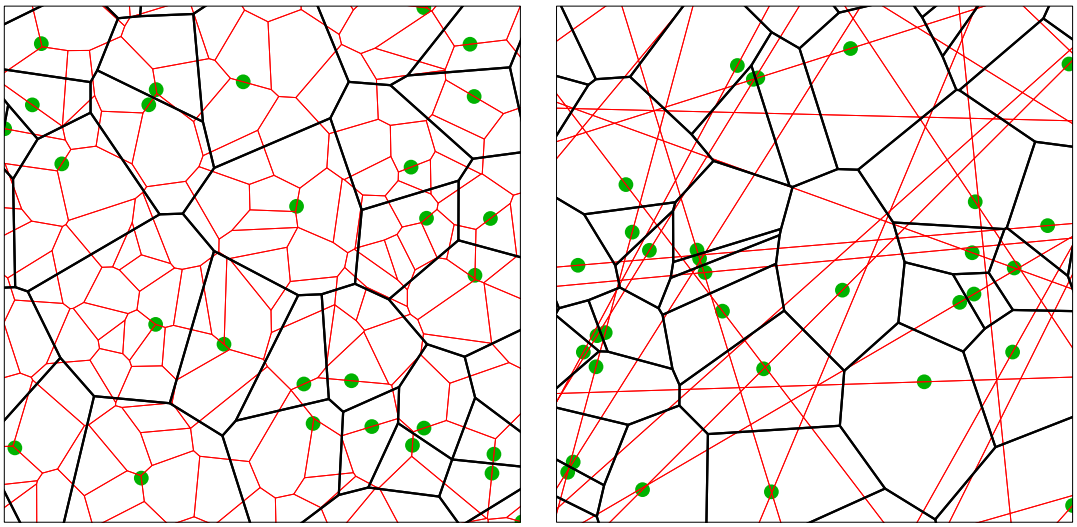

(a) PVT (b) PLT

Figure 3.7: Realizations of X_S and T_X for Cox processes on PVT and PLT.

e.g. street systems, which are modeled by the edge set $T^{(1)}$ of T. Therefore, it is also of interest to consider the edge set $S_{X,n} = T^{(1)} \cap \Xi_{X,n}$ inside $\Xi_{X,n}$ for each cell $\Xi_{X,n}$. In this way, we can construct the marked point process $X_S = \{(X_n, S^o_{X,n})\}$, where $S^o_{X,n} = S_{X,n} - X_n$ is the centered segment system associated with X_n. Note that X_S is a stationary marked point point process with mark space $\mathcal{L}^o$. The typical mark S^*_X of X_S is called the *typical segment system*. A realization of T_X and X_S is displayed in Figure 3.7 for Cox processes X on PVT and PLT.

Note that both S^*_X and Ξ^*_X are important characteristics in order to analyze hierarchical network models. For instance, in Chapter 5 it is shown that the distributions of connection lengths can be estimated based on samples of S^*_X and Ξ^*_X which can be obtained from Monte–Carlo simulation. We therefore derive simulation algorithms for Ξ^*_X and S^*_X for various network models in Chapter 4.

Chapter 4

Simulation algorithms for the typical cell of random tessellations

Many important characteristics of random tessellation models can be obtained as functionals of their typical cell, see e.g. the mean value formulae given in Theorem 3.1. Thus, the typical cell of a random tessellation is an important object in order to investigate distributional properties of random tessellation models. However, even for the typical cell of PVT it is hard to obtain closed analytical expressions for the distribution of cell characteristics like the perimeter or the area. On the other hand, it is often possible to construct simulation algorithms for the typical cell. Then, based on Monte-Carlo simulation, distributional properties of the considered random tessellation can be investigated. Another application of simulation algorithms for the typical Voronoi cell of random tessellations is the analysis of hierarchical network models. For instance, in Chapter 5 it is shown how the distribution of different cost functionals like direct Euclidean and shortest path connection lengths in two-level hierarchical models can be estimated based on samples of the typical cell of random tessellations. These observations motivate the investigations in this chapter.

In particular, we derive simulation algorithms for the typical Voronoi cell of point processes which are concentrated on the edges of random tessellations, where we focus on two different types of point processes. On the one hand, we consider Cox processes on the edges of random tessellations and, on the other hand, we regard thinnings of the set of vertices of random tessellations. Then, if the underlying tessellation is e.g. a PDT, PLT and PVT, respectively, we derive simulation algorithms for the typical Voronoi cell of the respective point process. The results which are presented here are partly based on material elaborated in [27, 96, 97, 100].

Note that in the ergodic case, the distribution of the typical cell can be interpreted as the empirical distribution of the cells of the tessellation in a large sampling window, see Theorem 2.8. Thus, we can either simulate the random tessellation in a large sampling window W and regard the cells whose nucleus lies

inside W or we can locally simulate i.i.d. samples of the typical cell in order to estimate spatial averages by sample means. However, there are several advantages for the simulation of the typical cell. If we simulate the tessellation in a large sampling window, then the cells are all correlated. Furthermore, there are edge effects which might be significant if W is too small. On the other hand, runtime and memory problems occur if W is too large. All these problems can be avoided if the typical Voronoi cell is simulated locally and the same characteristics can be estimated. However, the challenge is then to develop efficient simulation algorithms. Recall that the typical Voronoi cell Ξ_X^* of a point process X can be constructed as $\Xi_X^* = \cap_{n\in\mathbb{N}} H(o, X_n^*)$, where $X^* = \{X_n^*\}$ is the Palm version of X. Thus, we have to develop simulation algorithms for X^* if X is e.g. a Cox process or thinning of the vertices of PDT, PLT and PVT.

The present chapter is organized in the following way. At the beginning, we give a brief summary of existing simulation algorithms for the typical Voronoi cell of Poisson processes and Cox processes on PLT, see Section 4.1. In particular, we explain a radial simulation algorithm for stationary Poisson processes and we show how this algorithm can be used in order to efficiently simulate the typical cell of PVT. The concept of radial simulation is essential for all algorithms which are developed later on.

Afterwards, in Section 4.2, two new simulation algorithms for the typical Voronoi cell of Cox processes on PVT are introduced. On the one hand, we show how the typical cell can be simulated directly and, on the other hand, we derive an indirect simulation algorithm that allows to simulate random cells from which the distribution of the typical cell can be obtained by a weighting procedure. One advantage of the latter algorithm is that it can also be used to simulate the typical cell of Cox process on further tessellation models, whereas the direct algorithm is specifically designed to simulate the typical cell of Cox processes on PVT. In Section 4.3 we then introduce a new algorithm for the simulation of the typical Voronoi cell of Cox processes on PDT. Similarly as for PVT, an indirect algorithm is constructed which can be used in order to simulate random cells from which the distribution of the typical cell can be obtained by an appropriate weighting. Section 4.4 summarizes a new simulation algorithm for the typical Voronoi cell of Cox processes on nested tessellations. This algorithm is applicable if nested tessellations $T = T_0/T_1$ with initial tessellation T_0 and component tessellation T_1 are considered whose stationary and Palm versions T_i and $\widetilde{T}_i$, respectively, can be simulated for $i = 0, 1$.

In Section 4.5 we explain how the typical Voronoi cell can be simulated if the underlying point process is obtained by independent thinnings of the vertices of PDT, PLT and PVT, respectively. In all three cases it is possible to derive direct simulation algorithms for the typical Voronoi cell.

Finally, in Section 4.6, some numerical results obtained from a simulation study are presented. In particular, the efficiencies of the direct and indirect

algorithm for Cox processes on PVT are investigated in order to decide which algorithm is preferable. Furthermore, we compare distributional properties of the typical cells of the different considered models.

4.1 Typical Voronoi cells of Poisson processes and Cox processes on PLT

In this section, we briefly review existing simulation algorithms for the typical cell of certain Voronoi tessellations. To begin with, we discuss how stationary Poisson processes in $\mathbb{R}^2$ can be simulated radially. The radial simulation algorithm for stationary Poisson processes is the basis of all simulation algorithms developed later on. We use this result in order to explain how the typical cell of PVT can be simulated. Moreover, we briefly summarize a simulation algorithm for the typical Voronoi cell of Cox processes on PLT developed in [31]. This algorithm will be used in order to compute e.g. the distribution of shortest path lengths, see Chapters 5 and 7.

4.1.1 Radial simulation of stationary Poisson processes

In our applications it is useful to simulate the points of a Poisson process with increasing distance to the origin. This approach is also called radial simulation of point processes. Note that for a stationary Poisson process $X = \{X_n\}$ in $[0, \infty)$ with intensity λ it is well–known that the atoms X_n are given by $X_n = \sum_{i=1}^{n} Y_i$ for $n \geq 1$, where $Y_1, Y_2, \ldots$ is a sequence of independent random variables which are $Exp(\lambda)$–distributed, i.e., the density of Y_1 is given by $f_{Y_1}(x) = \lambda e^{-\lambda x} \mathbb{1}_{[0,\infty)}(x)$. We can use this construction principle directly in order to simulate the points of X with increasing distance to the origin. This method can be generalized to Poisson processes in $\mathbb{R}^d$ for any $d \geq 1$. In the following, we will focus on the case that X is a stationary Poisson processes in $\mathbb{R}^2$, for further details see [80].

Note that a point $x = (x_1, x_2) \in \mathbb{R}^2$ can be represented by its polar coordinates, i.e. $x = (r \cos \phi, r \sin \phi)$ for some $r \in [0, \infty)$ and $\phi \in [0, 2\pi)$. Let X denote a stationary Poisson process in $\mathbb{R}^2$ with intensity $\lambda > 0$ and consider a sequence $\Phi_1, \Phi_2, \ldots$ of independent and identically distributed random variables with $\Phi_1 \sim U[0, 2\pi)$ and another sequence $D_1, D_2, \ldots$ of independent and identically distributed random variables with $D_1 \sim Exp(1)$. Now define the sequence $R_1, R_2, \ldots$ by

$$R_i = \sqrt{\sum_{k=1}^{i} \frac{D_k}{\pi \lambda}},$$

then $X = \{X_n\}$ with $X_n = \{(R_n \cos \Phi_n, R_n \sin \Phi_n)\}$ is a stationary Poisson process in $\mathbb{R}^2$ of intensity λ, see [47], p. 20 for a proof. Based on this statement it is

easy to simulate a Poisson process radially based on the simulation of $U[0, 2\pi)$- and $Exp(1)$-distributed random variables which are independent. For details on the simulation of random variables, see e.g. [2, 29, 81].

4.1.2 Simulation of the typical Voronoi cell of PVT

Due to Slivnyak's theorem, see Theorem 2.6, the typical Voronoi cell of a PVT induced by a stationary Poisson process $X = \{X_n\}$ can be regarded as the Voronoi cell at the origin o with respect to $X^* = X \cup \{o\}$. Thus, we can place a point at the origin, simulate further points X_n according to a stationary Poisson process and construct the typical cell $\Xi_X^* = \cap_{n\in\mathbb{N}} H(o, X_n)$ as the intersection of the bisectors $H(o, X_n), n \in \mathbb{N}$. Clearly, the radial simulation procedure introduced in the preceding section has many advantages here compared to other simulation algorithms for stationary Poisson processes. For instance, a stationary Poisson process X of intensity λ can be simulated in a sampling window W as follows. First, a random variable $N \sim Poi(\lambda\nu_2(W))$ is simulated and then, given $N = n$, the n points $X_1, \ldots, X_n$ of X inside W are simulated as independent and uniformly distributed points in W. Although this procedure seems to be easy, it is not appropriate in order to simulate the typical cell of the induced PVT. On the one hand, it is not known in advance how large the sampling window W has to be chosen in order to construct the typical cell. On the other hand, this procedure is computationally inefficient since often too many points are simulated. However, if we simulate X radially, we can simulate the points $X_1, X_2, \ldots$ with increasing distance to the origin. In particular, we can simulate points radially until a bounded Voronoi cell at o can be constructed based on the already simulated points. This cell is called the *initial cell*. Afterwards we can check for each newly simulated point if the initial cell cannot be influenced by points anymore which are farer away to o than the last generated point. If this is the case, we stop the algorithm and otherwise we simulate further points. The main steps of this simulation algorithm are sketched below. Here, the points $X_1, X_2, \ldots$ are constructed from $\Phi_1, \Phi_2, \ldots$ and $D_1, D_2, \ldots$ as explained in Section 4.1.1.

1. Generate $X^* = \{o\}$.

2. Simulate independent random variables $\Phi_1, \Phi_2, \ldots$ and $D_1, D_2, \ldots$ with $U_i \sim U[0, 2\pi), D_i \sim Exp(1)$ for $i = 1, 2, \ldots$.

3. Add $X_1, \ldots, X_n$ to X^* until a compact initial cell $\Xi_X^* = \cap_{i=1}^n H(o, X_i)$ at o can be constructed from the already simulated points of X^*.

4. If $R_n \geq r_{max} = 2\max\{|v_i|\}$, were $\{v_i\}$ denotes the set of vertices of Ξ_X^*, then stop. Else add further points $X_j, j = n+1, n+2, \ldots$ to X^* and put $\Xi_X^* = \cap_{i=1}^j H(o, X_i)$ until $R_j \geq r_{max}$.

Some technical details have to be considered. First we have to construct an initial cell. If for $n \geq 3$ the points $X_1, \ldots, X_n$ are already generated, then a cone criterion can be used in order to check if a bounded Voronoi cell can be constructed around o, see e.g. [24]. Once the initial cell Ξ_X^* has been generated, points outside the ball $B(o, r_{max})$ cannot influence the typical Voronoi cell anymore since the bisectors between o and points $x \in B(o, r_{max})^c$ cannot intersect Ξ_X^*. Thus we can stop the simulation if $R_n \geq r_{max}$. The resulting cell Ξ_X^* of this simulation procedure is then the typical Cell of a stationary PVT with intensity λ.

In Figure 4.1 the main steps of the algorithm are visualized. Note that in the simulation algorithms developed later on, we always try to follow this way, i.e., we simulate the points of the underlying point process (approximately) radially and construct an initial cell in order to decide when to stop the simulation. However, if we are considering e.g. Cox processes X on PDT, PLT and PVT, then we cannot simulate the points of X radially, but we can simulate the Poisson process radially which induces the underlying tessellation.

4.1.3 Simulation of the typical Voronoi cell of Cox processes on PLT

We now describe a simulation algorithm for the typical cell of Voronoi tessellations induced by Cox processes X with linear intensity λ_ℓ on a stationary PLT of length intensity γ. Note that due to Theorem 3.3 we have that $X^* = \widetilde{X} \cup \{o\}$, where $\widetilde{X}$ is a Cox process on the Palm version $\widetilde{T}$ of the random tessellation T regarded as the random Hausdorff measure $\nu_1(\,\cdot \cap T^{(1)})$ on $T^{(1)}$. Thus, first the PLT has to be simulated according to its Palm distribution with respect to $\nu_1(\,\cdot \cap T^{(1)})$, i.e., under the condition that $o \in T^{(1)}$. Due to Slivnyak's theorem, the conditional PLT can be constructed by adding an isotropic line ℓ_0 through o to an independent and stationary PLT of length intensity γ. Note that a stationary PLT can be simulated radially which is a direct consequence of its definition. Let $\Phi_1, \Phi_2, \ldots$ and $D_1, D_2, \ldots$ be independent random variables, where $\Phi_i \sim U[0, 2\pi)$ and $D_i \sim Exp(2\gamma)$ for $i = 1, 2, \ldots$. Furthermore, we define the random variables $R_n = \sum_{i=1}^n D_i, n = 1, 2, \ldots$. Then $\{\ell_n\}$ with $\ell_n = \ell(R_n, \Phi_n)$ is a Poisson line process, where $\ell(R_n, \Phi_n) = \{(x, y) \in \mathbb{R}^2 : -x \sin \Phi_n + y \cos \Phi_n = R_n\}$, see also Section 3.4.3. Now the typical Voronoi cell of a Cox process X on a PLT can be simulated using similar ideas as for the simulation of the typical cell of PVT. However, we cannot simulate the conditional Cox process X^* radially, but we can simulate the underlying random tessellation radially. The main steps are briefly summarized below. Note that the points of $X^* \backslash \{o\}$ on a single line ℓ_n can be regarded as a stationary Poisson process in $\mathbb{R}$ with intensity λ_ℓ. Thus, we can choose one point on ℓ_n as the origin and then simulate the points of X^* using independent and exponentially distributed waiting times, see Section 4.1.1. This observation can be used in order to simulate points X_1, X_2, X_3 and X_4 of X^* first

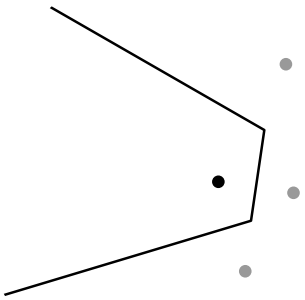

(a) Origin o (black) and radially simulated points X_1, X_2, X_3 (gray). Compact initial cell cannot be constructed yet.

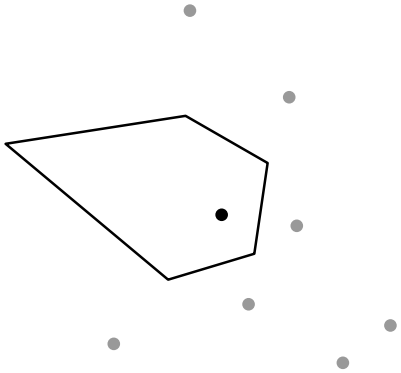

(b) Initial cell Ξ^* around o is constructed using the simulated points $X_1, \ldots, X_7$.

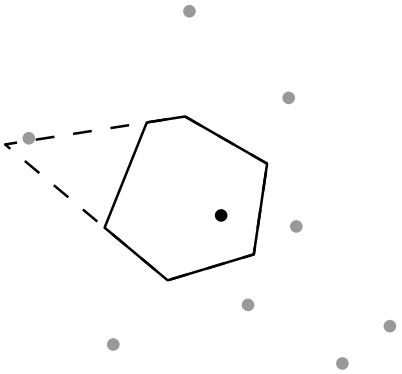

(c) Point X_8 is simulated radially and Ξ^* is cut by bisector.

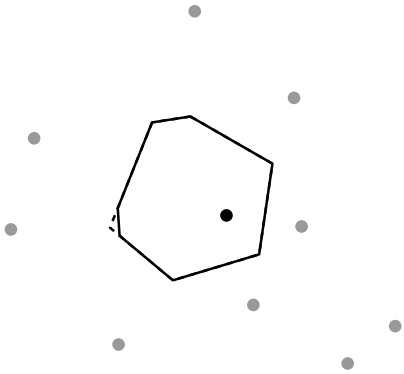

(d) Point X_9 is simulated radially and Ξ^* is cut by bisector.

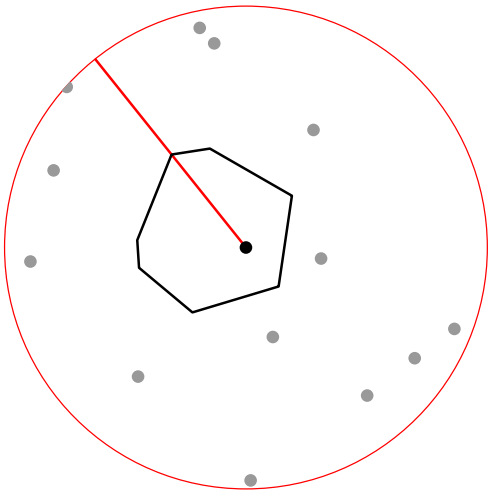

(e) Further points X_n are simulated radially until $|X_n| \geq r_{max}$.

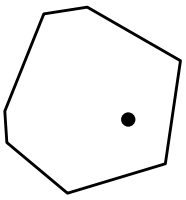

(f) Realization of the typical cell Ξ^* of PVT.

Figure 4.1: Simulation of the typical cell of a stationary PVT

which generate a compact initial cell around o. In particular, we place X_1 and X_2 on ℓ_0 as the two nearest points to the origin of a stationary Poisson process on ℓ_0. Afterwards, we place X_3 and X_4 on ℓ_1 as the two nearest points to $\ell_0 \cap \ell_1$ of a stationary Poisson process on ℓ_1. Then $\cap_{i=1}^4 H(o, X_i)$ is a compact polygon with probability 1.

1. Generate the line ℓ_0 with direction $\Phi_0 \sim U[0, 2\pi)$ through o which is identified with the unit vector $U_0 = (\cos\Phi_0, \sin\Phi_0)$.

2. Set $X^* = \{o\}$ and add the two points $X_1 = Y_1U_0, X_2 = -Y_2U_0$ on ℓ_0 to X^*, where Y_1 and Y_2 are independent and $Exp(\lambda_\ell)$–distributed.

3. Generate another line ℓ_1 with direction $\Phi_1 \sim U[0, 2\pi)$, unit vector $U_1 = (\cos\Phi_1, \sin\Phi_1)$ and distance $R_1 = D_1 \sim Exp(\gamma)$ to o.

4. Add the two points $X_3 = Z + Y_3U_1, X_4 = Z - Y_4U_1$ on ℓ_1 to X^*, where Y_3 and Y_4 are independent and $Exp(\lambda_\ell)$–distributed and $Z = \ell_0 \cap \ell_1$.

5. Construct initial cell Ξ_X^* at o with respect to X^* and put $r_{max} = 2\max\{|v_i|\}$, where $\{v_i\}$ are the vertices of Ξ_X^*.

6. Simulate further points X_n on ℓ_0 and ℓ_1 as the atoms of stationary (linear) Poisson process on $\ell_0 \cap B(o, r_{max})\backslash\{x \in \mathbb{R}^2 : -Y_2 \leq \langle x, U_0\rangle \leq Y_1\}$ and $\ell_1 \cap B(o, r_{max})\backslash\{x \in \mathbb{R}^2 : -Y_4 \leq \langle x - Z, U_1\rangle \leq Y_3\}$.

7. Simulate further lines $\ell_n = \ell(R_n, \Phi_n)$ with $\Phi_n \sim U[0, 2\pi)$ and $R_n = \sum_{i=1}^n D_i$, place points as linear Poisson processes on $\ell_n \cap B(o, r_{max})$, update both Ξ_X^* and r_{max} until $R_n \geq r_{max}$.

The resulting cell Ξ_X^* is then the typical Voronoi cell and $S_X^* = \Xi_X^* \cap \big(\cup_n \ell_n\big)$ is the typical segment system inside Ξ_X^*. A more detailed description of the algorithm can be found in [31] and [82]. In the following, we develop new simulation algorithms if the underlying tessellation is a PVT and PDT, respectively. The basic idea of simulating the Palm version $\widetilde{T}$ of the underlying tessellation T radially is also used there, although it is not directly possible as in the case of PLT.

4.2 Typical Voronoi cell of Cox processes on PVT

In this section, two algorithms are derived which can be used in order to estimate distributional properties of the typical Voronoi cell of Cox processes X on PVT. The first simulation algorithm is designed to simulate the typical Voronoi cell directly, whereas with the second algorithm it is possible to simulate random polygons from which all distributional properties of the typical Voronoi cell can be obtained by an appropriate weighting. However, the second algorithm can be applied to any Cox process on a stationary random tessellation T if T can be

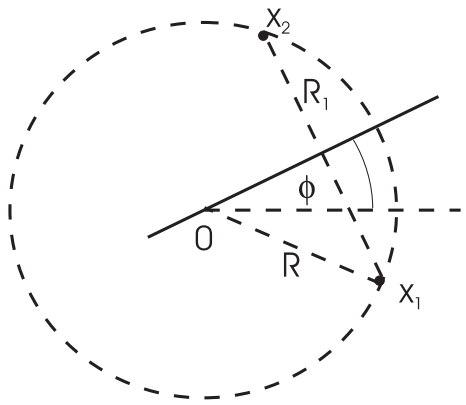

Figure 4.2: Line segment through the origin with its generating points

simulated starting from its typical cell, whereas the direct algorithm is specifically developed for Cox processes on PVT.

4.2.1 Direct simulation algorithm

In the following, let T denote a PVT induced by a stationary Poisson process of intensity λ. The direct simulation algorithm uses a result which has been recently derived in [13]. As in the preceding section, we have to simulate the Palm version $\widetilde{T}$ of T with respect to the Palm distribution P_Λ^*, where $\Lambda(\,\cdot\,) = \nu_1(\,\cdot\, \cap T^{(1)})$. Then the points of the Palm version X^* in $\mathbb{R}^2\backslash\{o\}$ can be simulated as linear Poisson processes on $\widetilde{T}^{(1)}$ with linear intensity λ_ℓ.

If T is a PVT, then it can be shown that the random tessellation $\widetilde{T}$ is a Voronoi tessellation with respect to some point process $X' = \{X_n'\}$. Note that under P_Λ^* one line segment of the Voronoi tessellation $\widetilde{T}$ contains the origin almost surely. Thus, it is obvious that there are two points X_1' and X_2' of the point process X' generating this Voronoi tessellation which are located on a circle around the origin. The locations of those two points can be described using random variables R, R_1 and Φ, where Φ is the angle of the line segment through the origin, $R = |X_1'|$ is the distance of the two points X_1' and X_2' to the origin and finally $R_1 = |X_1' - X_2'|/2$ is half of the distance between the points, see Figure 4.2. Note that $X'(B(o, |X_1'|)) = 0$ almost surely.

Now we state the result which is used for the direct simulation algorithm. It is a special case of Theorem 1.1 in [13].

Lemma 4.1 *Under P_Λ^* the following holds.*

(i) *The random variables $(\{X_n' : |X_n'| > R\}, R)$, R_1^2/R^2 and Φ are independent.*

(ii) *R^2 is Γ-distributed with shape parameter 1.5 and scale parameter $1/(\lambda\pi)$.*

(iii) *The conditional distribution of* $\{X'_n : |X'_n| > R\}$ *given* $R = r$ *is the distribution of a stationary Poisson process in* $\mathbb{R}^2 \backslash B(o, r)$ *with intensity* λ.

(iv) R_1^2/R^2 *is beta distributed with parameters* 1 *and* $1/2$.

(v) Φ *is uniformly distributed on* $[0, 2\pi)$.

Lemmas 3.4 and 4.1 can be used in order to obtain the following algorithm for the simulation of the typical Voronoi cell Ξ_X^* of a Cox process X with linear intensity λ_ℓ on T. In the following, let $\widetilde{T}$ denote the Voronoi tessellation induced by X'. First, we give an overview of the simulation algorithm and some technical details are explained later on.

1. Simulate two independent random variables given by $R^2 \sim \Gamma(1.5, 1/(\lambda\pi))$ and $\widetilde{R}^2 \sim B(1, 1/2)$.
2. Compute $R_1 = R\widetilde{R}$ and construct the two points $X'_1 = (\sqrt{R^2 - R_1^2}, R_1)$ and $X'_2 = (\sqrt{R^2 - R_1^2}, -R_1)$.
3. Given R, simulate a Poisson process $\{X'_n, n \geq 3\}$ radially outside the ball $B(o, R)$ and add the points X'_1 and X'_2 to obtain $X' = \{X'_n, n \geq 1\}$.
4. Construct the cells of the Voronoi tessellation $\widetilde{T}$ induced by X'.
5. Set $X^* = \{o\}$, simulate points $X_1, X_2, \ldots$ on $\widetilde{T}^{(1)}$ according to linear Poisson processes and add them to X^*.
6. Construct the Voronoi cell Ξ_X^* around o with respect to X^*.
7. Construct $S_X^* = \Xi_X^* \cap \widetilde{T}^{(1)}$.

In order to obtain a realization of the typical Voronoi cell Ξ_X^* and the typical segment system S_X^* we have to apply in addition an isotropic rotation. However, all characteristics which are considered in this thesis are rotation invariant. Thus we can omit this final rotation step for our purposes. The different steps of the simulation algorithm are sketched in Figure 4.3.

Naturally, some further technical details have to be considered. The simulation of points of X' and the construction of Voronoi cells of $\widetilde{T}$ on the one hand and the simulation of points of X^* on the other hand have to be performed in an alternating fashion. At the beginning, X'_1 and X'_2 have to be constructed and, given $R = |X'_1|$, the points of X' outside $B(o, R)$ are simulated radially conditioned to $B(o, R) \cap X' = \emptyset$ until the first Voronoi cell Ξ_1 around X'_1 with respect to the point process $X' = \{X'_n\}$ can be generated. Then the first points of X^* are simulated on $\partial\Xi_1$ as (linear) Poisson processes and o is added to X^*. This is done in the usual way by first simulating the total number of points $N \sim Poi(\lambda_\ell \nu_1(\partial\Xi_1))$ on the boundary $\partial\Xi_1$ and then, under the condition $N = n$, by

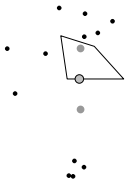

(a) Start: X_1', X_2' (gray) generating the line segment through o (gray with black boundary). The cell around X_1' is already constructed.

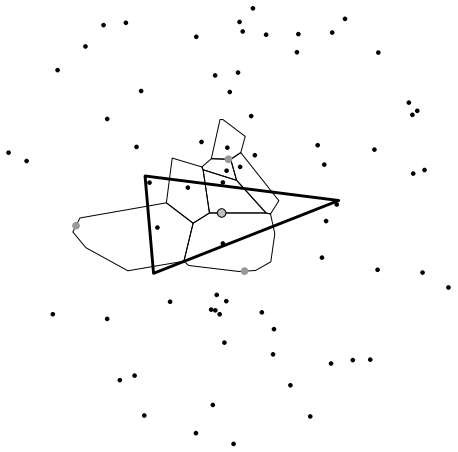

(b) Initial cell: The initial cell around o is constructed using the previously simulated points (gray) of X^*.

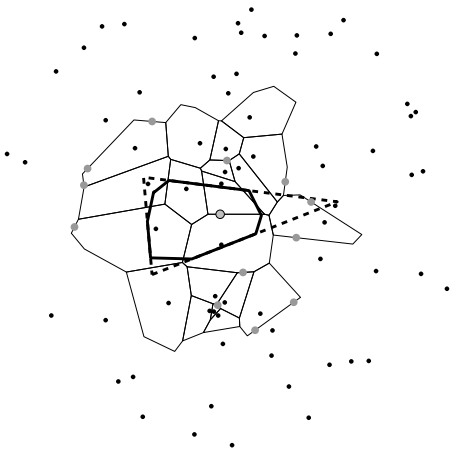

(c) Further points of X^* are simulated (gray) and the initial cell is intersected by the bisectors.

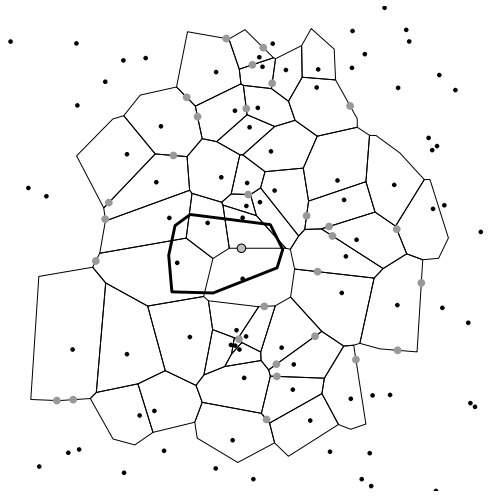

(d) A realization of the typical Voronoi cell is constructed and the algorithm stops.

Figure 4.3: Direct simulation of the typical Voronoi cell of Cox processes on PVT

placing n independent points uniformly distributed on $\partial\Xi_1$. In the next step, new points of X' are simulated and further cells Ξ_n of $\widetilde{T}$ are constructed. On the new line segments additional points of X^* are placed again as linear Poisson processes. If it is already possible, an initial cell is built around o using the points of X^* which have been simulated so far. In order to check if an initial cell can be constructed, we can use a cone criterion, see [26], [80] and [103]. If this is not yet possible, further cells of $\widetilde{T}$ are simulated and further points of X^* are positioned on the new edges until an initial cell can be constructed. The initial cell can only be influenced by points of X^* in the ball $B(o, r_{max})$ with radius $r_{max} = 2\max_{i=1,\dots,m} |v_i|$, where $\{v_i, i = 1\dots, m\}$ denotes the set of vertices of the initial cell. If all edges of $\widetilde{T}$ which can intersect the ball $B(o, r_{max})$ are constructed, the simulation algorithm can be stopped since all points of X^* are located on the edge set $\widetilde{T}^{(1)}$. Therefore we use the following criterion to stop the simulation algorithm. All vertices of $\widetilde{T}$ located on the boundary of only one already constructed cell are connected in clockwise order. If the resulting (not necessarily convex) polygon contains $B(o, r_{max})$, then all edges necessary for the simulation are constructed and the algorithm is stopped. This is a consequence of the property of PVT that almost surely three edges are emanating from each vertex and the convexity of the cells. Of course, if we intersect the initial cell with the bisector $H(o, X_n)$ of o and a newly generated point X_n, then the maximal radius r_{max} is updated in order to reduce runtime. In Figure 4.4 the stopping criterion is illustrated together with a simulated realization of the typical cell Ξ_X^*. If we are interested in the typical segment system S_X^* inside Ξ_X^*, we have to intersect Ξ_X^* with $\widetilde{T}^{(1)}$, i.e., we put $S_X^* = \Xi_X^* \cap \widetilde{T}^{(1)}$.

Then, except of the missing rotation around the origin, the constructed cell Ξ_X^* at the origin is the typical cell of a Voronoi tessellation induced by a Cox process X on PVT and $S_X^* = \Xi_X^* \cap \widetilde{T}^{(1)}$ is the typical segment system inside Ξ_X^*.

4.2.2 An indirect simulation algorithm

Now we derive an alternative simulation algorithm. This new algorithm allows us to simulate random cells which are not realizations of the typical cell. However, the simulated cells can be used in order to obtain distributional properties of the typical Voronoi cell of a Cox process X which is concentrated on the edge set of a stationary random tessellation T with length intensity γ. It is simply required that the random tessellation T^* distributed according to the Palm distribution P_T^* with respect to the cell nuclei can be simulated. If the random tessellation T is a PVT, then this simulation can be easily achieved. We only have to generate the Voronoi tessellation induced by a stationary Poisson process with an additional point located at the origin, see Section 4.1.2. But this technique can also be used to simulate the typical Voronoi cell of Cox processes X on random tessellations T

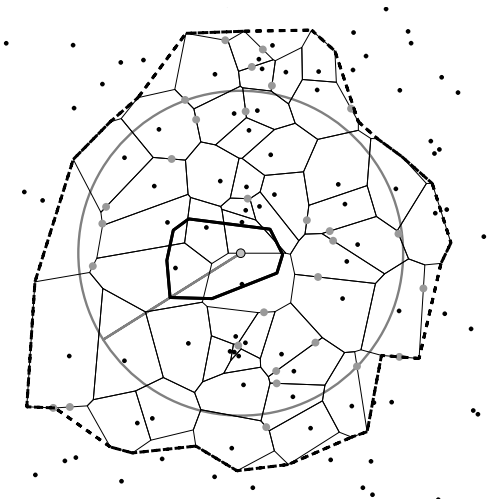

(a) Stopping criterion: If the circle (gray) is contained in the polygon of the outer vertices (dashed segments) the algorithm stops.

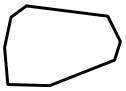

(b) A realization of the typical cell.

Figure 4.4: Stopping criterion and simulated cell for the direct algorithm

different from PVT. Possible models for T are Voronoi tessellations based on Cox processes on PLT ([31] and Section 4.1.3), Poisson-Laguerre tessellations ([42, 50, 52]) or Voronoi tessellations induced by so–called modulated Cox processes ([26]) whose random intensity measures are based on Boolean models ([69]). Note that in [54] related techniques are used in order to estimate distributional properties of characteristics of the typical cell of stationary iterated tessellations. Similarly, the typical cell is not simulated directly there, but a sequence of cells is simulated from which the distribution of the typical cell can be obtained.

We now focus on a Cox process X on some stationary random tessellation T with linear intensity λ_ℓ. Furthermore, we use the notion T_X for the Voronoi tessellation induced by X. The indirect simulation algorithm is then based on a formula stated in Theorem 4.3 below. But first we derive an auxiliary result in order to prove the theorem.

Note that the Voronoi tessellation T_X induced by the Cox process X together with the random tessellation T can be viewed as a random element $Y = (T_X, T)$ of $\mathsf{N}^2_{\mathcal{P}^o}$. In the following, we use the notation $T_X = \{(X_n^{(1)}, \Xi_n^{(1)})\}$ and $T = \{(X_n^{(2)}, \Xi_n^{(2)})\}$, respectively, and denote the joint distribution of the vector Y by P_Y. Furthermore, let λ_1 and λ_2 be the cell intensities of T_X and T, respectively, seen as the marked point processes of cell nuclei marked with the centered cells.

We are then interested in the distributions of the whole vector Y and in particular of T_X with respect to $P_Y^{(2)}$. Here $P_Y^{(2)}$ is the Palm distribution of Y with respect to the second component $T = \{(X_n^{(2)}, \Xi_n^{(2)})\}$, see Section 2.3.4. In the following, $(T_{\widetilde{X}}, T^*)$ denotes a vector of two random tessellations whose

joint distributed is given by $P_Y^{(2)}$. Note that $T_{\widetilde{X}}$ is then a Voronoi tessellation induced by some point process $\widetilde{X}$ on the edges of T^*. Thus, $\widetilde{X}$ denotes the point process of the nuclei of the Voronoi tessellation $T_{\widetilde{X}}$ on the edges of T^* under the distribution $P_Y^{(2)}$.

Lemma 4.2 *The point process $\widetilde{X}$ defined above is a (non-stationary) Cox process in $\mathbb{R}^2$ whose random intensity measure is given by $\Lambda_{\widetilde{X}}(B) = \lambda_\ell \nu_1(B \cap T^{*(1)})$ for $B \in \mathcal{B}(\mathbb{R}^2)$, where $T^{*(1)}$ is the edge set of T^*.*

Proof For arbitrary bounded sets $B_1, \dots, B_n \in \mathcal{B}(\mathbb{R}^2)$ which are pairwise disjoint and for any $n \geq 1, k_1, \dots, k_n \in \mathbb{N}$ regard the set A given by

$$A = \{\psi \in \mathsf{N}_{\mathcal{P}^o} : \psi(B_1 \times \mathcal{P}^o) = k_1, \dots, \psi(B_n \times \mathcal{P}^o) = k_n\}\,.$$

In order to show that $\widetilde{X}$ is the desired Cox process, it is sufficient to show that

$$P_Y^{(2)}(A \times \mathsf{N}_{\mathcal{P}^o} \times \mathcal{P}^o) = \mathbb{E}\Big(\prod_{i=1}^{n} \frac{(\lambda_\ell \nu_1(B_i \cap T^{*(1)}))^{k_i}}{k_i!}\, e^{-\lambda_\ell \nu_1(B_i \cap T^{*(1)})}\Big)\,, \tag{4.1}$$

since the finite–dimensional distributions determine the distribution of a point process uniquely. Recall that

$$P_Y^{(2)}(A \times \mathsf{N}_{\mathcal{P}^o} \times \mathcal{P}^o) = \frac{1}{\lambda_2}\, \mathbb{E}\#\{n : X_n^{(2)} \in [0,1)^2, t_{X_n^{(2)}} Y \in A \times \mathsf{N}_{\mathcal{P}^o}\}\,. \tag{4.2}$$

Notice that we can identify the Cox process X with its Voronoi tessellation T_X, thus we can use the definition of Cox processes in order to decompose the expectation in (4.2), i.e. the integral with respect to the distribution P_Y of Y, into an outer integration with respect to the distribution P_T of T and, given $T = \tau$, an inner integral with respect to the the conditional distribution $P_{X|T=\tau}$ of a non-stationary Poisson process with intensity measure $\lambda_\ell \nu_1(\,\cdot \cap \tau^{(1)})$. Then, using the notation $A' = \{\varphi \in \mathsf{N} : \varphi(B_1) = k_1, \dots, \varphi(B_n) = k_n\}$, we have

$$\begin{aligned}
&P_Y^{(2)}(A \times \mathsf{N}_{\mathcal{P}^o} \times \mathcal{P}^o)\\
&\quad= \frac{1}{\lambda_2} \int_{\mathsf{N}_{\mathcal{P}^o}} \int_{\mathsf{N}} \int_{[0,1)^2 \times \mathcal{P}^o} \mathbb{1}_{A'}(t_x\varphi)\, \tau(d(x,\xi))\, P_{X|T=\tau}(d\varphi)\, P_T(d\tau)\\
&\quad= \frac{1}{\lambda_2} \int_{\mathsf{N}_{\mathcal{P}^o}} \int_{[0,1)^2 \times \mathcal{P}^o} \int_{\mathsf{N}} \mathbb{1}_{A'}(t_x\varphi)\, P_{X|T=\tau}(d\varphi)\, \tau(d(x,\xi))\, P_T(d\tau)\\
&\quad= \frac{1}{\lambda_2} \int_{\mathsf{N}_{\mathcal{P}^o}} \int_{[0,1)^2 \times \mathcal{P}^o} \int_{\mathsf{N}} \mathbb{1}_{A'}(\varphi)\, P_{X|T=t_x\tau}(d\varphi)\, \tau(d(x,\xi))\, P_T(d\tau)\\
&\quad= \frac{1}{\lambda_2} \int_{\mathsf{N}_{\mathcal{P}^o}} \int_{[0,1)^2 \times \mathcal{P}^o} \prod_{i=1}^{n} \frac{(\lambda_\ell \nu_1(B_i \cap (t_x\tau)^{(1)}))^{k_i}}{k_i!\, e^{\lambda_\ell \nu_1(B_i \cap (t_x\tau)^{(1)})}}\, \tau(d(x,\xi))\, P_T(d\tau)\,.
\end{aligned}$$

Finally, we can apply the refined Campbell theorem, see Theorem 2.7, and obtain

$$\begin{aligned} P_Y^{(2)}(A \times \mathsf{N}_{\mathcal{P}^o} \times \mathcal{P}^o) &= \int_{[0,1)^2} \int_{\mathsf{N}_{\mathcal{P}^o}\times\mathcal{P}^o} \prod_{i=1}^{n} \frac{(\lambda_\ell \nu_1(B_i \cap \tau^{(1)}))^{k_i}}{k_i!\, e^{\lambda_\ell \nu_1(B_i\cap\tau^{(1)})}}\, P_T^*(d(\tau,\xi))\, dx \\ &= \mathbb{E}\Big(\prod_{i=1}^{n} \frac{(\lambda_\ell \nu_1(B_i \cap T^{*(1)}))^{k_i}}{k_i!}\, e^{-\lambda_\ell \nu_1(B_i\cap T^{*(1)})}\Big), \end{aligned}$$

which proves equation (4.1). □

Now we can use Lemma 4.2 and Neveu's exchange formula (Theorem 2.9) in order to derive the following representation formula for the typical Voronoi cell of a Cox process X on the random tessellation T. This result is the basis of the indirect simulation algorithm introduced later.

Theorem 4.3 *Let $h : \mathcal{P}^o \to [0,\infty)$ be measurable. Then,*

$$\mathbb{E}\, h(\Xi_X^*) = \frac{1}{\mathbb{E}\, \nu_1(\partial\Xi_T^*)}\, \mathbb{E}\left(\nu_1(\partial\Xi_T^*)\, \mathbb{E}\left(h(\Xi^o_{\widetilde{X}\cup\{Z\}}(Z)) \mid T^*\right)\right), \tag{4.3}$$

where Ξ_X^* denotes the typical cell of T_X and Ξ_T^* denotes the (typical) cell of T^* located at o. Moreover, $\Xi^o_{\widetilde{X}\cup\{Z\}}(Z)$ denotes the centered Voronoi cell around an additional point $Z \in \partial\Xi_T^*$ with respect to $\widetilde{X} \cup \{Z\}$. This point Z is conditionally uniformly distributed on $\partial\Xi_T^*$ and conditionally independent of $\widetilde{X}$ given T^*.

Proof First consider the function $f : \mathbb{R}^2 \times \mathcal{P}^o \times \mathcal{P}^o \times \mathsf{N}^2_{\mathcal{P}^o} \to [0,\infty)$ defined by

$$f(x,\xi,\xi_T,\psi) = \begin{cases} h(\xi) & \text{if } o \in \partial\xi_T + x, \\ 0 & \text{otherwise,} \end{cases} \tag{4.4}$$

i.e., we have $f(x,\xi,\xi_T,\psi) = h(\xi)$ if the origin is on the boundary of the shifted cell $\xi_T + x$ centered at x. Then, applying Lemma 2.9, we have that

$$\begin{aligned} \mathbb{E}\, h(\Xi_X^*) &= \int_{\mathsf{N}^2_{\mathcal{P}^o}\times\mathcal{P}^o} h(\xi)\, P_Y^{(1)}(d(\psi,\xi)) \\ &= \frac{1}{2}\int_{\mathsf{N}^2_{\mathcal{P}^o}\times\mathcal{P}^o} \int_{\mathbb{R}^2\times\mathcal{P}^o} f(x,\xi,\xi_T,t_x\psi)\, \psi^{(2)}(d(x,\xi))\, P_Y^{(1)}(d(\psi,\xi)) \\ &= \frac{\lambda_2}{2\lambda_1}\int_{\mathsf{N}^2_{\mathcal{P}^o}\times\mathcal{P}^o} \int_{\mathbb{R}^2\times\mathcal{P}^o} f(-x,\xi,\xi_T,\psi)\, \psi^{(1)}(d(x,\xi))\, P_Y^{(2)}(d(\psi,\xi_T)). \end{aligned}$$

Notice that the factor $1/2$ appears here since each point X_n of X is located on one (and only one) segment of T. Thus, there are precisely two cells of T which have X_n on their boundary. Moreover, we decompose the outer integral in the latter expression into an integral with respect to P_T^* and an inner integral with

respect to $P_{T_{\widetilde{X}}|T^*}$. Thus, we can use the definition of the function f which is given in (4.4), and get

$$\mathbb{E}\, h(\Xi_X^*) = \frac{\lambda_2}{2\lambda_1}\, \mathbb{E}\left(\mathbb{E}\left(\int_{\partial\Xi_T^*\times\mathcal{P}^o} h(\xi)\, T_{\widetilde{X}}(d(x,\xi)) \mid T^*\right)\right). \tag{4.5}$$

We can now apply Lemma 4.2 which yields that the conditional expectation given T^* can be regarded as the expectation with respect to a non-stationary PVT which is induced by a Poisson process concentrated on the edges of T^* with linear intensity λ_ℓ. In particular, this means that for given T^* the number N of points of $\widetilde{X}$ on the boundary $\partial\Xi_T^*$ of the zero cell Ξ_T^* of T^* has a Poisson distribution with mean $\eta = \lambda_\ell \nu_1(\partial\Xi_T^*)$. For given T^* and $N = n$, it is well known that the locations of the n points are distributed according to a n-dimensional random vector $(Z_1, \ldots, Z_n)$ whose components are independent and uniformly distributed on $\partial\Xi_T^*$. Furthermore, the vector $(Z_1, \ldots, Z_n)$ is conditionally independent of those points of $\widetilde{X}$ that are not located on $\partial\Xi_T^*$.

Now let $\Xi_1^o, \ldots, \Xi_n^o$ denote the centered Voronoi cells of the (conditional) PVT whose nuclei are given by the points $Z_1, \ldots, Z_n$. Notice that the cells $\Xi_1, \ldots, \Xi_n$ are then identically distributed, but not independent. This gives

$$\begin{aligned}
\mathbb{E}\Big(\int_{\partial\Xi_T^*\times\mathcal{P}^o} h(\xi)\, T_{\widetilde{X}}(d(x,\xi)) \mid T^*\Big) &= \sum_{n=1}^{\infty} \mathbb{P}(N = n \mid T^*)\, \mathbb{E}\Big(\sum_{i=1}^{n} h(\Xi_i^o) \mid N = n,\, T^*\Big) \\
&= \sum_{n=1}^{\infty} \mathbb{P}(N = n \mid T^*)\, n\, \mathbb{E}\Big(h(\Xi_1^o) \mid N = n,\, T^*\Big) \\
&= \eta \sum_{n=1}^{\infty} \mathbb{P}(N = n-1 \mid T^*)\, \mathbb{E}\Big(h(\Xi_1^o) \mid N = n,\, T^*\Big) \\
&= \eta \sum_{n=0}^{\infty} \mathbb{P}(N = n \mid T^*)\, \mathbb{E}\Big(h(\Xi_1^o) \mid S = n+1,\, T^*\Big).
\end{aligned}$$

It holds that $\mathbb{E}\big(h(\Xi_1^o) \mid N = n+1,\, T^*\big) = \mathbb{E}\left(h(\Xi^o_{\widetilde{X}\cup\{Z\}}(Z)) \mid S = n,\, T^*\right)$, where $\Xi^o_{\widetilde{X}\cup\{Z\}}(Z)$ denotes the centered Voronoi cell around a random point $Z \in \partial\Xi_T^*$ with respect to the point process $\widetilde{X} \cup \{Z\}$. This additional random point Z is conditionally independent of $\widetilde{X}$ and conditionally uniformly distributed on $\partial\Xi_T^*$ given $N = n$ and T^*. Hence, using (4.5), we finally get that

$$\mathbb{E}\, h(\Xi_X^*) = \frac{\lambda_\ell \lambda_2}{2\lambda_1}\, \mathbb{E}\left(\nu_1(\partial\Xi_T^*)\, \mathbb{E}\left(h(\Xi^o_{\widetilde{X}\cup\{Z\}}(Z)) \mid T^*\right)\right).$$

Moreover, we have $\lambda_1 = \lambda_\ell \gamma$ and $\mathbb{E}\nu_1(\partial\Xi_T^*) = 2\gamma/\lambda_2$, see Theorem 3.1. Thus, the proof is completed. □

A representation formula similar to equation (4.3) can be derived for the typical segment system S_X^*. In the following theorem we use the same notation as in Theorem 4.3.

Theorem 4.4 *Let $h : \mathcal{L}^o \to [0,\infty)$ be measurable. Then,*

$$\mathbb{E}\, h(S_X^*) = \frac{1}{\mathbb{E}\, \nu_1(\partial \Xi_T^*)}\, \mathbb{E}\left(\nu_1(\partial \Xi_T^*)\, \mathbb{E}\left(h(\Xi^o_{\widetilde{X}\cup\{Z\}}(Z) \cap (T^{*(1)} - Z)) \mid T^*\right)\right), \quad (4.6)$$

where $T^{*(1)}$ is the edge set of the random tessellation T^*.

Proof The statement can be proven in the same way as Theorem 4.3 using the function $f : \mathbb{R}^2 \times \mathcal{L}^o \times \mathcal{P}^o \times \mathsf{N}_{\mathcal{L}^o,\mathcal{P}^o} \to [0,\infty)$ defined by

$$f(x,\zeta,\xi_T,\psi) = \begin{cases} h(\zeta) & \text{if } o \in \partial \xi_T + x, \\ 0 & \text{otherwise.} \end{cases} \quad (4.7)$$

□

Now we are able to construct the following indirect simulation algorithm for the typical Voronoi cell of Cox processes on PVT which is justified by Theorem 4.3. From now on we assume that the tessellation T is a PVT induced by a stationary Poisson process $X' = \{X'_n\}$ with intensity λ, Ξ_T^* is the typical cell of T and $h : \mathcal{P}^o \to [0,\infty)$ is some measurable function. Notice that we then have $\mathbb{E}\nu_1(\partial \Xi_T^*) = 4/\sqrt{\lambda}$, see Theorem 3.1.

1. Simulate a Poisson process $X' = \{X'_i\}$ radially with intensity λ and add the origin o to the points of X' which gives $X'^* = X' \cup \{o\}$.

2. Construct the Voronoi cell Ξ_T^* induced by X'^* around o.

3. Simulate a random variable $N \sim \mathrm{Poi}(\lambda_\ell \nu_1(\partial \Xi_T^*))$. Given $N = n$, place independent points $X_1, \ldots, X_n$ uniformly distributed on the boundary of Ξ_T^* and set $\widetilde{X} = \{X_1, \ldots, X_n\}$. Place one additional point Z uniformly distributed on $\partial \Xi_T^*$ independently of the other points.

4. Construct further edges of the Voronoi tessellation T^* induced by X'^* and place points X_i on the edges according to linear Poisson processes which are added to $\widetilde{X}$.

5. Construct the centered Voronoi cell $\Xi^o_{\widetilde{X}\cup\{Z\}}$ at Z with respect to $\widetilde{X} \cup \{Z\}$.

6. Weight $h(\Xi^o_{\widetilde{X}\cup\{Z\}})$ by $\nu_1(\partial \Xi_T^*)\sqrt{\lambda}/4$.

Finally, it is possible to obtain the distribution of $h(\Xi_X^*)$ using the weighted value $\sqrt{\lambda}/4\, \nu_1(\partial \Xi_T^*)\, h(\Xi^o_{\widetilde{X}\cup\{Z\}})$. In Figure 4.5 the different steps of the simulation algorithm are shown. Altogether, the direct and indirect simulation algorithms are similar, but now we have to construct a cell around the additional point Z. Thus we have to adjust the stopping criterion which has been used for the direct simulation algorithm. In particular, we have to choose the maximal radius as

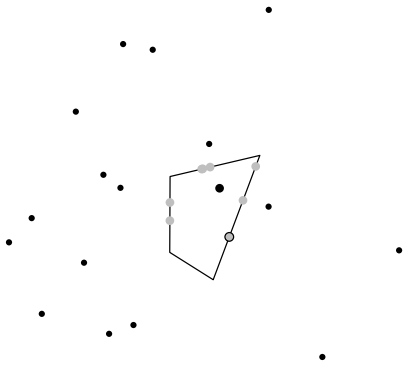

(a) Start: The cell around the origin is constructed, points (gray) of $\widetilde{X}$ are placed on the boundary and one further point Z (gray with black boundary) is added.

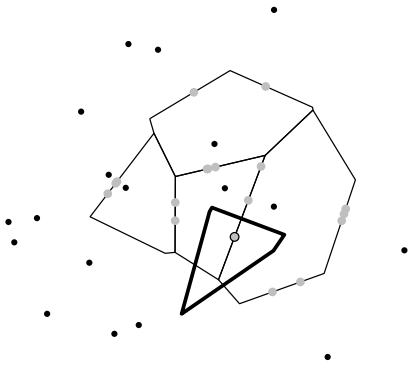

(b) Initial cell: The initial cell around Z is constructed using the previously simulated points (gray) of $\widetilde{X} \cup \{Z\}$.

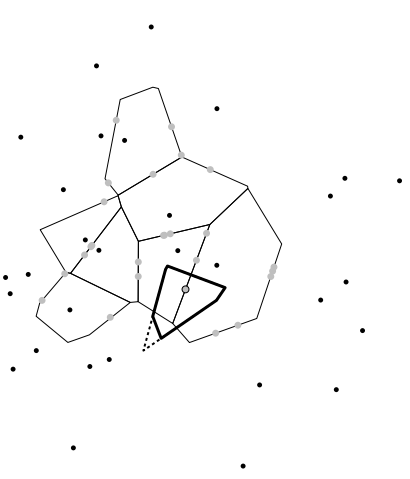

(c) Further points of $\widetilde{X}$ are simulated (gray) and the initial cell is intersected by the bisectors.

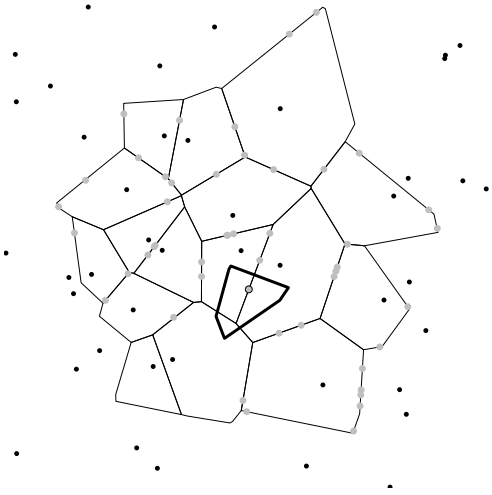

(d) The cell around Z is completed and the algorithm stops.

Figure 4.5: Indirect simulation of the typical cell of Cox processes on PVT

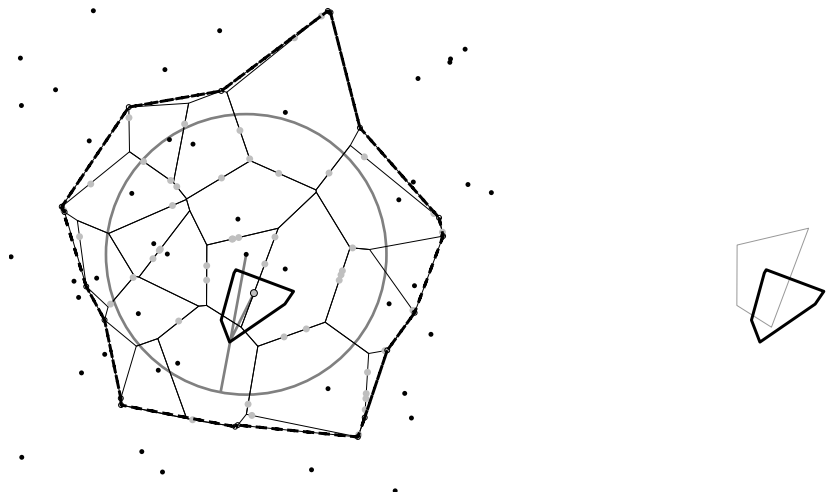

(a) Stopping criterion: If the circle (gray) is contained in the polygon of the outer vertices (dashed segments) the algorithm stops.

(b) Simulated cell (black) with typical cell (gray) of the PVT used for the weighting

Figure 4.6: Stopping criterion and simulated cell for the indirect algorithm

$r_{max} = \max_{i=1,\dots,m}(|v_i| + |v_i - Z|)$, where $\{v_i, i = 1, \dots, m\}$ denotes again the set of vertices of the initial cell, see also Figure 4.6. The final result of the indirect simulation algorithm is then a cell $\Xi^o_{\widetilde{X}\cup\{Z\}}$ which can be used in order to estimate distributional properties of the typical Voronoi cell Ξ^*_X of the Cox process X on the PVT T. Suppose that we regard independent copies $Y_1, \dots, Y_n$ of the random variable $\nu_1(\partial\Xi^*_T)h(\Xi^o_{\widetilde{X}\cup\{Z\}})$, then we define the estimator $\widehat{h(\Xi^*_X)}$ by

$$\widehat{h(\Xi^*_X)} = \frac{\sqrt{\lambda}}{4}\,\frac{1}{n}\sum_{i=1}^{n} Y_i \tag{4.8}$$

Using Theorem 4.3, it is easy to see that $\widehat{h(\Xi^*_X)}$ is unbiased and strongly consistent for $\mathbb{E}\,h(\Xi^*_X)$.

If we are interested in the typical segment system S^*_X inside the typical serving zone, then we can regard $\Xi^o_{\widetilde{X}\cup\{Z\}} \cap (T^{*(1)} - Z)$ and the weighting factor $\sqrt{\lambda}\nu_1(\partial\Xi^*_T)/4$. Let $h : \mathcal{L}^o \to [0, \infty)$ be a measurable function and assume that $Y_1, \dots, Y_n$ is an i.i.d. sample of $\nu_1(\partial\Xi^*_T)\, h(\Xi^o_{\widetilde{X}\cup\{Z\}} \cap (T^{*(1)} - Z))$. Then, using Theorem 4.4, we get that

$$\widehat{h(S^*_X)} = \frac{\sqrt{\lambda}}{4}\,\frac{1}{n}\sum_{i=1}^{n} Y_i \tag{4.9}$$

is an unbiased and strongly consistent estimator for the expectation $\mathbb{E}h(S^*_X)$.

4.3 Typical Voronoi cell of Cox processes on PDT

In this section we introduce a simulation algorithm for the typical Voronoi cell of Cox processes on PDT. More precisely, we derive an indirect simulation algorithm for the typical Voronoi cell of Cox processes on random tessellations which is applicable if the underlying tessellation can be simulated starting from the typical vertex. This algorithm is similar to the indirect simulation algorithm introduced in the preceding section which can be used if the underlying tessellation can be simulated starting from the typical cell. In particular, we derive an algorithm for the simulation of random cells from which all distributional properties of the typical Voronoi cell Ξ_X^* of Cox processes on PDT together with its typical segment system S_X^* can be computed by a subsequent weighting.

Assume that T is an arbitrary stationary tessellation with length intensity γ and X a Cox process on T with linear intensity λ_ℓ. Recall that T can be identified with the stationary marked point processes $\{(V_n, E_n^o)\}$ with mark space $\mathcal{L}^o$, where $\{V_n\}$ denotes the (unmarked) point process of vertices of T and E_n^o denotes the centered edge star corresponding to V_n. Thus, $E_n = E_n^o + V_n$ denotes the system of edges emanating from the vertex V_n, see Section 3.2.1. Furthermore, we can identify the Voronoi tessellation T_X induced by X with the marked point process $\{(X_n, \Xi_n^o)\}$ with mark space $\mathcal{P}^o$, where Ξ_n^o denotes the centered cell at X_n. In the same way as in the preceding section, we define the vector $Y = (T_X, T)$ which can be regarded as a random element of $\mathsf{N}_{\mathcal{P}^o,\mathcal{L}^o}$ and we can consider the Palm distributions $P_Y^{(i)}$ of Y with respect to the i-th component, see Section 2.3.4.

Let $(T_{\widetilde{X}}, T^*)$ denote the vector of marked point processes distributed according to the Palm distribution $P_Y^{(2)}$ with respect to $\{(V_n, E_n^0)\}$. Thus, $T_{\widetilde{X}}$ is a Voronoi tessellation induced by a point process $\widetilde{X}$ on the edges of the Palm version T^* of T with respect to $\{(V_n, E_n^o)\}$. It can be shown that $\widetilde{X}$ is a Cox process on T^* with linear intensity λ_ℓ.

Lemma 4.5 *The point process $\widetilde{X}$ is a (non-stationary) Cox process in $\mathbb{R}^2$ whose random intensity measure is given by $\Lambda_{\widetilde{X}}(B) = \lambda_\ell \nu_1(B \cap T^{*(1)})$ for $B \in \mathcal{B}(\mathbb{R}^2)$, where $T^{*(1)}$ is the edge set of T^*.*

Proof The lemma can be proven in the same way as Lemma 4.2. □

Now let E^* denote the typical edge star of T^*, i.e., the union of edges of T^* emanating from the origin. Using the notation introduced above, we can state the following theorem.

Theorem 4.6 *Let $h : \mathcal{P}^o \to [0, \infty)$ be a measurable function. Then*

$$\mathbb{E}h(\Xi_X^*) = \frac{1}{\mathbb{E}\,\nu_1(E^*)} \mathbb{E}\left(\nu_1(E^*)\, h(\Xi^o_{\widetilde{X}\cup\{Z\}}(Z))\right), \tag{4.10}$$

where $\widetilde{X}$ denotes the Cox process concentrated on the edge set $T^{*(1)}$ of T^* with linear intensity λ_ℓ and $\Xi^o_{\widetilde{X}\cup\{Z\}}(Z)$ denotes the centered Voronoi cell around an

additional point $Z \in E^*$ with respect to $\widetilde{X} \cup \{Z\}$. This point Z is conditionally uniformly distributed on E^* and conditionally independent of $\widetilde{X}$ given T^*.

Proof We define the function $f : \mathbb{R}^2 \times \mathcal{P}^o \times \mathcal{L}^o \times \mathsf{N}_{\mathcal{P}^o,\mathcal{L}^o} \to [0,\infty)$ by

$$f(x,\xi,\zeta,\psi) = \begin{cases} h(\xi) & \text{if } o \in \partial\zeta + x, \\ 0 & \text{otherwise,} \end{cases} \tag{4.11}$$

In the same way as in the proof of Theorem 4.3 we get

$$\mathbb{E}h(\Xi_X^*) = \frac{1}{2}\int_{\mathsf{N}_{\mathcal{P}^o,\mathcal{L}^o\times\mathcal{P}}} \int_{\mathbb{R}^2\times\mathcal{L}^o} f(x,\xi,\zeta,t_x\psi)\,\psi^{(2)}(d(x,\zeta))\,P_Y^{(1)}(d(\psi,\xi))\,,$$

since there are exactly two edge stars which contain the origin. Now we can apply Lemma 2.9 and use the same arguments as in the proof of Theorem 4.3 above in order to obtain

$$\mathbb{E}\,h(\Xi_X^*) = \frac{\lambda_\ell \lambda^{(0)}}{2\lambda}\,\mathbb{E}\left(\nu_1(E^*)\left(h(\Xi^o_{\widetilde{X}\cup\{Z\}}(Z))\right)\right), \tag{4.12}$$

where $\lambda^{(0)}$ denotes the intensity of the point process $\{V_n\}$ and λ is the spatial intensity of X. Moreover, it holds that $\lambda = \lambda_\ell\gamma$ and $\mathbb{E}\nu_1(E^*) = 2\gamma/\lambda^{(0)}$, see Theorem 3.1, which completes the proof. □

Notice that a formula which is similar to (4.10) is valid for the typical segment system S_X^*.

Theorem 4.7 *For each measurable function $h : \mathcal{L}^o \to [0,\infty)$ we have*

$$\mathbb{E}h(S_X^*) = \frac{1}{\mathbb{E}\,\nu_1(E^*)}\mathbb{E}\left(\nu_1(E^*)\,h(\Xi^o_{\widetilde{X}\cup\{Z\}}(Z)\cap(T^{*(1)}-Z))\right). \tag{4.13}$$

Proof The arguments of the proof of Theorem 4.6 can be used in the same way as above if we mark each point of $X = \{X_n\}$ with the centered segment system $S_n^o = (\Xi_n \cap T^{(1)}) - X_n$ inside its Voronoi cell. Then we can regard $Y = (T_X, T)$ as a random element of $\mathsf{N}_{\mathcal{L}^o,\mathcal{L}^o}$ and define $f : \mathbb{R}^2 \times \mathcal{L}^o \times \mathcal{L}^o \times \mathsf{N}_{\mathcal{L}^o,\mathcal{L}^o} \to [0,\infty)$ by

$$f(x,\xi,\zeta,\psi) = \begin{cases} h(\xi) & \text{if } o \in \partial\zeta + x, \\ 0 & \text{otherwise.} \end{cases} \tag{4.14}$$

Now exactly the same arguments as above can be used in order to complete the proof. □

Theorem 4.6 and Slivnyak's theorem can be used in order to obtain the following indirect simulation algorithm for the typical Voronoi cell of a Cox process X with linear intensity λ_ℓ on a PDT T. In the following, we regard $T = \{(V_n, E_n^o)\}$ as the point process of vertices marked with the edge stars. Furthermore, we use the

notation V for the stationary Poisson process of intensity λ which induces T and denote the Palm versions of T and V by T^* and V^*, respectively. Now assume that $h : \mathcal{P}^o \to [0, \infty)$ is some measurable function, then the following simulation algorithm can be constructed.

1. Simulate a Poisson process $V = \{V_n\}$ radially with intensity λ, add the origin o to V, i.e., $V^* = V \cup \{o\}$.

2. Construct the edge star E^* of the tessellation T^* induced by V^* at o.

3. Simulate a random variable $N \sim \mathrm{Poi}(\lambda_\ell \nu_1(E^*))$. Given $N = n$, place independent points $X_1, \ldots, X_n$ uniformly distributed on E^* and set $\widetilde{X} = \{X_1, \ldots, X_n\}$. Place one additional point Z independent of $\widetilde{X}$ uniformly distributed on $\partial \Xi_T^*$.

4. Construct further edges of T^* based on points of V^* and place points X_i on the edges according to linear Poisson processes. Add X_i to $\widetilde{X}$.

5. Construct the Voronoi cell $\Xi^o_{\widetilde{X} \cup \{Z\}}$ around Z with respect to $\widetilde{X}$.

6. Weight $h(\Xi^o_{\widetilde{X} \cup \{Z\}})$ by $\nu_1(E^*) 3\pi\sqrt{\lambda}/64$.

Then we can estimate the distribution of $h(\Xi_X^*)$ using the weighted quantity $\nu_1(E^*) 3\pi\sqrt{\lambda}/64\, h(\Xi^o_{\widetilde{X} \cup \{Z\}})$. The weighting factor which appears here is due to the fact that $\mathbb{E}\nu_1(E^*) = 64/(3\pi\sqrt{\lambda})$ if E^* is the typical edge star of a PDT induced by a Poisson process with intensity λ, see Section 3.4.

An overview of the different steps is shown in Figure 4.7. Naturally some details have to be considered which are briefly summarized below. Note that the algorithm is similar to the indirect algorithm explained in Section 4.2.2. We generate the Delaunay triangles of T^* and place points X_n on the new edges in an alternating fashion, where the points of V^* are simulated radially. At the beginning, the points of V^* are simulated until the edge star E^* at o with respect to V^* can be constructed. Now points X_n are placed on the edges of E^* including one additional point Z. Then further points of V^* are simulated, the corresponding Delaunay cells are constructed and points of $\widetilde{X}$ are placed on the new edges until an initial cell around Z can be generated from the already simulated points of $\widetilde{X}$. If the initial cell is constructed, we can use the stopping criterion already used in Section 4.2.2. Since the typical cell is contained in the initial cell, only points X_n of $\widetilde{X}$ inside the ball $B(o, r_{max})$ can influence the typical cell, where $r_{max} = \max_{i=1,\ldots,m}(|v_i| + |v_i - Z|)$. Here $\{v_i, i = 1, \ldots, m\}$ is again the set of vertices of the initial cell. If the ball $B(o, r_{max})$ is contained in the polygon of the already simulated Delaunay cells, then we can stop the simulation, see also Figure 4.7 (d). Like for Cox processes on PVT, we can use

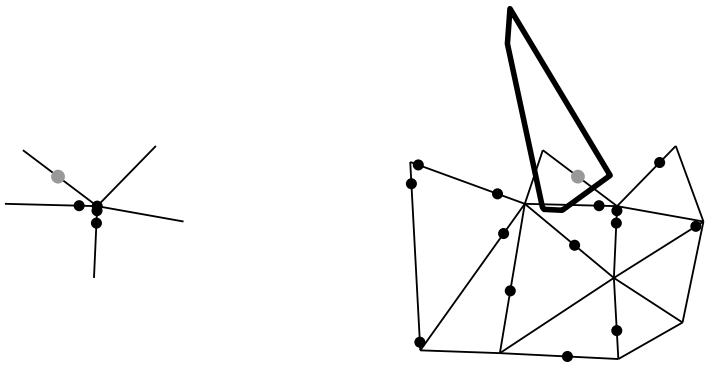

(a) Typical edge star E^* is generated and points are placed on its edges including an additional point Z (gray).

(b) The initial Voronoi cell around Z is constructed using those points of $\widetilde{X}$ which were simulated until this step.

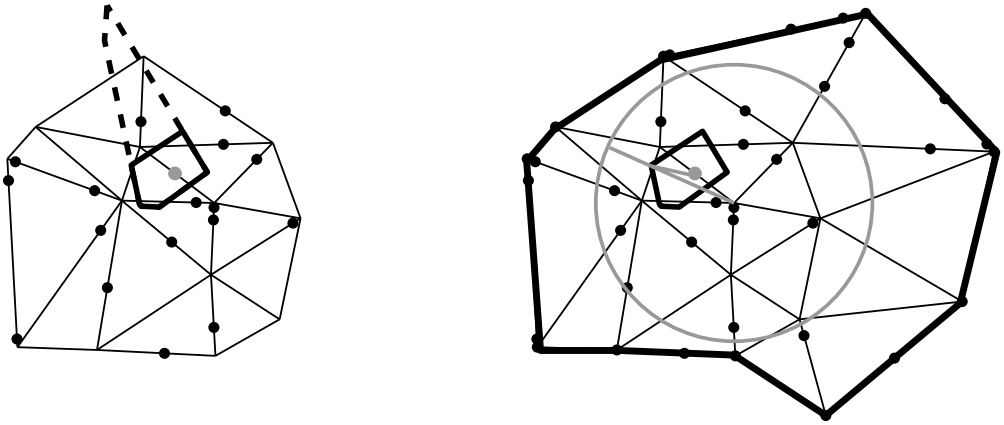

(c) Further points of $\widetilde{X}$ are simulated and the initial cell is intersected by their bisectors.

(d) The Voronoi cell around Z is completed and the algorithm stops if the circle with radius r_{max} (gray circle) is contained in the polygon of outer vertices (thick segments).

Figure 4.7: Indirect simulation of the typical cell of Cox processes on PDT

i.i.d. samples $Y_1, \ldots, Y_n$ of $\nu_1(E^*)\, h(\Xi^o_{\widetilde{X}\cup\{Z\}})$ in order compute the unbiased and consistent estimator $\widehat{h(\Xi^*_X)} = 3\pi\sqrt{\lambda}/64 \sum_{i=1}^n Y_i$ for $\mathbb{E}\, h(\Xi^*_X)$.

Now assume that we are interested in the simulation of the typical segment system S^*_X. Then we can consider $\Xi^o_{\widetilde{X}\cup\{Z\}} \cap (T^{*(1)} - Z)$ together with the weighting

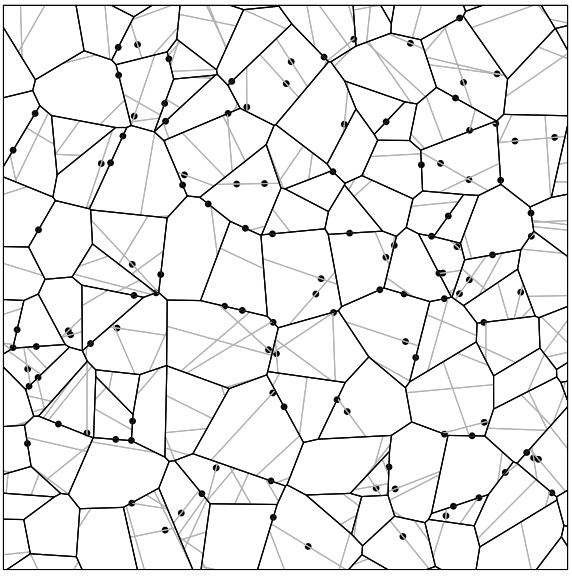

Figure 4.8: Cox process (black points) on an iterated tessellation with PVT (black) and PLT (gray) as T_0 and T_1

factor $\nu_1(E^*)3\pi\sqrt{\lambda}/64$. For every measurable function $h : \mathcal{L}^o \to [0,\infty)$ we can use i.i.d. samples of $\nu_1(E^*)3\pi\sqrt{\lambda}/64\, h(\Xi_{\widetilde{X}\cup\{Z\}} \cap T^{*(1)})$ in order to estimate $\mathbb{E}h(S_X^*)$ without bias by the sample mean, see Theorem 4.7 .

4.4 Typical Voronoi cell of Cox processes on nested tessellations

In this section we assume that $X = \{X_n\}$ is a Cox process with linear intensity λ_ℓ on a stationary iterated random tessellation T. More precisely, we assume that T is given by a nesting with initial tessellation T_0 and i.i.d. component tessellations $T_1, T_2, \ldots$ which are independent of T_0. Recall that the edge set of T is then defined by $T^{(1)} = \bigcup_{n=1}^{\infty} \partial\Xi_{0n} \cup (\Xi_{0n} \cap T_n^{(1)})$, where $\Xi_{01}, \Xi_{02}, \ldots$ are the cells of T_0. In particular, Ξ_{01} denotes the so–called zero cell of the initial tessellation T_0, i.e., the cell of T_0 which contains the origin. Furthermore, we assume that the inner structure of Ξ_{01} is given by $\Xi_{01} \cap T_1$. For brevity, we use the notation $T = \tau(T_0 \mid T_1, T_2, \ldots)$ for a nested tessellation induced by the initial tessellation T_0 and the independent component tessellations $T_1, T_2, \ldots$. Note that $T = \tau(T_0 \mid T_1, T_2, \ldots)$ is stationary with length intensity $\gamma = \gamma_0 + \gamma_1$ if T_0 is stationary with length intensity γ_0 and T_1 is stationary with length intensity γ_1.

A realization of a Cox process together with the underlying iterated tessellation is displayed in Fig. 4.8.

4.4.1 Representation formula for the Palm version $\widetilde{T}$ of T

Recall that the typical Voronoi cell Ξ_X^* of X can be regarded as the Voronoi cell at the origin induced by $X^* = \widetilde{X} \cup \{o\}$, where $\widetilde{X}$ is a Cox process with linear intensity λ_ℓ on the Palm version $\widetilde{T}$ of T seen as the random measure $\nu_1(\,\cdot \cap T^{(1)})$. Thus, in order to simulate Ξ_X^* we have to simulate first $\widetilde{T}$. In the following, we derive a representation formula for $\widetilde{T}$ which is suitable to construct simulation algorithms for $\widetilde{T}$. This formula is based on the stationary random tessellations T_0 and T_1 as well as their Palm versions $\widetilde{T}_0$ and $\widetilde{T}_1$. In particular, it is shown that the distribution of $\widetilde{T}$ can be expressed by the distributions of the iterated tessellations $\tau(\widetilde{T}_0 \mid T_1, T_2, \ldots)$ and $\tau(T_0 \mid \widetilde{T}_1, T_2, T_3, \ldots)$. In the latter case, the zero-cell Ξ_{01} of the initial tessellation T_0 is subdivided by the component tessellation $\widetilde{T}_1$ whereas the other cells of T_0 are subdivided by $T_2, T_3, \ldots$, respectively. This representation formula is suitable to derive simulation algorithms for $\widetilde{T}$ if T is a nestings of PDT, PLT and PVT, respectively, since in all cases simulation algorithms for $\widetilde{T}_0$ and $\widetilde{T}_1$ have been developed above.

Theorem 4.8 *For any measurable function $h : \mathbb{T} \to [0, \infty)$, it holds that*

$$\mathbb{E}h(\widetilde{T}) = \frac{\gamma_0}{\gamma}\, \mathbb{E}h(\tau(\widetilde{T}_0 \mid T_1, T_2, \ldots)) + \frac{\gamma_1}{\gamma}\, \mathbb{E}h(\tau(T_0 \mid \widetilde{T}_1, T_2, T_3, \ldots))\,. \tag{4.15}$$

Proof We can use the definition of the Palm distribution of the random measure $\nu_1(\,\cdot \cap T^{(1)})$ in order to write $\mathbb{E}h(\widetilde{T})$ as

$$\begin{aligned}\mathbb{E}h(\widetilde{T}) &= \frac{1}{\gamma}\, \mathbb{E}\Big[\int_{T^{(1)}\cap[0,1]^2} h(T-x)\, \nu_1(dx)\Big] \\ &= \frac{\gamma_0}{\gamma}\left[\frac{1}{\gamma_0}\mathbb{E}\int_{T_0^{(1)}\cap[0,1]^2} h(T-x)\, \nu_1(dx)\right] + \frac{\gamma_1}{\gamma}\left[\frac{1}{\gamma_1}\mathbb{E}\sum_{i=1}^{\infty}\int_{T_i^{(1)}\cap\Xi_{0i}\cap[0,1]^2} h(T-x)\, \nu_1(dx)\right],\end{aligned}$$

Furthermore, we can use that $T_0, T_1, T_2, \ldots$ are stationary and independent to get that

$$\begin{aligned}&\frac{1}{\gamma_0}\, \mathbb{E}\Big[\int_{T_0^{(1)}\cap[0,1]^2} h(T-x)\, \nu_1(dx)\Big] \\ &\quad= \frac{1}{\gamma_0}\, \mathbb{E}\Big[\int_{T_0^{(1)}\cap[0,1]^2} h(\tau(T_0 - x \mid T_1 - x, T_2 - x, \ldots))\, \nu_1(dx)\Big] \\ &\quad= \frac{1}{\gamma_0}\, \mathbb{E}\Big[\int_{T_0^{(1)}\cap[0,1]^2} h(\tau(T_0 - x \mid T_1, T_2, \ldots))\, \nu_1(dx)\Big] \\ &\quad= \mathbb{E}h(\tau(\widetilde{T}_0 \mid T_1, T_2, \ldots))\,,\end{aligned}$$

where the last equality is a consequence from the definition of the Palm distribution of $\nu_1(\,\cdot \cap T_0^{(1)})$. Thus, it remains to show that

$$\mathbb{E}h(\tau(T_0 \mid \widetilde{T}_1, T_2, T_3, \ldots)) = \frac{1}{\gamma_1}\mathbb{E}\Big[\sum_{i=1}^{\infty}\int_{T_i^{(1)}\cap\Xi_{0i}\cap[0,1]^2} h(T-x)\, \nu_1(dx)\Big]. \tag{4.16}$$

In the following we use the notation $\mathbb{E}_{T_i}$, $\mathbb{E}_{T_0,T_i}$ and $\mathbb{E}_{\{T_j\}}$ if expectation is taken with respect to one single tessellation T_i, two tessellations T_0 and T_i, or the infinite sequence of tessellations $\{T_j\}$, respectively. Since the tessellations $T_0, T_1, T_2, \ldots$ are independent and stationary, we get that

$$\begin{aligned}
&\mathbb{E}\Big[\sum_{i=1}^{\infty}\int_{T_i^{(1)}\cap\Xi_{0i}\cap[0,1]^2} h(T-x)\,\nu_1(dx)\Big]\\
&\quad=\sum_{i=1}^{\infty}\mathbb{E}_{T_0,T_i}\Big[\int_{T_i^{(1)}\cap[0,1]^2}\mathbb{E}_{\{T_j\}_{j\neq i}}\Big[\mathbb{1}_{\Xi_{0i}}(x)h(\tau(T_0-x\mid T_1-x,T_2-x,\ldots))\Big]\nu_1(dx)\Big]\\
&\quad=\sum_{i=1}^{\infty}\mathbb{E}\Big[\int_{T_1^{(1)}\cap[0,1]^2}\mathbb{1}_{\Xi_{0i}-x}(o)\,h(\tau(T_0-x\mid T_1-x,T_2,T_3,\ldots))\,\nu_1(dx)\Big],
\end{aligned}$$

where T_1-x is the component tessellation which subdivides the zero cell of the shifted tessellation T_0-x for each $x\in\Xi_{0i}$. Moreover, we have

$$\begin{aligned}
&\sum_{i=1}^{\infty}\mathbb{E}\Big[\int_{T_1^{(1)}\cap[0,1]^2}\mathbb{1}_{\Xi_{0i}-x}(o)\,h(\tau(T_0-x\mid\ T_1-x,T_2,T_3,\ldots))\,\nu_1(dx)\Big]\\
&\qquad=\mathbb{E}\Big[\int_{T_1^{(1)}\cap[0,1]^2}\sum_{i=1}^{\infty}\mathbb{1}_{\Xi_{0i}}(x)h(\tau(T_0-x\mid T_1-x,T_2,T_3,\ldots))\,\nu_1(dx)\Big]\\
&\qquad=\mathbb{E}\Big[\int_{T_1^{(1)}\cap[0,1]^2}h(\tau(T_0-x\mid T_1-x,T_2,T_3,\ldots))\,\nu_1(dx)\Big],
\end{aligned}$$

where we used that $\sum_{i=1}^{\infty}\mathbb{1}_{\Xi_{0i}}(x)=1$. Finally,

$$\begin{aligned}
&\mathbb{E}\Big[\int_{T_1^{(1)}\cap[0,1]^2}h(\tau(T_0-x\mid T_1-x,T_2,T_3,\ldots))\,\nu_1(dx)\Big]\\
&\qquad=\mathbb{E}_{\{T_j\}_{j\geq1}}\Big[\int_{T_1^{(1)}\cap[0,1]^2}\mathbb{E}_{T_0}\big[h(\tau(T_0-x\mid T_1-x,T_2,T_3,\ldots))\big]\,\nu_1(dx)\Big]\\
&\qquad=\mathbb{E}_{\{T_j\}_{j\geq1}}\Big[\int_{T_1^{(1)}\cap[0,1]^2}\mathbb{E}_{T_0}\big[h(\tau(T_0\mid T_1-x,T_2,T_3,\ldots))\big]\,\nu_1(dx)\Big]\\
&\qquad=\mathbb{E}_{T_0,\{T_j\}_{j\geq2}}\mathbb{E}_{T_1}\Big[\int_{T_1^{(1)}\cap[0,1]^2}h(\tau(T_0\mid T_1-x,T_2,T_3,\ldots))\nu_1(dx)\Big]\\
&\qquad=\gamma_1\mathbb{E}\big[h(\tau(T_0\mid\widetilde{T}_1,T_2,T_3,\ldots))\big],
\end{aligned}$$

where the last equality is a consequence of Theorem 2.13. Thus, the proof is completed. □

We can interpret equation (4.15) in the following way. A point of X is located on $T_0^{(1)}$ with probability γ_0/γ and on one of the edge sets of the tessellations $T_1, T_2, T_3, \ldots$ with the complementary probability γ_1/γ since the ratio of edge

lengths of the initial and component tessellations is γ_0/γ_1. Thus, the random tessellations $\tau(\widetilde{T}_0 \mid T_1, T_2, \ldots)$ and $\tau(T_0 \mid \widetilde{T}_1, T_2, T_3, \ldots)$ which are considered in (4.15) can be regarded as conditional versions of $\widetilde{T}$ under the condition that the origin is located on an edge of the initial tessellation and a component tessellation, respectively. These events occur with probabilities γ_0/γ and γ_1/γ, respectively. Using this interpretation, we can directly construct a simulation algorithm for $\widetilde{T}$ and hence X^* if $T_0, T_1, \widetilde{T}_0$ and $\widetilde{T}_1$ can be simulated.

4.4.2 The simulation algorithm

The representation formula for $\widetilde{T}$ given in Theorem 4.8 leads to a simulation algorithm of $\widetilde{T}$ and hence X^* if simulation algorithms for both T_0 and T_1 as well as their Palm versions $\widetilde{T}_0$ and $\widetilde{T}_1$ are available. This is the case if T_j, $j = 0, 1$ is a PVT, PLT or PDT, respectively, see the preceding sections. In particular, the remark after Theorem 4.8 directly yields the following simulation algorithm for the Palm version X^* of the stationary Cox process X on T. The main steps are summarized below.

1. Simulate a random variable $U \sim U[0, 1]$. If $U < \gamma_0/\gamma$, go to step 2, else go to step 3.

2. Simulate $\widetilde{T}_0 = \{\widetilde{\Xi}_{0n}\}$ and $T_1, T_2, \ldots$ independent from each other and subdivide the cells $\widetilde{\Xi}_{01}, \widetilde{\Xi}_{02}, \ldots$ by $T_1, T_2, \ldots$, respectively, which yields $\widetilde{T}$.

3. Simulate $T_0 = \{\Xi_{0n}\}$ and $\widetilde{T}_1, T_2, T_3, \ldots$ independent from each other, subdivide the zero cell Ξ_{01} of T_0 by $\widetilde{T}_1$ and subdivide the cells $\Xi_{02}, \Xi_{03}, \ldots$ of T_0 by $T_2, T_3, \ldots$, which yields $\widetilde{T}$.

4. Construct $X^* = \{o\}$ and place further points of X^* onto each edge of $\widetilde{T}$ as linear Poisson processes with linear intensity λ_ℓ.

5. Construct the Voronoi cell Ξ_X^* around o induced by X^*.

6. Construct $S_X^* = \Xi_X^* \cap \widetilde{T}^{(1)}$.

Then Ξ_X^* and S_X^* are the typical Voronoi cell and its typical segment system for a Cox process X on T.

In order to implement the algorithm above we have to consider some technical details. The random tessellation T_0 and $\widetilde{T}_0$, respectively, are simulated radially, i.e., their cells are constructed with increasing distance to the origin. If T_0 is e.g. a PVT, then the simulation algorithms in Section 4.1.1 and 4.2 can be applied in order to generate the underlying point process of the Voronoi tessellations T_0 and $\widetilde{T}_0$, respectively. Each generated cell is then independently subdivided and points of X^* are placed on each new generated edge according to linear

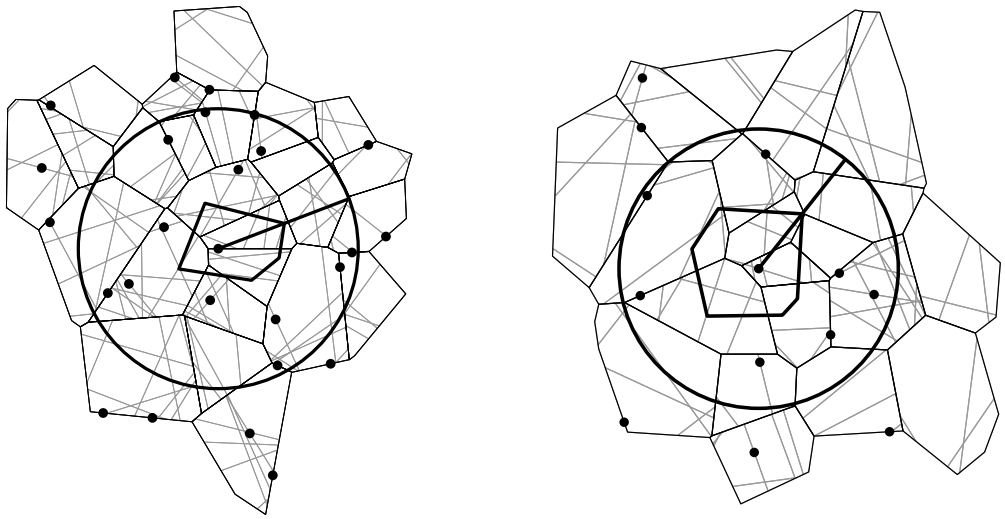

(a) Origin on initial tessellation (b) Origin on component tessellation

Figure 4.9: Simulated typical cell for PVT/PLT–nesting together with $B(o, r_{max})$

Poisson processes. If an initial cell Ξ_X^* is constructed, the following stopping criterion can be used. Let $r_{max} = 2\max_{i=1,\dots,m} |v_i|$, where $\{v_i, i = 1\dots, m\}$ is the set of vertices of the initial cell. Then we stop the simulation if all cells of T_0 and $\widetilde{T}_0$, respectively, which intersect $B(o, r_{max})$ are already generated and subdivided since only points of X^* on these segments can influence the typical cell. If the stopping criterion is not fulfilled, then we simulate further points of X^*, intersect Ξ_X^* with the corresponding bisectors and update r_{max} until we can stop the algorithm. Realizations of the simulation algorithm are shown in Figure 4.9 for a Cox process on a PVT/PLT–nesting. The resulting cell Ξ_X^* is then the typical Voronoi cell of X and $S_X^* = \Xi_X^* \cap \widetilde{T}^{(1)}$ is the typical segment system.

Note that Theorem 4.6 has to be used in order to generate $\widetilde{T}_0$ and $\widetilde{T}_1$ if T_0 and T_1 is a PDT, respectively.

4.5 Typical Voronoi cell for thinned vertex sets

We now consider another type of point processes X on the edges of random tessellations. In particular, we regard the point process which consists of the independently thinned set of vertices $V = \{V_n\}$ of the tessellation T. Thus, each point V_n of V survives with probability $p \in (0, 1)$ independently of all other points. In the following, we concentrate on the case that T is a PDT, PLT and PVT, respectively. Then we can again construct simulation algorithms for the typical cell Ξ_X^* and the segment system S_X^* within it. In this section, T^* is always distributed according to the Palm distribution with respect to V, i.e., we identify

T with $\{(V_n, E_n^o)\}$ and regard the Palm version T^* of $\{(V_n, E_n^o)\}$. Recall that the Palm version of a p-thinning of V is obtained by a p-thinning of the vertices of the Palm version T^*, where all vertices of T^* are independently thinned according to the survival probability p, but the origin survives almost surely, see Section 3.5.3.

We briefly summarize the algorithms below and omit some technical details which are similar as in the case of Cox processes.

4.5.1 Vertices of PDT

Let T be a PDT induced be the stationary Poisson process V with intensity λ. Thus, the vertices of T are given by V. Then, due to Slivnyak's theorem, we get that T^* is the Delaunay tessellation with respect to the point process $V^* = V \cup \{o\}$ and hence Ξ_X^* and S_X^* can be simulated in the following way.

1. Simulate a stationary Poisson process $V = \{V_n\}$ radially, set $V^* = V \cup \{o\}$ and construct the Delaunay tessellation T^* with respect to V^*.

2. Define $X^* = \{o\}$ and add each point V_i to X^* if $U_i < p$, where $U_1, U_2, \ldots$ are i.i.d. with $U_i \sim U[0, 1)$.

3. Generate the Voronoi cell Ξ_X^* at o with respect to X^*.

4. Construct $S_X^* = T^{*(1)} \cap \Xi_X^*$.

Again, we first have to generate an initial cell. If the initial cell is constructed, we simulate further points of X^* and intersect the initial cell with the corresponding bisectors until $|V_n| > r_{max} = 2 \max_{i=1,\ldots,n} |v_i|$, where $\{v_i, i = 1, \ldots, m\}$ are the vertices of the initial cell. However, if we are interested in S_X^*, then it may happen that further points of V^* have to be simulated until all segments which intersect Ξ_X^* are constructed. Note that a p-thinning of a stationary Poisson process with intensity λ is a Poisson process whose intensity is given by $p\lambda$. Thus, the resulting cell Ξ_X^* of this simulation algorithm is the typical cell of a PVT induced by a stationary Poisson of intensity $p\lambda$.

4.5.2 Vertices of PLT

Now assume that T is a PLT. We have to simulate the tessellation T^* distributed according to the Palm distribution with respect to the vertices V of T, i.e., under the condition that there are two lines through the origin. It is well–known that the angle Φ between the two lines ℓ_1 and ℓ_2 at the typical point of V is distributed according to the density $f_\Phi(x) = \sin(x)/2$ for $x \in [0, \pi)$, see e.g. [65]. Moreover, the lines ℓ_1 and ℓ_2 are isotropic since T is isotropic. Using these considerations, we can simulate Ξ_X^* and S_X^* as follows.

1. Simulate two angles $\Phi_1 \sim U[0,\pi)$ and $\Phi \sim f_\Phi$ independently from each other and generate the lines ℓ_1 and ℓ_2 through o with angles Φ_1 and $\Phi_2 = \Phi_1 + \Phi$, respectively.

2. Simulate a stationary and isotropic Poisson line process $\{\ell_3, \ell_4, \ldots\}$ radially which is independent of ℓ_1 and ℓ_2. Then define T^* as the tessellation induced by $\{\ell_1, \ell_2, \ell_3, \ldots\}$.

3. Construct V^* as the union of all intersection points $\ell_j \cap \ell_k$ in $\mathbb{R}^2 \backslash \{o\}$ of line pairs $\ell_j, \ell_k \in \{\ell_1, \ell_2, \ell_3, \ldots\}$ with $j \neq k$.

4. Define $X^* = \{o\}$ and add the i-th point of V^* to X^* if $U_i < p$, where $U_1, U_2, \ldots$ are i.i.d. with $U_i \sim U[0,1)$.

5. Construct the Voronoi cell Ξ_X^* at o induced by X^*.

6. Construct $S_X^* = T^{*(1)} \cap \Xi_X^*$.

As always, we generate points of V^* until an initial cell can be constructed. Then we generate further points and intersect the initial cell with the corresponding bisectors. The simulation stops if the distance to the origin from the last simulated line is larger than $r_{max} = 2\max_{i=1,\ldots,n} |v_i|$, where $v_i, i = 1, \ldots, m$ are the vertices of the initial cell. The resulting cell Ξ_X^* and the segment system S_X^* are then the typical Voronoi cell and typical segment system, respectively, of a p-thinning of the vertices of T.

4.5.3 Vertices of PVT

Finally, if T is a PVT, we can proceed in the following way. Since PVT and PDT are dual tessellations we get that the dual tessellation of T^* is a PDT with respect to the Palm distribution of its nuclei. This means that we can simulate a PDT starting from its typical cell and then generate the dual tessellation in order to obtain T^*. Note that the distribution of the typical cell Ξ_D^* of a PDT is explicitly known, see [71] and [87], Theorem 10.4.4. Let $Y_1 = RZ_1, Y_2 = RZ_2$ and $Y_3 = RZ_3$ denote the three vertices of Ξ_D^*, where the random variables $Z_i, i = 1,2,3$ are unit vectors which we identify with their polar angles. Then random radius R is distributed according to the density f_R given by $f_R(r) = 2\lambda^2\pi^2 r^3 \exp(-\lambda\pi r^2)$ for $r \geq 0$ and the joint density of (Z_1, Z_2, Z_3) is given by $\nu_2(\mathrm{conv}\{z_1, z_2, z_3\})/(12\pi^2)$ for $z_1, z_2, z_3 \in [0, 2\pi)^3$. These results yield the following simulation algorithm for Ξ_X^* and S_X^*.

1. Simulate the three points $Y_1 = RZ_1, Y_2 = RZ_2$ and $Y_3 = RZ_3$. Given R, simulate an independent and stationary Poisson process $\{Y_4, Y_5, \ldots\}$ of intensity λ radially in $\mathbb{R}^2 \backslash B(o,R)$.

2. Generate T^* as the Voronoi tessellation with respect to $\{Y_n\}$.

3. Define $X^* = \{o\}$ and add each vertex $V_i \neq o$ of T^* to X^* if $U_i < p$, where $U_1, U_2, \ldots$ are i.i.d. with $U_i \sim U[0,1)$.

4. Construct the Voronoi cell Ξ_X^* at o with respect to X^*.

5. Construct $S_X^* = T^{*(1)} \cap \Xi_X^*$.

Note that we can use here the same stopping criterion as in the simulation algorithm for the typical cell of Cox process on the edges of PVT. The resulting cell Ξ_X^* and the segment system S_X^* are then distributed as the typical cell and the typical segment system of a p-thinning of the vertices of a PVT, respectively..

4.6 Numerical results obtained by Monte Carlo simulation

In this section we present some results which were obtained from Monte–Carlo simulation using the algorithms introduced above. To begin with, we compare the results of the direct and indirect algorithm for the typical Voronoi cell of Cox processes on PVT. The numerical results for the typical Voronoi cell of Cox processes on PVT were obtained in cooperation with P. Saffert and are partially documented in his diploma thesis ([84]).

4.6.1 Scaling invariance for Cox processes and thinnings

Let T be a random tessellation with length intensity 1 and consider the Cox processes X and X' on $T_\gamma = T/\gamma$ and $T_{\gamma'} = T/\gamma'$, respectively, where λ_ℓ and λ'_ℓ denote the linear intensities of X and X'. In Section 3.5.2 it was shown that $X \stackrel{\mathrm{d}}{=} \frac{\gamma'}{\gamma} X'$ if $\kappa = \gamma/\lambda_\ell$ and $\kappa' = \gamma'/\lambda'_\ell$ are equal. Moreover, a similar scaling invariance holds if X and X' are thinnings of the vertices of T_γ and $T_{\gamma'}$, respectively. Then again $X \stackrel{\mathrm{d}}{=} \frac{\gamma'}{\gamma} X'$ if $\kappa = \gamma/\lambda_\ell$ is equal to $\kappa' = \gamma'/\lambda'_\ell$, see Section 3.5.3, where λ_ℓ is defined by $\lambda_\ell = p\lambda^{(0)}\gamma$ for p-thinnings of $T_\gamma^{(0)}$. Thus, in both considered cases, it holds that $\Xi_X^* \stackrel{\mathrm{d}}{=} \frac{\gamma'}{\gamma}\Xi_{X'}^*$ if $\kappa = \kappa'$, where Ξ_X^* and $\Xi_{X'}^*$ are the typical Voronoi cells of X and X', respectively. From this observation we directly get that e.g. $\mathbb{E}\nu_1(\partial\Xi_X^*) = \frac{\gamma'}{\gamma}\mathbb{E}\nu_1(\partial\Xi_{X'}^*)$ and $\sqrt{\mathbb{E}\nu_2(\Xi_X^*)} = \frac{\gamma'}{\gamma}\sqrt{\mathbb{E}\nu_2(\Xi_{X'}^*)}$.

Therefore, we focus in the following only on single values of the parameter γ, but different values of κ. Then numerical results for $\gamma' \neq \gamma$ with $\kappa' = \kappa$ can be obtained from the corresponding results for γ by an appropriate scaling.

4.6.2 Comparison of direct and indirect simulation algorithms

The sample means of different cell characteristics obtained from the cells generated with the direct simulation algorithm and the sample means of the corresponding weighted characteristics for the cells generated with the indirect algorithm have to be equal. However, the variances may differ since we generate different random variables with the same mean. Thus, we computed the sample variances of different characteristics like the (weighted) number of vertices (ν_0), perimeter (ν_1) and area (ν_2) for samples simulated with both algorithms. In Table 4.1 the results are summarized for different values of the scaling factor κ. The variance of the output is always smaller for the direct algorithm compared with the variance of the indirect algorithm. Since both algorithms have a similar runtime, the variance of the (random) output is the main criterion in order to decide which algorithm is preferable for the computation of distributional properties. In the following, we therefore concentrate only on results obtained from the directly simulated cells, although the indirect algorithm yields similar results.

In particular, for the computation of cost functionals like Euclidean distances and shortest path lengths, see Chapter 5, it is important that the simulation algorithm has low variance of the output. Due to time-consuming calculations only a relatively small sample size can be considered there. Thus, especially for this purpose, the direct algorithm is preferable.

4.6.3 Comparison of the typical cell of PVT and Cox processes on PDT, PLT and PVT

For different values of κ samples of the typical Voronoi cell Ξ_X^* induced by a Cox process X on T were simulated, where T is either a PDT, PLT or PVT. Based on each sample, the probability densities of cell characteristics like the area and perimeter were estimated. Note that for $\kappa = \gamma/\lambda_\ell \to \infty$ with $\lambda = \lambda_\ell \gamma$ fixed, the distribution of these cell characteristics converge to the distribution of the corresponding characteristic of the typical cell of a PVT with cell intensity λ. This is a consequence of Lemma 6.1 in Chapter 6. Thus, it is interesting to compare the distributions of cell characteristics of the typical Voronoi cell based on Cox processes and Poisson processes.

In Figure 4.10 histograms for the area and perimeter of Ξ_X^* are displayed which were estimated based on samples of size 1 000 000. For both the area and perimeter of the typical Voronoi cell of a Cox process on PVT, the estimated probability densities converge fast to the corresponding densities for the typical cell of a PVT. It is even hard to distinguish between the histograms for Cox processes on PVT and PVT itself if $\kappa = 50$. However, the convergence is not that fast if we consider Cox processes on PDT and PLT. For both models a difference to the PVT–case can be observed even for $\kappa = 50$, although this difference is

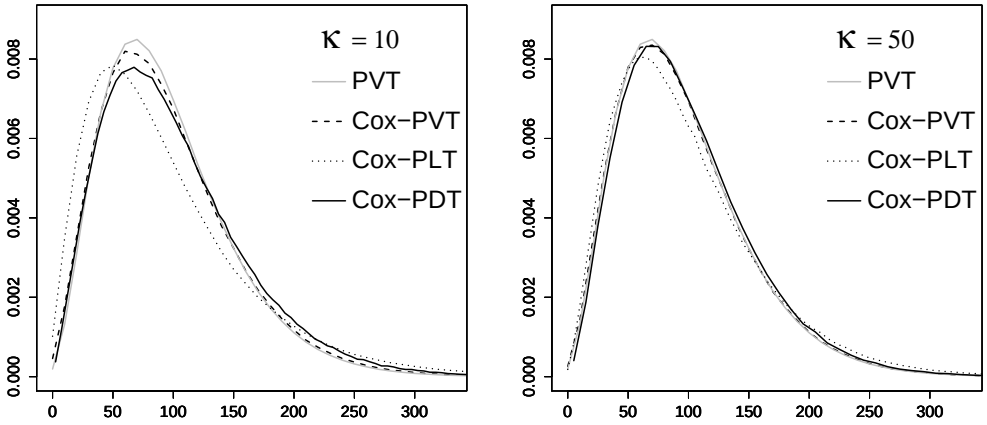

(a) Area, $\kappa = 10$

(b) Area, $\kappa = 50$

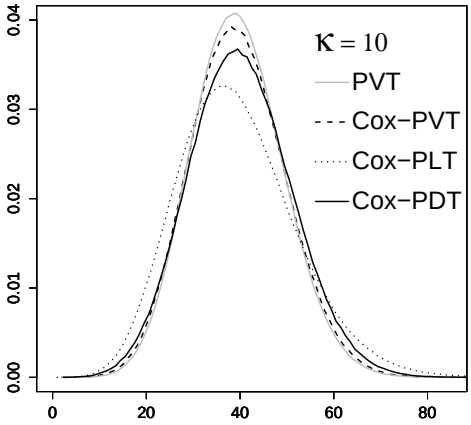

(c) Perimeter, $\kappa = 10$

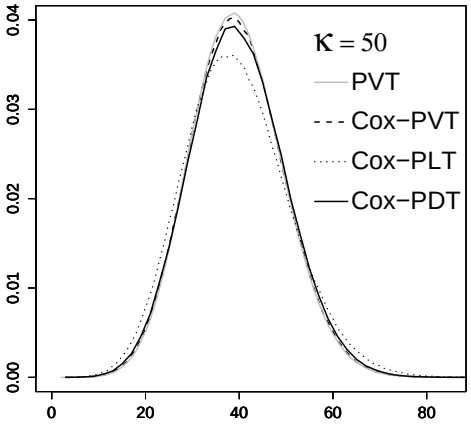

(d) Perimeter, $\kappa = 50$

Figure 4.10: Histograms for area and perimeter of the typical Voronoi cell for Cox processes on T

less for PDT. Actually, this is the behavior one would expect because the edges of PVT are shorter and more evenly spread in the plane compared to the edges of PDT. Moreover, the most irregular cells with the longest segments among the three basic models are observed for PLT. Thus, from this point of view, it is plausible that the dependencies between the points of X are decreasing faster if the underlying tessellation T is a PVT rather than a PDT and PLT. Thus, the convergence to the PVT–case is faster for Cox processes concentrated on PVT than for PDT which is in turn faster than for PLT. The same behavior can also be observed in Table 4.2, where the coefficients of variation (cv, $\mathrm{cv}X := 100 \cdot \sqrt{\mathrm{Var}X}/\mathbb{E}X$) of the number of vertices $\nu_0(\Xi_X^*)$ and the area $\nu_2(\Xi_X^*)$ are shown for different values of κ.

κ	Direct Algorithm			Indirect Algorithm		
	$\mathbb{E}\nu_1$	$\mathbb{E}\nu_2$	$\mathbb{E}\nu_0$	$\mathbb{E}\nu_1$	$\mathbb{E}\nu_2$	$\mathbb{E}\nu_0$
10	652.75	124680.35	1.87	1497.86	175659.46	4.36
20	1266.92	479859.33	1.82	2812.88	653731.80	4.26
30	1874.68	1065937.19	1.81	4086.39	1426403.79	4.22
40	2484.18	1881871.79	1.81	5354.02	2492851.63	4.17
50	3098.75	2931215.45	1.80	6624.04	3855095.79	4.17
60	3689.98	4194702.08	1.79	7882.49	5510771.23	4.15
90	5511.02	9384330.87	1.79	11644.29	12187366.14	4.11
120	7336.33	16670645.20	1.79	15406.61	21481790.15	4.10

Table 4.1: Sample variances for different characteristics of Ξ_X^* obtained for the direct (left) and indirect (right) simulation algorithm, respectively, where $\gamma = 0.125$ was fixed.

κ	cv ν_0				cv ν_2			
	Cox-PVT	Cox-PDT	Cox-PLT	PVT	Cox-PVT	Cox-PDT	Cox-PLT	PVT
10	22.784	23.694	24.091	22.240	55.174	59.145	69.538	52.947
20	22.496	22.857	23.454	22.240	54.085	56.373	64.819	52.947
30	22.431	22.823	23.200	22.240	53.733	55.399	62.638	52.947
40	22.386	22.638	23.056	22.240	53.564	54.860	61.340	52.947
50	22.378	22.629	22.929	22.240	53.544	54.546	60.516	52.947
60	22.324	22.548	22.870	22.240	53.342	54.217	59.792	52.947
90	22.292	22.459	22.752	22.240	53.203	53.940	58.595	52.947
120	22.303	22.457	22.669	22.240	53.173	53.713	57.836	52.947

Table 4.2: Estimates for the cv of the number of vertices (ν_0) and area (ν_2) of the typical Voronoi cell Ξ_X^* of Cox processes on PVT, PLT and PDT as well as the typical cell of PVT for different values of κ, using the direct algorithm

κ	Cox-PVT		Cox-PDT		Cox-PLT		PVT	
	$\mathbb{E}\nu_1$	$\mathrm{cv}\nu_1$	$\mathbb{E}\nu_1$	$\mathrm{cv}\nu_1$	$\mathbb{E}\nu_1$	$\mathrm{cv}\nu_1$	$\mathbb{E}\nu_1$ (exact)	$\mathrm{cv}\nu_1$
10	40.010	25.242	40.094	27.019	39.726	31.469	40.0	24.315
20	40.005	24.869	40.067	25.699	39.766	29.580	40.0	24.315
30	40.008	24.698	40.033	25.412	39.791	28.684	40.0	24.315
40	40.010	24.621	40.021	25.146	39.810	28.130	40.0	24.315
50	39.982	24.613	40.011	25.087	39.812	27.776	40.0	24.315
60	39.997	24.508	40.010	24.916	39.834	27.474	40.0	24.315
90	39.992	24.458	40.007	24.777	39.849	26.944	40.0	24.315
120	39.994	24.438	39.995	24.716	39.884	26.590	40.0	24.315

Table 4.3: Estimates for expectation and cv of the boundary length $\nu_1(\partial\Xi_X^*)$ of the typical Voronoi cell of Cox processes on PVT, PLT and PDT as well as PVT for different values of κ (where $\mathbb{E}\nu_2(\Xi_X^*) = 100$ was fixed)

4.6.4 Comparison of the typical cell of Cox processes on PVT/PVT and PVT/PLT nestings

In this section we present some numerical results for the typical Voronoi cell of a Cox process X on the edges of a PVT/PLT nesting and compare them to results for Cox processes on PVT and PLT, respectively. Notice that other nested tessellations based on PVT, PDT and PLT, respectively, can be analyzed similarly.

Scaling invariance for nestings

Let T be a T_0/T_1 nesting and let γ_0 and γ_1 denote the length intensities of T_0 and T_1, respectively. If T is scaled by a constant $c > 0$, then we have $cT \stackrel{\mathrm{d}}{=} T'$, where T' is a nesting of initial tessellation T_0' and component tessellation T_1' with $T_0' \stackrel{\mathrm{d}}{=} cT_0$ and $T_1' \stackrel{\mathrm{d}}{=} cT_1$. Thus, the length intensities γ_0' and γ_1' of T_0' and T_1' are given by $\gamma_0' = \gamma_0/c$ and $\gamma_1' = \gamma_1/c$, respectively.

Now assume that X and X' are Cox processes on the random tessellations T and T' with linear intensities λ_ℓ and $\lambda_\ell' = \lambda_\ell/c$, respectively, then $cX \stackrel{\mathrm{d}}{=} X'$. That means, if $\gamma_0/\gamma_1 = \gamma_0'/\gamma_1'$ and if in addition the scaling factors $\kappa = (\gamma_0 + \gamma_1)/\lambda_\ell$ and $\kappa' = (\gamma_0' + \gamma_1')/\lambda_\ell'$ are equal, then the two Cox processes X and $\gamma_0/\gamma_0' \cdot X'$ have the same distributions, see also Section 3.5.2. Thus, we only have to do numerical computations for one parameter vector $(\gamma_0, \gamma_1, \lambda_\ell)$ with given ratio γ_0/γ_1 and scaling factor κ. Numerical results for all other parameter vectors $(\gamma_0', \gamma_1', \lambda_\ell')$ with ratio $\gamma_0/\gamma_1 = \gamma_0'/\gamma_1'$ and scaling factor $\kappa = (\gamma_0' + \gamma_1')/\lambda_\ell'$ can then be computed from the corresponding results for the parameter vector $(\gamma_0, \gamma_1, \lambda_\ell)$

by an appropriate scaling. We therefore fix $\gamma = 1$ below and only vary $\gamma_0 \in [0, 1]$ and $\lambda_\ell > 0$, where γ_1 is put to $1 - \gamma_0$.

Area and perimeter of the typical Voronoi cell

We now assume that T is a T_0/T_1 nesting with a PVT as initial tessellation and a PLT as component tessellation. For different values of κ, γ_0 and γ_1 with $\gamma_0 + \gamma_1 = 1$ we simulated the typical Voronoi cell of a Cox process X on T as explained in Section 4.4. Based on the generated samples of the typical cell, we estimated the distribution of cell characteristics like perimeter and area. Some results are shown in Fig. 4.11 together with the corresponding results for Cox processes on PVT and PLT. The difference between the different considered models decreases for increasing κ as expected. However, for $\kappa = 10$ there is a clear difference between the densities of the different considered cases. Note that the distributions for Cox processes on PVT and PLT seem to appear as extremal cases as γ_0 tends to 0 and 1, respectively, and for Cox processes on PVT/PLT–nestings we can interpolate between these extremal distributions. Thus, using Cox processes on T_0/T_1-nestings we get more flexible models and we can in a way shift between the distributions of the typical Voronoi cell of Cox processes on the initial tessellation T_0 and the component tessellation T_1, respectively, as γ_0 tends from 1 to 0.

4.6.5 Numerical results for thinnings

In this section some results are presented which are obtained from a simulation study using the simulation algorithms for the typical Voronoi cell of thinnings of the vertices of PDT, PLT and PVT. Recall that the vertices of a PDT form a stationary Poisson process, thus a p-thinning of the vertices of a PDT is again a stationary Poisson process. Hence, the typical cell of a PVT and the typical Voronoi cell of a thinning of the vertices of a PDT have the same distribution.

Histograms of the area and perimeter of the typical Voronoi cell were estimated for thinnings of the vertices of PDT, PLT and PVT. Some results are displayed in Figure 4.12. Because of the scaling invariance for thinnings of the vertex sets, we focus again on the case that the length intensity γ of T is equal to 1 and we consider different values for the scaling factor κ. Results for $\gamma \neq 1$ can then be obtained from the results for $\gamma = 1$ by a suitable scaling. The results are quite similar as for Cox processes on T, therefore they are only discussed briefly. Again, we expect that for large κ the distribution of cell characteristics of the typical cell like the perimeter and area converge to the distribution of the corresponding characteristics for the typical cell of a stationary PVT. This can also be shown theoretically using the same methods as for Cox processes. If the underlying tessellation is a PVT, then the convergence of the distributions of the considered cell characteristics to the corresponding distribution of the typical cell of PVT is very fast. Even for small values of κ one can hardly distinguish

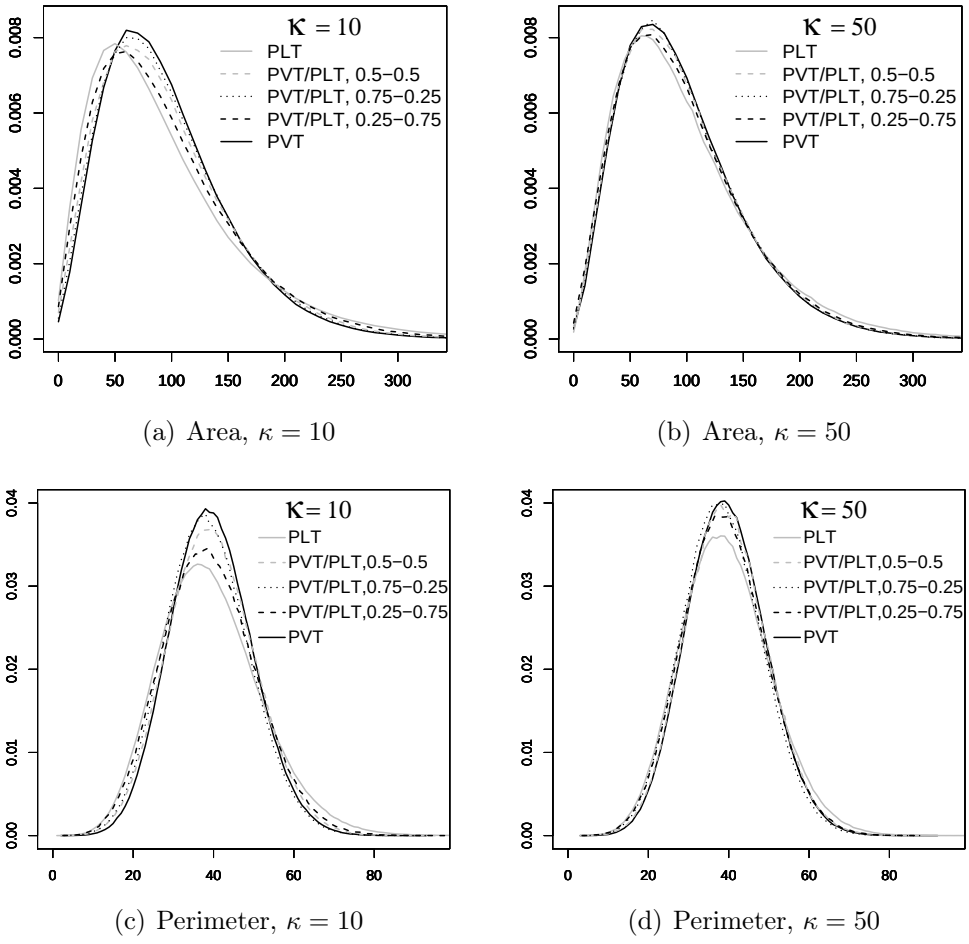

(a) Area, $\kappa = 10$

(b) Area, $\kappa = 50$

(c) Perimeter, $\kappa = 10$

(d) Perimeter, $\kappa = 50$

Figure 4.11: Histograms for area and perimeter of the typical Voronoi cell of Cox processes on PVT/PLT nestings.

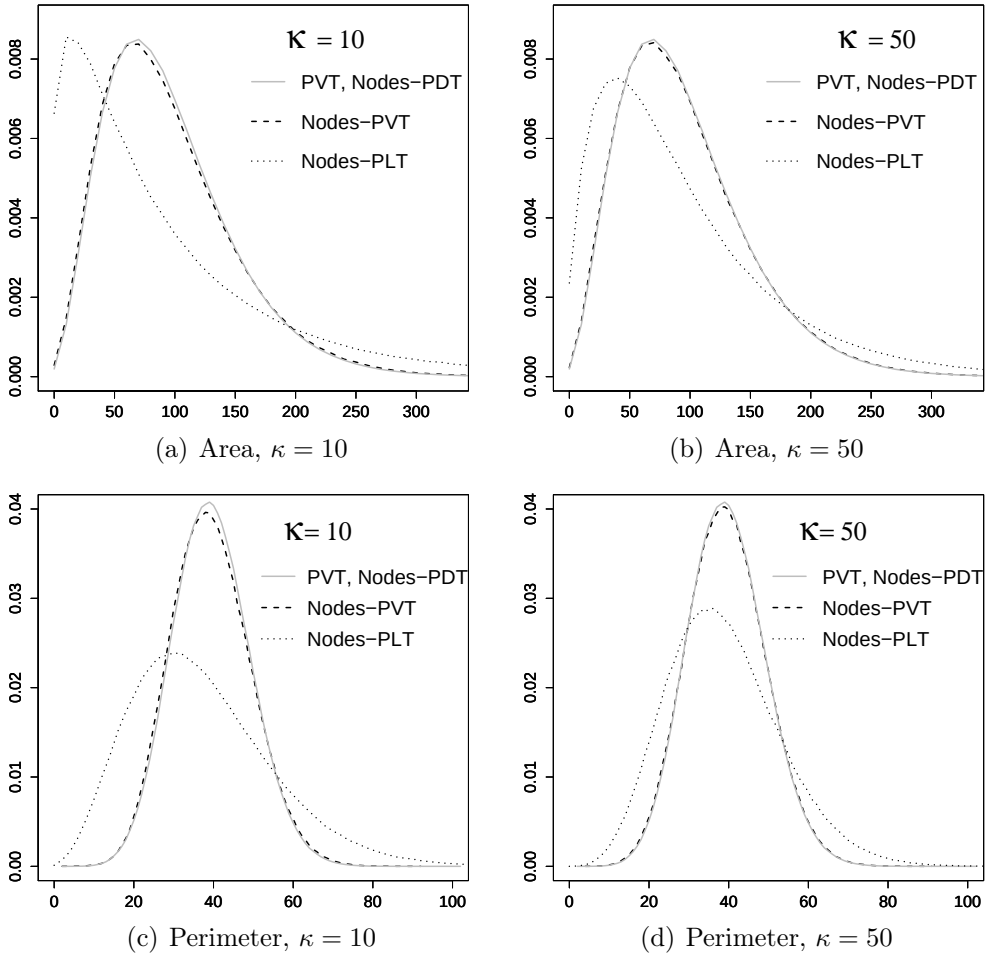

(a) Area, $\kappa = 10$ (b) Area, $\kappa = 50$

(c) Perimeter, $\kappa = 10$ (d) Perimeter, $\kappa = 50$

Figure 4.12: Histograms for area and perimeter of the typical cell for thinnings of the vertices of T

the distributions between the area and perimeter of the typical Voronoi cell for thinned nodes and the typical cell of PVT. However, if T is a PLT, then there is a large deviation from the PVT case between the distributions of these cell characteristics. This is the expected behavior since for PLT there are e.g. infinitely many point located on each single line yielding a point process which is quite different from a Poisson process.

4.6.6 Implementation tests

It is always important to test the implementations of the developed algorithms. Methods for software tests with random output are suitable for this purpose, see e.g. [24, 31, 60]. Note that these tests are based on statistical significance tests. For the algorithms introduced here we used samples of simulated cells in order to test the correctness of the implementation of the algorithms. More

precisely, we generated for different parameters large i.i.d. samples $Z_1, \ldots, Z_n$ of cell characteristics like the area and number of vertices. Let Z denote the considered cell characteristic. Then the mean $\mathbb{E}Z$ is known in the cases regarded above. For instance, the mean area of the typical Voronoi cell is equal to $1/\lambda$ if λ is the intensity of the cell nuclei and the mean number of vertices of the typical Voronoi cell is 6 for all considered point process models. This information can be used to perform e.g. asymptotic Gaussian two sample test for equal means ([19]). If the implementation is incorrect, then it is likely that random cells are generated and cell characteristics $\widetilde{Z}_1, \ldots, \widetilde{Z}_n$ are computed which do not have the correct mean value, i.e., $\mathbb{E}Z \neq \mathbb{E}\widetilde{Z}_1$. Consequently, if the sample size n is large enough these tests are rejected. However, all the tests showed the expected behavior, so we assume that our implementations are correct. More detailed test results for the implementation of the simulation algorithm for the typical Voronoi cell Ξ_X^* of a Cox process X on PVT can be found in [84].

Chapter 5

Euclidean and shortest path connection distances in hierarchical network models

In this chapter, we investigate cost functionals (or performance characteristics) which can be associated with hierarchical telecommunication networks, where we focus especially on networks with two hierarchy levels. Thus, there are network components of low and high hierarchy. Each *low–level component* (LLC) is linked to a unique *high–level component* (HLC) and the physical connection has to be established either via the cable system of the network or wireless by radio transmissions. Then cost functionals like connection lengths can be associated with the network. Clearly, the geometry of the network and its components influences connection lengths and hence the overall performance of the network. Thus, it is an important task to investigate connection lengths of the network and their dependence on e.g. different network geometries and connection rules. A promising approach in order to achieve this goal is the analysis of cost functionals based on spatial stochastic models which can represent existing or future networks. This is the topic of the present chapter which is organized in the following way.

First, in Section 5.1, we introduce the *Stochastic Subscriber Line Model* (SSLM), a spatial stochastic model for hierarchical telecommunication networks. In particular, we explain how the underlying infrastructure of the network as well as LLC and HLC are modeled. Furthermore, it is specified how connections between LLC and HLC are established. In order to specify the connection rules, we use the concept of so–called serving zones, i.e., we associate to each HLC a domain called serving zone and all LLC inside this serving zone are connected to the corresponding HLC. Subsequently, we define cost functionals based on this model using Palm calculus. More precisely, we are interested in the distributions of cost functionals associated with the connection from the typical LLC to its associated HLC and investigate in detail the distributions of direct Euclidean connection lengths in Section 5.2 and shortest path connection lengths in Section 5.4. These

are important performance characteristics of telecommunication networks since they provide information about the connection length of the typical user. For instance, for some network technologies it is important that the connection length is shorter than a given threshold in order to assure that a connection can be established.

For both considered cost functionals we derive formulae for the distribution function and probability density which are based on expectations of certain functionals of the typical serving zone and its inner structure. These formulae lead directly to estimators for the distribution function and density, respectively, which can be calculated based on samples of the typical serving zone. Such samples can be generated using the simulation algorithms developed in Chapter 4. Afterwards statistical properties of the considered estimators are investigated and it is shown that they are e.g. uniformly strong consistent.

The content of this chapter is partly based on results which were obtained in [96] and [97].

5.1 Spatial stochastic models for two-level hierarchical networks

In this section, we introduce the SSLM as a spatial stochastic model for hierarchical telecommunication networks which takes the underlying infrastructure of the network like street systems into account. Since detailed network data is often unavailable, we do not model the cable system directly, but we model the street system along which the cables of the network are deployed. The edge sets of random tessellations are used for this purpose. In a second step, we model both HLC and LLC by planar point processes whose points are either scattered freely in the plane or along the edges of the underlying random tessellation representing the support of the cable system. Finally, we introduce the concept of serving zones in order to specify to which HLC a LLC is connected. Based on this modeling approach, we can define cost functionals associated with the connection from the typical LLC to its associated HLC like shortest path connection lengths and direct Euclidean connection distances which are studied in more detail in Sections 5.2 and 5.4

5.1.1 Components of low and high hierarchy levels on random tessellations

We represent the underlying infrastructure of the telecommunication network by the edge set $T^{(1)}$ of a random tessellation T in $\mathbb{R}^2$. In the following, we assume that T is stationary with length intensity γ, i.e., the mean length of $T^{(1)}$ per unit area is $\gamma = \mathbb{E}\nu_1(T^{(1)} \cap [0,1]^2)$. For a given stationary tessellation T, we model

the locations of both HLC and LLC by stationary point processes $H = \{H_n\}$ and $L = \{L_n\}$, respectively.

In particular, we assume that the point process H is concentrated on the edge set $T^{(1)}$ almost surely, i.e., $\mathbb{P}(H_n \in T^{(1)} \text{ for all } n \in \mathbb{N}) = 1$. Possible models for H have been introduced in Section 3.5. For instance, H can be a Cox processes on T or a thinning of the set of vertices of T. Now assume that H is stationary with (planar) intensity $\lambda > 0$, then we define the quotient $\lambda_\ell = \lambda/\gamma$ as the planar intensity of H divided by the length intensity of T. If H is a Cox process, then the intensity quotient λ_ℓ is just the linear intensity of the Poisson processes on the edge set $T^{(1)}$. However, we can define λ_ℓ for any point process whose points are concentrated on the edges of T.

For the point process L representing LLC we distinguish two different scenarios. On the one hand, we consider the case that L is a stationary Poisson process with intensity λ' which is independent of H and T. On the other hand, we assume that L is a Cox process on T with linear intensity λ'_ℓ which is independent of H given T. Thus, in the latter case, L is stationary since the tessellation T is stationary and its planar intensity λ' can be calculated as $\lambda' = \lambda'_\ell\gamma$. So we have defined the basic components of the SSLM. Below, we specify the connection rules between LLC and HLC.

5.1.2 Service zones and their inner structure

Now we define to which HLC a LLC is connected. This is done by the definition of so–called serving zones. A *serving zone* is a domain which is associated to each HLC such that the serving zones of distinct HLC do not overlap, but their union covers the whole Euclidean plane. Thus, the serving zones form a tessellation in $\mathbb{R}^2$. A LLC is then linked to the HLC in whose serving zone it is located. In our stochastic framework we define serving zones using random tessellations.

In the following, $T_H = \{\Xi_{H,n}\}$ denotes a random tessellation, where we assume that the nuclei $\{\alpha(\Xi_{H,n})\}$ of T_H are given by the locations of the point process $H = \{H_n\}$. There are various possible models for T_H. For instance, T_H can be constructed as the Voronoi tessellation induced by H which will be done in order to obtain the numerical results presented later on. However, there are more complex models for T_H which can be considered like random Laguerre tessellations ([50, 52]) or aggregated Voronoi tessellations ([91]). Now assume that T_H is specified, then a point L_j of L is linked to the point H_n of H if and only if $L_j \in \Xi_{H,n}$, i.e., all LLC inside $\Xi_{H,n}$ are linked to H_n. In this context, the cell $\Xi_{H,n}$ of T_H is also called the *serving zone* of the point H_n and the typical cell Ξ^*_H of T_H is called the *typical serving zone*.

Furthermore, we define the stationary marked point process $H_S = \{(H_n, S^o_{H,n})\}$ whose marks are given by $S^o_{H,n} = (T^{(1)} \cap \Xi_{H,n}) - H_n$. Thus, each point of H is marked with the segment system inside its serving zone and hence H_S is a stationary marked point process with intensity λ whose mark space is given by

the family of finite segment systems $\mathcal{L}^o$ which contain the origin. If L is a Cox process on T, then a point L_n of L is linked to H_j if and only if $L_n \in S^o_{H,j} + H_j$. Note that the typical mark $S^*_H : \Omega \to \mathcal{L}^o$ of H_S is a random segment system which contains the origin. We call S^*_H the *typical segment system*, see also Section 3.5.4. Note that Campbell's theorem for stationary marked point processes yields

$$\begin{aligned}
\gamma &= \mathbb{E} \sum_{H_i \in H} \nu_1(S^o_{H,i} + H_i \cap [0,1)^2) \\
&= \lambda \int_{\mathbb{R}^2} \mathbb{E}\nu_1(S^*_H \cap ([0,1)^2 - x))\, \nu_2(dx) \\
&= \lambda \mathbb{E}\left[\int_{S^*_H} \int_{\mathbb{R}^2} \mathbb{I}_{[0,1)^2 - x}(y)\, \nu_2(dy)\, \nu_1(dx) \right] \\
&= \lambda \mathbb{E}\nu_1(S^*_H)\,.
\end{aligned}$$

Thus, it holds that $\mathbb{E}\nu_1(S^*_H) = \gamma/\lambda = 1/\lambda_\ell$. This observation is used later on.

5.1.3 Cost functionals for two-level hierarchical models

So far, we introduced four modeling components, namely T, H_S, L and T_H. They can be used in order to construct the marked point process $L_M = \{(L_n, M_n)\}$, where each point L_n is marked with a random variable M_n which represents the associated cost of the connection from L_n to H_j provided that $L_n \in \Xi_{H,j}$. In the following, we assume that M_n is either the direct Euclidean connection length, i.e., $M_n = |L_n - H_j|$ provided that $L_n \in \Xi_{H,j}$, or M_n is the length of the shortest path from L_n to H_j along $T^{(1)}$ provided that $L_n \in S_{H,j} = S^o_{H,j} + H_j$. Note that in the latter case, we only consider Cox processes L on T as models for LLC. However, further cost functionals could be considered like the length of least nodes paths or the number of passed nodes on the shortest path between LLC and HLC, see [104]. Realizations of the model for Voronoi tessellations as serving zones and Cox processes H and L on PVT and PLT are displayed in Figure 5.1(a) and (b), where LLC are connected to HLC on the shortest path as well as the direct Euclidean distance. It is easy to see that the marked point process L_M is stationary if the random tessellation T is stationary. In the following, the main research goal is to investigate the Palm mark distribution $P^o_{L_M}$ of L_M. Thus, we are interested in the distribution of the typical mark M^* of L_M.

An important fact is that realizations of the marked point process L_M can be constructed from realizations of L and H_S if L is a Cox process and from realizations of L and T_H if L is a Poisson process. Hence, instead of L_M, we can regard the vectors $Y = (L, H_S)$ and $Y = (L, T_H)$, respectively, together with the Palm distribution P^*_L of Y with respect to the first component L, see Section 2.3.4 for details on Palm distributions of jointly stationary marked point processes. Now assume that $(L^*, \widetilde{H}_S)$ and $(L^*, T_{\widetilde{H}})$, respectively, are distributed

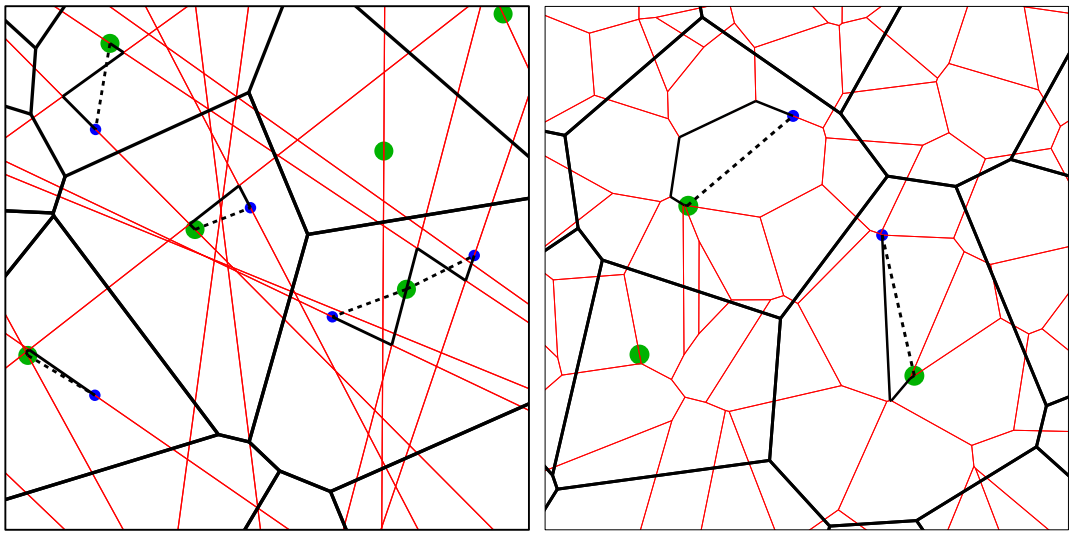

(a) PLT (b) PVT

Figure 5.1: HLC with their serving zones (black) and LLC (blue) with Euclidean distances and shortest paths along the edge set

according to the Palm distribution P_L^*, where the notation $\widetilde{H}_S = \{(\widetilde{H}_n, \widetilde{S}^o_{H,n})\}$ is used and

$$\widetilde{T}^{(1)} = \bigcup_{n\geq 1} (\widetilde{S}^o_{H,n} + \widetilde{H}_n) \tag{5.1}$$

denotes the edge set corresponding to $\widetilde{H}_S$. Then M^* can be regarded as the associated cost for the connection from the origin o to the point $\widetilde{H}_n$ of $\widetilde{H}$ in whose serving zone o is located. Note that $L^*\backslash\{o\}$ is a stationary Poisson process and a Cox process on $\widetilde{T}$ if L is a stationary Poisson process and Cox process on T, respectively, see Theorems 2.6 and 3.3.

Similarly, we regard the vectors $(\widetilde{L}, H_S^*)$ and $(\widetilde{L}, T_H^*)$ which are distributed according to the Palm distributions $P^*_{H_S}$ and $P^*_{T_H}$, respectively, where $T^{*(1)}$ denotes the edge set of H_S^*. On the one hand, if L is a Cox process on T, then $\widetilde{L}$ is a (non-stationary) Cox process on $T^{*(1)}$ with linear intensity λ'_ℓ which is independent of H^* given $T^{*(1)}$. This can be proven basically in the same way as Lemma 4.2. On the other hand, if L is a stationary Poisson process independent of H, then $\widetilde{L} \overset{\mathrm{d}}{=} L$ and $\widetilde{L}$ is independent of H^*, see Section 2.3.4.

5.2 The typical Euclidean distance D^*

We consider in this section as a basis the hierarchical model defined in Section 5.1 and we assume that the cost functional is given by the direct Euclidean connection length. Thus, we consider the marked point process $L_D = \{(L_n, D_n)\}$, where

$D_n = |L_n - H_j|$ provided that $L_n \in \Xi_{H,j}$. That means, the cost functional associated with the connection of L_n to H_j is the Euclidean distance between L_n and H_j. Moreover, we always assume that L is either a Cox process on the edges of T conditionally independent of H given T or a stationary Poisson process in $\mathbb{R}^2$ which is independent of T and H. Realizations for different considered models are displayed in Figure 5.2, where the underlying tessellation T is a PDT, PLT and PVT, respectively, and the serving zones are modeled by the Voronoi tessellation induced by a Cox process H on T.

We are then interested in the distribution of the typical mark D^* of L_D which we call the *typical Euclidean distance*.

5.2.1 Distributional properties

In this section we derive representation formulae which represent the distribution function and the probability density of the typical Euclidean connection distance D^* as expectations of functionals of the typical serving zone and the segment system within it. These formulae lead to estimators for the distribution of these characteristics which can be computed based on samples of the typical serving zone and its segment system, respectively.

Representation by the typical serving zone

Applying Neveu's exchange formula (see Lemma 2.9) we can represent the distribution function of D^* in terms of the typical cell Ξ_H^* of T_H and in terms of the typical segment system S_H^* within Ξ_H^* if L is a Poisson process and Cox process, respectively. An important fact is that this representation does not depend on parameters or points of L anymore. Thus, the distribution of D^* is uniquely determined by T_H and H_S, respectively.

Theorem 5.1 *If L is a Poisson process that is independent of H, then the distribution function $F_{D^*} : [0,\infty) \to [0,1]$ of D^* is given by*

$$F_{D^*}(x) = \lambda_\ell \, \gamma \, \mathbb{E} \, \nu_2(\Xi_H^* \cap B(o,x)) \,, \qquad x \geq 0 \,, \tag{5.2}$$

where $\nu_2(\Xi_H^* \cap B(o,x))$ denotes the area of Ξ_H^* intersected with the ball $B(o,x) \subset \mathbb{R}^2$ centered at o with radius x. If L is a Cox processes on T which is conditionally independent of H given T, then the distribution function of D^* is given by

$$F_{D^*}(x) = \lambda_\ell \, \mathbb{E} \, \nu_1(S_H^* \cap B(o,x)) \,, \qquad x \geq 0 \,. \tag{5.3}$$

Proof We use Lemma 2.9 in order to prove Theorem 5.1. First let L be a Poisson process of intensity λ', then we can regard the vector $Y = (L_D, T_H)$ as a random element of $\mathsf{N}_{[0,\infty),\mathcal{P}^o}$ and we use the notations $(L_D^*, T_{\widetilde{H}})$ and $(\widetilde{L}_D, T_H^*)$ for the Palm versions of Y distributed according to $P_{L_D}^*$ and $P_{T_H}^*$, respectively. For

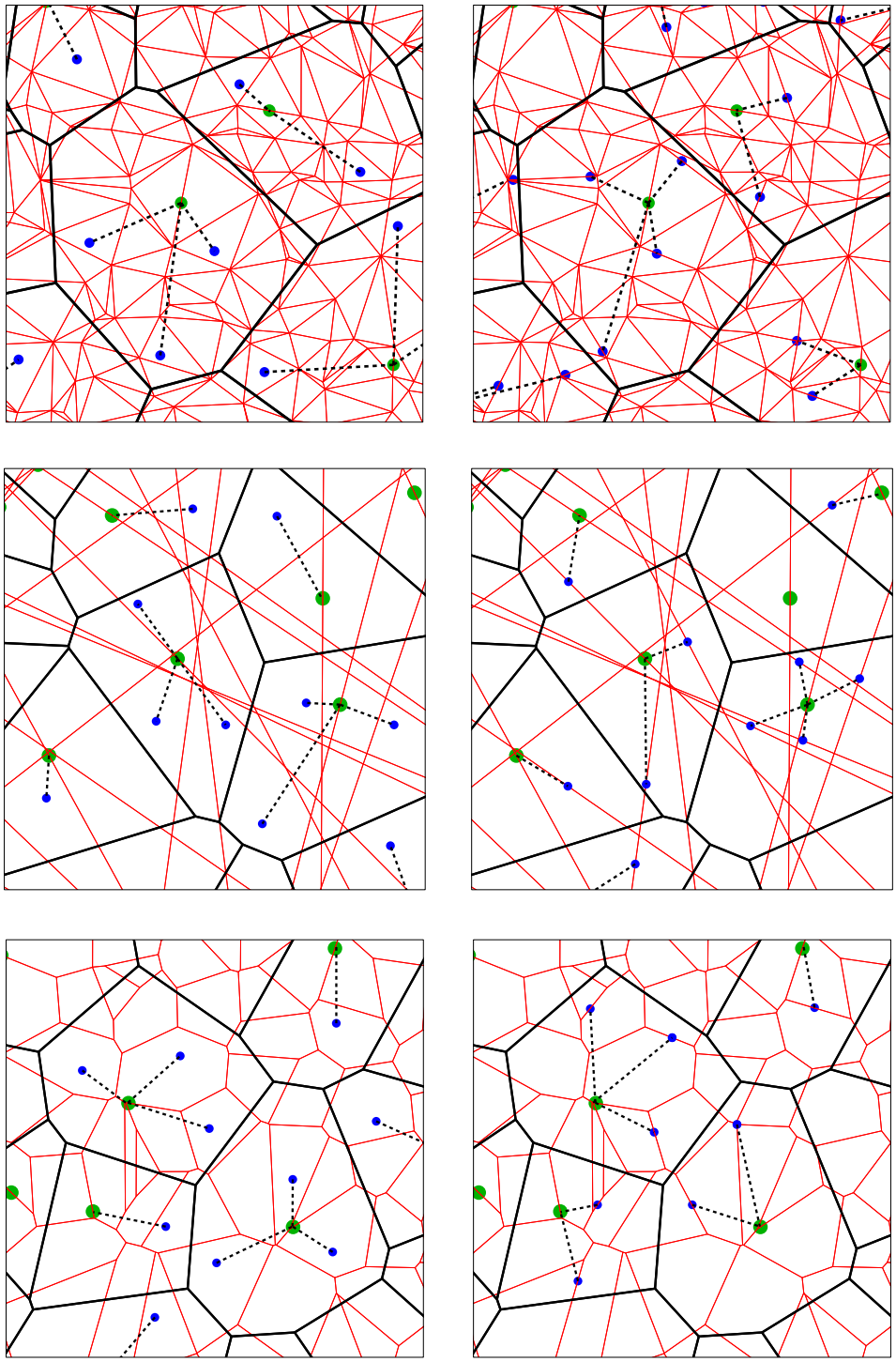

Figure 5.2: H on PDT (top), PLT (middle), PVT (bottom) with serving zones (black) and connection distances (dashed) for L Poisson (left) and Cox (right)

some measurable $h : [0,\infty) \to [0,\infty)$ we define the function $f : \mathbb{R}^2 \times [0,\infty) \times \mathcal{P}^o \times \mathsf{N}_{[0,\infty),\mathcal{P}^o} \to [0,\infty)$ by

$$f(x,m,\xi,\psi) = \begin{cases} h(m) & \text{if } o \in \xi + x, \\ 0 & \text{otherwise.} \end{cases} \tag{5.4}$$

Now we can apply Lemma 2.9 and get

$$\begin{aligned} \mathbb{E}\, h(D^*) &= \int_{\mathsf{N}_{[0,\infty),\mathcal{P}^o}} \int_{\mathbb{R}^2\times\mathcal{P}^o} f(x,\xi,m,\psi)\, \psi^{(2)}(d(x,\xi))\, P^*_{L_D}(d(\psi,m)) \\ &= \frac{\lambda}{\lambda'} \int_{\mathsf{N}_{[0,\infty),\mathcal{P}^o}} \int_{\mathbb{R}^2\times[0,\infty)} f(-x,\xi,m,t_x\psi)\, \psi^{(1)}(d(x,m))\, P^*_{T_H}(d(\psi,\xi)) \\ &= \frac{\lambda}{\lambda'} \int_{\mathsf{N}_{[0,\infty),\mathcal{P}^o}} \int_{\mathbb{R}^2\times[0,\infty)} h(|x|)\mathbb{1}_\xi(x)\, \psi^{(1)}(d(x,m)) P^*_{T_H}(d(\psi,\xi)) \\ &= \frac{\lambda}{\lambda'} \mathbb{E}\left(\mathbb{E}\Big(\sum_{\widetilde{L}_n \in \Xi^*_H} h(|\widetilde{L}_n|) \,\Big|\, \Xi^*_H \Big) \right). \end{aligned}$$

Since L and H are independent we get that T^*_H and $\widetilde{L}$ are also independent and in addition that $\widetilde{L} \stackrel{\mathrm{d}}{=} L$, see Section 2.3.4. Thus, given Ξ^*_H, we have that $\widetilde{L}$ is a stationary Poisson process of intensity λ'. Using Campbell's theorem, we get

$$\mathbb{E}\Big(\sum_{\widetilde{L}_n \in \Xi^*_H} h(|\widetilde{L}_n|) \,\Big|\, \Xi^*_H \Big) = \lambda' \int_{\Xi^*_H} h(|u|)\, \nu_2(du)$$

which yields for $h(|u|) = \mathbb{1}_{[0,x]}(|u|)$ that

$$F_{D^*}(x) = \mathbb{E}\, \mathbb{1}_{[0,x]}(D^*) = \lambda\, \mathbb{E}\, \nu_2(\Xi^*_H \cap B(o,x)).$$

On the other hand, if L is a Cox process concentrated on $T^{(1)}$, then we can regard the vector $Y = (L_D, H_S)$ as a random element of $\mathsf{N}_{[0,\infty),\mathcal{L}^o}$. Recall that we use the notation $(L^*_D, \widetilde{H}_S)$ and $(\widetilde{L}_D, H^*_S)$ for the Palm versions of Y with respect to $P^*_{L_D}$ and $P^*_{X_S}$, respectively. In the same way as above we can apply Neveu's exchange formula and get

$$\mathbb{E}\, h(D^*) = \frac{\lambda}{\lambda'}\, \mathbb{E}\left(\mathbb{E}\Big(\sum_{\widetilde{L}_n \in S^*_H} h(|\widetilde{L}_n|) \,\Big|\, S^*_H \Big) \right).$$

Again, $\widetilde{L}$ is independent of H^*_S under $P^*_{H_S}$ given S^*_H. Moreover, $\lambda' = \lambda'_\ell \gamma$ and $\widetilde{L} \cap S^*_H$ is a Cox process whose random intensity measure is given by $\lambda'_\ell \nu_1(B \cap S^*_H)$ for $B \in \mathcal{B}(\mathbb{R}^2)$. Thus, given S^*_H, we can apply Campbell's theorem which yields

$$\mathbb{E}\Big(\sum_{\widetilde{L}_n \in S^*_H} h(|\widetilde{L}_n|) \,\Big|\, S^*_H \Big) = \lambda'_\ell \int_{S^*_H} h(|u|)\, \nu_1(du).$$

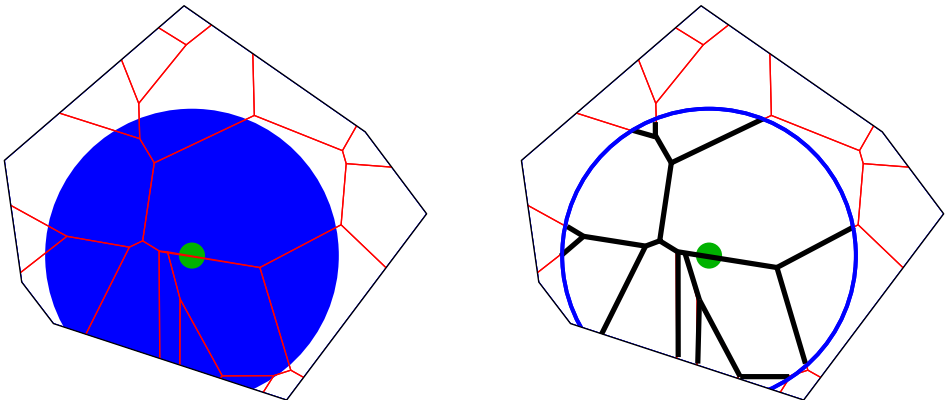

(a) $\Xi_H^* \cap B(o,x)$ (blue) (b) $S_H^* \cap B(o,x)$ (black)

Figure 5.3: The typical cell and the typical segment system intersected by $B(o,x)$.

Hence, choosing $h(|u|) = \mathbb{1}_{[0,x]}(|u|)$ we obtain

$$F_{D^*}(x) = \mathbb{E}\,\mathbb{1}_{[0,x]}(D^*) = \lambda_\ell\,\mathbb{E}\,\nu_1(S_H^* \cap B(o,x))\,,$$

which completes the proof. □

The quantities which are considered in equations (5.2) and (5.3) are illustrated in Figure 5.3. Using Theorem 5.1 it is possible to derive also representation formulae for the probability density of D^*.

Theorem 5.2 *If L is a Poisson process, which is independent of H, then the probability density $f_{D^*} : [0,\infty) \to [0,\infty)$ of D^* is given by*

$$f_{D^*}(x) = \lambda_\ell\,\gamma\,\mathbb{E}\,\nu_1(\Xi_H^* \cap \partial B(o,x))\,, \qquad x \geq 0\,, \tag{5.5}$$

where $\nu_1(\Xi_H^* \cap \partial B(o,x))$ denotes the curve length of the circle $\partial B(o,x)$ centered at o with radius x inside Ξ_H^*. If L is a Cox processes on T which is conditionally independent of H given T, then the probability density of D^* is given by

$$f_{D^*}(x) = \lambda_\ell\,\mathbb{E}\left(\sum_{i=1}^{N_x^*} \frac{1}{\sin\alpha_i^*}\right), \qquad x \geq 0\,, \tag{5.6}$$

where $N_x^* = |S_H^* \cap \partial B(o,x)|$ is the number of intersection points of the segment system S_H^* with $\partial B(o,x)$ and $\alpha_1^*, \ldots, \alpha_{N_x^*}^*$ are the angles at the corresponding intersection points between their tangents to $\partial B(o,x)$ and the intersecting segments.

Proof If L is a Poisson process, then we can use the polar decomposition of the 2-dimensional Lebesgue measure in order to get from (5.2) that

$$\begin{aligned} F_{D^*}(x) &= \lambda_\ell \gamma\, \mathbb{E} \int_{\mathbb{R}^2} \mathbb{1}_{\Xi_H^* \cap B(o,x)}(y)\, \nu_2(dy) \\ &= \lambda_\ell \gamma\, \mathbb{E} \int_0^\infty \int_0^{2\pi} r\, \mathbb{1}_{\Xi_H^* \cap B(o,x)}((r\cos t, r\sin t)\, dt\, dr \\ &= \lambda_\ell \gamma\, \mathbb{E} \int_0^x \int_0^{2\pi} r\, \mathbb{1}_{\Xi_H^*}((r\cos t, r\sin t)))\, dt\, dr \\ &= \int_0^x \lambda_\ell \gamma \mathbb{E} \nu_1(\Xi_H^* \cap \partial B(o,r))\, dr\,, \end{aligned}$$

If L is a Cox process, then we can use a decomposition of the Hausdorff measure ν_1 which is given in Lemma A.14 in the appendix. Similar as above, we get that

$$\begin{aligned} F_{D^*}(x) &= \lambda_\ell\, \mathbb{E}\, \nu_1(S_H^* \cap B(o,x)) \\ &= \lambda_\ell\, \mathbb{E} \int_0^\infty \sum_{i=1}^{N_y^*} \frac{1}{\sin\alpha_i^*}\, \mathbb{1}_{[0,x]}(y)\, dy \\ &= \int_0^x \lambda_\ell\, \mathbb{E}\Big(\sum_{i=1}^{N_y^*} \frac{1}{\sin\alpha_i^*} \Big)\, dy\,, \end{aligned}$$

which proves Theorem 5.2. □

The quantities considered in equations (5.5) and (5.6) are shown Figure 5.4 for a PVT as underlying tessellation. Note that the results of this section can be generalized in the following way. In the proof of Theorem 5.1 we never used that L is a Poisson process and a Cox process on T, respectively. On the one hand, for a Poisson process L, we only used that L is a stationary point process of intensity λ' independent of T. On the other hand, for a Cox process L on T, we only used that given T its conditional intensity measure is given by $\lambda'_\ell \nu_1(\,\cdot \cap T^{(1)})$ and that L is independent of H given T. Thus, the result of Theorem 5.1 remains valid if L is a stationary point process independent of T and a point process whose conditional intensity measure is given by $\lambda'_\ell \nu_1(\,\cdot \cap T^{(1)})$ conditioned on T which is in addition independent of H given T.

For $n \geq 1$, assume that Ξ_H^* denotes the n-th nearest-neighbor Voronoi cell ([79]). Then F_{D^*} given in (5.2) and (5.3) is the distribution function of the distance from a typical point of L to its n-th nearest neighbor of H. Moreover, if L is a Cox process, then F_{D^*} is the distribution function of the typical n-th nearest-neighbor distance between points of H. These distributions have applications e.g. in the analysis of interference in wireless networks ([38]).

Finally, it is worth mentioning that the distribution of D^* does not depend on the choice of the point process L if H is not a Cox process, but a stationary Poisson process in $\mathbb{R}^2$ which is independent of L. Then, the typical Euclidean distance

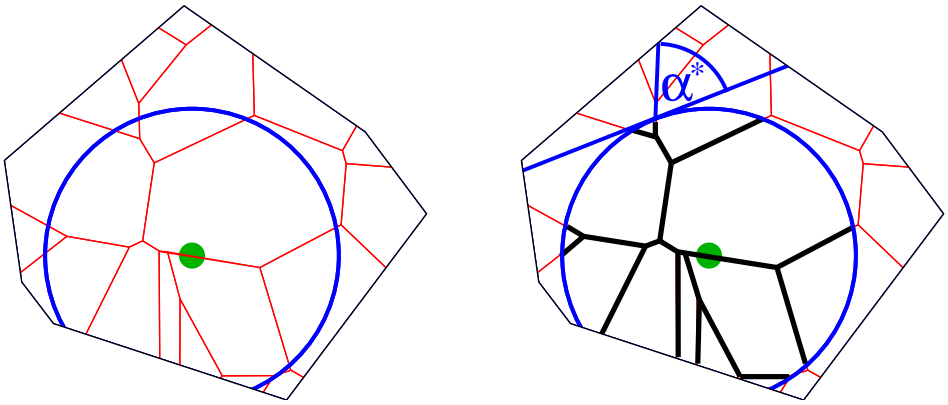

(a) $\Xi_H^* \cap \partial B(o,x)$ (blue) (b) $S_H^* \cap \partial B(o,x)$ (blue) and an angle α^*

Figure 5.4: The typical cell and the typical segment system intersected by $\partial B(o,x)$.

D^* has the same distribution as the distance from o to the nearest point of H, which is a *Weibull distribution* with parameters $\lambda\pi$ and 2, see e.g. [38, 89]. Thus, in this case the density of D^* is given by $f_{D^*}(x) = \lambda\pi x \exp(-\lambda\pi x^2)\mathbb{1}_{[0,\infty)}(x)$.

5.2.2 Example: Cox processes on PLT

In the specific case that H is a Cox process on a PLT with serving zones T_H modeled by the Voronoi tessellation induced by H, it is possible to derive analytical formulae for the distribution functions F_{D^*} considered in (5.2) and (5.3), respectively.

Theorem 5.3 *Let T be a PLT, H a Cox process on T and T_H the Voronoi tessellation induced by H. Then, for $x > 0$, the distribution function considered in (5.2) is given by*

$$F_{D^*}(x) = 1 - \exp\Big(-\lambda_\ell\,\gamma\,x^2 \int_0^2 e^{-\lambda_\ell\, xs}\sqrt{4-s^2}\,ds\Big)\,, \tag{5.7}$$

and the distribution function considered in (5.3) is given by

$$F_{D^*}(x) = 1 - e^{-2\lambda_\ell\, x}\exp\Big(-\lambda_\ell\,\gamma\,x^2 \int_0^2 e^{-\lambda_\ell\, xs}\sqrt{4-s^2}\,ds\Big)\,. \tag{5.8}$$

Proof Let H be a Cox process which is concentrated on the PLT T and let L be a Poisson process independent of H. Then, using the independence of the processes L and H, we get for each $x \geq 0$ that $F_{D^*}(x) = 1 - \mathbb{P}(H(B(o,x)) = 0)$

and

$$\begin{aligned}\mathbb{P}(H(B(o,x))=0) &= \mathbb{E}\exp(-\lambda_\ell \nu_1(B(o,x)\cap T))\\ &= \mathbb{E}\exp\Big(-\lambda_\ell x \nu_1(B(o,1)\cap \frac{1}{x}T)\Big).\end{aligned}$$

The latter expectation can be calculated in the following way. Suppose that K denotes the random number of lines of T which intersect $B(o,x)$. Then K is Poisson distributed with mean $2\gamma x$ and, given $K=k$, these k lines $\ell_1,\dots,\ell_k$ are independent and isotropic uniform random (IUR) lines ([66]). Thus we get

$$\begin{aligned}&\mathbb{E}\exp\Big(-\lambda_\ell x \nu_1(B(o,1)\cap\frac{1}{x}T)\Big)\\ &= \sum_{k=0}^{\infty}\mathbb{P}(K=k)\,\mathbb{E}\Big(\exp\big(-\lambda_\ell x\nu_1(B(o,1)\cap\frac{1}{x}T)\big)\;\big|\;K=k\Big)\\ &= \sum_{k=0}^{\infty}\mathbb{P}(K=k)\,\mathbb{E}\Big(\prod_{i=1}^{k}\exp\big(-\lambda_\ell x\nu_1(B(o,1)\cap\ell_i)\big)\;\big|\;K=k\Big)\\ &= \sum_{k=0}^{\infty}\mathbb{P}(K=k)\,\Big(\mathbb{E}\exp\big(-\lambda_\ell x Z\big)\Big)^k\\ &= \exp(-2\gamma x)\sum_{k=0}^{\infty}\frac{\big(2\gamma x\mathbb{E}\exp(-\lambda_\ell x Z)\big)^k}{k!}\\ &= \exp\big(-2\gamma x\big(1-\mathbb{E}\exp(-\lambda_\ell x Z)\big)\big)\,,\end{aligned}$$

where Z denotes the intersection length of an IUR line hitting $B(o,1)$. The distribution function of Z can be computed as $F_Z(s)=1-\sqrt{1-s^2/4}$ for $s\in[0,2]$. By partial integration we finally get that

$$\mathbb{E}\exp(-\lambda_\ell x Z) = 1-\frac{\lambda_\ell x}{2}\int_0^2 e^{-\lambda_\ell x s}\sqrt{4-s^2}\,ds\,,$$

which proves (5.7). If L is a Cox process, then we can do in principle the same calculations. However, due to Slivnyak's theorem, there is almost surely one additional line through the origin which yields the additional factor $\exp(-2\lambda_\ell x)$ appearing in (5.8). □

Notice that we can also derive analytical formulae for the probability densities of D^* if T is a PLT, by simply computing the derivatives of the functions given in (5.7) and (5.8), respectively. But, if the random tessellation T is different from a PLT, H is not a Cox process or T_H is not a Voronoi tessellation, then analytical solutions seem to be impossible.

5.3 Statistical estimators

Formulae (5.2) – (5.5) can be used in order to define estimators for the density and distribution function of the typical Euclidean distance D^* which are based on samples of the typical serving zone Ξ_H^* and its line segment system S_H^*, respectively. Such samples can be obtained from simulations for various models, see Chapter 4.

5.3.1 Estimators for distribution function and density of D^*

The representation formulae (5.2) – (5.5) directly lead to estimators for the distribution function and probability density of D^* which can be calculated based on Monte-Carlo simulations of Ξ_H^* and S_H^*. Note that we do not have to simulate points of L.

Assume that $\Xi_{H,1}^*, \ldots, \Xi_{H,n}^*$ and $S_{H,1}^*, \ldots, S_{H,n}^*$ are n independent copies of Ξ_H^* and S_H^*, respectively. If L is a Poisson process, then estimators $\widehat{F}_{D^*}(x;n)$ and $\widehat{f}_{D^*}(x;n)$ for the distribution function $F_{D^*}(x)$ and the density $f_{D^*}(x)$, respectively, can be defined by

$$\widehat{F}_{D^*}(x;n) = \frac{\lambda_\ell \, \gamma}{n} \sum_{i=1}^{n} \nu_2(\Xi_{H,i}^* \cap B(o,x)) \tag{5.9}$$

and by

$$\widehat{f}_{D^*}(x;n) = \frac{\lambda_\ell \, \gamma}{n} \sum_{i=1}^{n} \nu_1(\Xi_{H,i}^* \cap \partial B(o,x)) \,. \tag{5.10}$$

If L is a Cox process, we define an estimator $\widehat{F}_{D^*}(x;n)$ for the distribution function $F_{D^*}(x)$ by

$$\widehat{F}_{D^*}(x;n) = \frac{\lambda_\ell}{n} \sum_{i=1}^{n} \nu_1(S_{H,i}^* \cap B(o,x)) \,. \tag{5.11}$$

It is easy to see that the estimators in (5.9) – (5.11) are unbiased and in addition strongly consistent for fixed $x \geq 0$. However, if L is a Cox process, then it is not recommended to use equation (5.6) in order to define an analogous estimator $\widehat{f}_{D^*}(x;n)$ for $f_{D^*}(x)$ by just omitting the expectation in (5.6). Computer experiments have shown that this estimator is numerically unstable due to the measurements of small angles. In the latter case, a better way to estimate the density seems to be the computation of the estimated distribution function $\widehat{F}_{D^*}(x;n)$ by formula (5.11) and then to consider difference quotients obtained from this estimated distribution function as estimators $\widehat{f}_{D^*}(x;n)$ for the values of the density $f_{D^*}(x)$. Note that all estimators introduced in this section have advantages compared to estimators which are based on simulations of the whole model in a large sampling window. These methods are computationally more

intensive and they only approximate the distribution of D^*. In addition, they demand to simulate also the points of L and thus lead to a larger variability, see also Section 5.5.3. Moreover, using the estimators for F_{D^*} and f_{D^*} given in equations (5.9) – (5.11), it is possible to unbiasedly estimate even functionals of D^*, like moments of any order.

5.3.2 Almost sure convergence of the maximal error

Note that the estimators $\widehat{f}_{D^*}(x;n)$ and $\widehat{F}_{D^*}(x;n)$ defined in (5.10) and (5.11), respectively, are strongly consistent for each $x \in \mathbb{R}$. But we can even show that they are uniformly consistent. For instance, we can prove that the maximal deviation between the estimator $\widehat{f}_{D^*}(x;n)$ introduced in equation (5.10) and the true density f_{D^*} converges almost surely to zero if L is a Poisson process.

Theorem 5.4 *Let L be a Poisson process, then*

$$\mathbb{P}\left(\lim_{n\to\infty} \sup_{x\in\mathbb{R}} |\widehat{f}_{D^*}(x;n,\omega) - f_{D^*}(x)| = 0\right) = 1\,.$$

Proof Let $\varepsilon > 0$, then we have to show that for almost all $\omega \in \Omega$ there exists $N(\varepsilon,\omega)$ with

$$|\widehat{f}_{D^*}(x;n,\omega) - f_{D^*}(x)| \le \varepsilon$$

for all $n \ge N(\varepsilon,\omega)$ and $x \in [0,\infty)$. Suppose that $0 = q_0 < q_1 < \cdots < q_m < q_{m+1} = \infty$ with $|q_{i+1} - q_i| \le \delta$ for $i = 1,\ldots,m-1$, where δ, m and q_m depend on ε. Then $x \in [q_i, q_{i+1})$ for some $i = 0,\ldots,m$ and we get

$$\begin{aligned} |\widehat{f}_{D^*}(x;n,\omega) - f_{D^*}(x)| &\le |\widehat{f}_{D^*}(x;n,\omega) - \widehat{f}_{D^*}(q_i;n,\omega)| \\ &+ |\widehat{f}_{D^*}(q_i;n,\omega) - f_{D^*}(q_i)| + |f_{D^*}(q_i) - f_{D^*}(x)|\,. \end{aligned} \tag{5.12}$$

Now the law of large numbers yields

$$|\widehat{f}_{D^*}(q_i;n,\omega) - f_{D^*}(q_i)| \overset{a.s.}{\to} 0$$

for $n \to \infty$. Thus, $|\widehat{f}_{D^*}(q_i;n,\omega) - f_{D^*}(q_i)| < \varepsilon/3$ for all $n > N_i(\varepsilon,\omega)$ almost surely. Since f_{D^*} is continuous and $\lim_{x\to\infty} f_{D^*}(x) = 0$, we can choose δ and q_m such that $|f_{D^*}(q_i) - f_{D^*}(x)| < \varepsilon/3$. For the remaining term we get

$$\begin{aligned} |\widehat{f}_{D^*}(x;n,\omega) &- \widehat{f}_{D^*}(q_i;n,\omega)| \\ &\le \frac{\lambda_\ell \gamma}{n} \sum_{j=1}^{n} |\nu_1\big(\Xi^*_{H,j} \cap \partial B(o,x)\big) - \nu_1\big(\Xi^*_{H,j} \cap \partial B(o,q_i)\big)|\,. \end{aligned}$$

On the one hand, it holds that

$$\begin{aligned} \nu_1\big(\Xi^*_{H,j} \cap \partial B(o,x)\big) - \nu_1\big(\Xi^*_{H,j} \cap \partial B(o,q_i)\big) &\le \nu_1\big(\Xi^*_{H,j} \cap \partial B(o,q_i)\big)\Big(\frac{q_{i+1}}{q_i} - 1\Big) \\ &\le 2\pi(q_{i+1} - q_i)\,. \end{aligned}$$

On the other hand, we have

$$\begin{aligned}\nu_1\big(\Xi^*_{H,j}\cap\partial B(o,q_i)\big) \;-\; & \nu_1\big(\Xi^*_{H,j}\cap\partial B(o,x)\big)\\ &\leq\; \nu_1(\Xi^*_{H,j}\cap\partial B(o,q_i)) - \nu_1\bigg(\Big(\frac{q_i}{q_{i+1}}\Xi^*_{H,j}\Big)\cap\partial B(o,q_i)\bigg)\\ &=\; \nu_1\left(\Xi^*_{H,j}\backslash\Big(\frac{q_i}{q_{i+1}}\Xi^*_{H,j}\Big)\cap\partial B(o,q_i)\right).\end{aligned}$$

These considerations yield

$$\begin{aligned}|\widehat{f}_{D^*}(x;n,\omega) \;-\; & \widehat{f}_{D^*}(q_i;n,\omega)|\\ &\leq\; 2\pi\lambda_\ell\gamma(q_{i+1}-q_i)+\frac{\lambda_\ell\gamma}{n}\sum_{j=1}^{n}\nu_1\left(\Xi^*_{H,j}\backslash\Big(\frac{q_i}{q_{i+1}}\Xi^*_{H,j}\Big)\cap\partial B(o,q_i)\right).\end{aligned}$$

Note that the function $g(q,q')=\lambda_\ell\gamma\mathbb{E}\nu_1(\Xi^*_H\backslash(\frac{q}{q'}\Xi^*_H)\cap\partial B(o,q))$ is continuous on $[0,\infty)\times[0,\infty)$ if we put $g(q,0)=0$ for all $q\in[0,\infty)$. Furthermore, we have $g(q,q)=0$ for all $q\in[0,\infty)$ and $g(q,q')\leq\lambda_\ell\gamma\mathbb{E}\nu_1(\Xi^*_H\cap\partial B(o,q))=h(q)$ with $h(q)\to 0$ for $q\to\infty$. Thus, we can choose δ, m and q_m with $g(q_i,q_{i+1})<\varepsilon/6$ for all $i=0,\ldots,m$. Since the law of large numbers yields almost surely

$$\lim_{n\to\infty}\frac{\lambda_\ell\gamma}{n}\sum_{j=1}^{n}\nu_1\left(\Xi^*_{H,j}\backslash\Big(\frac{q_i}{q_{i+1}}\Xi^*_{H,j}\Big)\cap\partial B(o,q_i)\right) \;=\; g(q_i,q_{i+1})<\frac{\varepsilon}{6},$$

we can choose $N_i(\varepsilon,\omega)$ such that

$$2\lambda_\ell\gamma\pi(q_{i+1}-q_i)+\frac{\lambda_\ell\gamma}{n}\sum_{j=1}^{n}\nu_1\left(\Xi^*_{H,j}\backslash\Big(\frac{q_i}{q_{i+1}}\Xi^*_{H,j}\Big)\cap\partial B(o,q_i)\right) \;\leq\; \frac{\varepsilon}{3}$$

for all $n>N_i(\varepsilon,\omega)$. Thus, we have almost surely that

$$|\widehat{f}_{D^*}(x;n,\omega)-f_{D^*}(x)| \;\leq\; \varepsilon$$

for all $x\in[0,\infty)$ and $n\geq\max\{N(\varepsilon,\omega),N_1(\varepsilon,\omega),\ldots,N_{m-1}(\varepsilon,\omega)\}$. □

Furthermore, it can be shown that the maximal deviation between $\widehat{F}_{D^*}(x;n)$ and the true distribution function $F_{D^*}(x)$ converges almost surely to 0 if L is a Cox process.

Theorem 5.5 *Let L be a Cox process. Then*

$$\mathbb{P}\left(\lim_{n\to\infty}\sup_{x\in\mathbb{R}}|\widehat{F}_{D^*}(x;n,\omega)-F_{D^*}(x)|=0\right)=1.$$

Proof The proof is similar as the proof above. Let $\varepsilon > 0$ and suppose that $0 = q_0 < q_1 < \cdots < q_m < q_{m+1} = \infty$ with $q_{i+1} - q_i < \delta$ for $i = 0, \ldots, m-1$, where δ, m and q_m depend on ε. For each $x \in [0, \infty)$, we have $x \in [q_i, q_{i+1})$ for some $i = 0, \ldots, m$ and the law of large numbers yields

$$\begin{aligned} |\widehat{F}_{D^*}(x; n, \omega) - F_{D^*}(x)| &\leq |\widehat{F}_{D^*}(q_i; n, \omega) - F_{D^*}(q_i)| \\ &+ F_{D^*}(q_{i+1}) - F_{D^*}(q_i) + \widehat{F}_{D^*}(q_{i+1}; n, \omega) - \widehat{F}_{D^*}(q_i; n, \omega) \\ &\overset{a.s.}{\to} 2(F_{D^*}(q_{i+1}) - F_{D^*}(q_i)) \end{aligned}$$

for $n \to \infty$, where we put $\widehat{F}_{D^*}(q_{m+1}; n, \omega) = F_{D^*}(q_{m+1}) = 1$. Since $2(F_{D^*}(q_{i+1}) - F_{D^*}(q_i)) < \varepsilon$ for $i = 0, \ldots, m$ if δ is small enough, we can choose $N(\varepsilon, \omega)$ such that almost surely

$$|\widehat{F}_{D^*}(x; n, \omega) - F_{D^*}(x)| \leq \varepsilon \quad \text{for all} \quad x \in \mathbb{R}, n \geq N(\varepsilon, \omega)\,.$$

□

5.3.3 Numerical results from Monte-Carlo simulation

In order to estimate the distribution of D^*, we simulated the typical cell Ξ_H^* together with its typical segment system S_H^* for the case that T_H is the Voronoi tessellation induced by the Cox process H on PDT and PVT, respectively. Thus, we assumed that a point of L is connected to the nearest point of H. Because of the scaling invariance of Cox processes on random tessellations, the length intensity γ of T was set to 1 and only different values of the scaling factor $\kappa = \gamma/\lambda_\ell$ were considered. Results corresponding to other parameter pairs (γ', λ'_ℓ) with $\kappa = \gamma'/\lambda'_\ell$ can then be obtained from the results for $\gamma = 1$ be an appropriate scaling, compare Section 4.6.

From the simulated data the density and distribution of D^* was then estimated using the estimators introduced in Section 5.3.1 for a Cox process and Poisson process L, respectively. Note that for Cox processes L the estimated distribution function $\widehat{F}_{D^*}(x; n)$ was used in order to estimate the density $f_{D^*}(x)$ by difference quotients. Furthermore, for a Cox process H on PLT, the density of D^* was calculated by means of (5.7) and (5.8), respectively. The obtained results are shown in Figures 5.5 and 5.6 together with the density of a $Wei(\lambda_\ell \gamma \pi, 2)$-distribution. Some estimated distribution functions are displayed in Figure 5.7. Note that the $Wei(\lambda_\ell \gamma \pi, 2)$-distribution is the distribution of the random distance from the typical point of L to the nearest point of an independent stationary Poisson process H of intensity $\lambda = \lambda_\ell \gamma$. Thus, it is interesting to compare the distribution of D^* with the $Wei(\lambda_\ell \gamma \pi, 2)$-distribution. In Chapter 6 it is even shown that D^* converges in distribution to the $Wei(\lambda\pi, 2)$-distribution for $\kappa = \gamma/\lambda_\ell \to \infty$ provided that $\gamma \lambda_\ell = \lambda$ if the underlying tessellation T is ergodic. This observation can be explained intuitively by the fact that, for large κ, we have only few points per

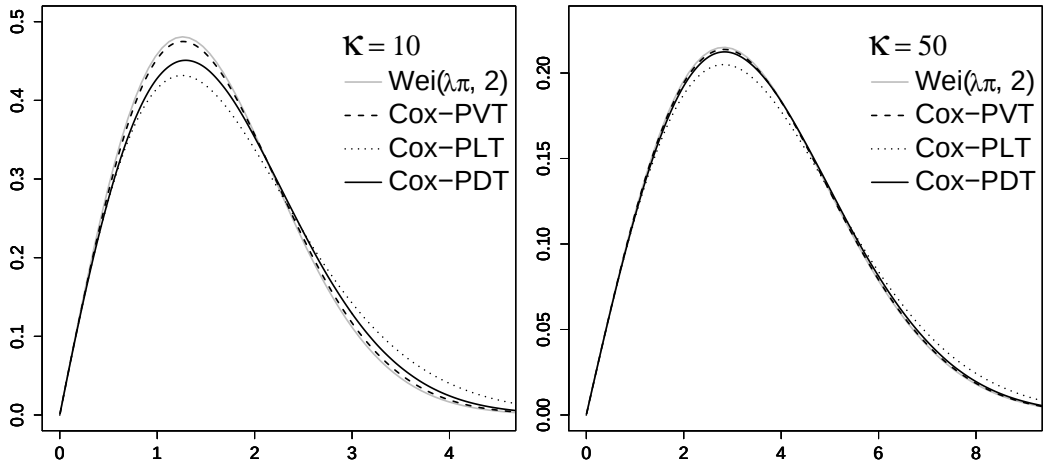

(a) Density of D^*, $\kappa = 10$ (b) Density of D^*, $\kappa = 50$

Figure 5.5: Estimated density of D^* if L is a Poisson process

segment of T. Thus, the dependence between the points decreases for increasing κ yielding a point process H which is similar to a stationary Poisson process.

On the one hand, if L is a Poisson process and H a Cox process on PVT, the histogram of D^* can hardly be distinguished from the one corresponding to a $Wei(\gamma\lambda_\ell\pi, 2)$-distribution, even for small values of κ. For PDT and, in particular, for PLT this is not the case. On the other hand, if L is a Cox process, then the distribution of D^* is considerably different from the $Wei(\gamma\lambda_\ell\pi, 2)$-distribution, even if H is a Cox process on PVT. Then, also for larger values of κ, a clear difference between the Weibull-distribution and the distribution of the typical Euclidean distance D^* can be observed. A fact which may cause this discrepancy is that for a Poisson process L the typical connection distance D^* solely depends on the shape of the typical cell Ξ_H^*. However, for a Cox process L, the distribution of D^* depends in addition on the structure of the typical segment system S_H^* within Ξ_H^*.

Furthermore, we considered the case that T_H is modeled by a the Voronoi tessellation of a Cox process on a PVT/PLT-nesting, i.e., we considered the case that T is a T_0/T_1-nesting with a PVT T_0 of length intensity γ_0 and a PLT T_1 of length intensity γ_1, where we again assumed that $\gamma = \gamma_0 + \gamma_1 = 1$. We used the simulation algorithm developed for the typical Voronoi cell Ξ_H^* and the typical segment system S_H^* of Cox processes on PVT/PLT-nestings in order to generate samples of Ξ_H^* and S_H^* which were used to estimate the density of D^* for Poisson processes and Cox processes L as explained above. Some densities estimated from these samples are displayed in Figure 5.8, where $\gamma_0 = 0.25, 0.5$ and 0.75. The behavior of the densities is similar as for Cox processes H on PDT, PLT and PVT. For increasing κ the difference between the densities decreases, but for small values of κ a clear difference between the densities is observable for the

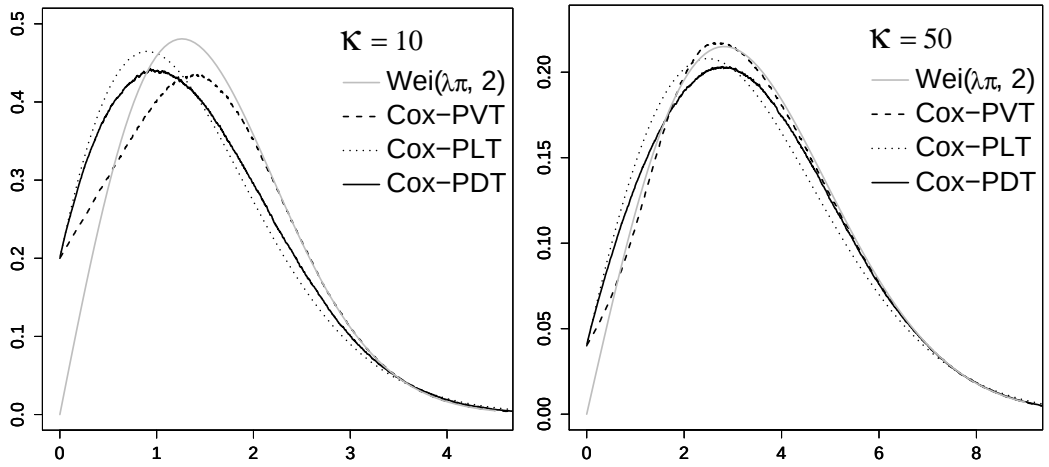

(a) Density of D^*, $\kappa = 10$ (b) Density of D^*, $\kappa = 50$

Figure 5.6: Estimated density of D^* if L is a Cox process

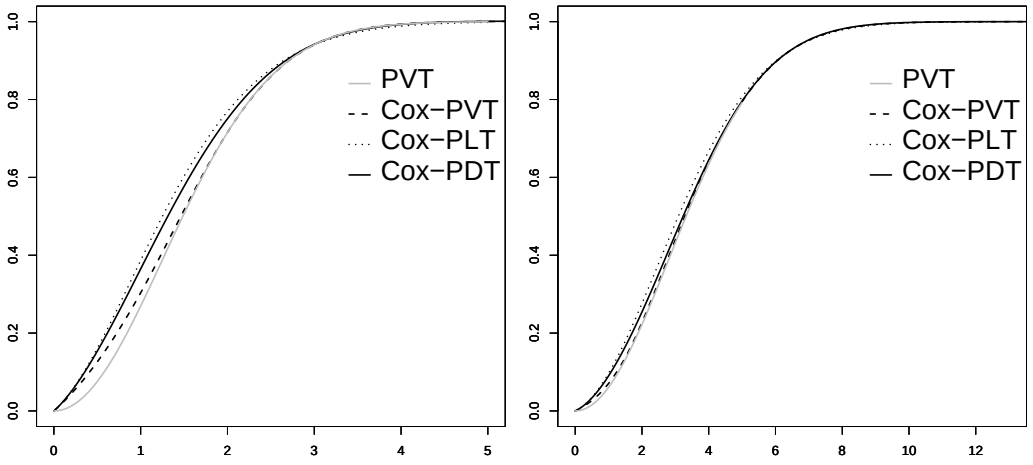

(a) Distribution function of D^*, $\kappa = 10$ (b) Distribution function of D^*, $\kappa = 50$

Figure 5.7: Estimated distribution function of D^* if L is a Poisson process

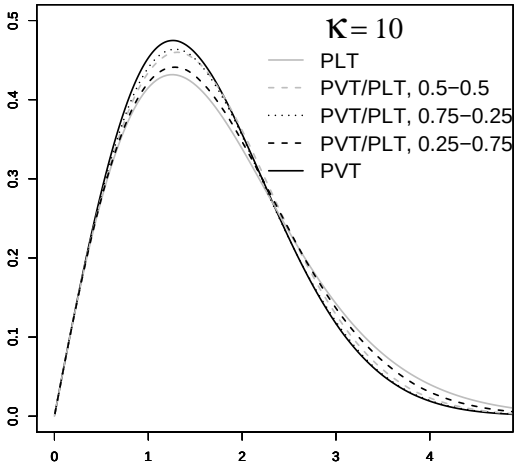

(a) Density of D^* for Poisson process L

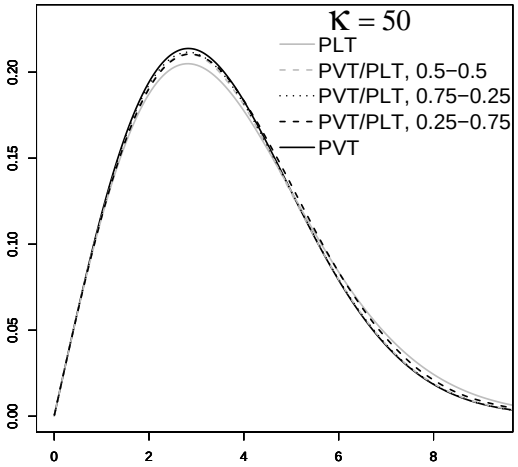

(b) Density of D^* for Poisson process L

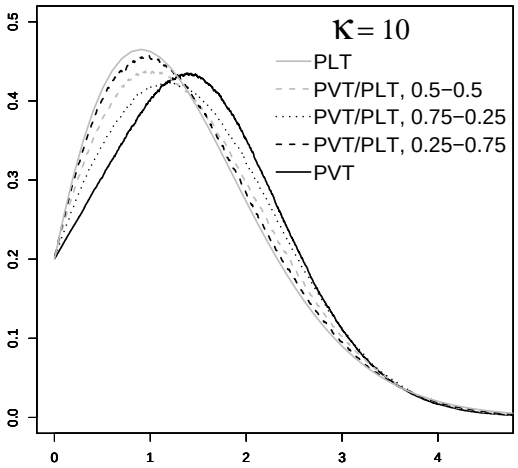

(c) Density of D^* for Cox process L, $\kappa = 10$

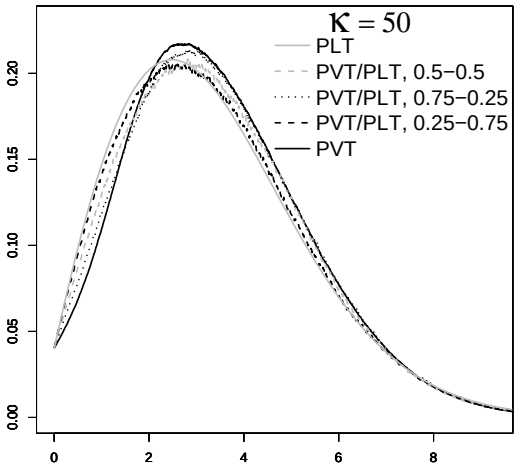

(d) Density of D^* for Cox process L, $\kappa = 50$

Figure 5.8: Density of D^* if L is a Poisson process and Cox process

considered models. Note that the distributions of D^* for PVT and PLT occur as extremal cases and we can interpolate from PVT to PLT if γ_0 goes from 1 to 0. Thus, if we consider iterated tessellations as street model, we arrive at more flexible classes of distance distributions which include the distance distributions for the simple tessellation models.

5.4 Shortest path connection lengths

In this section we consider basically the same model as in the preceding section, but we assume that points of L are connected to their associated point of H on the shortest path along the edges of the underlying tessellation and we are interested in the length of this path.

5.4.1 Typical shortest path length C^*

In principle, we consider the stochastic model introduced in Section 5.1, where we always assume that L is a Cox process on $T^{(1)}$ with linear intensity λ'_ℓ which is conditionally independent of H given T. We then link each point L_n of L to the point H_j of H if and only if $L_n \in S_{H,j} = S^o_{H,j} + H_n$. However, this time we mark L_n with the shortest path length C_n from L_n to H_j along $T^{(1)}$. A realization of the model is shown in Figure 5.9 for a Cox process H on T, where the serving zones T_H are constructed as the Voronoi tessellation induced by H. In this way we obtain the stationary marked point process $L_C = \{(L_n, C_n)\}$. The cost functional considered here is the *typical shortest path length* C^*, i.e., we are interested in the Palm mark distribution $P^o_{L_C}$ of L_C.

5.4.2 Representation formula

In this section we investigate the distribution of the typical shortest path length C^*. To start with, we derive a representation formula for the density f_{C^*} of C^* which expresses the distribution of C^* as the expectation of functionals of the typical segment system S^*_H by the help of Neveu's exchange formula given in Lemma 2.9. This representation formula can be used in order to construct estimators for f_{C^*} which are based on i.i.d. samples of the typical segment system S^*_H. Recall that such samples can be obtained from Monte Carlo simulation of S^*_H which is e.g. possible for Voronoi tessellations T_H if T is a PLT, PVT and PDT, respectively, and H is a Cox process on $T^{(1)}$ or a thinning of the vertices $T^{(0)}$ of T, see Chapter 4.

However, first we show that the quantity $\mathbb{E}h(C^*)$ for non-negative measurable functions h can be represented in terms of the Palm distribution of H_S.

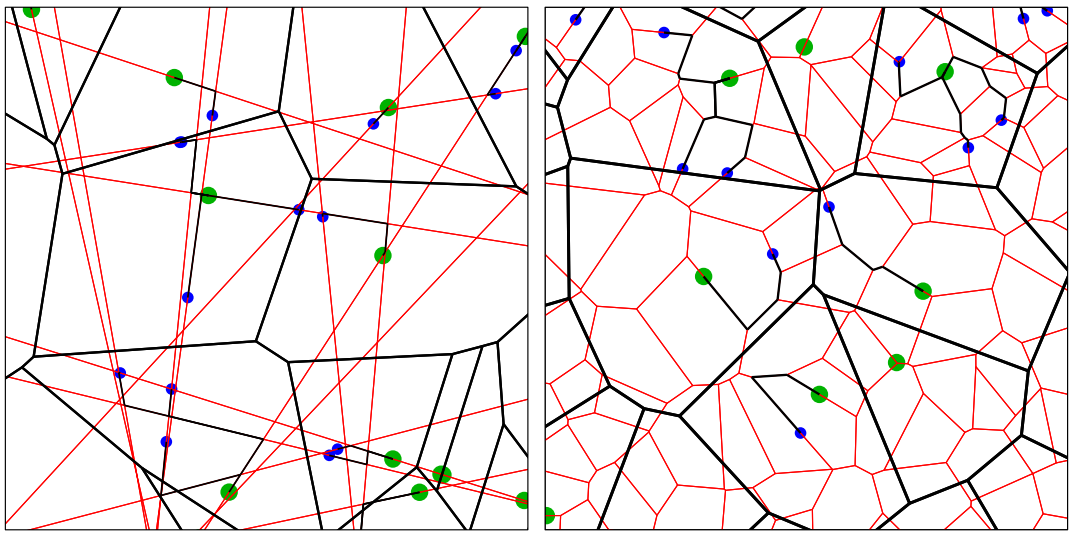

(a) PLT (b) PVT

Figure 5.9: HLC with their serving zones (black) and LLC (blue) with shortest paths along the edge set (red) for different street models

Lemma 5.6 *Let $h : \mathbb{R} \to [0, \infty)$ be a measurable function which is non-negative. Then,*

$$\mathbb{E}\, h(C^*) = \lambda_\ell\, \mathbb{E} \int_{S_H^*} h(c(y))\, \nu_1(dy)\,, \tag{5.13}$$

where $c(y)$ is the shortest path length from y to o along the edges of H_S^*, H_S^* is distributed according to the Palm distribution $P_{H_S}^*$ of H_S and S_H^* denotes the typical segment system centered at o of H_S^*.

Proof The proof is similar to the proof of Theorem 5.1. We can apply Neveu's exchange formula to the vector $Y = \{(L_C, H_S)\}$ of marked point processes. Let $(\widetilde{L}_C, H_S^*)$ be distributed according to $P_{H_S}^*$ and let $T^{*(1)}$ be the edge set of H_S^*. Furthermore, we use the notation $\widetilde{L}_C = \{(\widetilde{L}_n, \widetilde{C}_n)\}$. Using the function $f : \mathbb{R}^2 \times [0, \infty) \times \mathcal{L}^o \times \mathsf{N}_{[0,\infty),\mathcal{L}^o} \to [0, \infty)$ defined by

$$f(x, c, \zeta, \psi) = \begin{cases} h(c) & \text{if } x \in \zeta\,, \\ 0 & \text{otherwise}\,, \end{cases} \tag{5.14}$$

we get with Neveu's exchange formula that

$$\begin{aligned} \mathbb{E}h(C^*) &= \frac{\lambda}{\gamma \lambda_\ell'} \mathbb{E}\Big(\int_{S_H^*} h(c(x)) \widetilde{L}(dx) \Big) \\ &= \frac{\lambda_\ell}{\lambda_\ell'} \mathbb{E}\Big(\mathbb{E}\Big(\int_{S_H^*} h(c(x)) \widetilde{L}(dx) \Big| T^{*(1)} \Big) \Big)\,. \end{aligned} \tag{5.15}$$

Now the point process $\widetilde{L}$ is a Poisson process given $T^{*(1)}$ with intensity measure $\lambda'_\ell \nu_1(\,\cdot\, \cap T^{*(1)})$ concentrated on $T^{*(1)}$. Thus we can apply Campbell's Theorem which yields

$$\mathbb{E}\Big(\int_{S_H^*} h(c(x)) \widetilde{L}(dx) \Big| T^{*(1)} \Big) \;=\; \lambda'_\ell \int_{S_H^*} h(c(y)) \nu_1(dy)\,.$$

□

Recall that $\mathbb{E}\nu_1(S_H^*) = 1/\lambda_\ell$, thus we can rewrite the representation formula of $\mathbb{E}h(C^*)$ given in (5.13) as

$$\mathbb{E}\, h(C^*) = \frac{1}{\mathbb{E}\nu_1(S_H^*)}\, \mathbb{E} \int_{S_H^*} h(c(y))\, \nu_1(dy)\,. \tag{5.16}$$

It is important that the expectation $\mathbb{E}\, h(C^*)$ does not depend on the linear intensity λ'_ℓ of the process L anymore. Furthermore, we can rewrite equation (5.13) as

$$\mathbb{E}\, h(C^*) = \lambda_\ell\, \mathbb{E} \sum_{i=1}^{N} \int_{c(A_i)}^{c(B_i)} h(u)\, du\,, \tag{5.17}$$

where the segment system S_H^* is subdivided into line segments $S_1, \ldots, S_N$, where $A_1, B_1, \ldots, A_N, B_N$ denote the endpoints of these segments which are defined such that

- $S_H^* = \bigcup_{i=1}^N S_i$,
- $\nu_1(S_i \cap S_j) = 0$ for $i \neq j$ and
- $c(A_i) < c(B_i) = c(A_i) + \nu_1(S_i)$,

see also Figure 5.10. Some segments of S_H^* are divided in this way at so–called *distance peaks*. We call a point z on S_H^* distance peak if there are two different shortest paths from z to o. Notice that N is the random number of line segments of S_H^* after the division and it is not difficult to show that

$$\mathbb{E}N \leq a\mathbb{E}\nu_0(E^*) < \infty\,,$$

where $a > 0$ is some constant and $\nu_0(E^*)$ denotes the number of segments emanating from the typical vertex of T. Using the notation introduced above and Lemma 5.6, we can prove a representation formula for the probability density f_{C^*} of the typical shortest path length C^* which can be applied in order to estimate this density.

Theorem 5.7 *The typical shortest path length C^* is an absolutely continuous random variable and the density is given by*

$$f_{C^*}(x) = \begin{cases} \lambda_\ell\, \mathbb{E} \sum\limits_{i=1}^{N} \mathbb{1}_{[c(A_i),c(B_i))}(x) \text{ if } x \geq 0\,, \\ \\ 0 \quad \text{otherwise.} \end{cases} \tag{5.18}$$

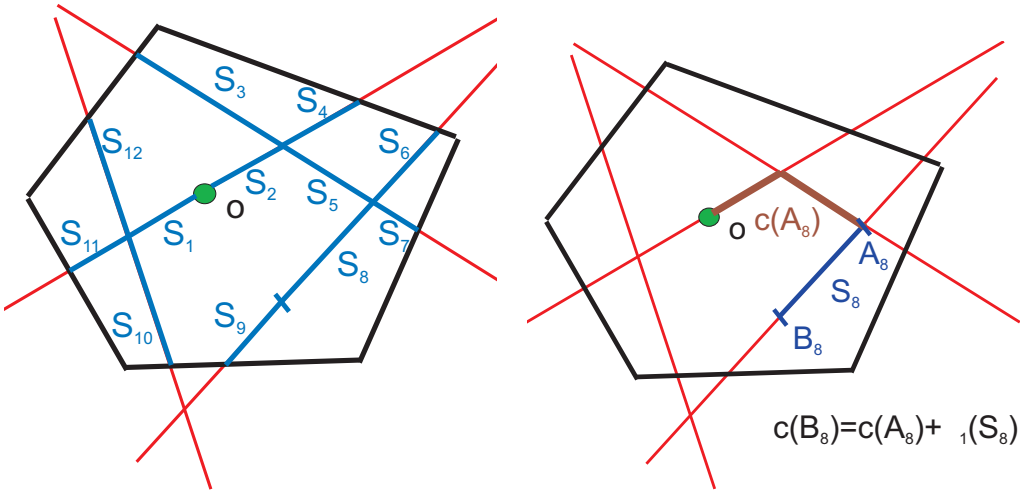

(a) Segments of S_H^* (b) Split segment

Figure 5.10: S_H^* divided into segments $S_1, \ldots, S_N$

Proof Note that the distribution of C^* is given by $P_{C^*}(B) = \mathbb{E}\mathbb{1}_B(C^*)$ for all $B \in \mathcal{B}(\mathbb{R})$, thus we can use equation (5.17) with $h(x) = \mathbb{1}_B(x)$ and get

$$\begin{aligned}
\mathbb{P}_{C^*}(B) &= \lambda_\ell \mathbb{E} \sum_{i=1}^{N} \int_{c(A_i)}^{c(B_i)} \mathbb{1}_B(u) 1 \, du \\
&= \lambda_\ell \mathbb{E} \sum_{i=1}^{N} \int_B \mathbb{1}_{[c(A_i),c(B_i))}(u) \, du \\
&= \int_B \lambda_\ell \mathbb{E} \sum_{i=1}^{N} \mathbb{1}_{[c(A_i),c(B_i))}(u) \, du \,,
\end{aligned}$$

hence the proof is completed. □

We now use Theorem 5.7 to show that f_{C^*} belongs to the space of cadlag functions on $[0, \infty)$, i.e., f_{C^*} is right-continuous and the left-hand limits exist.

Lemma 5.8 *The density f_{C^*} defined in (5.18) is a cadlag function on $[0, \infty)$. Moreover, f_{C^*} is bounded and if H has no points in the set of vertices $T^{(0)}$ of T with probability 1, then $f_{C^*}(0) = 2\lambda_\ell$. If H is a thinning of $T^{(0)}$, then $f_{C^*}(0) = \lambda_\ell \mathbb{E}\nu_0(E^*)$.*

Proof Let $x_0 \in \mathbb{R}$, then we get almost surely

$$\lim_{x \searrow x_0} \sum_{i=1}^{N} \mathbb{1}_{[c(A_i),c(B_i))}(x) = \sum_{i=1}^{N} \mathbb{1}_{[c(A_i),c(B_i))}(x_0) \,,$$

thus the dominated convergence theorem yields that f_{C^*} is right-continuous since $\mathbb{E}N < \infty$. Moreover, it is not difficult to see that

$$g_{C^*}(x) := \lambda_\ell \mathbb{E} \sum_{i=1}^{N} \mathbb{1}_{(c(A_i),c(B_i)]}(x)$$

is a version of the density f_{C^*} that is left-continuous with $f_{C^*}(x) = g_{C^*}(x)$ for every continuity point of f_{C^*}. Thus the left-hand limits of f_{C^*} exist. In addition, $f_{C^*}(x) \leq \lambda_\ell \mathbb{E}N < \infty$ for all $x \in \mathbb{R}$ and hence f_{C^*} is bounded.

On the one hand, if H has almost surely no points in $T^{(0)}$, then the origin is located in the relative interior of a line segment of S_H^* with probability 1. Thus there are almost surely 2 segments emanating from o which means that $f_{C^*}(0) = 2\lambda_\ell$. On the other hand, if H is a thinning of $T^{(0)}$, then the mean number of segments emanating from o under $P_{H_S}^*$ is $\mathbb{E}\nu_0(E^*)$ which completes the proof. □

Using equation (5.18) it is possible to derive estimators $\widehat{f_{C^*}}(x)$ for $f_{C^*}(x)$ which can be calculated from data obtained by simulations of typical serving zones. This is explained in more detail in the next section. However, equation (5.18) can also be used in order to estimate f_{C^*} from information in a large sampling window, where the lower–level components do not have to be regarded. Note that due to Theorem 5.7 and the definition of the Palm mark distribution it holds that

$$f_{C^*}(x) = \frac{1}{\gamma \nu_2(W)} \mathbb{E} \sum_{H_j \in W} \sum_{i=1}^{N_j} \mathbb{1}_{[c(A_i^{(j)}),c(B_i^{(j)}))}(x)\,, \tag{5.19}$$

where $W \in \mathcal{B}_0(\mathbb{R}^2)$ with $\nu_2(W) > 0$, N_j is the number of segments of $S_{H,j}^o$ and $c(A_i^{(j)}), c(B_i^{(j)})$ are the shortest path lengths along $T^{(1)}$ from the endpoints of the i-th segment of $S_{H,j}^o + H_j$ to H_j.

5.5 Statistical estimators

5.5.1 Estimators for the density of C^*

In this section we construct estimators for the density of the typical shortest path length which are based on equation (5.18) in Theorem 5.7. Our aim is to construct estimators which are based on independent samples of the typical segment system S_H^*. Recall that such samples can be obtained from Monte-Carlo simulation for various models, see Chapter 4. However, notice that some shortest paths may lie partly outside Ξ_H^* which means that the line segment system has to be simulated also outside the typical serving zone Ξ_H^* for a certain distance. Now assume that an i.i.d. sample $S_{H,1}^*, \ldots, S_{H,n}^*$ of S_H^* is given. Then, for each $j = 1, \ldots, n$, the shortest path length for all nodes of $S_{H,j}^*$ can be calculated using

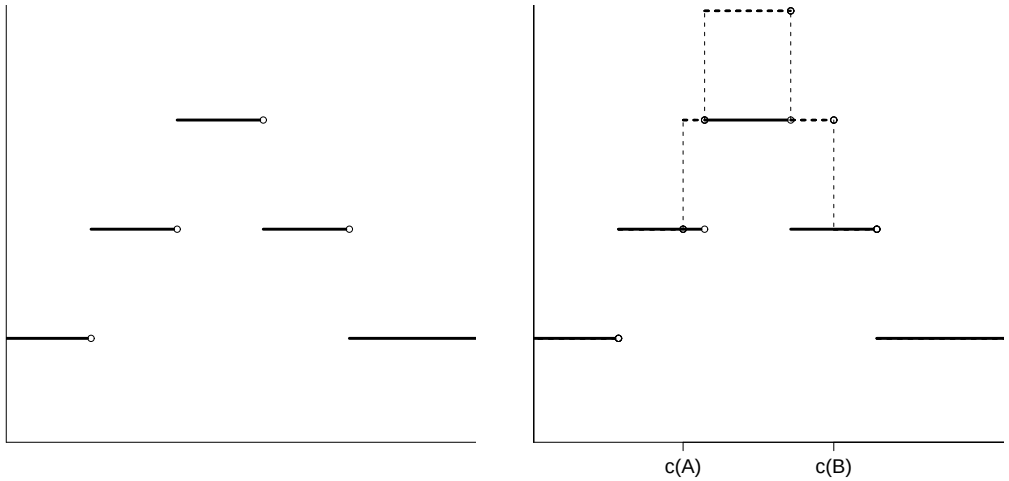

(a) $\widehat{f}_{C^*}(\,\cdot\,;n)$ before adding a segment

(b) Segment with endpoints A and B is added

Figure 5.11: Construction of $\widehat{f}(\,\cdot\,;n)$

e.g. Dijkstra's algorithm ([22]). If there are line segments with a distance peak in their relative interior, then they are split into two segments as mentioned in Section 5.4.2. In this way we obtain the segments $S_1^{(j)},\dots,S_{N_j}^{(j)}$ and the shortest path lengths $c(A_1^{(j)}),c(B_1^{(j)}),\dots,c(A_{N_j}^{(j)}),c(B_{N_j}^{(j)})$ from their endpoints to o. On the basis of this data, we can construct two slightly different estimators. The first one is defined by

$$\widehat{f}_{C^*}(x;n)=\lambda_\ell\,\frac{1}{n}\sum_{j=1}^{n}\sum_{i=1}^{N_j}\mathbb{1}_{[c(A_i^{(j)}),c(B_i^{(j)}))}(x)\;. \tag{5.20}$$

Another estimator can be constructed if we also estimate the expected length of the line segment system in the typical cell from the simulated data. This procedure yields

$$\widetilde{f}_{C^*}(x;n)=\frac{1}{\sum\limits_{j=1}^{n}\nu_1(S_{H,j}^*)}\sum_{j=1}^{n}\sum_{i=1}^{N_j}\mathbb{1}_{[c(A_i^{(j)}),c(B_i^{(j)}))}(x)\;. \tag{5.21}$$

Notice that both functions $\widehat{f}_{C^*}(x;n)$ and $\widetilde{f}_{C^*}(x;n)$, respectively, are step functions. For each line segment $S_i^{(j)}$ with shortest path lengths $c(A_i^{(j)})$ and $c(B_i^{(j)})$ from its endpoints, we add λ_ℓ/n to $\widehat{f}_{C^*}(x;n)$ if $x\in[c(A_i^{(j)}),c(B_i^{(j)}))$. Thus, we obtain a step function and for for each simulation run we add further steps with each generated segment, see Figure 5.11. We now summarize some statistical properties of $\widehat{f}_{C^*}(x;n)$ and $\widetilde{f}_{C^*}(x;n)$.

Theorem 5.9 *Let $\widehat{f}_{C^*}(x;n)$ and $\widetilde{f}_{C^*}(x;n)$ be the estimators defined in (5.20) and (5.21), respectively. Then, for $x \in \mathbb{R}$,*

$$\mathbb{P}\Big(\lim_{n\to\infty} \widehat{f}_{C^*}(x;n) = f_{C^*}(x)\Big) = \mathbb{P}\Big(\lim_{n\to\infty} \widetilde{f}_{C^*}(x;n) = f_{C^*}(x)\Big) = 1 \tag{5.22}$$

and

$$\mathbb{E}\widehat{f}_{C^*}(x;n) = f_{C^*}(x). \tag{5.23}$$

Let $h : \mathbb{R} \to [0,\infty)$ be a measurable function, then

$$\mathbb{E}\left[\int_{\mathbb{R}} h(x)\widehat{f}_{C^*}(x;n)\,dx\right] = \mathbb{E}h(C^*) \tag{5.24}$$

and

$$\mathbb{P}\left(\lim_{n\to\infty}\int_{\mathbb{R}} h(x)\widehat{f}_{C^*}(x;n)\,dx = \lim_{n\to\infty}\int_{\mathbb{R}} h(x)\widetilde{f}_{C^*}(x;n)\,dx = \mathbb{E}h(C^*)\right) = 1\,. \tag{5.25}$$

Proof We get from Theorem 5.7 that the estimator $\widehat{f}_{C^*}(x;n)$ is unbiased. Moreover, the law of large numbers implies that $\lim_{n\to\infty}\widehat{f}_{C^*}(x;n) = f(x)$ with probability 1 for every $x \in \mathbb{R}$. Note that $\mathbb{E}\nu_1(S_H^*) = 1/\lambda_\ell$, thus we have almost surely $\lim_{n\to\infty} 1/n \ \sum_{j=1}^n \nu_1(S_{H,j}^*) = 1/\lambda_\ell$ which yields $\lim_{n\to\infty}\widetilde{f}_{C^*}(x;n) = f(x)$ almost surely. Furthermore, using Fubini's theorem we get that

$$\mathbb{E}\int_{\mathbb{R}} h(x)\widehat{f}_{C^*}(x;n)\,dx \;\; = \;\; \mathbb{E}h(C^*)\,,$$

where we have used the unbiasedness of the estimator $\widehat{f}_{C^*}(x;n)$. The law of large numbers yields the final result since

$$\int_{\mathbb{R}} h(x)\widehat{f}_{C^*}(x;n)\,dx = \frac{\lambda_\ell}{n}\sum_{j=1}^{n}\int_{\mathbb{R}}\sum_{i=1}^{N_j} \mathbb{I}_{[c(A_i^{(j)}),c(B_i^{(j)}))}(x)h(x)\,dx\,.$$

□

Note that the estimator $\widetilde{f}_{C^*}(x;n)$ has an advantage compared to $\widehat{f}_{C^*}(x;n)$, although it is not unbiased. For instance, we always get

$$\int_{\mathbb{R}} \widetilde{f}_{C^*}(x;n)\,dx = 1$$

for any $n = 1,2,\ldots,$ whereas the integral over $\widehat{f}_{C^*}(x;n)$ is not equal to 1 in general and hence $\widehat{f}_{C^*}(x;n)$ is in this case not a probability density. Theorem 5.9 states that we can estimate the density f_{C^*} at every $x \in \mathbb{R}$ unbiasedly and consistently. Furthermore, the expectation of $h(C^*)$ can be estimated consistently

for every non–negative measurable function based on the estimated density. If the estimator $\widehat{f}_{C^*}(x;n)$ is used, then we can even estimate the expectation of $h(C^*)$ unbiasedly. This is not possible if the density f_{C^*} is e.g. estimated by kernel methods.

Remark: Note that we can also define estimators based on the data in large sampling windows by

$$\widehat{f}_W(x;n) = \frac{\lambda_\ell}{\#\{j : H_j \in nW\}} \sum_{H_j \in nW} \sum_{i=1}^{N_j} \mathbb{1}_{[c(A_i^{(j)}),c(B_i^{(j)}))}(x)\,. \tag{5.26}$$

Then the consistency results of Theorem 5.9 remain valid for this estimator if e.g. $B(o,r) \subset W$ for some $r > 0$ due to the ergodic theorem, see Theorem 2.8. Nevertheless, we concentrate on estimators based on samples of the typical segment system S_H^* since these estimators are computationally less intensive. Furthermore, some problems appear if large sampling windows are used for the estimation. For instance, we do not know how large the window W has to be chosen in order to have a good approximation of the true distribution. Moreover, neighboring serving zones are highly correlated and there are always edge effects at the boundary. All these problems can be avoided if we regard i.i.d. samples of S_H^*.

5.5.2 Almost sure convergence of the maximal error

In the preceding section we have seen that for every fixed $x \in \mathbb{R}$ the empirical density $\widehat{f}_{C^*}(x;n)$ is an unbiased estimator for the true density $f_{C^*}(x)$ of the typical shortest path length C^*. Furthermore, Theorem 5.9 states that $\widehat{f}_{C^*}(x;n) \overset{a.s.}{\to} f_{C^*}(x)$ for $n \to \infty$. It is possible to show that $\widehat{f}_{C^*}(x;n,\omega)$ converges even uniformly to f_{C^*} with probability 1, i.e., we can show that

$$\lim_{n\to\infty} \sup_{x\in\mathbb{R}} |\widehat{f}_{C^*}(x;n,\omega) - f_{C^*}(x)| = 0$$

almost surely as it is also the case for the estimators for the density of the typical Euclidean distance D^*. In the proof of this statement we use the following notation. We define $Z_j(A) := \sum_{i=1}^{N_j}(\mathbb{1}_A(c(A_i^{(j)})) + \mathbb{1}_A(c(B_i^{(j)})))$ for $A \in \mathcal{B}(\mathbb{R})$ and $j = 1,\ldots,n$. Then $Z_1,\ldots,Z_n$ are i.i.d. (non-simple) point processes on the non-negative axis $[0,\infty)$ with finite intensity measure since $\mathbb{E}Z_j(\mathbb{R}) \le 2\mathbb{E}N < \infty$. Now the following theorem can be proven.

Theorem 5.10 *It holds that*

$$\mathbb{P}\left(\lim_{n\to\infty} \sup_{x\in\mathbb{R}} |\widehat{f}_{C^*}(x;n,\omega) - f_{C^*}(x)| = 0\right) = 1\,.$$

Proof It suffices to show that for almost all $\omega \in \Omega$ and $\varepsilon > 0$ there is some $N(\varepsilon, \omega) \in \mathbb{N}$ such that for all $n > N(\varepsilon, \omega)$ we have

$$|\widehat{f}_{C^*}(x; n, \omega) - f_{C^*}(x)| \leq \varepsilon$$

for all $x \in \mathbb{R}$. Now let $q \in \mathbb{Q}$, then we immediately get

$$\begin{aligned} &|\widehat{f}_{C^*}(x; n, \omega) - f_{C^*}(x)| \\ &\quad \leq |\widehat{f}_{C^*}(x; n, \omega) - \widehat{f}_{C^*}(q; n, \omega)| + |\widehat{f}_{C^*}(q; n, \omega) - f_{C^*}(q)| + |f_{C^*}(q) - f_{C^*}(x)| \,. \end{aligned} \tag{5.27}$$

Let $\varepsilon > 0, q, q' \in \mathbb{Q}$ with $q < q'$ and $x \in [q, q')$, then we have

$$|\widehat{f}_{C^*}(x; n, \omega) - \widehat{f}_{C^*}(q; n, \omega)| \leq \frac{\lambda_\ell}{n} \sum_{j=1}^{n} Z_j(\omega)((q, q')) \tag{5.28}$$

and, since the point processes $Z_1, \ldots, Z_n$ are i.i.d., it holds that

$$\frac{1}{n} \sum_{j=1}^{n} Z_j(\omega)((q, q')) \overset{a.s.}{\to} \mathbb{E} Z_1((q, q')) \,.$$

Recall that the intensity measure of Z_1 is finite, i.e., $\mathbb{E} Z_1([0, \infty)) < \infty$. Furthermore, $\lim_{x \to \infty} f_{C^*}(x) = 0$ and f_{C^*} is a cadlag function on $[0, \infty)$. Thus, we can choose $q_0, \ldots, q_m \in \mathbb{Q}$ with $q_0 = 0 < q_1 < \cdots < q_m < q_{m+1} = \infty$ such that for all $i = 0, \ldots, m$ and $x \in [q_i, q_{i+1})$ we have

$$\lambda_\ell \mathbb{E} Z_1((q_i, q_{i+1})) < \frac{\varepsilon}{3} \,, \quad |f_{C^*}(x) - f_{C^*}(q_i)| < \frac{\varepsilon}{3} \,. \tag{5.29}$$

Additionally, we get almost surely that

$$\begin{aligned} \lim_{n \to \infty} \frac{\lambda_\ell}{n} \sum_{j=1}^{n} Z_j(\omega)((q_i, q_{i+1})) &= \lambda_\ell \mathbb{E} Z_1((q_i, q_{i+1})) < \frac{\varepsilon}{3} \,, \\ \lim_{n \to \infty} \widehat{f}_{C^*}(q_i; n, \omega) &= f_{C^*}(q_i) \end{aligned}$$

for all $i = 0, \ldots, m$. Thus we can choose $N(\varepsilon, \omega) \in \mathbb{N}$ such that

$$\frac{\lambda_\ell}{n} \sum_{j=1}^{n} Z_j(\omega)((q_i, q_{i+1})) < \frac{\varepsilon}{3} \,, \tag{5.30}$$

$$|\widehat{f}_{C^*}(q_i; n, \omega) - f_{C^*}(q_i)| < \frac{\varepsilon}{3} \tag{5.31}$$

for all $i = 0, \ldots, m$ and $n > N(\varepsilon, \omega)$. Finally, we can combine the inequalities given in (5.27) – (5.31) which yields that for all $\varepsilon > 0$ and almost all $\omega \in \Omega$ there exists $N(\varepsilon, \omega)$ such that

$$|\widehat{f}_{C^*}(x; n, \omega) - f_{C^*}(x)| < \varepsilon$$

for all $x \in \mathbb{R}$ and $n \geq N(\varepsilon, \omega)$. Hence, the proof is completed. □

Remark: The result of Theorem 5.10 is also true for the estimator defined in (5.26) for an averaging sequence of unboundedly increasing sampling windows, i.e.,

$$\mathbb{P}\left(\lim_{n\to\infty} \sup_{x\in\mathbb{R}} |\widehat{f}_W(x;n,\omega) - f_{C^*}(x)| = 0\right) = 1\,.$$

5.5.3 Rates of convergence and variances

In the approach to estimate f_{C^*} which has been introduced in this chapter we avoid the simulation of LLC in the estimation procedure of the distribution of C^*. This has some advantages on the performance of the considered estimators compared to classical estimation procedures based e.g. on observations of LLC and their shortest path lengths themselves.

A common measure which is used to quantify the deviation of a density estimator $\widehat{f}$ from the true density f is the mean integrated squared error of $\widehat{f}$ which we denote by $MISE(\widehat{f})$. It is given by

$$MISE(\widehat{f}) = \mathbb{E}\int_{\mathbb{R}} (\widehat{f}(x) - f(x))^2\,dx\,. \tag{5.32}$$

If we consider the estimator $\widehat{f}_{C^*}(x;n)$ defined in equation (5.20), then we get

$$\begin{aligned}
MISE(\widehat{f}_{C^*}) &= \mathbb{E}\int_{\mathbb{R}} (\widehat{f}_{C^*}(x;n) - f_{C^*}(x))^2\,dx \\
&= \frac{\lambda_\ell^2}{n}\int_{\mathbb{R}} \mathrm{Var}\Big(\sum_{i=1}^{N} \mathbb{1}_{[c(A_i),c(B_i))}(x)\Big)\,dx \\
&\leq \frac{\lambda_\ell^2}{n}\int_{\mathbb{R}} \mathbb{E}\Big(\sum_{i,j=1}^{N} \mathbb{1}_{[c(A_i),c(B_i))}(x)\mathbb{1}_{[c(A_j),c(B_j))}(x)\Big)\,dx \\
&= \frac{\lambda_\ell^2}{n}\mathbb{E}\sum_{i,j=1}^{N} \nu_1([c(A_i),c(B_i)) \cap [c(A_j),c(B_j))) \leq \frac{\lambda_\ell^2}{n}\mathbb{E}(N\nu_1(S_H^*))\,.
\end{aligned}$$

Thus we get that the rate of convergence of $MISE(\widehat{f}(x;n))$ is of order $1/n$ provided that $\mathbb{E}(N\nu_1(S_H^*)) < \infty$. Now assume that we simulate the points of $\widetilde{L}$ on S_H^*, compute the shortest path lengths $\widetilde{C}_i$ of each point $\widetilde{L}_i \in S_H^*$ and finally construct a kernel estimator for f_{C^*}. Then, on the one hand, the rate of convergence of the mean integrated squared error of kernel estimators is of order $n^{-4/5}$ or even slower, see [101]. On the other hand, the computational effort in order to obtain the kernel estimator and $\widehat{f}_{C^*}$ is similar since for every point $\widetilde{L}_i$ we have to compute the shortest path lengths to the endpoints of the segment S_j with

$\widetilde{L}_i \in S_j$. Thus, from this point of view, the estimator $\widehat{f}_{C^*}$ defined in this section is superior to kernel estimators.

Now we regard the estimator $\widehat{F}_{C^*}(x)$ for the distribution function F_{C^*} of C^* which is defined by

$$\widehat{F}_{C^*}(x;n) = \frac{\lambda_\ell}{n} \sum_{i=1}^{n} \nu_1(S^*_{H,i}(x)) \,, \tag{5.33}$$

where $S^*_{H,i}(x) = \{y \in S^*_{H,i} : c(y) \le x\}$ for all $x \in \mathbb{R}$. Then

$$\widehat{F}_{C^*}(x;n) = \int_0^x \widehat{f}_{C^*}(t;n)\, dt$$

and Theorem 5.9 implies that this estimator is unbiased and strongly consistent for $F_{C^*}(x)$. On the other hand, assume that we simulate the points $\widetilde{L}^{(i)}_j$ of $\widetilde{L}^{(i)}$ on $S^*_{H,i}$ and additionally compute the shortest path lengths $\widetilde{C}^{(i)}_j$. Then a natural estimator for $F_{C^*}(x)$ is given by

$$\widetilde{F}_{C^*}(x;n) = \frac{\lambda_\ell}{\lambda'_\ell} \frac{1}{n} \sum_{i=1}^{n} \#\{\widetilde{L}^{(i)}_j \in S^*_{H,i} : \widetilde{C}^{(i)}_j \le x\} \,. \tag{5.34}$$

Note that $\widetilde{F}_{C^*}(x;n)$ is an unbiased estimator for $F_{C^*}(x)$, see equation (5.15) in the proof of Lemma 5.6. We get that

$$\mathbb{E}(\widetilde{F}_{C^*}(x;n) \mid S^*_{H,i}, i = 1,\dots,n) \;=\; \frac{\lambda_\ell}{\lambda'_\ell} \frac{1}{n} \sum_{i=1}^{n} \mathbb{E}(\#\{\widetilde{L}^{(i)}_j \in S^*_{H,i} : \widetilde{C}^{(i)}_j \le x\} \mid S^*_{H,i}) \,.$$

Now $\widetilde{L}^{(i)}$ is a Poisson process with intensity measure $\lambda'_\ell \nu_1(\,\cdot \cap S^*_{H,i})$ given $S^*_{H,i}$, thus we can apply Campbell's theorem which yields

$$\mathbb{E}(\#\{\widetilde{L}^{(i)}_j \in S^*_{H,i} : \widetilde{C}^{(i)}_j \le x\} \mid S^*_{H,i}) = \lambda'_\ell \nu_1(S^*_{H,i}(x)) \,.$$

Hence we get

$$\widehat{F}_{C^*}(x;n) = \mathbb{E}(\widetilde{F}_{C^*}(x;n) \mid S^*_{H,i}, i = 1,\dots,n) \,,$$

and thus $\operatorname{Var} \widehat{F}_{C^*}(x;n) \le \operatorname{Var} \widetilde{F}_{C^*}(x;n)$. This means that our estimator is again superior to the natural estimator which is based on measurements of real shortest path lengths for $\widetilde{L}$.

5.5.4 Numerical results

In this section we present some numerical results obtained with the estimator $\widehat{f}_{C^*}(x;n)$ based on samples of S^*_H generated with the simulation algorithms introduced in Chapter 4 for different models. In particular, we regard a random

tessellation T which is in the following a PDT, PLT and PVT, respectively, whose length intensity is given by γ. Moreover, two different models for H are considered. We assume that H is either a Cox process on $T^{(1)}$ or a thinning of the vertices $T^{(0)}$ of T. Finally, we assume that the serving zones are given by the Voronoi tessellation T_H induced by H, i.e., each point of L is connected to the nearest point of H.

To start with, we first recall that all considered models are scaling invariant. This means that for all $\lambda_\ell, \gamma > 0$ with fixed quotient $\kappa = \gamma/\lambda_\ell$ we obtain the same model, but only on a different scale. Using this scaling invariance, it is sufficient to compute the density for a single value of κ. The density for other values of κ can then be obtained by a suitable scaling.

Scaling invariance

Suppose that $\gamma = a\widetilde{\gamma}$ and $\lambda_\ell = a\widetilde{\lambda}_\ell$, where $\widetilde{\gamma} > 0, \widetilde{\lambda}_\ell > 0$ and $a > 0$ are fixed. Recall that a scaling of the parameter pair by some $a > 0$ corresponds to a scaling of the whole model corresponding to the parameters $\widetilde{\gamma}, \widetilde{\lambda}_\ell$ by the factor $1/a$, see Sections 3.5.2, 3.5.3 and 4.6.1. For instance, we have that $S_H^*(\gamma, \lambda_\ell) \stackrel{\mathrm{d}}{=} 1/a\, S_H^*(\widetilde{\gamma}, \widetilde{\lambda}_\ell)$, where $S_H^*(\gamma, \lambda_\ell)$ is the typical segment system with parameters γ and λ_ℓ. We can use this scaling invariance in order to calculate the probability density $f_{C^*}(x; \gamma, \lambda_\ell)$ from the knowledge of the density $f_{C^*}(x; \widetilde{\gamma}, \widetilde{\lambda}_\ell)$ by an appropriate scaling.

Theorem 5.11 *For any pair (γ, λ_ℓ) of parameters $\gamma, \lambda_\ell > 0$, regard the density $f_{C^*}(x; \gamma, \lambda_\ell)$ in (5.18). Then we have that*

$$f_{C^*}(x; \gamma, \lambda_\ell) = a f_{C^*}(ax; \widetilde{\gamma}, \widetilde{\lambda}_\ell) \tag{5.35}$$

if $\gamma/\lambda_\ell = \widetilde{\gamma}/\widetilde{\lambda}_\ell$ and $a > 0$ with $\lambda_\ell = a\widetilde{\lambda}_\ell$.

Proof Let $x > 0$ and recall that $S_H^*(\gamma, \lambda_\ell) \stackrel{\mathrm{d}}{=} 1/a\, S_H^*(\widetilde{\gamma}, \widetilde{\lambda}_\ell)$. This yields

$$\begin{aligned} f_{C^*}(x; \gamma, \lambda_\ell) &= \lambda_\ell\, \mathbb{E} \sum_{i=1}^{N} \mathbb{1}_{[c(A_i), c(B_i))}(x) \\ &= a\widetilde{\lambda}_\ell\, \mathbb{E} \sum_{i=1}^{N} \mathbb{1}_{[c(\widetilde{A}_i), c(\widetilde{B}_i))}(a\,x) = a f_{C^*}(ax; \widetilde{\gamma}, \widetilde{\lambda}_\ell)\,, \end{aligned}$$

where we used that the shortest path does not change if the model is scaled, but its length grows linearly as a 1-dimensional quantity. □

Note that the same scaling invariance is true for the density f_{D^*} of the typical Euclidean distance D^* which can be shown in the same way. In the following, we concentrate our study on the case that $\gamma = 1$ and different values of κ.

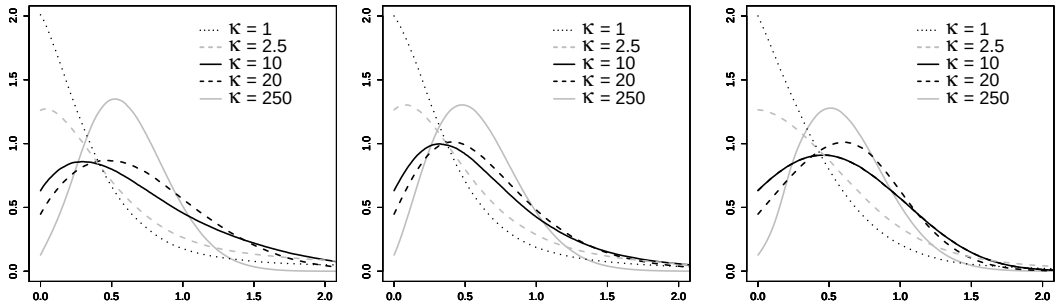

(a) PDT (b) PLT (c) PVT

Figure 5.12: f_{C^*} for Cox process H with $\lambda_\ell \gamma = 1$ and different values of κ

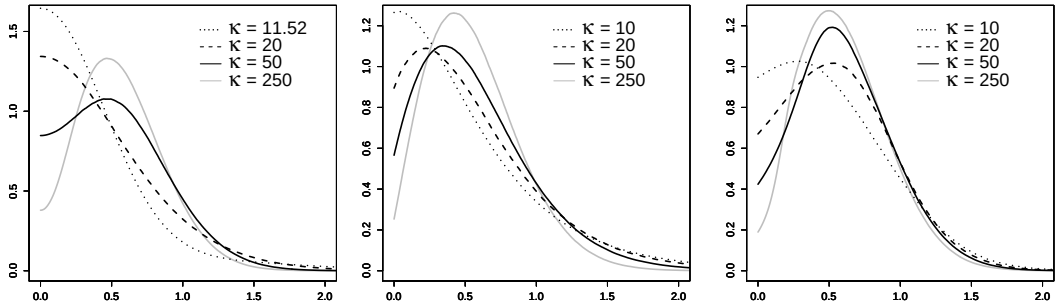

(a) PDT (b) PLT (c) PVT

Figure 5.13: f_{C^*} for a p-thinning H with $p\lambda^{(0)} = 1$ and different values of κ

Empirical densities

We simulated 50 000 cells for different values of κ and used the generated segment systems in order to estimated the density $\widehat{f}_{C^*}(x; n)$ as explained in Section 5.5.1. In Figures 5.12 and 5.13 some densities which are obtained in this manner are shown. There are clear differences between the shapes of the densities for all values of κ and the different considered models. However, for Cox processes H on T it seems that the density f_{C^*} is close to the density of an exponential distribution whereas for larger values of κ the shape of f_{C^*} changes to the shape of a Weibull distribution. This observation motivates the study of so–called scaling limits in the next chapter. In particular, we prove that the distribution of C^* converges to known distributions for $\kappa \to 0$ and $\kappa \to \infty$, respectively, if C^* is appropriately scaled. If H is a thinning of $T^{(0)}$, then the densities look similar to the densities of Cox processes for larger values of κ, but note that there is a clear difference for small values of κ. A more comprehensive analysis of the estimated densities of C^* can be found in Chapter 7, where moments of C^* are compared for different considered models. Furthermore, parametric densities are fitted to the estimated ones in order to obtain analytical formulae for the distributions of C^* for different parameters γ and λ_ℓ and tessellation models

T. These parametric distributions are compared to distributions of connection lengths estimated from real network data. This comparison reveals an excellent fit between the parametric densities obtained via Monte–Carlo methods and the densities observed in real data.

Chapter 6

Scaling limits for the typical Euclidean distance and the typical shortest path lengths

In the present chapter we investigate the behavior of the typical Euclidean distance and the typical shortest path length as the parameters of the model considered in Chapter 5 tend to extremal cases. We focus here on the case that the HLC are modeled by Cox processes H on the edges of a stationary tessellation T. Recall that the distributions of both the typical shortest path length and the typical Euclidean distance depend on two parameters, namely the length intensity γ of the underlying tessellation and the linear intensity λ_ℓ of H. Moreover, the quotient $\kappa = \gamma/\lambda_\ell$ of both parameters defines the structure of the model, i.e., for fixed κ the same model is obtained up to a scaling. Note that only few segments of the underlying tessellation intersect each serving zone if κ is small, whereas large values of κ yield a dense segment system in each serving zone. Thus, we can consider the two limiting cases that κ tends to zero and infinity if the model is simultaneously scaled in an appropriate way. In particular, we investigate the case that $\kappa = \gamma/\lambda_\ell \to 0$ with λ_ℓ fixed and $\gamma \to 0$ and the case $\kappa = \gamma/\lambda_\ell \to \infty$ with $\lambda_\ell \to 0$ and $\gamma \to \infty$ such that $\gamma\lambda_\ell = \lambda$ for some fixed value of $\lambda > 0$. The main result of this chapter states that the distribution of the typical shortest path length converges to an exponential distribution with parameter $2\lambda_\ell$ for $\kappa \to 0$ and to a Weibull distribution with parameters $\lambda\pi/\xi^2$ and 2 for $\kappa \to \infty$, respectively, where $\xi \geq 1$ is some constant depending on the underlying tessellation model.

The chapter is organized as follows. In Section 6.1 we briefly discuss the model we are considering. Afterwards, in Section 6.2, it is shown that the typical shortest path length converges in distribution to an exponential distribution for $\kappa \to 0$. This result is valid if the underlying tessellation is stationary. In this case, the limiting distribution does not depend on the specific model of the underlying tessellation. If the LLC are modeled by a Cox process, then the typical Euclidean distance converges to the same distribution.

Subsequently, in Section 6.3 we state that the typical Euclidean distance converges to a Weibull distribution with parameters $\lambda\pi$ and 2 for $\kappa \to \infty$. This result is obtained using classical results on weak convergence of rescaled thinnings of point processes, where the limiting point process is a stationary Poisson process. Afterwards it is shown that there exists a constant $\xi \geq 1$ such that the difference between the typical Euclidean distance and shortest path length converges in probability to zero which implies that the typical shortest path lengths converges to a Weibull distribution with parameters $\lambda\pi$ and 2 scaled by ξ, see Theorem 6.2 in Section 6.3. The main steps of the proof of Theorem 6.2 are given in Section 6.4. However, in order to keep the proof more transparent, we use a Lemma whose proof is postponed to Section 6.5.

Afterwards, in Section 6.6 we show that for various models the conditions of Theorem 6.2 are fulfilled and hence the typical shortest path length converges to a Weibull distribution with parameters $\lambda\pi/\xi^2$ and 2. Therefore, we have to show that the considered tessellation models are mixing and that some integrability condition is fulfilled which is indeed the case for the basic tessellation models PDT, PLT and PVT, iterated tessellations based on these basic tessellations of Poisson type and STIT tessellations. Furthermore, we can even show that the constant ξ is equal to 1 if the underlying tessellation is a PLT or an iterated tessellation with a PLT as initial tessellation.

The material presented in this chapter is partly based on results elaborated in [99].

6.1 Scaled typical Euclidean distances and shortest path lengths

In this chapter we consider basically the same model as defined in Chapter 5, although we concentrate on the case that both LLC and HLC are modeled by Cox processes on the edges of a stationary random tessellation.

In the following, we assume that T is a stationary random tessellation with length intensity 1 and we use the notation $T_\gamma = T/\gamma$ for the random tessellation obtained from T by a scaling with the factor γ. Note that $\mathbb{E}\nu_1(T_\gamma^{(1)} \cap [0,1)^2) = \mathbb{E}\nu_1(T^{(1)} \cap [0,\gamma)^2)/\gamma = \gamma$, thus the length intensity of T_γ is equal to γ for all $\gamma > 0$. Using this construction, we define the structure (or model) of T_γ by T and then scale T by $1/\gamma$ in order to obtain the length intensity we are interested in. Then, given T_γ, both LLC and HLC are modeled by Cox processes L and H with linear intensities λ'_ℓ and λ_ℓ, respectively, on the edges of T_γ and each point of L is linked to the nearest point of H. Thus, the serving zones T_H of H are modeled by the Voronoi tessellation induced by H and the connection is obtained either on the direct Euclidean distance or on the shortest path. In this way we can construct the marked point processes $L_D = \{(L_n, D_n)\}$ and $L_C = \{(L_n, C_n)\}$,

where D_n and C_n denotes the Euclidean distance and shortest path connection length, respectively, from L_n to the nearest point of H, see also Sections 5.2 and 5.4. We are then interested in the typical Euclidean distance $D^* = D^*(\lambda_\ell, \gamma)$ and the typical shortest path length $C^* = C^*(\lambda_\ell, \gamma)$, respectively, which only depend on the parameters $\lambda_\ell > 0$ and $\gamma > 0$, see Theorems 5.1 and 5.7. Recall that $D^*(\lambda_\ell, \gamma) \stackrel{\mathrm{d}}{=} aD^*(a\lambda_\ell, a\gamma)$and $C^*(\lambda_\ell, \gamma) \stackrel{\mathrm{d}}{=} aC^*(a\lambda_\ell, a\gamma)$ for all $a > 0$. Thus, if $\kappa = \gamma/\lambda_\ell$ and $\kappa' = \gamma'/\lambda'_\ell$ are equal, then we obtain the same distributions up to a scaling.

Let $\widetilde{T}_\gamma$ and $\widetilde{H}$ denote the Palm versions of T_γ and H distributed according to the Palm distribution P_L^* with respect to L. Note that D^* and C^* can then be regarded as the Euclidean distance $|\widetilde{H}_0|$ and the shortest path length $c(\widetilde{H}_0)$ from o to $\widetilde{H}_0$ along $\widetilde{T}_\gamma^{(1)}$, respectively, where $\widetilde{H}_0$ denotes the closest point of $\widetilde{H}$ to o. In the following, we assume that the joint distribution of $D^*, C^*, \widetilde{H}$ and $\widetilde{T}_\gamma$ is given by P_L^*. For further details on the model see Chapter 5.

Now we investigate the limiting behavior of D^* and C^* if $\kappa \to 0$ and $\kappa \to \infty$, where D^* and C^* are appropriately scaled. In Figure 6.1 realizations of the model for small and large values of κ are shown. Recall that for $\kappa \to 0$ and $\kappa \to \infty$ the edge set of T_γ inside each serving zones becomes infinitely sparse and infinitely dense, respectively. Thus, for small values of κ only one edge of $T_\gamma^{(1)}$ intersects most of the serving zones whereas for large κ the serving zones are intersected by a dense segment system.

6.2 Asymptotic exponential distribution for $\kappa \to 0$

To start with, we regard the case that $\kappa = \gamma/\lambda_\ell \to 0$, where λ_ℓ fixed and $\gamma \to 0$. Thus, the mean number of points per edge length of $T_\gamma^{(1)}$ is constant, but the length intensity of T_γ tends to zero.

Theorem 6.1 *Let T be an arbitrary stationary tessellation. Then, for any fixed $\lambda_\ell > 0$, it holds that*

$$C^*(\gamma, \lambda_\ell) \stackrel{\mathrm{d}}{\to} Z \qquad as \quad \gamma \to 0\,, \tag{6.1}$$

where $\stackrel{\mathrm{d}}{\to}$ denotes convergence in distribution and $Z \sim Exp(2\lambda_\ell)$, i.e., the random variable Z is exponentially distributed with expectation $1/(2\lambda_\ell)$.

Proof Define $R_\gamma = \max\{r > 0 : B(o,r) \cap \widetilde{S}_\gamma^o = B(o,r) \cap \widetilde{T}_\gamma^{(1)}\}$, where $\widetilde{S}_\gamma^o$ denotes the segment containing the origin of the random edge set $\widetilde{T}_\gamma^{(1)}$ defined in (5.1). It is easy to see that

$$\lim_{\gamma \to 0} R_\gamma = \infty \qquad \text{a.s.} \tag{6.2}$$

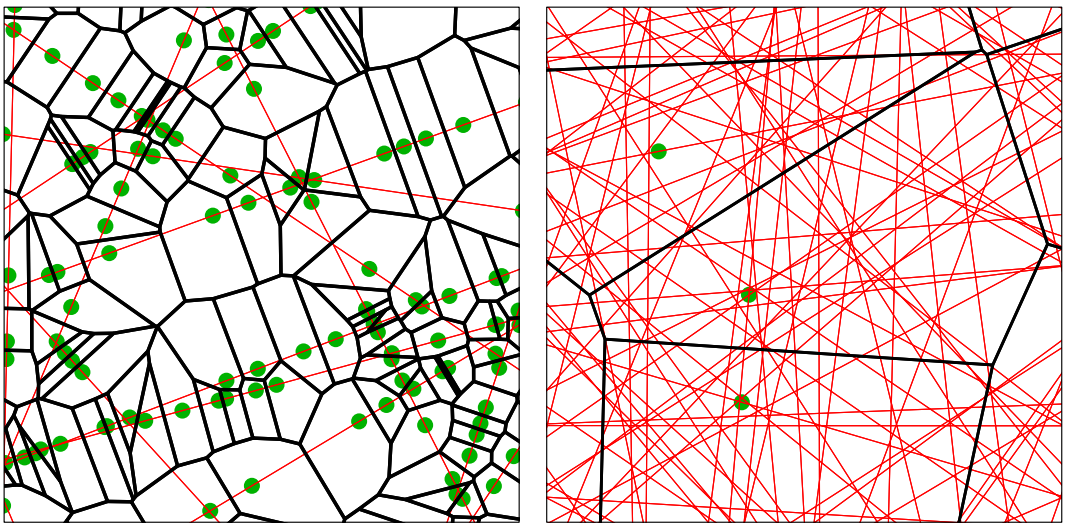

(a) $\kappa = 1$ (b) $\kappa = 1000$

Figure 6.1: Realizations of extreme values of κ

Now recall that C^* is shortest path length from o to the closest point $\widetilde{H}_0$ of the point process $\widetilde{H} = \{\widetilde{H}_n\}$ of HLC under the Palm distribution P_L^* with respect to L. Furthermore, note that the distribution function $F_{C^*}(x)$ of C^* can be written for all $x \geq 0$ as

$$\begin{aligned} F_{C^*}(x) &= \mathbb{P}(\widetilde{H}_0 \in B(o, R_\gamma))\, \mathbb{P}(C^* \leq x \mid \widetilde{H}_0 \in B(o, R_\gamma)) \\ &\quad + \mathbb{P}(\widetilde{H}_0 \notin B(o, R_\gamma))\, \mathbb{P}(C^* \leq x \mid \widetilde{H}_0 \notin B(o, R_\gamma))\,. \end{aligned}$$

Since $\widetilde{H}$ is a Cox process on S_H^* with linear intensity λ_ℓ, we get that

$$\mathbb{P}(C^* \leq x \mid \widetilde{H}_0 \in B(o, R_\gamma)) = \frac{\mathbb{P}(\min\{Z_1, Z_2\} \leq x, \min\{Z_1, Z_2\} \leq R_\gamma)}{\mathbb{P}(\widetilde{H}_0 \in B(o, R_\gamma))}$$

for each $x > 0$. Here, Z_1 and Z_2 are independent, exponentially distributed random variables with parameter λ_ℓ which are independent of R_γ. This yields

$$\mathbb{P}(\widetilde{H}_0 \notin B(o, R_\gamma)) = \mathbb{P}(\min\{Z_1, Z_2\} > R_\gamma) = \mathbb{E}\exp(-2\lambda_\ell R_\gamma)\,,$$

since $\min\{Z_1, Z_2\}$ is exponentially distributed with parameter $2\lambda_\ell$ and independent of R_γ. Now equation (6.2) implies that

$$\lim_{\gamma \to 0} \mathbb{P}(\widetilde{H}_0 \notin B(o, R_\gamma)) = 0 \qquad \text{and} \qquad \lim_{\gamma \to 0} \mathbb{P}(\widetilde{H}_0 \in B(o, R_\gamma)) = 1$$

and as a consequence

$$\lim_{\gamma \to 0} F_{C^*}(x) = \mathbb{P}(\min\{Z_1, Z_2\} \leq x) \;=\; 1 - \exp(-2\lambda_\ell x)$$

for each $x \geq 0$. Thus, the proof is completed. □

Note that the case $\kappa = \gamma/\lambda_\ell \to 0$ with γ fixed and $\lambda_\ell \to \infty$ can also be treated using Theorem 6.1. Due to the scaling invariance of the shortest path lengths we get that

$$\lambda_\ell \; C^*(\gamma, \lambda_\ell) \stackrel{\mathrm{d}}{=} C^*(\gamma/\lambda_\ell, 1)$$

for any $\gamma, \lambda_\ell > 0$. Thus, we can apply Theorem 6.1 which yields that

$$\lambda_\ell \; C^*(\gamma, \lambda_\ell) \stackrel{\mathrm{d}}{\to} Z \qquad \text{as} \quad \lambda_\ell \to \infty \,,$$

where $Z \sim \mathit{Exp}(2)$.

Furthermore, if L is a Cox process on T_γ, then it is easy to see that the typical Euclidean distance $D^*(\gamma, \lambda_\ell)$ converges also in distribution to an exponential distribution with parameter $2\lambda_\ell$ for $\gamma \to 0$ and fixed λ_ℓ, since the shortest path connection length is obtained in the limit by the direct Euclidean distance, see the proof of Theorem 6.1. However, if L is a planar Poisson process, then the distribution of $D^*(\gamma, \lambda_\ell)$ does not converge for $\gamma \to 0$, but $D^*(\gamma, \lambda_\ell)$ converges in distribution to the spherical contact distribution of T_γ if γ is fixed and $\lambda_\ell \to \infty$.

6.3 Asymptotic Weibull distribution for $\kappa \to \infty$

We now study the asymptotic behavior of the distributions of $D^* = D^*(\gamma, \lambda_\ell)$ and $C^* = C^*(\gamma, \lambda_\ell)$ if the scaling factor κ tends to ∞, where we assume that $\gamma \to \infty$ and $\lambda_\ell \to 0$ such that $\lambda_\ell \gamma = \lambda$ is fixed. This means that the spatial intensity λ of H is constant, but the edge set of T_γ gets denser as $\kappa \to \infty$. In particular, we show that D^* converges in distribution to the (random) Euclidean distance Z from the origin to the nearest point of a stationary Poisson process of intensity λ and C^* converges in distribution to ξZ, where $\xi \geq 1$ is some constant depending on T which is multiplied by Z. Then, it is not difficult to see that Z as well as ξZ have Weibull distributions, see also [38, 105].

Theorem 6.2 *Let T be ergodic and $Z \sim \mathit{Wei}(\lambda\pi, 2)$ for some $\lambda > 0$, then*

$$D^*(\gamma, \lambda_\ell) \stackrel{\mathrm{d}}{\to} Z \qquad \textit{as} \quad \kappa \to \infty \tag{6.3}$$

if $\gamma \to \infty$ and $\lambda_\ell \to 0$ such that $\lambda = \gamma\lambda_\ell$. Furthermore, let T be isotropic, mixing and

$$\mathbb{E}\, \nu_1^2(\partial \Xi^*) < \infty \,, \tag{6.4}$$

where we denote with $\nu_1(\partial\Xi^*)$ the circumference of the typical cell Ξ^* of T. Then there exists a constant $\xi \geq 1$ such that

$$C^*(\gamma, \lambda_\ell) \stackrel{\mathrm{d}}{\to} \xi Z \qquad \textit{as} \quad \kappa \to \infty \tag{6.5}$$

provided that $\gamma \to \infty$ and $\lambda_\ell \to 0$ with $\lambda_\ell \gamma = \lambda$, where $\xi Z \sim \mathit{Wei}(\lambda\pi/\xi^2, 2)$.

We split the *proof* of Theorem 6.2 into several steps. First we show that, under the Palm probability measure P_L^*, the typical Euclidean distance $|\widetilde{H}_0|$ from the origin to the nearest point $\widetilde{H}_0$ of $\widetilde{H} = \{\widetilde{H}_n\}$ converges in distribution to the corresponding characteristic of a stationary Poisson process with intensity λ, see Lemma 6.2. Moreover, in Lemma 6.4 we then show that there exists a constant $\xi \geq 1$ such that the difference between $\xi|\widetilde{H}_0|$ and the shortest path length $C^* = C^*(\gamma, \lambda_\ell)$ from the origin to $\widetilde{H}_0$ along the edge set $\widetilde{T}_\gamma^{(1)}$ converges to zero in probability. Finally, combining the results of Lemmas 6.2 and 6.4, the statement of Theorem 6.2 follows.

6.4 Proof of Theorem 6.2

6.4.1 Some auxiliary results

In order to prove Lemmas 6.1 and 6.2 we use two classical results regarding the weak convergence of point processes that will be given below, see e.g. [21, 44, 58]. Note that a sequence of point processes $X^{(1)}, X^{(2)}, \ldots$ in $\mathbb{R}^2$ converges weakly or in distribution to a point process X in $\mathbb{R}^2$ if and only if

$$\lim_{m\to\infty} \mathbb{P}(X^{(m)}(B_1) = i_1, \ldots, X^{(m)}(B_k) = i_k) = \mathbb{P}(X(B_1) = i_1, \ldots, X(B_k) = i_k)$$

for all $k \geq 1$, $i_1, \ldots, i_k \geq 0$ and for all finite sequences of bounded continuity sets $B_1, \ldots, B_k \in \mathcal{B}(\mathbb{R}^2)$ of X, see also Theorem A.9. Note that a set $B \in \mathcal{B}(\mathbb{R}^2)$ is called (stochastic) continuity set of X if $\mathbb{P}(X(\partial B) > 0) = 0$. If the sequence $X^{(1)}, X^{(2)}, \ldots$ converges weakly, then we shortly write $X^{(m)} \Longrightarrow X$.

Now assume that $X = \{X_n\}$ is an arbitrary ergodic point process in $\mathbb{R}^2$ which fulfills the condition $\mathbb{P}(X(\mathbb{R}^2) = 0) = 0$ and let $\lambda \in (0, \infty)$ denote its intensity. Then the following limit theorem for independently thinned and appropriately re-scaled versions of X can be proven. For each $p \in (0, 1)$, let $X^{(p)}$ be a point process which is obtained from X by independent thinning, where each point X_n of X survives with probability p and is removed with probability $1 - p$ independently of the other points of X. Moreover, let $Y^{(p)}$ be a re-scaled version of the thinned process $X^{(p)}$, i.e., we define $Y^{(p)}$ by $Y^{(p)}(B) = X^{(p)}(B/\sqrt{p})$ for each $B \in \mathcal{B}(\mathbb{R}^2)$. Thus, for each $p \in (0, 1)$, the point processes $Y^{(p)}$ and X are both stationary with the same intensity λ and it can be shown that

$$Y^{(p)} \Longrightarrow Y \qquad \text{if } p \to 0, \tag{6.6}$$

where Y is a stationary Poisson process in $\mathbb{R}^2$ whose intensity is equal to λ, see e.g. Section 11.3 of [21] or Theorem 7.3.1 in [58]. Intuitively, this result can be explained in the following way. The dependence between points of the point process in domains A and B decreases with increasing distance between A and B. Thus, if the point process is thinned independently only points far away of

each other survive with high probability yielding a point process with complete spatial randomness, i.e., a Poisson process.

Moreover, the following continuity property of Palm distributions is true. Let $X^{(1)}, X^{(2)}, \ldots$ be a sequence of stationary point processes in $\mathbb{R}^2$ with intensities $\lambda_1, \lambda_2, \ldots$, and let X be another stationary point process in $\mathbb{R}^2$ with $\mathbb{P}(X(\mathbb{R}^2) = 0) = 0$ whose intensity is given by λ. If $\lambda_m = \lambda$ for all $m \geq 1$ and in addition $X^{(m)} \Longrightarrow X$ as $m \to \infty$, then the Palm versions $X^{(1)*}, X^{(2)*}, \ldots$ of $X^{(1)}, X^{(2)}, \ldots$ converge weakly to the Palm version X^* of X, i.e.,

$$X^{(m)*} \Longrightarrow X^* \qquad \text{as } m \to \infty, \tag{6.7}$$

see e.g. Proposition 10.3.6 in [58].

6.4.2 Typical Euclidean distance

In the whole section we assume that the underlying tessellation T is an ergodic tessellation. We first show that the Cox process H on T converges weakly to a stationary Poisson process of intensity λ if $\kappa \to \infty$ under the condition that $\lambda_\ell \gamma = \lambda$ is constant. This result is then used in order to prove that the typical Euclidean distance $D^* = |\widetilde{H}_0|$ from the typical LLC to its nearest HLC is asymptotically Weibull distributed.

Lemma 6.1 *If $\kappa = \gamma/\lambda_\ell \to \infty$ provided that $\lambda_\ell \gamma = \lambda$ for some constant $\lambda \in (0, \infty)$, then $H \Longrightarrow Y$, where Y is a stationary Poisson process with intensity λ.*

Proof For all $\gamma > 1$, let $H = H(\gamma)$ be the Cox process of HLC with parameters γ and λ_ℓ, where $\lambda_\ell = \lambda/\gamma$ for some constant $\lambda \in (0, \infty)$. Then the Cox process $H(\gamma)$ can be constructed from $H(1)$ by independent thinning with survival probability $p = 1/\gamma$ followed by a re-scaling with the scaling factor $\sqrt{1/\gamma}$, i.e.,

$$H(\gamma) \stackrel{\mathrm{d}}{=} H(1)^{(p)} .$$

Moreover, the Cox process $H(1)$ is ergodic since the underlying tessellation T and hence the random intensity measure of $H(1)$ is ergodic. Thus we can use (6.6) which yields

$$H(\gamma) \Longrightarrow Y \quad \text{as} \quad \gamma \to \infty.$$

□

Using Lemma 6.1 we can now show that $|\widetilde{H}_0|$ converges in distribution to a Weibull distribution.

Lemma 6.2 *Let $Z \sim Wei(\lambda\pi, 2)$ for some $\lambda > 0$. Then $|\widetilde{H}_0| \stackrel{\mathrm{d}}{\to} Z$ as $\kappa \to \infty$ provided that $\gamma \to \infty$ and $\lambda_\ell \to 0$ such that $\lambda_\ell \gamma = \lambda$.*

Proof Let $H^* = H^*(\gamma)$ be the Palm version of the stationary point process $H = H(\gamma)$. Moreover, let Y be a stationary Poisson process with intensity λ. Then the distribution of $Y \cup \{o\}$ is equal to the Palm distribution of Y due to Slivnyak's theorem, see Theorem 2.6. Thus, Lemma 6.1 and (6.7) yield that

$$H^*(\gamma) \Longrightarrow Y \cup \{o\} \tag{6.8}$$

if $\gamma \to \infty$ and $\lambda_\ell \to 0$ with $\lambda_\ell \gamma = \lambda$. Since both L and H are Cox processes on T_γ that are conditionally independent given T_γ, we have that $\widetilde{H} \cup \{o\}$ and the Palm version H^* of H have the same distributions. This follows from Slivnyak' theorem for stationary Cox processes, see Theorem 3.3. Thus, for each $r > 0$ we get

$$\begin{aligned}
\lim_{\gamma\to\infty} \mathbb{P}(|\widetilde{H}_0| > r) &= \lim_{\gamma\to\infty} \mathbb{P}(\widetilde{H}(B(o,r)) = 0) \\
&= \lim_{\gamma\to\infty} \mathbb{P}((\widetilde{H} \cup \{o\})(B(o,r)) = 1) \\
&= \lim_{\gamma\to\infty} \mathbb{P}(H^*(B(o,r)) = 1) \\
&= \mathbb{P}((Y \cup \{o\})(B(o,r)) = 1) \\
&= \mathbb{P}(Y(B(o,r)) = 0)\,,
\end{aligned}$$

where in the last but one equality formula (6.8) was used. Hence, for each $r > 0$, we have

$$\lim_{\gamma\to\infty} \mathbb{P}(|\widetilde{H}_0| > r) \;=\; \mathbb{P}(Y(B(o,r)) = 0) \;=\; \exp(-\lambda\pi r^2)\,,$$

which proves that $|\widetilde{H}_0| \xrightarrow{\mathrm{d}} Z \sim \mathit{Wei}(\lambda\pi, 2)$. □

6.4.3 Shortest path length vs. scaled Euclidean distance

In this section we investigate the difference between the typical shortest path length and the typical Euclidean distance. Intuitively, one might expect that the shortest path oscillates around the direct Euclidean connection for large κ. Realizations of L and H together with their shortest paths and Euclidean connections are shown in Figure 6.2 for large κ. It seems that the shortest path lengths deviate from the direct Euclidean distances by a constant factor for $\kappa \to \infty$. In the following we prove that under reasonable assumptions on T this is indeed the case.

Throughout this section we assume that T is a stationary and isotropic random tessellation which is also mixing. Moreover, we assume that the typical cell Ξ^* of T satisfies the integrability condition (6.4). Then it can be shown that for some constant $\xi \geq 1$ the difference between the scaled Euclidean distance $\xi|\widetilde{H}_0|$ and the shortest path length $C^* = C^*(\gamma, \lambda_\ell)$ from the origin to $\widetilde{H}_0$ along the edges of $\widetilde{T}_\gamma$ converges in probability to zero. In the proof of this statement we make use of the following auxiliary result.

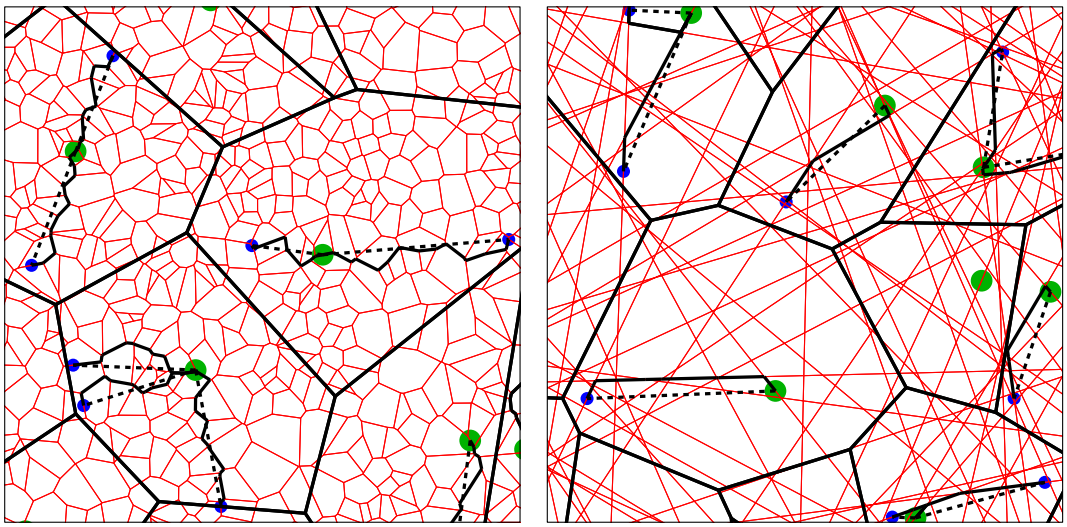

(a) PVT (b) PLT

Figure 6.2: Euclidean distances and shortest path for large κ.

Lemma 6.3 *Let* $\widetilde{T}^{(1)}_{\gamma,\varepsilon} = \big\{u \in \widetilde{T}^{(1)}_{\gamma} : \big|c(u) - \xi|u|\big| < \varepsilon\big\}$, *where* $\xi \geq 1$ *is some constant and* $c(u)$ *denotes the length of the shortest path from* u *to the origin along the edges of* $\widetilde{T}^{(1)}_{\gamma}$. *If* $\gamma \to \infty$ *and* $\lambda_\ell \to 0$, *where* $\lambda_\ell \gamma = \lambda$ *is fixed, then there exists* $\xi \geq 1$ *such that for each* $\varepsilon > 0$ *and* $r > 0$

$$\lim_{\gamma\to\infty} \mathbb{E} \exp\Big(- \frac{\lambda}{\gamma}\, \nu_1\big(\widetilde{T}^{(1)}_{\gamma} \backslash \widetilde{T}^{(1)}_{\gamma,\varepsilon} \cap B(o,r)\big)\Big) = 1\,. \tag{6.9}$$

The *proof* of this lemma is shifted to Section 6.5 in order to make the proof of Theorem 6.2 more transparent. Now we can use Lemma 6.3 in order to prove the following lemma which completes the proof of Theorem 6.2.

Lemma 6.4 *If* $\gamma \to \infty$ *and* $\lambda_\ell \to 0$ *such that* $\lambda_\ell \gamma = \lambda$, *then there is a constant* $\xi \geq 1$ *with* $C^*(\gamma, \lambda_\ell) - \xi|\widetilde{H}_0| \xrightarrow{\mathrm{P}} 0$, *where* $\xrightarrow{\mathrm{P}}$ *denotes convergence in probability.*

Proof We have to show that there exists some constant $\xi \geq 1$ such that for any $\varepsilon > 0$ and $\delta > 0$ we can choose $\gamma_0 > 0$ with

$$\mathbb{P}\big(\big|C^* - \xi|\widetilde{H}_0|\big| > \varepsilon\big) \leq \delta$$

for all $\gamma > \gamma_0$. Note that we can rewrite $\mathbb{P}\big(\big|C^* - \xi|\widetilde{H}_0|\big| > \varepsilon\big)$ as

$$\begin{aligned}&\mathbb{P}\big(\big|C^* - \xi|\widetilde{H}_0|\big| > \varepsilon\big)\\ &\quad = \mathbb{P}\big(\big|C^* - \xi|\widetilde{H}_0|\big| > \varepsilon, |\widetilde{H}_0| \leq r\big) + \mathbb{P}\big(\big|C^* - \xi|\widetilde{H}_0|\big| > \varepsilon, |\widetilde{H}_0| > r\big)\,,\end{aligned}$$

where $r > 0$ is an arbitrary fixed number. Lemma 6.2 yields

$$\mathbb{P}\big(|\widetilde{H}_0| > r\big) \to e^{-\lambda\pi r^2} \quad \text{as} \quad \gamma \to \infty\,,$$

thus we can choose $r > 0$ with $\mathbb{P}\big(|\widetilde{H}_0| > r\big) < \delta/2$ for all $\gamma > 0$ sufficiently large. Hence, it suffices to show that there exists $\gamma_0 > 0$ such that

$$\mathbb{P}\big(\big|C^* - \xi|\widetilde{H}_0|\big| > \varepsilon, |\widetilde{H}_0| \le r\big) \le \delta/2$$

for all $\gamma > \gamma_0$. Now let $\widetilde{N} = \widetilde{H}(B(o,r))$ denote the random number of atoms of $\widetilde{H}$ in the ball $B(o,r)$. Since $\widetilde{H}$ is a Poisson process with intensity measure $\lambda_\ell \nu_1(\,\cdot \cap \widetilde{T}_\gamma^{(1)})$ given $\widetilde{T}_\gamma$, we get

$$\begin{aligned}
&\mathbb{P}\big(\big|C^* - \xi|\widetilde{H}_0|\big| > \varepsilon, |\widetilde{H}_0| \le r\big) \\
&\quad \le \mathbb{E}\left(\sum_{k=1}^{\infty} \mathbb{P}(\widetilde{N} = k \mid \widetilde{T}_\gamma)\, \mathbb{P}\Big(\max_{i=1,\dots,k} \big(\big|c(Y_i) - \xi|Y_i|\big|\big) > \varepsilon \;\Big|\; \widetilde{T}_\gamma, \widetilde{N} = k\Big)\right) \\
&\quad = \mathbb{E}\left(\sum_{k=1}^{\infty} \mathbb{P}(\widetilde{N} = k \mid \widetilde{T}_\gamma) \left(1 - \mathbb{P}\big(\big|c(Y_1) - \xi|Y_1|\big| \le \varepsilon \mid \widetilde{T}_\gamma\big)^k\right)\right),
\end{aligned}$$

where the points $Y_1, \dots, Y_k$ are conditionally independent and identically distributed according to the probability measure $\nu_1\big(\,\cdot \cap \widetilde{T}_\gamma^{(1)} \cap B(o,r)\big)/\nu_1\big(\widetilde{T}_\gamma^{(1)} \cap B(o,r)\big)$ given $\widetilde{T}_\gamma$ and $\widetilde{N} = k$. In particular, for the conditional probability in the latter expression, we have

$$\begin{aligned}
\mathbb{P}\big(\big|c(Y_1) - \xi|Y_1|\big| \le \varepsilon \mid \widetilde{T}_\gamma\big) &= \frac{\displaystyle\int_{\widetilde{T}_\gamma^{(1)} \cap B(o,r)} \mathbb{1}_{[-\varepsilon,\varepsilon]}(c(u) - \xi|u|)\, \nu_1(du)}{\nu_1(\widetilde{T}_\gamma^{(1)} \cap B(o,r))} \\
&= \frac{\nu_1\big(\widetilde{T}_{\gamma,\varepsilon}^{(1)} \cap B(o,r)\big)}{\nu_1\big(\widetilde{T}_\gamma^{(1)} \cap B(o,r)\big)}\,.
\end{aligned}$$

Given $\widetilde{T}_\gamma$ we can use that $\widetilde{N} \sim Poi(\widetilde{\lambda})$ with $\widetilde{\lambda} = \lambda_\ell \nu_1\big(\widetilde{T}_\gamma^{(1)} \cap B(o,r)\big)$ which yields

$$\begin{aligned}
&\sum_{k=1}^{\infty} \mathbb{P}(\widetilde{N} = k \mid \widetilde{T}_\gamma) \left(1 - \mathbb{P}\big(\big|c(Y_1) - \xi|Y_1|\big| \le \varepsilon \mid \widetilde{T}_\gamma\big)^k\right) \\
&\qquad = 1 - \sum_{k=0}^{\infty} e^{-\tilde{\lambda}} \frac{\widetilde{\lambda}^k}{k!} \Big(\frac{\lambda_\ell \nu_1\big(\widetilde{T}_{\gamma,\varepsilon}^{(1)} \cap B(o,r)\big)}{\widetilde{\lambda}}\Big)^k \\
&\qquad = 1 - \sum_{k=0}^{\infty} e^{-\tilde{\lambda}} \frac{1}{k!} \Big(\lambda_\ell \nu_1\big(\widetilde{T}_{\gamma,\varepsilon}^{(1)} \cap B(o,r)\big)\Big)^k \\
&\qquad = 1 - \exp\big(-\lambda_\ell \big(\nu_1(\widetilde{T}_\gamma^{(1)}) \backslash \nu_1(\widetilde{T}_{\gamma,\varepsilon}^{(1)} \cap B(o,r))\big)\big)\,.
\end{aligned}$$

Thus we have

$$\lim_{\gamma\to\infty} \mathbb{P}\big(\big|C^* - |\widetilde{H}_0|\big| > \varepsilon, |\widetilde{H}_0| \le r\big) \;\le\; 1 - \lim_{\gamma\to\infty} \mathbb{E} \exp\Big(-\frac{\lambda}{\gamma}\, \nu_1\big(\widetilde{T}_\gamma^{(1)} \backslash \widetilde{T}_{\gamma,\varepsilon}^{(1)} \cap B(o,r)\big)\Big)\,.$$

Now, using Lemma 6.3, we get that

$$\lim_{\gamma\to\infty} \mathbb{P}\big(\big|C^* - \xi|\widetilde{H}_0|\big| > \varepsilon, |\widetilde{H}_0| \le r\big) \;=\; 0\,,$$

which completes the proof. □

6.5 Proof of Lemma 6.3

This section is devoted to the proof of Lemma 6.3. In order to prove Lemma 6.3 we make use of some well-known results from measure theory, the theory of subadditive processes, and geometric measure theory which are summarized in the appendix. In particular, applying Theorems A.7, A.10 and A.12 it is possible to prove Lemma 6.3. It is obvious that

$$\limsup_{\gamma\to\infty} \mathbb{E}\exp\Big(-\frac{\lambda}{\gamma}\,\nu_1\big(\widetilde{T}_\gamma^{(1)} \setminus \widetilde{T}_{\gamma,\varepsilon}^{(1)} \cap B(o,r)\big)\Big) \le 1.$$

Thus it suffices to show that

$$\liminf_{\gamma\to\infty} \mathbb{E}\exp\Big(-\frac{\lambda}{\gamma}\,\nu_1\big(\widetilde{T}_\gamma^{(1)} \setminus \widetilde{T}_{\gamma,\varepsilon}^{(1)} \cap B(o,r)\big)\Big) \ge 1\,. \tag{6.10}$$

Proof of (6.10)

Note that the random intensity measure of the Cox process L is given by the stationary random measure $\Lambda(B) = \lambda'_\ell \nu_1(B \cap T_\gamma^{(1)})$ for $B \in \mathcal{B}(\mathbb{R}^2)$. Due to Slivnyak's theorem for Cox processes (Theorem 3.3) we can identify the edge set $\widetilde{T}_\gamma^{(1)}$ with the Palm version $\Lambda^*_{T_\gamma^{(1)}}$ of the stationary random measure $\Lambda_{T_\gamma^{(1)}}$ given by $\Lambda_{T_\gamma^{(1)}}(B) = \nu_1(B \cap T_\gamma^{(1)})$ for $B \in \mathcal{B}(\mathbb{R}^2)$, see e.g. Lemma 3.4. We now use the the abbreviation

$$h(\tau^{(1)}) = \exp\Big(-\frac{\lambda}{\gamma}\,\nu_1(\tau^{(1)} \setminus \tau_\varepsilon^{(1)} \cap B(o,r))\Big)\,,$$

where $\tau_\varepsilon^{(1)} = \big\{u \in \tau^{(1)} : \big|c(u) - \xi|u|\big| < \varepsilon\big\}$ and $c(u)$ is the length of the shortest path from u to the origin along the edges $\tau^{(1)}$ of a tessellation τ which fulfills the condition $o \in \tau^{(1)}$. Then the Campbell theorem for stationary random measures (Theorem 2.13) yields that

$$\begin{aligned}
\mathbb{E}h(\widetilde{T}_\gamma^{(1)}) &= \frac{1}{\gamma\nu_2(B(o,1/\gamma))}\mathbb{E}\Big(\int_{T_\gamma^{(1)}\cap B(o,1/\gamma)} h(T_\gamma^{(1)} - x)\nu_1(dx)\Big)\\
&= \frac{1}{\pi}\mathbb{E}\Big(\int_{T^{(1)}\cap B(o,1)} h\big(T_\gamma^{(1)} - \frac{z}{\gamma}\big)\nu_1(dz)\Big)\,,
\end{aligned}$$

where in the last expression we used the substitution $z = \gamma x$ keeping in mind that $(1/\gamma)T^{(1)} = T_\gamma^{(1)}$. Moreover, we define $T_{\gamma,\varepsilon,z}^{(1)} = \{y \in T_\gamma^{(1)} : |c(y, z/\gamma) - \xi|y - z/\gamma|| < \varepsilon\}$, where we denote by $c(y, z/\gamma)$ the length of the shortest path from y to z/γ along the edges of the considered graph. Using this notation, we get for each $\gamma \geq 1$ that

$$\begin{aligned}
\mathbb{E}h\big(\widetilde{T}_\gamma^{(1)}\big) &= \frac{1}{\pi}\,\mathbb{E}\Big(\int_{T^{(1)}\cap B(o,1)} \exp\Big(-\frac{\lambda}{\gamma}\,\nu_1\big(T_\gamma^{(1)}\backslash T_{\gamma,\varepsilon,z}^{(1)} \cap B(z/\gamma, r)\big)\Big)\nu_1(dz)\Big) \\
&\geq \frac{1}{\pi}\,\mathbb{E}\Big(\nu_1\big(T^{(1)}\cap B(o,1)\big) \inf_{z\in T^{(1)}\cap B(o,1)} \exp\Big(-\frac{\lambda}{\gamma}\,\nu_1\big(T_\gamma^{(1)}\backslash T_{\gamma,\varepsilon,z}^{(1)}\cap B(z/\gamma, r)\big)\Big)\Big) \\
&= \frac{1}{\pi}\,\mathbb{E}\Big(\nu_1\big(T^{(1)}\cap B(o,1)\big) \exp\Big(-\sup_{z\in T^{(1)}\cap B(o,1)} \frac{\lambda}{\gamma}\,\nu_1\big(T_\gamma^{(1)}\backslash T_{\gamma,\varepsilon,z}^{(1)}\cap B(z/\gamma, r)\big)\Big)\Big) \\
&\geq \frac{1}{\pi}\,\mathbb{E}\Big(\nu_1\big(T^{(1)}\cap B(o,1)\big) \exp\Big(-\sup_{z\in T^{(1)}\cap B(o,1)} \frac{\lambda}{\gamma}\,\nu_1\big(T_\gamma^{(1)}\backslash T_{\gamma,\varepsilon,z}^{(1)}\cap B(o, r+1)\big)\Big)\Big).
\end{aligned}$$

Thus, in order to prove (6.10), it suffices to show that

$$X_\gamma = \sup_{z\in T^{(1)}\cap B(o,1)} \frac{1}{\gamma}\,\nu_1\Big(T_\gamma^{(1)}\backslash T_{\gamma,\varepsilon,z}^{(1)}\cap B(o, r+1)\Big) \xrightarrow{L^1} 0 \qquad \text{for } \gamma \to \infty. \quad (6.11)$$

This can be seen in the following way. First (6.11) implies that X_γ converges in probability to 0 which means that the random variable $Y_\gamma = \exp(-\lambda X_\gamma)\nu_1(T^{(1)} \cap B(o,1))$ converges in probability to $\nu_1\big(T^{(1)}\cap B(o,1)\big)$. Furthermore, it holds that $Y_\gamma \leq \nu_1(T^{(1)} \cap B(o,1))$ for all $\gamma \geq 1$ and $\mathbb{E}\nu_1(T^{(1)} \cap B(o,1)) = \pi < \infty$. Thus, the family $\{Y_\gamma,\, \gamma \geq 1\}$ is uniformly integrable and we get with Theorem A.7 that Y_γ converges in L^1 to $\nu_1\big(T^{(1)} \cap B(o,1)\big)$. In particular, we have $\lim_{\gamma\to\infty} 1/\pi\mathbb{E}Y_\gamma = 1/\pi\mathbb{E}\nu_1\big(T^{(1)}\cap B(o,1)\big) = 1$ if (6.11) holds. Thus, (6.10) is a consequence of (6.11) and it is hence sufficient to show (6.11).

Proof of (6.11)

Note that $X_\gamma \geq 0$, thus it is sufficient to show that $\mathbb{E}X_\gamma \to 0$. Moreover, the segment system $T_\gamma^{(1)} \cap B(o, r+1)$ satisfy the conditions of Theorem A.12 almost surely since no segment of $T_\gamma^{(1)} \cap B(o, r+1)$ „points" to the origin with probability 1. Let ℓ_Φ^+ denote the half line starting at o with direction Φ, then we can apply

Theorem A.12 in order to get that

$$\begin{aligned}
\mathbb{E}X_\gamma &= \mathbb{E}\Big(\sup_{z\in T^{(1)}\cap B(o,1)} \frac{1}{\gamma} \int_{T_\gamma^{(1)}\cap B(o,r+1)} \mathbb{1}_{[\varepsilon,\infty)}\Big(\big|c(y,\frac{z}{\gamma}) - \xi|y-\frac{z}{\gamma}|\big|\Big)\,\nu_1(dy)\Big) \\
&= \mathbb{E}\Big(\frac{1}{\gamma} \sup_{z\in T^{(1)}\cap B(o,1)} \int_0^{2\pi} \sum_{\substack{X_i\in T_\gamma^{(1)}\cap \ell_\Phi^+:\\ |X_i|\le r+1}} \frac{|X_i|}{\sin\alpha_i} \mathbb{1}_{[\varepsilon,\infty)}\Big(\big|c(X_i,\frac{z}{\gamma}) - \xi|X_i-\frac{z}{\gamma}|\big|\Big)\,d\Phi\Big) \\
&\le \frac{r+1}{\gamma}\mathbb{E}\Big(\int_0^{2\pi} \sup_{z\in T^{(1)}\cap B(o,1)} \sum_{\substack{X_i\in T_\gamma^{(1)}\cap \ell_\Phi^+:\\ |X_i|\le r+1}} \frac{1}{\sin\alpha_i} \mathbb{1}_{[\varepsilon,\infty)}\Big(\big|c(X_i,\frac{z}{\gamma}) - \xi|X_i-\frac{z}{\gamma}|\big|\Big)\,d\Phi\Big) \\
&= \frac{2\pi(r+1)}{\gamma}\mathbb{E}\Big(\sup_{z\in T^{(1)}\cap B(o,1)} \sum_{\substack{X_i\in T_\gamma^{(1)}\cap \ell^+:\\ |X_i|\le r+1}} \frac{1}{\sin\alpha_i} \mathbb{1}_{[\varepsilon,\infty)}\Big(\big|c(X_i,\frac{z}{\gamma}) - \xi|X_i-\frac{z}{\gamma}|\big|\Big)\Big) \\
&= 2\pi(r+1)\mathbb{E}g_\gamma\big(T^{(1)}\big)\,,
\end{aligned}$$

where the last but one line is a consequence of Fubini's theorem and the isotropy of $T_\gamma^{(1)}$. Here, we denote by $\ell^+ = \ell_0^+$ the half line with direction $\Phi = 0$, and in the last expression we used the notation

$$g_\gamma\big(T^{(1)}\big) = \frac{1}{\gamma} \sup_{z\in T^{(1)}\cap B(o,1)} \sum_{\substack{X_i\in T_\gamma^{(1)}\cap \ell^+:\\ |X_i|\le r+1}} \frac{1}{\sin\alpha_i} \mathbb{1}_{[\varepsilon,\infty)}\Big(\big|c(X_i,\frac{z}{\gamma}) - \xi|X_i-\frac{z}{\gamma}|\big|\Big)\,. \quad (6.12)$$

Note that the point process $T^{(1)}\cap\mathbb{R}$ is stationary with intensity $2/\pi$ ([87], Theorem 4.5.3), where we identify $\mathbb{R}$ with the x-axis. Thus the inversion formula for Palm distributions of stationary point processes on $\mathbb{R}$ can be applied, see e.g. Proposition 11.3 (iii) in [45]. Now, if $T^{(1)*}$ denotes the Palm version of $T^{(1)}$ with respect to the point process $T^{(1)}\cap\mathbb{R}$, it follows that

$$\mathbb{E}g_\gamma\big(T^{(1)}\big) \;=\; \frac{2}{\pi}\,\mathbb{E}\Big(\int_0^\infty \mathbb{1}_{[0,X_1^*]}(x)\, g_\gamma\big(T^{(1)*}-x\big)\,dx\Big)\,,$$

where we number the points of $\{X_i^*\} = T^{(1)*}\cap\mathbb{R}$ in ascending order such that $\ldots < X_{-1}^* < X_0^* = 0 < X_1^* < X_2^* < \ldots$. Thus, we have shown that, in order to prove (6.11), it is sufficient to prove that

$$\lim_{\gamma\to\infty} \mathbb{E}\Big(\int_0^\infty \mathbb{1}_{[0,X_1^*]}(x)\, g_\gamma\big(T^{(1)*}-x\big)\,dx\Big) = 0\,, \quad (6.13)$$

where the function $g_\gamma : \mathcal{F} \to [0,\infty)$ is defined in (6.12). We split the proof of (6.13) into two main steps. In the first step, we show that

$$\lim_{\gamma\to\infty} \widetilde{g}_\gamma\big(x, T^{(1)*}\big) = 0 \quad (6.14)$$

almost everywhere with respect to the product measure $\nu_1 \otimes P^*$, where P^* denotes the distribution of $T^{(1)*}$ and we use the abbreviation $\widetilde{g}_\gamma(x, T^{(1)*}) = \mathbb{1}_{[0,X_1^*]}(x)\, g_\gamma(T^{(1)*} - x)$. Then, in the second step, we show that the family $\{\widetilde{g}_\gamma,\, \gamma > 0\}$ is uniformly $(\nu_1 \otimes P^*)$-integrable. Thus the assumptions of Theorem A.7 are then fulfilled which implies that (6.13) holds.

Proof of (6.14)

Notice that we get for each $x \in [0, X_1^*]$ that

$$\begin{aligned}
&g_\gamma\big(T^{(1)*} - x\big) \\
&\quad\le \frac{1}{\gamma} \sup_{z \in (T^{(1)*}-x)\cap B(o,1)} \sum_{\substack{X_i \in (T_\gamma^{(1)*} - \frac{x}{\gamma}) \cap \ell^+: \\ |X_i| \le r+1}} \frac{1}{\sin\alpha_i} \mathbb{1}_{[\varepsilon,\infty)}\Big(\big|c(X_i, \frac{z}{\gamma}) - \xi|X_i - \frac{z}{\gamma}|\big|\Big) \\
&\quad= \frac{1}{\gamma} \sup_{z \in T^{(1)*}\cap B(x,1)} \sum_{\substack{X_i^* \in T^{(1)*}\cap(\ell^+ + x): \\ X_i^* \in B(x,(r+1)\gamma)}} \frac{1}{\sin\alpha_i} \mathbb{1}_{[\varepsilon,\infty)}\Big(\frac{1}{\gamma}\big|c(X_i^*, z) - \xi|X_i^* - z|\big|\Big) \\
&\quad\le \frac{1}{\gamma} \sum_{\substack{X_i^* \in T^{(1)*}\cap(\ell^+ + x): \\ X_i^* \in B(x,(r+1)\gamma)}} \frac{1}{\sin\alpha_i} \sup_{z \in T^{(1)*}\cap B(x,1)} \mathbb{1}_{[\varepsilon,\infty)}\Big(\frac{1}{\gamma}\big|c(X_i^*, z) - \xi|X_i^* - z|\big|\Big).
\end{aligned}$$

Thus,

$$\begin{aligned}
&g_\gamma\big(T^{(1)*} - x\big) \\
&\quad\le \frac{1}{\gamma} \sum_{\substack{X_i^* \in T^{(1)*}\cap\ell^+: \\ |X_i^*| \le (r+a)\gamma}} \frac{1}{\sin\alpha_i} \sup_{z \in T^{(1)*}\cap B(o,a)} \mathbb{1}_{[\varepsilon,\infty)}\Big(\frac{1}{\gamma}\big|c(X_i^*, z) - \xi|X_i^* - z|\big|\Big) \\
&\quad= \frac{1}{\gamma} \sum_{\substack{X_i^* \in T^{(1)*}\cap\ell^+: \\ |X_i^*| \le (r+a)\gamma}} \frac{1}{\sin\alpha_i} \mathbb{1}_{[\varepsilon,\infty)}\Big(\frac{1}{\gamma} \sup_{z \in T^{(1)*}\cap B(o,a)} \big|c(X_i^*, z) - \xi|X_i^* - z|\big|\Big),
\end{aligned}$$

where we put $a = 1 + X_1^*$. Moreover, we have

$$\begin{aligned}
\frac{1}{\gamma} \sup_{z \in T^{(1)*}\cap B(o,a)} \big|c(X_i^*, z) - \xi|X_i^* - z|\big| \;&\le\; \frac{1}{\gamma}\big(c(X_0^*, X_i^*) - \xi|X_i^*|\big) \\
&+\; \frac{1}{\gamma}\left(\sup_{z \in T^{(1)*}\cap B(o,a)} c(z, X_0^*) + \xi a\right),
\end{aligned}$$

which is due to the fact that $c(X_0^*, X_i^*) - c(X_0^*, z) \le c(X_i^*, z) \le c(X_0^*, X_i^*) + c(X_0^*, z)$ and $\xi|X_i^*| - \xi a \le \xi|X_i^* - z| \le \xi|X_i^*| + \xi a$ for all $i \ge 1$ and $z \in T^{(1)*} \cap B(o,a)$. Obviously, the second term of this upper bound tends to zero P^*-almost surely

as $\gamma \to \infty$. Now, in order to show that (6.14) holds, it is sufficient to show that P^*-almost surely there is $i_0 \in \mathbb{N}$ with

$$\frac{1}{\gamma}\left(c(X_0^*, X_i^*) - \xi X_i^*\right) \in \left(-\frac{\varepsilon}{2}\,,\ \frac{\varepsilon}{2}\right) \tag{6.15}$$

for all $i \geq i_0, \gamma \geq 1$ with $X_i^* \leq (r+a)\gamma$.

Proof of (6.15)

It is easy to see that $\mathbf{X} = \{|X_i^* - X_j^*|, i, j \geq 1, i < j\}$ is an additive process since $|X_i^* - X_k^*| = |X_i^* - X_j^*| + |X_j^* - X_k^*|$ for $i < j < k$. Moreover, $T^{(1)*} \cap \mathbb{R}$ is cycle-stationary (see e.g. [94]) which yields that $\{|X_i^* - X_j^*|\} \stackrel{\mathrm{d}}{=} \{|X_{i+1}^* - X_{j+1}^*|\}$, where $0 < \mathbb{E}X_1^* < \infty$. Thus, using Theorem A.10 it follows that the finite limit $\lim_{i\to\infty} X_i^*/i = \zeta_{\mathbf{X}}$ exists P^*-almost surely. Now consider the family $\mathbf{Y} = \{Y_{ij}, i, j \geq 1, i < j\}$ of non-negative random variables which is given by $Y_{ij} = c(X_i^*, X_j^*)$, where $c(X_i^*, X_j^*)$ denotes the shortest path length from X_i^* to X_j^* on $T^{(1)*}$. Then, it is not difficult to see that $Y_{ik} \leq Y_{ij} + Y_{jk}$ for $i < j < k$. Due to the cycle-stationarity of $T^{(1)*} \cap \mathbb{R}$, we get that $\{Y_{ij}\} \stackrel{\mathrm{d}}{=} \{Y_{i+1,j+1}\}$ and $\mathbb{E}Y_{01} = \mathbb{E}c(X_0^*, X_1^*) < \infty$ is a consequence of condition (6.4), see the next paragraph below. Thus we get that $\mathbf{Y}$ is a subadditive process and hence Theorem A.10 can be applied in order to get that the finite limit $\lim_{j\to\infty} c(X_0^*, X_j^*)/j = \zeta_{\mathbf{Y}}$ exists P^*-almost surely. Since both $\mathbf{X}$ and $\mathbf{Y}$ are ergodic, see the paragraphs below, the limits $\zeta_{\mathbf{X}}$ and $\zeta_{\mathbf{Y}}$ are constant. Bearing in mind that $0 < \mathbb{E}X_1^* = \zeta_{\mathbf{X}} \leq \zeta_{\mathbf{Y}} < \infty$, this gives that

$$\lim_{j\to\infty} \frac{c(X_0^*, X_j^*)}{X_j^*} = \lim_{j\to\infty} \frac{j}{X_j^*}\,\frac{c(X_0^*, X_j^*)}{j} = \xi\,, \tag{6.16}$$

where $\xi = \zeta_{\mathbf{Y}}/\zeta_{\mathbf{X}} \in [1, \infty)$. Now assume that $\widetilde{\varepsilon} > 0$ with $\widetilde{\varepsilon}(r+a) < \varepsilon/2$. Then, using (6.16), it follows that with probability 1

$$\frac{c(X_0^*, X_i^*)}{X_i^*} - \xi \in (-\widetilde{\varepsilon}, \widetilde{\varepsilon})$$

for all i which are sufficiently large and, as a consequence,

$$\frac{1}{\gamma}\left(c(X_0^*, X_i^*) - \xi X_i^*\right) \in \left(-\frac{\varepsilon}{2}\,,\ \frac{\varepsilon}{2}\right)$$

if i is sufficiently large, $\gamma \geq 1$ and $X_i^*/\gamma \leq r + a$.

Proof of $\mathbb{E}c(X_0^*, X_1^*) < \infty$

We consider the stationary marked point process $\{(X_n, \Xi_n^+)\}$, where $\{X_n\} = T^{(1)} \cap \mathbb{R}$ denotes the point process of intersection points of the edge set $T^{(1)}$ with

the x-axis $\mathbb{R}$, and each point is marked with the cell Ξ_n^+ of T on the right of X_n. Let λ^+ be the intensity of the stationary marked point process $\{(X_n, \Xi_n^+)\}$, and let Ξ^{+*} denote its typical mark. Then we can use the definition of the Palm mark distribution in order to get that

$$\begin{aligned}\mathbb{E}\, c(X_0^*, X_1^*) &\leq \mathbb{E}\, \nu_1(\partial \Xi^{+*}) = \frac{1}{\lambda^+}\, \mathbb{E} \sum_{X_i \in T^{(1)} \cap [0,1)} \nu_1(\partial \Xi_i^+) \\ &= \frac{1}{\lambda^+}\, \mathbb{E} \sum_{\Xi_i \in T} \mathbb{1}_{\{\partial^+ \Xi_i \cap [0,1) \neq \emptyset\}} \nu_1(\partial \Xi_i)\,,\end{aligned}$$

where $\partial^+ \Xi$ denotes that part of the boundary of Ξ with outer unit normal vector in $[\pi/2, 3\pi/2)$. Now we can apply Campbell's theorem to the latter expression, which gives

$$\begin{aligned}\mathbb{E} c(X_0^*, X_1^*) &\leq \frac{\lambda_T}{\lambda^+}\, \mathbb{E}\nu_1(\partial \Xi^*) \int_{\mathbb{R}^2} \mathbb{1}_{\{\partial^+ \Xi^* + x \cap [0,1) \neq \emptyset\}} \nu_2(dx) \\ &= \frac{\lambda_T}{\lambda^+}\, \mathbb{E}\nu_1(\partial \Xi^*) \nu_2([0,1) \oplus \partial^+ \Xi^*)\,,\end{aligned}$$

where $\lambda_T = 1/\mathbb{E}\, \nu_2(\Xi^*)$. It is easy to see that $\nu_2([0,1) \oplus \partial^+ \Xi^*) \leq a\, \nu_1(\partial \Xi^*)$ for some constant $a < \infty$ which implies that $\mathbb{E}\, c(X_0^*, X_1^*) \leq (a \lambda_T / \lambda^+)\, \mathbb{E}\nu_1^2(\partial \Xi^*)$. Thus, the assertion is shown since it is assumed that $\mathbb{E}\nu_1^2(\partial \Xi^*) < \infty$.

Ergodicity

We only show that the subadditive process $\mathbf{X}$ is ergodic. The ergodicity of $\mathbf{Y}$ can be shown exactly in the same way. Let $\mathcal{I}_{\mathcal{S}} \subset \mathcal{B}(\mathcal{S})$ denote the σ-algebra of those subsets of the space $\mathcal{S}$ of double-indexed sequences, which are invariant under the shift defined by $\{|X_i^* - X_j^*|\} \longmapsto \{|X_{i+1}^* - X_{j+1}^*|\}$, see Chapter A.2. Moreover, note that we can write $\mathbf{X} = h(T_\gamma^{(1)*})$ for some measurable function $h : \mathcal{F} \to \mathcal{S}$. It holds that for any deterministic tessellation τ in $\mathbb{R}^2$ and all $A \in \mathcal{I}_{\mathcal{S}}$, we have $h(\tau^{(1)}) \in A$ if and only if $h(\tau^{(1)} - x) \in A$ for all $x \in [0, \infty)$. Thus, the definition of the Palm distribution of the stationary point process $\{X_i\} = T^{(1)} \cap \mathbb{R}$ with intensity $2/\pi$ yields for any $A \in \mathcal{I}_{\mathcal{S}}$ that

$$\begin{aligned}\mathbb{P}(\mathbf{X} \in A) &= \mathbb{P}(h(T^{(1)*}) \in A) \\ &= \frac{\pi}{2}\, \mathbb{E} \sum_{X_i \in T^{(1)} \cap B(o,1) \cap \ell^+} \mathbb{1}_A(h(T^{(1)} - X_i)) \\ &= \frac{\pi}{2}\, \mathbb{E}\big(\mathbb{1}_A(h(T^{(1)}))\, \#\{X_i \in T^{(1)} \cap B(o,1) \cap \ell^+\}\big) \\ &= \frac{\pi}{2}\, \mathbb{E}\big(\mathbb{1}_{h^{-1}(A)}(T^{(1)})\, \#\{X_i \in T^{(1)} \cap B(o,1) \cap \ell^+\}\big)\,.\end{aligned}$$

However, since the random tessellation T is mixing and $h^{-1}(A) = h^{-1}(A) + x$ for any $A \in \mathcal{I}_{\mathcal{S}}$ and $x \in \ell^+$, we get that

$$\begin{aligned}\mathbb{P}\big(T^{(1)} \in h^{-1}(A)\big) &= \lim_{|x|\to\infty, x\in\ell^+} \mathbb{P}\big(T^{(1)} \in h^{-1}(A), T^{(1)} - x \in h^{-1}(A)\big) \\ &= \mathbb{P}\big(T^{(1)} \in h^{-1}(A)\big)^2,\end{aligned}$$

which means that $\mathbb{P}\big(T^{(1)} \in h^{-1}(A)\big) = 0$ or $\mathbb{P}\big(T^{(1)} \in h^{-1}(A)\big) = 1$. Thus, altogether we have

$$\begin{aligned}\mathbb{P}(\mathbf{X} \in A) &= \mathbb{P}\big(T^{(1)} \in h^{-1}(A)\big)\, \frac{\pi}{2}\, \mathbb{E}\, \#\{X_i \in T^{(1)} \cap B(o,1) \cap \ell^+\} \\ &= \mathbb{P}\big(T^{(1)} \in h^{-1}(A)\big)\end{aligned}$$

which yields $\mathbb{P}(\mathbf{X} \in A) = 0$ or $\mathbb{P}(\mathbf{X} \in A) = 1$ for any $A \in \mathcal{I}_{\mathcal{S}}$. This implies that $\mathbf{X}$ is ergodic.

Uniform integrability

It only remains to show that the family $\{\widetilde{g}_\gamma,\, \gamma > 0\}$ considered in (6.14) is uniformly $(\nu_1 \otimes P^*)$-integrable. Note that we can apply the ergodic theorem for stationary marked point processes, see Theorem 2.8, in order to get that

$$\begin{aligned}\lim_{\gamma\to\infty} \frac{1}{\gamma} \sum_{\substack{X_i\in T^{(1)}\cap\ell^+:\\ |X_i|\le(r+1)\gamma}} \frac{1}{\sin\alpha_i} &= (r+1) \lim_{\gamma\to\infty} \frac{1}{(r+1)\gamma} \sum_{\substack{X_i\in T^{(1)}\cap\ell^+:\\ |X_i|\le(r+1)\gamma}} \frac{1}{\sin\alpha_i} \\ &= (r+1)\, \mathbb{E}\, \frac{1}{\sin\alpha^*}\end{aligned}$$

almost surely and in L^1 using the fact that the point process $T^{(1)} \cap \mathbb{R}$ marked with the intersection angles is ergodic, which can be shown in the same manner as the ergodicity of $\mathbf{X}$. Here we denote by α^* the typical intersection angle which is distributed according to the density $f_{\alpha^*}(\alpha) = \sin(\alpha)/2$ for $0 \le \alpha < \pi$, see e.g. [90], p. 288, which yields $\mathbb{E}(\sin\alpha^*)^{-1} = \pi/2 < \infty$. Thus

$$\begin{aligned}0 &= \lim_{\gamma\to\infty} \mathbb{E} \left| \frac{1}{\gamma} \sum_{\substack{X_i\in T^{(1)}\cap\ell^+:\\ |X_i|\le(r+1)\gamma}} \frac{1}{\sin\alpha_i} - (r+1)\, \mathbb{E}\, \frac{1}{\sin\alpha^*} \right| \\ &= \lim_{\gamma\to\infty} \frac{2}{\pi}\, \mathbb{E} \int_{\mathbb{R}} \mathbb{1}_{[0,X_1^*]}(x) \left| \frac{1}{\gamma} \sum_{\substack{X_i\in (T^{(1)*}-x)\cap\ell^+:\\ |X_i|\le(r+1)\gamma}} \frac{1}{\sin\alpha_i} - (r+1)\, \mathbb{E}\, \frac{1}{\sin\alpha^*} \right| dx\,,\end{aligned}$$

where in the last equality we applied the inversion formula for Palm distributions of stationary marked point processes on $\mathbb{R}$, see Proposition 11.3 (iii) in [45].

That means we have shown that

$$\mathbb{1}_{[0,X_1^*]}(x)\,\frac{1}{\gamma}\sum_{\substack{X_i\in(T^{(1)*}-x)\cap\ell^+:\\ |X_i|\le(r+1)\gamma}}\frac{1}{\sin\alpha_i}\;\to\;(r+1)\mathbb{1}_{[0,X_1^*]}(x)\,\mathbb{E}\,\frac{1}{\sin\alpha^*}$$

in $L^1(\nu_1\otimes\mathbb{P}^*)$ as $\gamma\to\infty$. Thus, Theorem A.7 implies that the family $\{h_\gamma,\,\gamma>0\}$ with

$$h_\gamma(x,T^{(1)*})=\mathbb{1}_{[0,X_1^*]}(x)\,\frac{1}{\gamma}\sum_{\substack{X_i\in(T^{(1)*}-x)\cap\ell^+:\\ |X_i|\le(r+1)\gamma}}\frac{1}{\sin\alpha_i}$$

is uniformly $(\nu_1\otimes P^*)$-integrable. Moreover, we have that

$$\mathbb{1}_{[0,X_1^*]}(x)g_\gamma(T^{(1)*}-x)\le\mathbb{1}_{[0,X_1^*]}(x)\,\frac{1}{\gamma}\sum_{\substack{X_i\in(T^{(1)*}-x)\cap\ell^+:\\ |X_i|\le(r+1)\gamma}}\frac{1}{\sin\alpha_i}\,.$$

As a consequence, Lemma A.8 implies that the family $\{\widetilde{g}_\gamma,\,\gamma>0\}$ considered in (6.14) is uniformly $(\nu_1\otimes P^*)$-integrable.

6.6 Examples

Note that we assumed in Theorem 6.2 that the underlying tessellation T is stationary and isotropic. All examples of tessellations which are considered in this section obviously have these properties. Moreover, it was assumed in Theorem 6.2 that T is in addition mixing and fulfills the integrability condition (6.4). To begin with, we show that the mixing condition is satisfied for a wide class of stationary tessellations. Furthermore, we also show that the integrability condition (6.4) is fulfilled.

The tessellation models which are considered in the literature concentrate mainly on PDT, PLT and PVT, iterated tessellations constructed from these basic tessellation models of Poisson type and STIT tessellations, see e.g. [1, 5, 6, 8, 34, 75]. In this chapter, wee assume that an iterated tessellation is either a T_I/T_{II}-nesting or a T_I/T_{II}-superposition of the random tessellations T_I and T_{II} as defined in Section 3.4.4, see also [5, 55, 102]. Recall that the edge set of a T_I/T_{II}-superposition is given by the union $T_I^{(1)}\cup T_{II}^{(1)}$ of the edge sets of T_I and T_{II} which are assumed to be independent. Moreover, a T_I/T_{II}-nesting is constructed by a subdivision of each cell of T_I based on independent copies of T_{II}. Note that a STIT tessellation can be regarded as the weak limit of nested tessellations, where the cells of T_I are subdivided infinitely often followed by an appropriate rescaling, see [74]. In the following, we show that for these important models the assumptions of Theorem 6.2 are fulfilled. Moreover, if the underlying tessellation T is a PLT or a T_I/T_{II}-superposition/nesting based on a PLT T_I, then we can even calculate the constant ξ explicitly which appears in Theorem 6.2. On the other hand, if T is a PDT, then we can obtain an upper bound for ξ.

6.6.1 Mixing tessellations

Suppose that the underlying tessellation T is isotropic and stationary. In order to apply Theorem 6.2 we have to show additionally that T is a mixing tessellation. A useful criterion to decide if a random closed set is mixing can be found in the following theorem which is a slight modification of Theorem 2.12.

Lemma 6.5 *A stationary random closed set Ξ in $\mathbb{R}^2$ is mixing if and only if*

$$\lim_{|x|\to\infty} \mathbb{P}(\Xi \cap C_1 = \emptyset,\, \Xi \cap (C_2 + x) = \emptyset) = \mathbb{P}(\Xi \cap C_1 = \emptyset)\, \mathbb{P}(\Xi \cap C_2 = \emptyset) \quad (6.17)$$

for all $C_1, C_2 \in \mathcal{R}$, where $\mathcal{R}$ is the family of all subsets of $\mathbb{R}^2$ which are finite unions of closed balls with rational radii and centers with rational coordinates.

Proof The statement of Lemma 6.5 is essentially Theorem 2.12, see also Lemma 4 in [40] and Theorem 9.3.2 in [87]. There, the slightly stronger condition is considered that equation (6.17) holds for all compact sets $C_1, C_2 \subset \mathbb{R}^2$. However, it is not difficult to see that it is sufficient to assume that (6.17) only holds for the separating class $\mathcal{R}$, see also Section 1.4 of [70] for similar statements. In order to prove the assertion, we only have to show that the system $\mathcal{E}$ defined by $\mathcal{E} = \{\mathcal{F}^{C_0}_{C_1,\dots,C_k} : C_0, \dots, C_k \in \mathcal{R}', k \geq 0\}$ is a semi-algebra that generates the σ–algebra $\mathcal{B}(\mathcal{F})$, where $\mathcal{R}' = \mathcal{R} \cup \{\emptyset\}$ and $\mathcal{F}^{C_0}_{C_1,\dots,C_k}$ is given by

$$\mathcal{F}^{C_0}_{C_1,\dots,C_k} = \{F \in \mathcal{F} : F \cap C_0 = \emptyset, F \cap C_1 \neq \emptyset, \dots, F \cap C_k \neq \emptyset\}\,.$$

Notice that the family $\mathcal{R}'$ is union-stable. Hence Lemma 2.2.2 in [87] can be applied which yields that $\mathcal{E}$ is a semi-algebra. Furthermore, let $G \subset \mathbb{R}^2$ be an open set, then $G = \bigcup_{i=1}^{\infty} C_i$ for a sequence $C_1, C_2, \dots \in \mathcal{R}'$ and $\mathcal{F}_G = \{F \in \mathcal{F} : F \cap G \neq \emptyset\} = \bigcup_{n=1}^{\infty} \mathcal{F}_{\bigcup_{i=1}^{n} C_i}$, thus we have $\mathcal{F}_G \in \sigma(\mathcal{E})$. Since the family $\{\mathcal{F}_G : G \subset \mathbb{R}^2 \text{ open}\}$ generates $\mathcal{B}(\mathcal{F})$, we get that $\sigma(\mathcal{E}) = \mathcal{B}(\mathcal{F})$. The assertion of Lemma 6.5 can now be proven using exactly the same arguments as in the proof of Lemma 4 in [40]. □

Note that it is well known that the basic tessellations of Poisson type, i.e., PDT, PVT and PLT, are mixing, see e.g. Chapter 10.5 in [87]. Very recently, it was shown in [49] that STIT tessellations are mixing. Moreover, we can use Lemma 6.5 in order to show that T is mixing if T is an iterated tessellation which is constructed based on these basic tessellations models.

Lemma 6.6 *The tessellation T is mixing if T is a T_I/T_{II}-superposition of two mixing tessellations T_I and T_{II}, or a T_I/T_{II}-nesting of a mixing initial tessellation T_I and any stationary component tessellation T_{II}.*

Proof We use Lemma 6.5 in order to proof the lemma. First assume that the tessellation T is a T_I/T_{II}-superposition. Then we get for any $C_1, C_2 \in \mathcal{R}$ that

$$\begin{aligned}
&\mathbb{P}(T^{(1)} \cap C_1 = \emptyset,\, T^{(1)} \cap (C_2 + x) = \emptyset) \\
&\quad = \mathbb{P}(T_I^{(1)} \cap C_1 = \emptyset,\, T_I^{(1)} \cap (C_2 + x) = \emptyset,\, T_{II}^{(1)} \cap C_1 = \emptyset,\, T_{II}^{(1)} \cap (C_2 + x) = \emptyset) \\
&\quad = \mathbb{P}(T_I^{(1)} \cap C_1 = \emptyset,\, T_I^{(1)} \cap (C_2 + x) = \emptyset)\, \mathbb{P}(T_{II}^{(1)} \cap C_1 = \emptyset,\, T_{II}^{(1)} \cap (C_2 + x) = \emptyset)\,,
\end{aligned}$$

since T_I and T_{II} are independent. Thus Lemma 6.5 yields that T is mixing if both T_I and T_{II} are mixing. Now let T be a T_I/T_{II}-nesting of a mixing initial tessellation T_I and a stationary component tessellation T_{II}. Furthermore, assume that $C_1 = \cup_{j=1}^{n} B_j, C_2 = \cup_{j=n+1}^{n+m} B_j$ for a finite family of closed balls $B_1, \ldots, B_{n+m} \subset \mathbb{R}^2$ with rational radii and centers with rational coordinates and let $\Xi_1, \Xi_2, \ldots$ denote the cells of the initial tessellation $T_I = \{\Xi_n\}$. We use the notation D for the family of all decompositions of the index set $\{1, \ldots, n+m\}$ into non-empty subsets, and for $J = \{J_1, \ldots, J_k\} \in D$ we consider the set

$$A_J(x) = \{\cup_{j \in J_i}(B_j + x\mathbb{1}_{\{j>n\}}) \subset \mathring{\Xi}_{j_i},\ i = 1, \ldots, k,\ \Xi_{j_i} \neq \Xi_{j_l} \text{ for } j_i \neq j_l\}\,, \quad (6.18)$$

i.e., each of the sets $\cup_{j \in J_i}(B_j + x\mathbb{1}_{\{j>n\}})$ is contained in a different cell of the initial tessellation T_I. Then, using this notation, we have

$$\begin{aligned}
&\lim_{|x|\to\infty} \mathbb{P}(T^{(1)} \cap C_1 = \emptyset,\, T^{(1)} \cap (C_2 + x) = \emptyset) \\
&\quad = \sum_{J \in D} \lim_{|x|\to\infty} \mathbb{P}(T^{(1)} \cap C_1 = \emptyset,\, T^{(1)} \cap (C_2 + x) = \emptyset,\, A_J(x))\,.
\end{aligned}$$

Notice that the cells $\Xi_1, \Xi_2, \ldots$ of T_I are bounded with probability 1, thus we get

$$\lim_{|x|\to\infty} \mathbb{P}(T^{(1)} \cap C_1 = \emptyset,\, T^{(1)} \cap (C_2 + x) = \emptyset,\, A_J(x)) = 0$$

if there are $i \leq n$ and $j > n$ such that $i, j \in J_l$ for some $l \in \{1, \ldots, k\}$. On the other hand, if we assume that $J = \{J_1, \ldots, J_k\}$ is a decomposition of $\{1 \ldots, n+m\}$ with $J_i \subset \{1, \ldots, n\}$ for $i = 1, \ldots, l$ and $J_i \subset \{n+1, \ldots, n+m\}$ for $i = l+1, \ldots, k$, then we get that

$$\begin{aligned}
&\mathbb{P}(T^{(1)} \cap C_1 = \emptyset,\, T^{(1)} \cap (C_2 + x) = \emptyset,\, A_J(x)) \\
&\quad = \mathbb{P}(A_J(x),\, B_{J_i} \cap T_{II,i}^{(1)} = \emptyset,\, i = 1, \ldots, l,\, B_{J_i} + x \cap T_{II,i}^{(1)} = \emptyset,\, i = l+1, \ldots, k),
\end{aligned}$$

where $B_{J_i} = \cup_{j \in J_i} B_j$ and $T_{II,1}, \ldots, T_{II,k}$ are independent copies of the component tessellation T_{II} that are independent of T_I. Using this independence and the definition of $A_J(x)$, we get that

$$\begin{aligned}
&\mathbb{P}(A_J(x),\, B_{J_i} \cap T_{II,i}^{(1)} = \emptyset,\, i = 1, \ldots, l,\, B_{J_i} + x \cap T_{II,i}^{(1)} = \emptyset,\, i = l+1, \ldots, k) \\
&\quad = \mathbb{P}(A_J(x))\, \mathbb{P}(B_{J_i} \cap T_{II,i}^{(1)} = \emptyset,\, i = 1, \ldots, l)\, \mathbb{P}(B_{J_i} \cap T_{II,i}^{(1)} = \emptyset,\, i = l+1, \ldots, k).
\end{aligned}$$

Furthermore, since T_I is mixing, we directly get from the definition of mixing random closed sets that

$$\lim_{|x|\to\infty} \mathbb{P}(A_J(x)) = \mathbb{P}(A_{J'}(o))\, \mathbb{P}(A_{J''}(o))\,,$$

where $J' = \{J_1, \dots, J_l\}$ and $J'' = \{J_{l+1}, \dots, J_k\}$ are the decompositions of $\{1, \dots, n\}$ and $\{n+1, \dots, n+m\}$, respectively, which are induced by J. Furthermore, $A_{J'}(o)$ and $A_{J''}(o)$ are defined analogously to (6.18). Summarizing all considerations from above, we get that

$$\begin{aligned}
&\lim_{|x|\to\infty} \mathbb{P}(T^{(1)} \cap C_1 = \emptyset,\, T^{(1)} \cap (C_2 + x) = \emptyset,\, A_J(x)) \\
&\quad = \mathbb{P}(A_{J'}(o),\, B_{J_i} \cap T^{(1)}_{II,i} = \emptyset,\, i = 1, \dots, l) \\
&\qquad\qquad \times\ \mathbb{P}(A_{J''}(o),\, B_{J_i} \cap T^{(1)}_{II,i} = \emptyset,\, i = l+1, \dots, k) \\
&\quad = \mathbb{P}(T^{(1)} \cap C_1 = \emptyset, A_{J'}(o))\, \mathbb{P}(T^{(1)} \cap C_2 = \emptyset, A_{J''}(o))\,,
\end{aligned}$$

which yields

$$\begin{aligned}
&\lim_{|x|\to\infty} \mathbb{P}(T^{(1)} \cap C_1 = \emptyset,\, T^{(1)} \cap (C_2 + x) = \emptyset) \\
&\quad = \sum_{J\in D} \lim_{|x|\to\infty} \mathbb{P}(T^{(1)} \cap C_1 = \emptyset,\, T^{(1)} \cap (C_2 + x) = \emptyset,\, A_J(x)) \\
&\quad = \sum_{J'\in D'} \sum_{J''\in D''} \mathbb{P}(T^{(1)} \cap C_1 = \emptyset, A_{J'}(o))\, \mathbb{P}(T^{(1)} \cap C_2 = \emptyset, A_{J''}(o)) \\
&\quad = \mathbb{P}(T^{(1)} \cap C_1 = \emptyset)\, \mathbb{P}(T^{(1)} \cap C_2 = \emptyset)\,,
\end{aligned}$$

where D' and D'' denote the families of all decompositions of $\{1, \dots, n\}$ and $\{n+1, \dots, n+m\}$, respectively. Thus we can apply Lemma 6.5 which yields that the nested tessellation T is mixing. □

6.6.2 Second moment of perimeter of the typical cell

Recall that, in order to apply Theorem 6.2, the random tessellation T has to fulfill the integrability condition (6.4). In this section we show that the second moment of the circumference of the typical cell is finite for the above considered tessellations. In the following, we use the notation $R(\Xi)$ for the radius of the minimal ball which can be circumscribed to the random convex polygon Ξ.

Lemma 6.7 *If T is a PVT, PDT, PLT and STIT tessellation, respectively, then $\mathbb{E}R^2(\Xi^*) < \infty$ and, consequently,*

$$\mathbb{E}\nu_1^2(\partial\Xi^*) < \infty\,. \tag{6.19}$$

Moreover, (6.19) *holds if T is a T_I/T_{II}-superposition/nesting such that*

$$\max\{\mathbb{E}R^2(\Xi_I^*), \mathbb{E}R^2(\Xi_{II}^*)\} < \infty\,, \tag{6.20}$$

where Ξ_I^* and Ξ_{II}^* is the typical cell of T_I and T_{II}, respectively.

Proof Since the boundary length is a monotonic increasing functional on the space of convex bodies in $\mathbb{R}^2$, we get that

$$\mathbb{E}\nu_1^2(\partial\Xi^*) \le 4\pi^2\mathbb{E}R^2(\Xi^*) \tag{6.21}$$

holds for the typical cell Ξ^* of any stationary tessellation T. If T is a PDT, then the distribution of $R(\Xi^*)$ is known, see e.g. [66], Theorem 7.5 in [71] and Theorem 10.4.4 in [87], and it can be easily shown that $\mathbb{E}R^2(\Xi^*) < \infty$. Moreover, it is well known that $\mathbb{E}R^2(\Xi^*) < \infty$ if T is either a PVT or PLT, see e.g. [18]. Since the interior of the typical cell of a STIT tessellation has the same distribution as the interior of the typical cell of a PLT, see [74], we directly get that $\mathbb{E}R^2(\Xi^*) < \infty$ for STIT tessellations.

If $T = T_I/T_{II}$ is an iterated tessellation with cell intensity λ_T, then Proposition 3.1 in [54] can be applied together with Campbell's theorem in order to get

$$\begin{aligned}
\mathbb{E}\nu_1^2(\partial\Xi^*) &= \frac{\lambda_I}{\lambda_T}\,\mathbb{E}\Big(\sum_{\Xi_i\in T_{II}} \nu_1^2(\partial(\Xi_i\cap\Xi_I^*))\,\mathbb{1}_{\{\Xi_i\cap\Xi_I^*\neq\emptyset\}}\Big)\\
&= \frac{\lambda_I\lambda_{II}}{\lambda_T}\,\mathbb{E}\int_{\mathbb{R}^2} \nu_1^2(\partial(\Xi_{II}^*+x\cap\Xi_I^*))\,\mathbb{1}_{\{\Xi_{II}^*+x\cap\Xi_I^*\neq\emptyset\}}\,\nu_2(dx)\,.
\end{aligned}$$

Here we denote with λ_I, λ_{II} and Ξ_I^*, Ξ_{II}^* the cell intensities and the typical cells of T_I and T_{II}, respectively. Note that we can assume that the typical cells Ξ_I^* and Ξ_{II}^* are independent. Furthermore, we have $\nu_1^2(\partial(\Xi_{II}^*+x\cap\Xi_I^*)) \le \min\{\nu_1^2(\partial\Xi_I^*), \nu_1^2(\partial\Xi_{II}^*)\}$, thus, we get

$$\begin{aligned}
\mathbb{E}\nu_1^2(\partial\Xi^*) &\le \frac{\lambda_I\lambda_{II}}{\lambda_T}\,\mathbb{E}\Big(\min\{\nu_1^2(\partial\Xi_I^*), \nu_1^2(\partial\Xi_{II}^*)\}\nu_2(\check{\Xi}_{II}^*\oplus\Xi_I^*)\Big)\\
&\le \frac{4\pi\,\lambda_I\lambda_{II}}{\lambda_T}\,\mathbb{E}\Big(\min\{\nu_1^2(\partial\Xi_I^*), \nu_1^2(\partial\Xi_{II}^*)\}\ \max\{R^2(\Xi_I^*), R^2(\Xi_{II}^*)\}\Big)\,,
\end{aligned}$$

where we used in the latter inequality that

$$\nu_2(\check{\Xi}_{II}^*\oplus\Xi_I^*) \ \le\ \pi R^2(\check{\Xi}_I^*\oplus\Xi_{II}^*) \ \le\ 4\pi\max\{R^2(\Xi_I^*), R^2(\Xi_{II}^*)\}\,.$$

Finally, using (6.21) and the independence of the cells Ξ_I^* and Ξ_{II}^*, we get

$$\begin{aligned}
\mathbb{E}\nu_1^2(\partial\Xi^*) &\le \frac{4\pi^3\,\lambda_I\lambda_{II}}{\lambda_T}\,\mathbb{E}\Big(\min\{R^2(\Xi_I^*), R^2(\Xi_{II}^*)\}\ \max\{R^2(\Xi_I^*), R^2(\Xi_{II}^*)\}\Big)\\
&= \frac{4\pi^3\,\lambda_I\lambda_{II}}{\lambda_T}\,\mathbb{E}R^2(\Xi_I^*)\,\mathbb{E}R^2(\Xi_{II}^*) \ <\ \infty\,,
\end{aligned}$$

if condition (6.20) is fulfilled. □

6.6.3 Asymptotic Weibull distribution of the typical shortest path lengths

We have shown in Sections 6.6.1 and 6.6.2 that the assumptions of Theorem 6.2 are fulfilled for a large class of random tessellations T and hence Theorem 6.2 can be applied. The results are summarized in the following corollary. Furthermore, we show that in same cases the constant ξ can be calculated explicitly.

Corollary 6.8 *Let $Z \sim Wei(\lambda\pi, 2)$ and let T be a PDT, PVT, PLT, STIT tessellation or an iterated tessellation $T = T_I/T_{II}$ such that condition* (6.20) *is fulfilled, where T is either*

1. *a superposition of two mixing tessellations T_I and T_{II}, or*
2. *a nesting of a mixing initial tessellation T_I and any stationary component tessellation T_{II}.*

Then $C^* \xrightarrow{\mathrm{d}} \xi Z$ for some constant $\xi \geq 1$ provided that $\gamma \to \infty$ and $\lambda_\ell \to 0$ such that $\lambda_\ell \gamma = \lambda$. Furthermore, if T is a PLT or a T_I/T_{II}-superposition/nesting, where T_I is a PLT, then $\xi = 1$. If T is a PDT, then $\xi \leq 4/\pi \approx 1.27$.

Proof In order to prove the first part of the assertion, we can apply Theorem 6.2 bearing in mind the results of Lemmas 6.6 and 6.7 as well as the comments immediately before Lemma 6.6.

Now we regard the cases that T is a PLT, a T_I/T_{II}-superposition/nesting with a PLT T_I, or a PDT. First assume that T is a PLT with intensity 1. The edge set $\widetilde{T}_\gamma^{(1)}$ of the tessellation $\widetilde{T}_\gamma$ is then induced by a random sequence of lines $\ell_0, \ell_1, \ldots$. Due to Slivnyak's theorem we have that $\ell_1, \ell_2, \ldots$ form the edge set $T_\gamma^{(1)}$ of the (stationary and isotropic) PLT T_γ and ℓ_0 is an additional line through the origin o which is isotropic and independent of T_γ. This yields

$$\frac{1}{\gamma}\,\nu_1(\widetilde{T}_\gamma^{(1)} \backslash \widetilde{T}_{\gamma,\varepsilon}^{(1)} \cap B(o,r)) \;\leq\; \frac{1}{\gamma}\,\nu_1(T_\gamma^{(1)} \cap B(o,r)) + \frac{2r}{\gamma}\,.$$

Note that due to formula (2.25)

$$\nu_1(T_\gamma^{(1)} \cap B(o,r))/\gamma = \pi r^2 \nu_1(T^{(1)} \cap B(o,r\gamma))/\nu_2(B(o,r\gamma))$$

converges to $r^2\pi$ in L^1 since T is a PLT which is mixing and, therefore, ergodic. Thus, using Theorem A.7, together with Lemma A.8, we have that the family of random variables $\{X_\gamma,\, \gamma > 0\}$ with $X_\gamma = \nu_1(\widetilde{T}_\gamma^{(1)} \backslash \widetilde{T}_{\gamma,\varepsilon}^{(1)} \cap B(o,r))/\gamma$ is uniformly integrable. Moreover, we have shown in Lemma 6.3 that the Laplace transform of X_γ converges to 1. This implies that $X_\gamma \xrightarrow{\mathrm{P}} 0$, see e.g. [45], Theorem 5.3. Thus we can apply Theorem A.7 again which yields

$$\lim_{\gamma\to\infty} \mathbb{E}\, X_\gamma = 0\,. \tag{6.22}$$

However, if $T_\gamma^{(1)}$ gets denser, there are lines which intersect the line through o close to o. Thus, all points on these lines have approximately the direct connections as shortest paths which can be used in order to show that $\xi = 1$. Assume that $\xi > 1$ and let $r > 2 > \varepsilon > 0$ with $\xi > 1 + \varepsilon$ and define the segment $S_{0,\varepsilon}$ by $S_{0,\varepsilon} = \ell_0 \cap B(o, \varepsilon/2)$. Then, if the line ℓ_i intersects $S_{0,\varepsilon}$, we get for each $y \in \ell_i$ that $0 \le c(y) - |y| \le \varepsilon$ since the length of the path from y to o via the intersection point $\ell_i \cap S_{0,\varepsilon}$ cannot be longer than $|y| + \varepsilon$. Thus, if $|y| > 2$ we get that $(\xi - 1)|y| \ge \varepsilon$ and hence

$$\big|c(y) - \xi|y|\big| \;=\; \big|c(y) - |y| - (\xi - 1)|y|\big| \;\ge\; \varepsilon(|y| - 1) \ge \varepsilon\,,$$

which implies that $y \in \widetilde{T}_\gamma^{(1)} \backslash \widetilde{T}_{\gamma,\varepsilon}^{(1)}$. Moreover, if $\ell_i \cap S_{0,\varepsilon} \neq \emptyset$, then it is easy to see that $\nu_1(\ell_i \cap B(o,r) \backslash B(o,2)) \ge a$ for some constant $a > 0$. With these two observations we get

$$\begin{aligned} X_\gamma \;=\; \frac{1}{\gamma}\nu_1(\widetilde{T}_\gamma^{(1)} \backslash \widetilde{T}_{\gamma,\varepsilon}^{(1)} \cap B(o,r)) \;&\ge\; \frac{1}{\gamma}\,\nu_1\Big(\bigcup_{i:\ell_i \cap S_{0,\varepsilon} \neq \emptyset} \{\ell_i \cap B(o,r) \backslash B(o,2)\}\Big) \\ &\ge\; \frac{a}{\gamma}\,\#\{\ell_i : \ell_i \cap S_{0,\varepsilon} \neq \emptyset\}\,. \end{aligned}$$

Furthermore, since T is a PLT, we have $\#\{\ell_i : \ell_i \cap S_{0,\varepsilon} \neq \emptyset\} \sim Poi(2\,\varepsilon\gamma/\pi)$ which yields

$$\liminf_{\gamma\to\infty} \mathbb{E}X_\gamma \;\ge\; \lim_{\gamma\to\infty} \frac{a}{\gamma}\,\mathbb{E}\#\{\ell_i : \ell_i \cap S_{0,\varepsilon} \neq \emptyset\} \;=\; \frac{2\,\varepsilon a}{\pi} > 0\,.$$

But this is a contradiction to (6.22) and hence $\xi = 1$.

Now assume that the tessellation $T = T_I/T_{II}$ is a superposition/nesting such that T_I is a PLT. Then we have

$$\frac{1}{\gamma}\,\nu_1(\widetilde{T}_\gamma^{(1)} \backslash \widetilde{T}_{\gamma,\varepsilon}^{(1)} \cap B(o,r)) \;\;\ge\;\; \mathbb{1}_{\{o \in \widetilde{T}_{I,\gamma}^{(1)}\}}\,\frac{1}{\gamma}\,\nu_1(\widetilde{T}_{I,\gamma}^{(1)} \backslash \widetilde{T}_{I,\gamma,\varepsilon}^{(1)} \cap B(o,r))\,,$$

where $\widetilde{T}_{I,\gamma}^{(1)}$ is that part of $\widetilde{T}_\gamma^{(1)}$ which corresponds to the initial tessellation T_I. However, T_I is assumed to be a PLT, thus the same arguments as above can be applied in order to show that $\xi = 1$.

Finally, assume that T is a PDT and let $N(y)$ denote that vertex of T which is closest to $y \in \mathbb{R}^2$. In [8] it was shown that for any $t > 0$ and $y \in \partial B(o,1)$, there is a path $P(ty)$ along $T^{(1)}$ from $N(o)$ to $N(ty)$ of length $c(P(ty))$ such that almost surely

$$\lim_{t\to\infty} \frac{c(P(ty))}{t} = \frac{4}{\pi}\,. \tag{6.23}$$

Now let $\ell = \{sy : s \in \mathbb{R}\}$ denote a line of direction y and consider the stationary point process $T^{(1)} \cap \ell$ of intersection points $\{X_i\}$ which are ordered such that $\cdots < X_{-1} < X_0 \le 0 < X_1 < \cdots$. Moreover, let $c(X_i, X_j)$ denote the shortest path length between X_i and X_j on $T^{(1)}$. We then consider the stationary marked

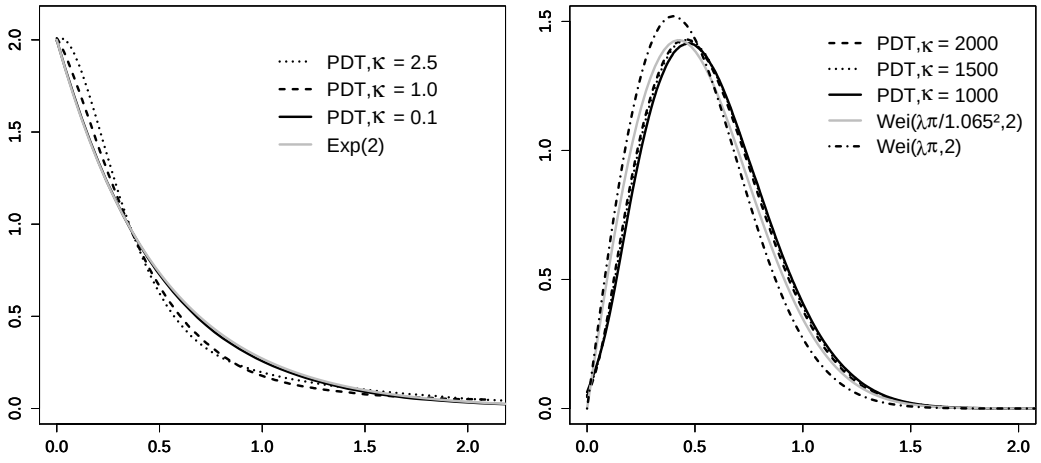

(a) $\kappa \to 0$ (where $\lambda_\ell = 1$) (b) $\kappa \to \infty$ (where $\gamma\lambda_\ell = 1$)

Figure 6.3: Density f_{C^*} for PDT together with corresponding limit distributions

point process $\{(X_i, c(X_i, N(X_i))\}$ and we denote its typical mark by c_N^*. Then we get for each $i > 0$ that

$$\begin{aligned} \frac{c(X_0, X_i)}{|X_i - X_0|} &\leq \frac{c(N(o), N(X_i))}{|X_i - X_0|} + \frac{c(X_0, N(o))}{|X_i - X_0|} + \frac{c(X_i, N(X_i))}{|X_i - X_0|} \\ &\leq \frac{c(P(X_i))}{|X_i|} + \frac{c(X_0, N(o))}{|X_i|} + \frac{c(X_i, N(X_i))}{|X_i|} \,. \end{aligned}$$

It is easy to see that the second summand of the latter expression tends to 0 as $i \to \infty$. The same is true for the third summand since the marked point process $\{(X_i, c(X_i, N(X_i))\}$ is ergodic and furthermore $\mathbb{E}\, c_N^* < \infty$. Thus, we can use (6.23) and get that

$$\limsup_{i\to\infty} \frac{c(X_0, X_i)}{|X_i - X_0|} \leq \frac{4}{\pi} \,. \tag{6.24}$$

On the other hand, it holds that $\mathbb{P}(\lim_{i\to\infty} c(X_0, X_i)/|X_i - X_0| = \xi) = 1$ if and only if $\mathbb{P}(\lim_{i\to\infty} c(X_0^*, X_i^*)/|X_i^* - X_0^*| = \xi) = 1$, where $\{X_i^*\}$ denotes the Palm version of $\{X_i\}$. Thus (6.24) and (6.16) yield that $\xi \leq 4/\pi$. □

6.7 Numerical results and possible extensions

In this section some results obtained from Monte-Carlo simulation are shown. Furthermore, we discuss some possible generalizations of Theorem 6.2 which can be obtained using the basically the same proof technique.

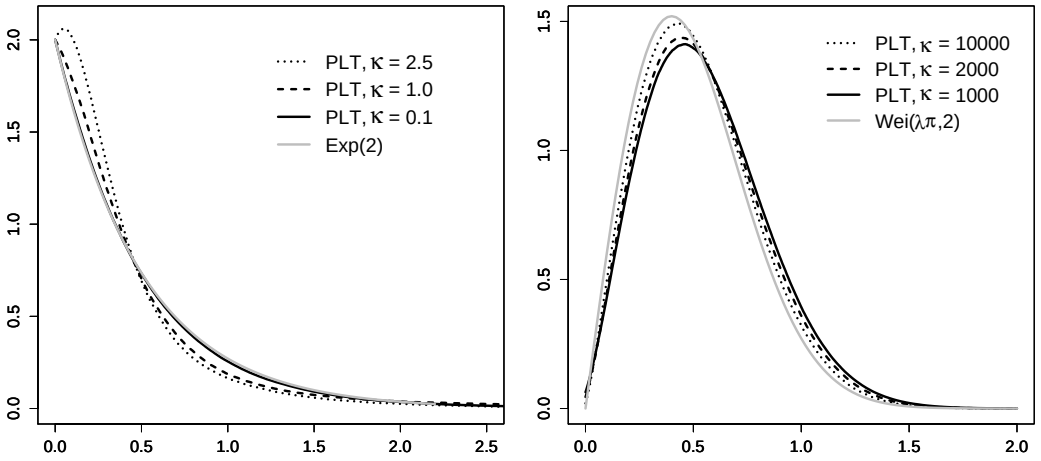

(a) $\kappa \to 0$ (where $\lambda_\ell = 1$) (b) $\kappa \to \infty$ (where $\gamma\lambda_\ell = 1$)

Figure 6.4: Density f_{C^*} for PLT together with corresponding limit distributions

6.7.1 Numerical results

For small and large κ we simulated the typical segment system S_H^* for PDT, PLT and PVT, respectively, and estimated the density of C^* with the estimator introduced in (5.20). In Figures 6.3–6.5 the estimated densities are shown shown for different values of κ together with the density of the exponential and Weibull distribution, respectively. The densities are already very close to an exponential distribution for $\kappa = 1$ and for $\kappa = 0.1$ one can hardly distinguish the density of C^* from the density of the exponential distribution for all considered models. In Figure 6.4(b) the estimated density for $\kappa = 1000, 2000, 10000$ and $\gamma\lambda_\ell = 1$ is displayed for PLT together with the density of the $Wei(\lambda\pi, 2)$-distribution. For $\kappa = 1000, 2000$ the densities still differ considerably from the density of the $Wei(\lambda\pi, 2)$-distribution, but for $\kappa = 10000$ the fit is already good. However, for PDT and PVT the convergence for $\kappa \to \infty$ seems to be faster. In Figures 6.3(b) and 6.5(b) estimated densities for large κ are shown for PDT and PVT, respectively, together with the densities of the $Wei(\lambda\pi, 2)$-distribution and $Wei(\lambda\pi/\xi^2, 2)$-distribution, where ξ was chosen by hand for both models. Already for $\kappa = 1000$ it seems like the density of C^* does not change considerably anymore for increasing κ. But note that a clear difference between the densities of C^* and the density of the $Wei(\lambda\pi, 2)$-distribution can be observed which is larger for PVT than for PDT. As can be seen in Figure 6.5 (b), the density of the $Wei(\lambda\pi/1.145^2, 2)$-distribution approximates the density of C^* very well for T being a PVT and $\kappa \geq 1000$. This suggests that in this case the constant ξ appearing in Theorem 6.2 and Corollary 6.8, respectively, is approximately 1.145. For PDT the density of the $Wei(\lambda\pi/1.065^2, 2)$-distribution is already very close to the density of C^* for $\kappa \geq 1000$, see Figure 6.5 (b). Thus, for PDT the constant ξ seems to be approximately 1.065.

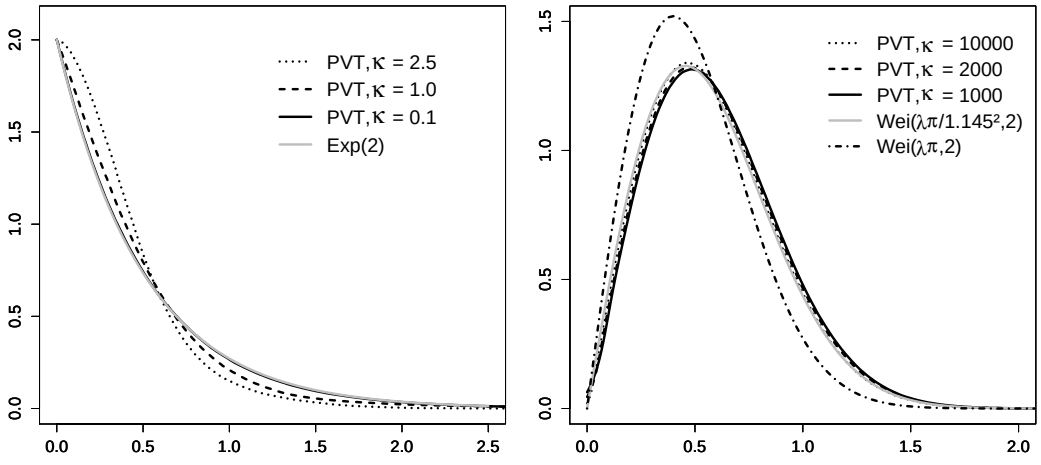

(a) $\kappa \to 0$ (where $\lambda_\ell = 1$) (b) $\kappa \to \infty$ (where $\gamma\lambda_\ell = 1$)

Figure 6.5: Density f_{C^*} for PVT together with corresponding limit distributions

6.7.2 Possible extensions

It is possible to generalize the setting of Theorem 6.2 in different ways. For instance, the statement of Theorem 6.2 is still valid if we consider instead of C^* the typical subscriber line length which is defined as the shortest path length from the origin to the nearest point H_0 of H, where we consider the sum of the Euclidean distance from the origin to the closest point of the edge set $T^{(1)}$ and the shortest path length on the edge set $T^{(1)}$ from the closest point to H_0, see also [24, 34]. Then the auxiliary results corresponding to Lemmas 6.3 and 6.4 can be proved basically by the same arguments and hence Theorem 6.2 is valid.

Moreover, it is not necessary to assume that the random segment system T is the edge set of a random tessellation in order to proof Theorem 6.2. But it is possible to regard an arbitrary stationary and isotropic segment process in $\mathbb{R}^2$ which is mixing and fulfills the additional condition that there is only one single cluster with probability 1. In particular, Theorem 6.2 can be extended to random geometric graphs.

Furthermore, we can relax the assumption that L_n is connected to its closest point of H, i.e., that the serving zones T_H are modeled by the Voronoi tessellation induced by H. For example, we can also connect L_n to its k-th nearest neighbor of H for any $k \geq 1$. This corresponds to the case that T_H is modeled by the k-th nearest neighbor Voronoi tessellation. Then Theorem 6.2 remains valid if we exchange the random variable Z by the random Euclidean distance from the origin to the k-th nearest point of a Poisson process which is known to be distributed according to a generalized Gamma distribution ([38, 105]). Further possible extensions include the cases that T_H is modeled by a certain Cox-Laguerre tessellation ([52]) or an aggregated Voronoi tessellation ([5, 91]). Again, Theorem 6.2 is still true, except that Z has to be replaced by another

random variable whose distribution can be calculated.

In the next chapter we use the limiting distributions derived in the present chapter in order to choose parametric densities which can be fitted to estimated density of C^* for a large range of κ. Parametric families which include both exponential distributions and Weibull distributions turn out to be good choices in order to obtain a good fit to the estimated densities for a large range of values of κ and all considered models, see Chapter 7.

Chapter 7

Empirical and parametric densities for shortest path length

This chapter is devoted to the application of the results which have been derive in Chapters 5 and 6. It is partly based on results in [36]. In particular, we derive parametric densities for the typical shortest path length C^*, where the parameters depend only on the underlying street model T and the scaling factor κ. The obtained parametric densities are compared to densities estimated from real connection lengths in the access network of Paris. This comparison reveals an excellent fit between connection lengths obtained from the SSLM and real data, respectively. Thus, if the optimal street model is known, realistic distributions for connection lengths, which only depend on κ, are directly available using the results of this chapter. Since κ can be estimated easily and efficient methods exist in order to obtain the optimal street model for given street data ([32, 85]), we thus demonstrate that the methodology developed in this thesis provides efficient tools in order to analyze existing telecommunication networks. In particular, we can avoid time–consuming network reconstructions and extensive Monte–Carlo simulation. Furthermore, for a given street model, we can investigate different network scenarios for future networks which are based on new technologies like optical fiber networks. Depending on κ, the distribution of connection lengths is directly available and hence various scenarios can be studied, whereas classical methods can only investigate few scenarios which may not be representative due to large computation times.

The present chapter is organized in the following way. We use the estimator

$$\widehat{f}_{C^*}(x;n) = \lambda_\ell \, \frac{1}{n} \sum_{j=1}^{n} \sum_{i=1}^{N_j} \mathbb{1}_{[c(A_i^{(j)}),c(B_i^{(j)}))}(x) \; . \tag{7.1}$$

which has been introduced in Section 5.5 in order to estimate the density of the typical shortest path length for different models. Below, the stationary random tessellation T is either a PDT, PLT or PVT. Furthermore, we focus on the case

that H is a Cox process on the random tessellation T or a thinning of the vertices $T^{(0)}$ of T. Then the simulation algorithms for S_H^* introduced in Chapter 4 can be used to generate samples of S_H^* in order to compute $\widehat{f}_{C^*}(x;n)$. To begin with, we analyze the distributions of C^* for the different considered models in Section 7.1. In particular, we compare first and second order moments of C^* for Cox processes and thinnings. Afterwards, in Section 7.2, we use the estimated densities in order to obtain parametric densities for the Cox process case, where the parameters depend only on the model type of T and the scaling factor κ.

The goal of the present chapter is to provide parametric densities which can be used to analyze real telecommunication networks. Thus, we have to check that the fitted parametric distributions are realistic distributions for connection distances. In a first step, we show that the fitted parametric densities are good approximations of the densities estimated by Monte–Carlo simulation. More precisely, we compare means and variance in Section 7.3. The comparison shows a quite good fit for a wide range of κ and all considered models. In the final Section 7.4, we compare the obtained parametric densities to densities estimated from real connection lengths of the access network in Paris which are stored in databases. Again, we observe a very good fit which demonstrates that our methods can be applied easily and efficiently in practice. Thus, the developed techniques provide efficient tools for the analysis and planning of telecommunication networks.

7.1 Distributional properties of C^* for Cox processes and thinnings

In order to estimate the density of shortest path lengths we simulated $n = 50\,000$ typical segment systems S_H^* within the typical Voronoi cell for different values of κ, where H is either a Cox process on T or a thinnings of $T^{(0)}$ and T is PDT, PLT and PVT, respectively. Thus, we assume that T_H is the Voronoi tessellation induced by H. Based on the generated samples, we estimated the density $\widehat{f}_{C^*}(x;n)$ as explained in Section 5.5.1. The estimated densities were then used to compute means and variances. Below, the numerical results are discussed in more detail.

7.1.1 Densities estimated from Monte–Carlo simulation

Some estimated densities are displayed in Figures 7.1 – 7.4 for Cox processes and thinnings. At first sight, a clear difference between the shapes of the densities for small and large κ as well as for the different considered model types can be observed.

For Cox processes H, the differences between the densities corresponding to the different tessellation types appear to decrease for $\kappa \to 0$ and $\kappa \to \infty$, respectively, although they are still noticeable, see Figure 7.1. On the one hand, recall

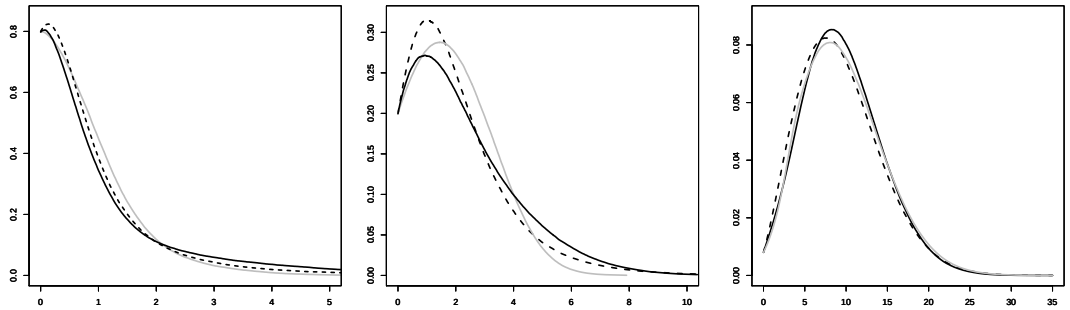

(a) $\kappa = 2.5$ (b) $\kappa = 10$ (c) $\kappa = 250$

Figure 7.1: Density for $\gamma = 1, \kappa = 10, 250, 750$ and Cox processes on PVT (gray), PDT (black), PLT (broken)

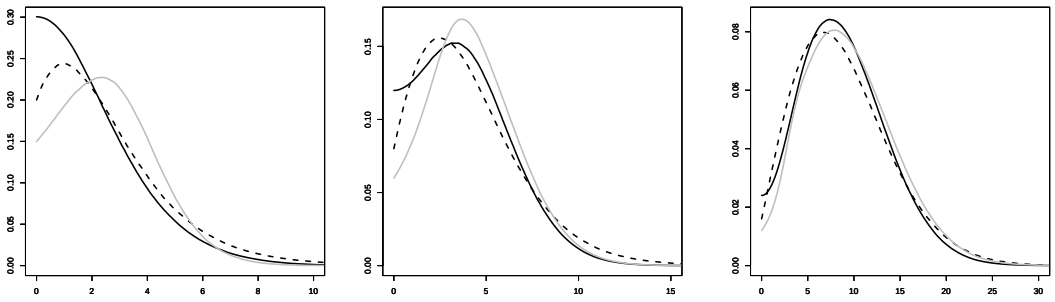

(a) $\kappa = 20$ (b) $\kappa = 50$ (c) $\kappa = 250$

Figure 7.2: Density for $\gamma = 1, \kappa = 20, 50, 250$ and thinned vertices of PVT (gray), PDT (black), PLT (broken)

that for Cox processes H the typical shortest path lengths C^* converges in distribution to ξZ for $\kappa \to \infty$ with $\lambda = \gamma\lambda_\ell$ fixed, where $Z \sim Wei(\lambda\pi, 2)$ and $\xi \geq 1$ is some constant which depends on the underlying tessellation T. For instance, $\xi = 1$ for PLT and $\xi > 1$ for PDT and PVT. Thus, there will always remain differences between the densities of C^* for PDT, PLT and PVT, respectively, if H is a Cox process and κ is increasing. On the other hand, for decreasing κ the differences between the densities vanish, see Figure 7.1 (a). This is the expected behavior since for PDT, PLT as well as PVT the distribution of C^* converges to an exponential distribution with the same parameter, see Theorem 6.1.

If H is a thinning of the vertices of T, then the behavior of the densities for increasing κ is quite similar as for Cox processes H, see Figure 7.2. We expect for thinnings H the same limit behavior for $\kappa \to \infty$ as for Cox processes, thus there will always remain a difference between the densities of C^* for PDT, PLT and PVT. In contrary to the Cox process case, the densities of C^* differ strongly from each other for small κ, see Figure 7.2. Note that the limit for $\kappa \to 0$ cannot be considered here since $\kappa > 1/\lambda^{(0)}$, where $\lambda^{(0)}$ is the intensity of the point process

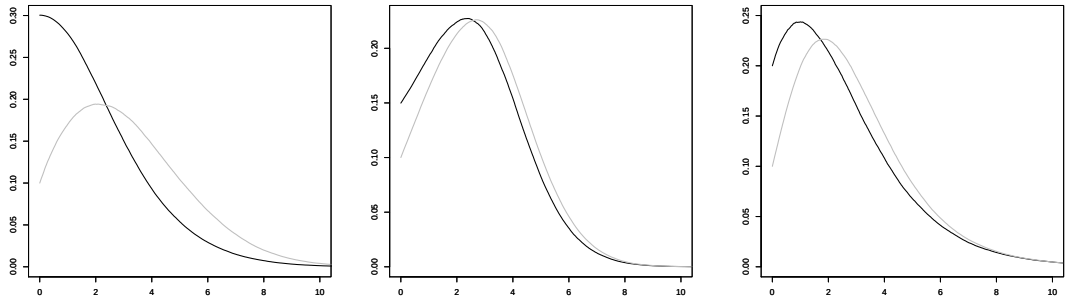

(a) PDT (b) PVT (c) PLT

Figure 7.3: Density for $\gamma = 1, \kappa = 20$ for thinned vertices (black) and Cox process (gray)

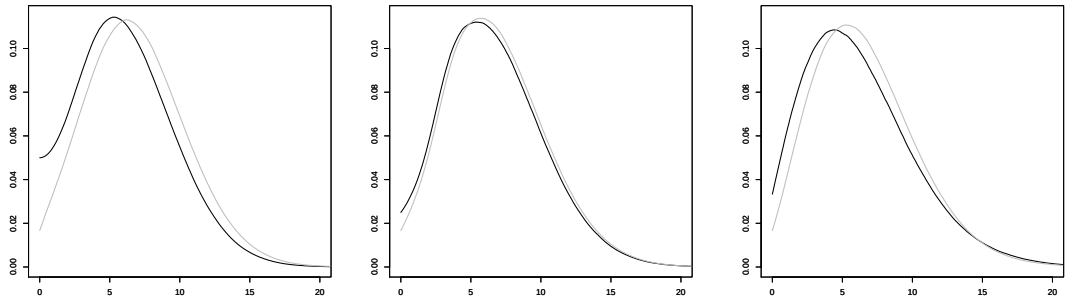

(a) PDT (b) PVT (c) PLT

Figure 7.4: Density for $\gamma = 1, \kappa = 120$ for thinned vertices (black) and Cox process (gray)

$T^{(0)}$ of vertices of T, see Section 3.5.3. Furthermore, $f_{C^*}(0) = \lambda_\ell \mathbb{E}\nu_0(E^*)$, where $\mathbb{E}\nu_0(E^*) = 3, 4$ and 6 if T is a PVT, PLT and PDT, respectively, see Lemma 5.8. Thus, there is a large difference between the densities corresponding to PVT, PLT and PDT near to 0 which is more pronounced for small κ.

In Figures 7.3 and 7.4 estimated densities are displayed for different values of κ and PDT, PLT and PVT, where H is a Cox process on T and a thinning of $T^{(0)}$, respectively. There is a large deviation between the densities corresponding to Cox processes and thinnings which decreases as κ increases. But, except for PVT, this deviation is still noticeable even for larger values of κ. The deviation is the largest for PDT, where e.g. at 0 the value of the density for thinnings is three times the value of the density for Cox processes. However, one may expect that the difference between the densities of C^* for thinnings and Cox processes on the same tessellation type T disappears as $\kappa \to \infty$.

7.1.2 Means and variances

Based on the estimated densities we calculated the expectations and the coefficients of variation (cv) for the typical shortest path length. In Figure 7.5(a) the means are shown for a Cox process H on T. First it is interesting that for small values of κ ($\kappa < 50$) the mean typical shortest path length $\mathbb{E}C^*$ is the smallest for PVT and the largest for PDT. However, for increasing κ things change. For instance, $\mathbb{E}C^*$ is smaller for PLT than for PVT if $\kappa = 50$, but $\mathbb{E}C^*$ is still the largest for PDT. Finally, if κ is large enough ($\kappa \geq 500$), $\mathbb{E}C^*$ is the smallest for PLT and the largest for PVT. This is the behavior which is intuitively expected since, compared to PDT and PLT, the edges of PVT are shorter and there are more nodes where the shortest path has to change its direction yielding longer shortest path along PVT than along PLT and PDT. Furthermore, for PLT the direct Euclidean distance is obtained in the limit for $\kappa \to \infty$, see Corollary 6.8. Thus, $\mathbb{E}C^*$ has to be the shortest for PLT if κ is large enough.

In Figure 7.5(b) the means of C^* are shown if H is a thinning of $T^{(0)}$. Here, $\mathbb{E}C^*$ is the smallest for PDT and the largest for PLT if κ is small ($\kappa < 20$). Then, for increasing κ, things change again and $\mathbb{E}C^*$ is the smallest for PDT and the largest PVT ($20 \leq \kappa \leq 250$). Finally, if $\kappa > 250$, $\mathbb{E}C^*$ is the smallest for PLT and the largest for PVT as it is the case for Cox processes with large κ. Compared to Cox processes, the means are smaller for thinnings. This difference is the largest for PDT which can be explained by the fact that there are in the mean 6 segments emanating from the typical point of H, whereas for Cox processes, there are only 2 segments emanating from the typical point of H. Hence, all LLC on these segments have the optimal Euclidean distance as their shortest path length which could be a reason that $\mathbb{E}C^*$ is smaller for thinnings. Although this difference is less for PVT and PLT, since only 3 and 4 segments are emanating from the typical point of H for thinnings, it is still observable.

The coefficients of variation are displayed in Figure 7.6(a) for Cox processes on PVT, PDT and PLT, respectively. Here we can see that for all three models cvC^* approaches cv$Z$=52.27 for large κ, were $Z \sim Wei(\lambda\pi, 2)$, as it is expected due to Theorem 6.2. On the other hand, the behavior for small κ is quite different for the three considered models. Recall that C^* converges to an $Exp(2\lambda_\ell)$-distribution for $\kappa \to 0$ if λ_ℓ is fixed, see Theorem 6.1 and Figure 7.1(a). Thus, one could expect that cvC^* converges to 100 for $\kappa \to 0$. However, this is only for PVT the case for the values of κ which are considered in our study. The reason might be that the convergence is much slower for PDT and PLT. For instance, if T is a PLT, then it is likely that even for small κ there is one line not containing the origin which intersects the typical serving zone, see also Figure 6.1. Then points on this additional intersecting line have very long shortest path lengths. With regard to equation (5.18) it is therefore likely that C^* has heavier tails for PLT than for PVT which yields a higher cv. However, note that the weak convergence of C^* to the $Exp(2\lambda_\ell)$–distribution does not necessarily imply that $\mathbb{E}C^*$ and cvC^*

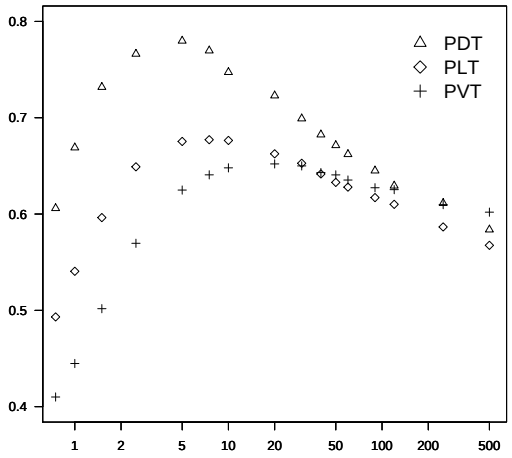

(a) Cox process with $\gamma\lambda_\ell = 1$

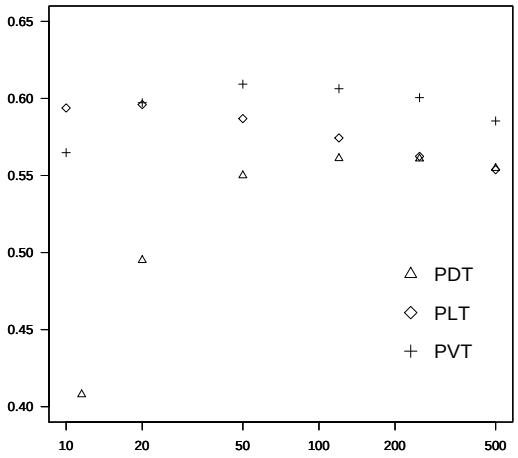

(b) Thinned vertices of T with intensity 1

Figure 7.5: $\mathbb{E}C^*$ for Voronoi tessellation T_H based on different models of H.

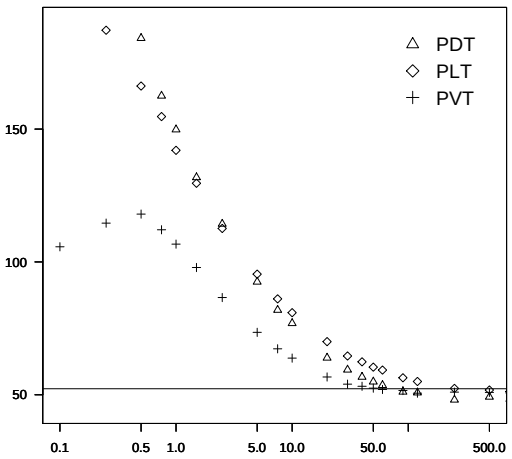

(a) Cox process H with $\gamma\lambda_\ell = 1$

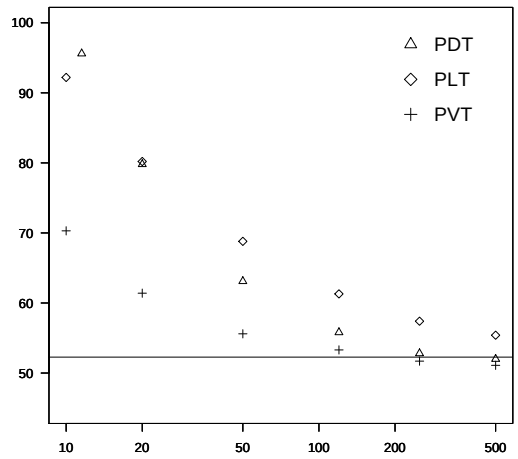

(b) Thinned vertices of T with intensity 1

Figure 7.6: cvC^* for Voronoi tessellation T_H and different models of H. The horizontal lines are at 52.27=cv$Z$, $Z \sim Wei(\lambda\pi, 2)$.

converge to $\mathbb{E}Z$ and cv$Z$ for $Z \sim Exp(2\lambda_\ell)$.

For the case that H is constructed by thinnings of $T^{(0)}$ the cv is shown in Figure 7.6(b). Here, the behavior is quite similar as for Cox processes. However, recall that the limit for $\kappa \to 0$ cannot be considered here since κ is bounded from below by $\kappa \geq 1/\lambda^{(0)}$. Compared to the results for Cox processes, the cv is larger for thinnings which may be caused by the fact that the densities for thinnings seem to have heavier tails, see e.g. Figures 7.3 and 7.4.

7.2 Parametric densities for the typical shortest path length

The goal of this section is to fit parametric densities to the empirical densities which were estimated based on Monte–Carlo simulation. Here, we focus on the case that the serving zones are modeled by Voronoi tessellations induced by Cox processes H on T, where T is a PDT, PLT and PVT, respectively. Our aim is to obtain a whole library of distributions for PDT, PLT and PVT as street models and $\kappa > 0$. Especially for large values of κ the estimation procedure for the densities f_{C^*} is time-consuming since we have to perform simulation experiments with long runtimes. Furthermore, means, variances and quantiles have to be calculated numerically. Thus, it would be of great benefit for applications if the densities were given as parametric functions, where the parameters only depend on κ and the type of the underlying street model T. Then, for real data, first an optimal tessellation model could be fitted to given data, see [32, 85] for details, and afterwards the appropriate density could be chosen from the library avoiding further simulations. Note that the fitting procedure for random tessellations introduced in [32, 85] is very fast and κ can be estimated easily. Thus, the distribution of shortest path lengths for given data would be directly available.

However, first it is important to choose an appropriate family of densities $\{f(x;\theta), \theta = (\theta_1, \ldots, \theta_k) \in \mathbb{R}^k\}$. Recall that the densities of C^* for different values of γ, but equal κ, are identical up to a scaling. Thus, we always regard $\gamma = 1$ in the following. From the results obtained so far we get that the family $\{f(x;\theta), \theta = (\theta_1, \ldots, \theta_k) \in \mathbb{R}^k\}$ should fulfill at least the following conditions:

1. $f(x;\theta)$ is a probability density, i.e., $\int_{\mathbb{R}} f(x;\theta)\, dx = 1$,
2. the number k of parameters $\theta_1, \ldots, \theta_k$ of $f(x;\theta)$ is small,
3. $f(0;\theta) = 2\lambda_\ell = \frac{2}{\kappa}$ due to Lemma 5.8,
4. the densities of $Wei(\alpha, 2), \alpha > 0$ and $Exp(\eta), \eta > 0$ are contained in the family $\{f(x;\theta), \theta \in \Theta\}$ as limiting cases due to Theorems 6.1 and 6.2, and
5. $f(x;\theta)$ fits well for PDT, PLT as well as PVT for a large range of κ, especially with regard to expectation and variance.

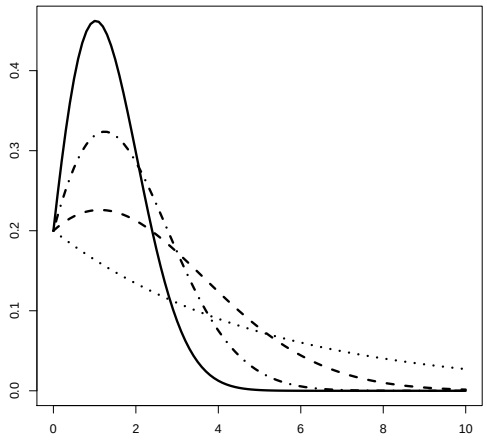

(a) Truncated Weibull distributions

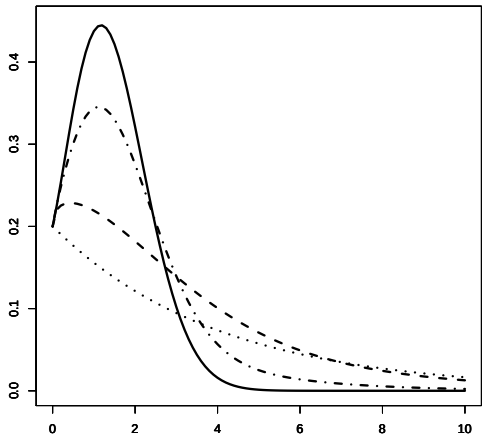

(b) Mixtures of exponential and Weibull distributions

Figure 7.7: Truncated Weibull and mixed exponential-and Weibull distributions for different parameters

It is not an easy task to choose a density which fulfills all conditions at once. Possible families are truncated Weibull distributions or a mixtures of exponential and Weibull distributions.

7.2.1 The truncated Weibull distribution

Note that the limit distributions $Wei(\lambda\pi/\xi^2, 2)$ and $Exp(2\lambda_\ell)$ in Theorems 6.1 and 6.2 are both specific cases of the $Wei(\alpha, \beta)$-distribution. However, condition 3 cannot be fulfilled in general by $Wei(\alpha, \beta)$-distributions, thus we shift their densities to the left and truncate them at 0 such that condition 3 is fulfilled. In this manner we obtain as one possible family of candidates the truncated Weibull distribution, where the density is given by

$$f(x;\alpha,\beta) = C\left(x + \left(\frac{2\lambda_\ell}{\alpha\beta}\right)^{\frac{1}{\beta-1}}\right)^{\beta-1} e^{-\alpha\left(x+\left(\frac{2\lambda_\ell}{\alpha\beta}\right)^{\frac{1}{\beta-1}}\right)^{\beta}} \tag{7.2}$$

for $x \geq 0$ and $C = \alpha\beta \exp((\alpha^{-1}(2\lambda_\ell/\beta)^\beta)^{1/(\beta-1)})$. Notice that this density has only two parameters, but it is flexible enough to approximate the shapes of f_{C^*} for different values of κ, see Figure 7.7(a) and the results shown in Section 7.3. Suppose that α and β are known for a specific value of κ and $\gamma = 1$ and assume that we want to choose parameters α' and β' for the same $\kappa = \gamma'/\lambda'_\ell$ but $\gamma' \neq 1$. Then we can use the scaling invariance of f_{C^*} in order to obtain the new

parameters, i.e.,

$$f(x;\alpha',\beta') = \frac{1}{\gamma'} f(x/\gamma';\alpha,\beta)$$
$$= C'\left(x+\left(\frac{2(\gamma')^\beta\lambda'_\ell}{\alpha\beta}\right)^{\frac{1}{\beta-1}}\right)^{\beta-1}\exp\left(-\frac{\alpha}{(\gamma')^\beta}\left(x+\left(\frac{2\lambda'_\ell(\gamma')^\beta}{\alpha\beta}\right)^{\frac{1}{\beta-1}}\right)^\beta\right), \quad (7.3)$$

where $C' = \alpha/(\gamma')^\beta\beta\exp(((2\lambda'_\ell/\beta)^\beta(\gamma')^\beta/\alpha)^{1/(\beta-1)})$. Since β is the shape parameter it is clear that it is constant. Furthermore, the scale parameter α' changes to $\alpha' = \alpha/(\gamma')^\beta$ and we have to correct the shift, i.e., λ_ℓ changes to $\lambda'_\ell = \lambda_\ell/\gamma'$. If $\beta = 2$, $\alpha' = \alpha/(\gamma')^2$ is constant and $\kappa \to \infty$ with $\lambda'_\ell \to 0$, then we obtain from (7.3) the density of the $Wei(\alpha', 2)$–distribution in the limit. On the other hand, if $\beta \searrow 1$ and $\gamma' \to 0$ such that $2\lambda'_\ell = \alpha/(\gamma')^\beta$ is constant, then we get from (7.3) the density of the $Exp(2\lambda_\ell)$–distribution in the limit. Thus, the family of truncated Weibull distributions considered here incorporates both limit distributions and fulfills conditions 1–4.

7.2.2 Mixtures of exponential and Weibull distributions

Another family of candidates which fulfill conditions 1–4 above are mixture $p\,f_1(x) + (1-p)f_2(x), p \in (0,1)$ of the densities f_1 of an $Exp(\eta)$–distribution and f_2 of a $Wei(\alpha,\beta)$–distribution with $\beta > 1$. Again, condition 3 should be fulfilled as well, thus we get

$$f(x;\alpha,\beta,\eta) = 2\lambda_\ell\, e^{-\eta x} + \left(1 - 2\frac{\lambda_\ell}{\eta}\right)\alpha\beta x^{\beta-1}e^{-\alpha x^\beta} \quad (7.4)$$

for $2\lambda_\ell \le \eta$. Note that this family has three parameters, thus one more than the family of truncated Weibull distributions. The densities of mixtures between exponential and Weibull distributions are also flexible and can imitate the behavior of the densities of C^* quite well, see Figure 7.7(b). Assume that α, β and η are known for some κ and $\gamma = 1$. Then we can choose the parameters α', β' and η' for the same κ but $\gamma' \neq 1$ using the scaling invariance of our model. We obtain the density corresponding to γ' and λ'_ℓ by

$$f(x;\alpha',\beta',\eta') = \frac{1}{\gamma'} f(x/\gamma';\alpha,\beta,\eta)$$
$$= 2\lambda'_\ell\, e^{-\eta/\gamma' x} + \left(1 - \frac{2\lambda'_\ell\gamma'}{\eta}\right)\frac{\alpha}{(\gamma')^\beta}\beta x^{\beta-1}e^{-\alpha/(\gamma')^\beta x^\beta}, \quad (7.5)$$

and hence the new parameters are given by $\alpha' = \alpha/(\gamma')^\beta, \beta' = \beta$ and $\eta' = \eta/\gamma'$. Note that we can put $\alpha' = 0$ and $\eta' = 2\lambda'_\ell$ in (7.5) in order to get the density of the exponential distribution with parameter $2\lambda'_\ell$. Moreover, we can put $\eta' = 0$ and $\beta' = 2$, then we get the density of the $Wei(\alpha, 2)$-distribution. Thus, both limiting distributions are included in this family of parametric densities and conditions 1–4 are satisfied.

	$\mathbb{E}C^*$			$\mathrm{Var}C^*$			$\mathrm{cv}C^*$		
κ	PVT	trunc.	mix	PVT	trunc.	mix	PVT	trunc.	mix
5	1.397	1.391	1.387	1.053	1.051	1.350	73.5	73.7	83.7
10	2.054	2.055	2.059	1.699	1.694	2.735	63.5	63.3	80.3
50	4.552	4.511	4.540	5.603	5.713	9.979	52.0	52.9	69.6
120	6.861	6.828	6.863	12.12	12.25	19.32	50.7	51.2	64.1
250	9.641	9.654	9.680	24.16	23.97	34.15	51.0	50.7	60.4
500	13.46	13.49	13.51	46.95	46.67	61.22	50.9	50.6	61.2
1000	18.89	18.86	18.87	91.32	91.59	111.8	50.7	50.7	56.0
1500	22.97	22.91	22.92	135.0	135.4	160.0	50.6	50.8	55.2
2000	26.34	26.34	26.36	180.7	180.0	208.0	51.0	50.9	54.7

Table 7.1: Mean, variance and cv of C^* for PVT together with these values for fitted truncated Weibull and mixed exponential-Weibull distribution

	$\mathbb{E}C^*$			$\mathrm{Var}C^*$			$\mathrm{cv}C^*$		
κ	PLT	trunc.	mix	PLT	trunc.	mix	PLT	trunc.	mix
5	1.510	1.450	1.511	2.073	1.846	3.330	95.4	93.8	120.8
10	2.181	2.111	2.175	3.354	2.710	5.081	83.9	78.0	103.6
50	4.505	4.469	4.450	7.344	7.125	10.16	60.2	59.7	70.8
120	6.664	6.646	6.682	13.46	13.33	18.83	55.1	54.9	64.9
250	9.275	9.252	9.265	23.66	23.71	30.70	52.4	52.6	59.8
500	12.69	12.71	12.72	43.11	42.71	53.51	51.8	51.4	57.5
1000	17.68	17.60	17.61	79.15	80.05	96.05	51.2	50.8	55.7
1500	21.22	21.28	21.29	118.1	116.8	136.2	51.2	50.8	54.8
2000	24.24	24.30	24.31	153.3	151.7	174.2	51.1	50.7	54.3

Table 7.2: Mean, variance and cv of C^* for PLT together with these values for fitted truncated Weibull and mixed exponential-Weibull distribution

	$\mathbb{E}C^*$			$\mathrm{Var}C^*$			$\mathrm{cv}C^*$		
κ	PDT	trunc.	mix	PDT	trunc.	mix	PDT	trunc.	mix
5	1.744	1.723	1.712	2.604	2.504	1.898	92.5	91.8	80.5
10	2.367	2.378	2.373	3.288	3.279	3.413	76.6	76.1	77.9
50	4.780	4.757	4.768	6.691	6.756	10.84	54.1	54.6	69.0
120	6.966	6.927	6.949	12.03	12.21	19.96	49.8	50.4	64.3
250	9.665	9.565	9.589	21.60	22.23	33.41	48.1	49.3	60.3
500	13.05	13.06	13.08	41.31	41.15	56.91	49.3	49.1	57.7
1000	17.89	17.95	17.97	79.81	78.68	99.55	49.9	49.4	55.5
1500	21.79	21.75	21.77	116.5	116.5	141.3	49.5	49.6	54.6
2000	24.72	24.64	24.85	155.3	157.0	180.4	50.4	50.8	54.0

Table 7.3: Mean, variance and cv of C^* for PDT together with these values for fitted truncated Weibull and mixed exponential-Weibull distribution

7.3 Fitting of parametric densities

Matlab was used in order to perform a weighted least squares fit, where the parametric families introduced above were fitted to data $(\widehat{f}_{C^*}(x_1), \ldots, \widehat{f}_{C^*}(x_n))$ which was obtained for a vector $(x_1, \ldots, x_n)$ with n equidistant components from the densities estimated by Monte–Carlo simulation. As weights we chose the reciprocals $1/\widehat{f}_{C^*}(x_1), \ldots, 1/\widehat{f}_{C^*}(x_n)$ in order to obtain a better fit at the tails of the densities. Note that then the optical fit of the obtained parametric densities is worse than without weighting. However, means and variances fit much better.

Both regarded types of parametric densities fit optically quite well for all considered models and a wide range of κ, see Figures 7.8 and 7.9, where some estimated densities are shown together with the fitted ones. If we compare expectations and variances of the fitted truncated Weibull distributions and the empirical distributions obtained from Monte–Carlo simulation, we see that they match almost perfectly for all models and a wide range of κ, see Tables 7.1–7.3. Moreover, the expectations fit quite well for the mixture of the exponential and Weibull distributions. However, the variances differ clearly from the variances which were obtained from the empirical densities. The reason seems be that the exponential term in the mixture dominates the tail behavior of these distributions which yields a too large variance. Thus, the truncated Weibull distribution was chosen to built the library of densities.

We calculated the parameters α and β of the truncated Weibull distribution for all three considered models and a wide range of κ. Moreover, functions $\alpha(\kappa, T), \beta(\kappa, T)$ depending on κ and the random tessellation T were fitted to the estimated parameters for $\gamma = 1$. Thus, for all three model types, the distribution of C^* is now immediately available up to a scaling via

$$f(x; \kappa, T) = f(x; \alpha(\kappa, T), \beta(\kappa, T)) \,. \tag{7.6}$$

Recall that for $W_m = [-m, m]^2$ and measurable $h : [0, \infty) \to [0, \infty)$ it holds that

$$\mathbb{E}h(C^*) = \lim_{m \to \infty} \frac{1}{\#\{n : L_n \in W_m\}} \sum_{L_n \in W_m} h(C_n) \tag{7.7}$$

with probability 1, where $\{L_n, C_n\}$ is the point process of LLC marked with the corresponding shortest path connection distances. Thus, using stochastic geometry and Monte-Carlo simulation, we are able to provide analytical formulae for distance distributions which are formally equivalent to empirical distributions obtained from spatial averages of huge networks. However, we do not have to handle huge data sets in our approach, but we only have to know the optimal tessellation model of the underlying street system of the network. This simplicity is a great advantage of the approach used here. In the following section, we compare the obtained parametric distributions to distance distributions computed from real network data in order to show that they are realistic distributions for connection distances.

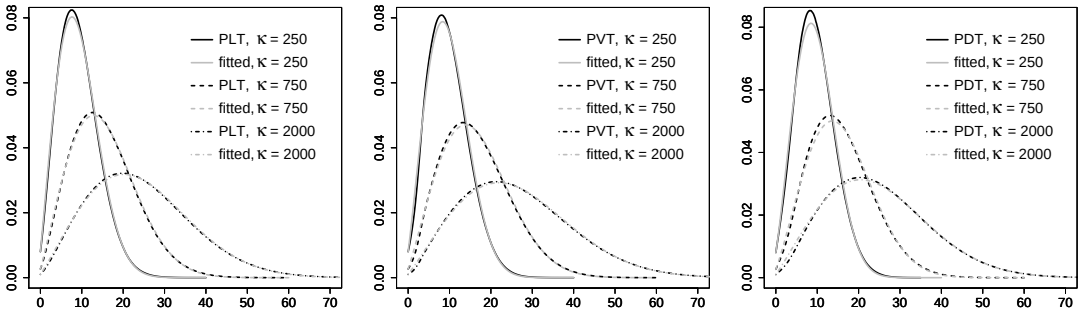

(a) PLT (b) PVT (c) PDT

Figure 7.8: Density for $\gamma = 1, \kappa = 250, 750, 2000$ and: (a) PLT, (b) PVT, (c) PDT with fitted truncated Weibull distributions

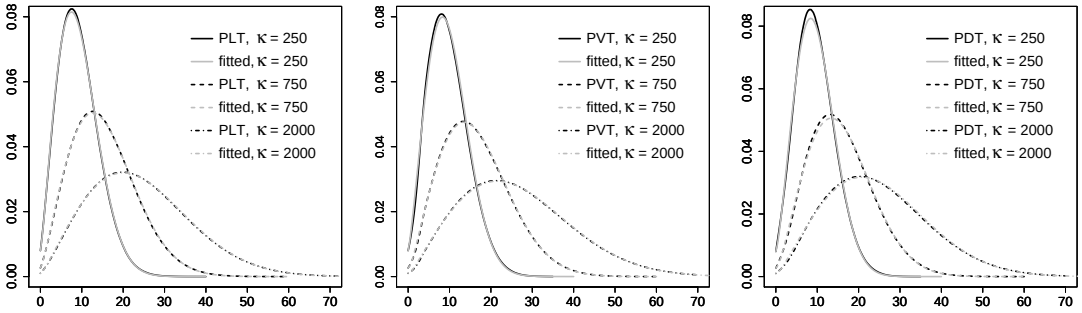

(a) PLT (b) PVT (c) PDT

Figure 7.9: Estimated densities for $\gamma = 1, \kappa = 250, 750, 2000$ and: (a) PLT, (b) PVT, (c) PDT with fitted mixtures of exponential and Weibull distributions

7.4 Application to real network data

It was shown in [35] that real street systems can be substituted by the optimal tessellation models as support for network nodes. In particular, histograms of shortest path connection distances have been compared for two distinct scenarios. For real serving zones, network nodes were randomly located on the real street system and on realizations of the best fitted model. The results showed that the histograms of the connection lengths for both settings are quite similar. Thus, it was shown that street systems can be represented by random tessellations in order to analyze connection lengths. Now we go one step further and compare the parametric distributions of the optimal model which were computed in the preceding section to real distance distributions obtained from databases. In particular, we show that real distance distributions of the access network in Paris can be approximated quite well by the parametric densities corresponding to the optimal street model and the appropriate value of κ which have been determined above.

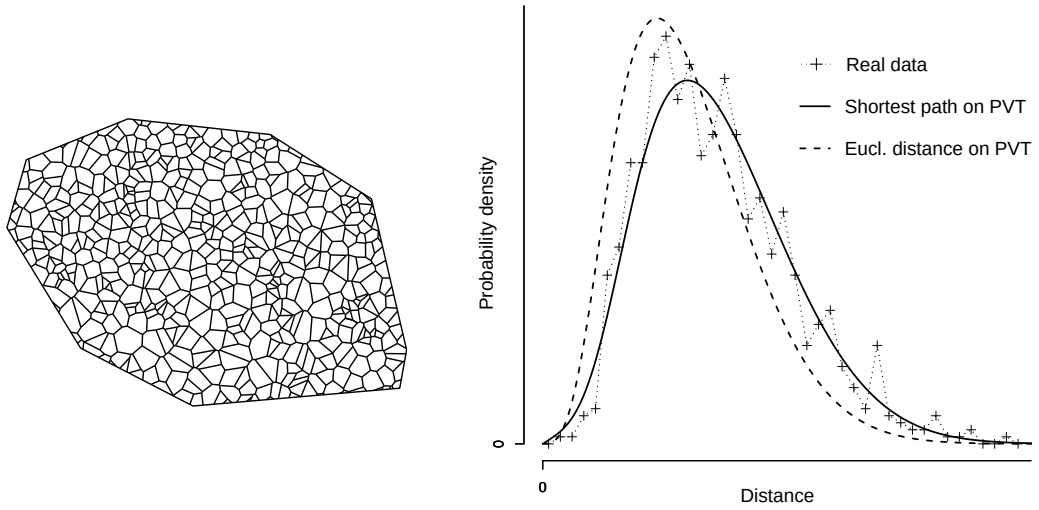

(a) Typical serving zone for $\kappa \simeq 1000$ (b) Densities of connection lengths

Figure 7.10: Typical serving zone of the larger scale subnetwork (a) with parametric density of C^* for the optimal street model compared to density of connection lengths estimated from real data (b), showing that the assumption of direct physical connections is incorrect.

We omit some technical details here, but note that real telecommunication networks have more than two hierarchy levels. However, real hierarchical networks can be subdivided into distinct subnetworks with two hierarchy levels. In particular, the access network in Paris was decomposed into three different subnetworks with two hierarchy levels, i.e., into a low–scale, middle–scale and large–scale subnetwork, where a HLC of the subnetwork at the lower scales can be a LLC of the subnetworks at the larger scales. Then histograms of connection distances were computed for these three subnetworks based on real connection lengths stored in databases.

The optimal tessellation model for the street system in Paris was determined to be a PVT using the fitting techniques in [32]. In the next step, the scaling factor κ was calculated for all three subnetworks as approximately $4, 35$ and 1000, respectively, based on the number of HLC at the respective scale. Finally, the appropriately rescaled parameters corresponding to κ and PVT as street model, which were determined in Section 7.2, were chosen for the truncated Weibull distribution. The resulting densities for the different subnetworks are displayed in Figures 7.10–7.12 together with the densities estimated from real connection lengths. In particular, at the large scale ($\kappa = 1000$) the fit is extremely good. Note that the parametric density is not fitted directly to the connection lengths from the database, but is obtained from the optimal street model and the number of HLC in the network. Thus, only the street system and the number of HLC are used in order to obtain the parametric density. Nevertheless, the fit between the

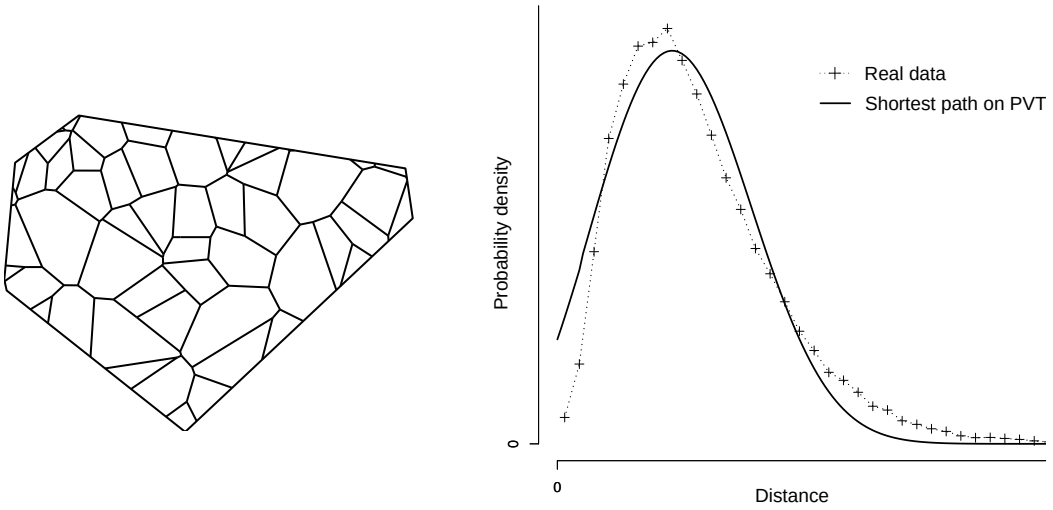

(a) Typical serving zone for $\kappa \simeq 35$ (b) Densities of connection lengths

Figure 7.11: Typical serving zone of the middle-scale subnetwork (a) and (rescaled) parametric density of C^* for optimal street model density compared to density of connection lengths estimated from real data (b).

densities estimated from the SSLM and the real connection lengths is excellent.

At the smaller scales, the parametric densities also approximate the real densities quite well. However, for $\kappa \approx 4$ and $\kappa \approx 35$ the densities were corrected in two different ways. If $\kappa \approx 4$, then only few streets cross each serving zone, see Figure 7.12(a). At this scale, the cable lengths e.g. from the street to the customers located in buildings along the street becomes therefore significant. Thus, the density was corrected by a shift for $\kappa \approx 4$, i.e., $f(x;\kappa,T) \to f(x-l;\kappa,T)$ for some $l > 0$. Similarly, for $\kappa \approx 35$, the density was corrected by a scaling in order to correct for curvatures of the cables in the network, i.e., $f(x;\kappa,T) \to f(x/c;\kappa,T)/c$ for some $c > 0$.

Note that Figure 7.10 shows that it is important to take the underlying street system into account. There, the distribution of the direct (Euclidean) connection lengths (dashed graph) is included in the plot. One can see that it does not fit to the histogram estimated from real data. In particular, it clearly underestimates the real connection lengths. This is the reason why classical studies usually introduce a correction factor for the direct connection lengths. But with the approach developed here, this correction factor can be directly related to the structure of the underlying street system.

Thus, we have shown that the SSLM is a realistic model in order to analyze connection lengths of telecommunication networks. Since an optimal street model can be determined easily for given street data, the methods developed in Chapters 4 – 7 can be used to efficiently analyze and plan telecommunication networks. In particular, time–consuming network reconstructions and simulations

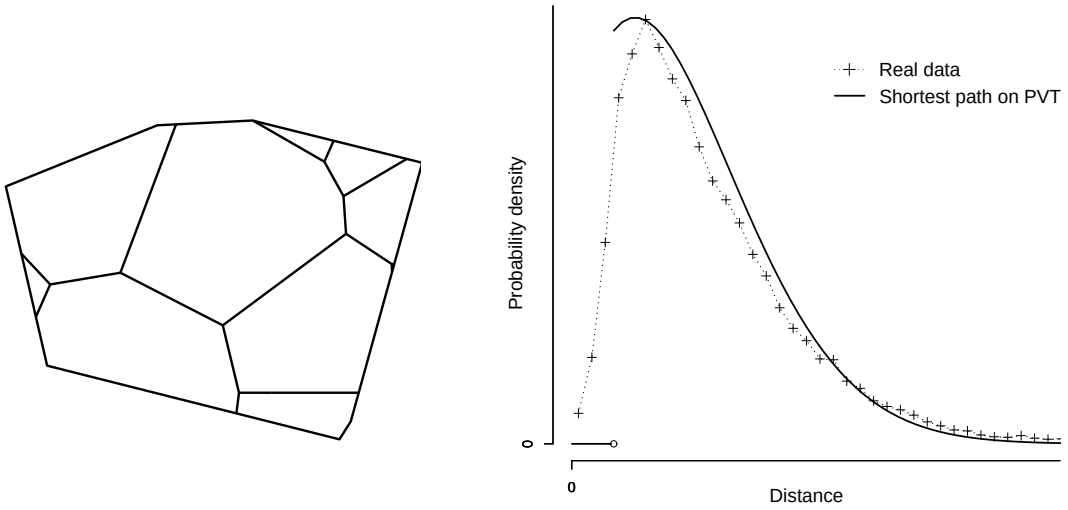

(a) Typical serving zone for $\kappa \simeq 4$ (b) Densities of connection lengths

Figure 7.12: Typical serving zone of the lower-scale subnetwork (a) and (shifted) parametric density of C^* for optimal street model compared to density of connection lengths estimated from real data (b).

can be avoided. Furthermore, for a given street model, various scenarios can be investigated since the parameters of the distance distributions are known and only depend on the scaling factor κ. This enables us to analyze possible settings for future networks based on new technologies like optical fiber networks, see also [36]. Using classical methods like network reconstructions, this is impossible since, due to large computation times, only few scenarios can be explored.

Chapter 8

Capacity distributions

In this chapter we investigate required capacities in hierarchical telecommunication networks at given locations on the cable system. Throughout this chapter we assume that all LLC are connected to their associated HLC on the shortest path along the cable system. We then define the required capacity at a given point x on the cable system as the sum of the capacities which are requested by all LLC whose shortest path connections cross x. This is an important performance characteristic of telecommunication networks. After the initial construction of the network all cables are already installed and, if the demand is higher than the capacity at a given location, the demand of some LLC cannot be served. So for strategic planning of telecommunication networks the capacity needed a certain locations is an important quantity.

This chapter is organized as follows. First, in Section 8.1, we extend the model considered in the previous chapters in order to introduce the notion of capacity in the SSLM. More precisely, we consider a random tessellation which models the street system and place LLC and HLC as point processes on the edges of the random tessellation. Each LLC is then connected to its associated HLC on the shortest path. Furthermore, we consider a third point process on the edges of the underlying tessellation that models the locations at which we are interested in the required capacity. In particular, we investigate the typical capacity, i.e., the capacity required at the typical point of this additional point process. It is shown that the distribution of the typical capacity is uniquely determined by the so–called typical subtree length which is defined in Section 8.1.

Subsequently, in Sections 8.2 and 8.3, we consider then specific cases of the model and show how the distribution of the typical subtree length can be estimated based on samples of the typical serving zone. In particular, we introduce estimators for the distribution of the typical subtree length for locations with a fixed shortest path length to the associated HLC and for locations formed by Cox processes on the underlying random tessellation. Furthermore, some statistical properties of these estimators are investigated. Finally, in Section 8.4, some numerical results obtained from Monte Carlo simulations are discussed.

The content of the present chapter is partly based on results obtained in [98].

8.1 Modeling of capacities

The topic of this chapter is the modeling and analysis of capacities which are required at various locations in telecommunication networks. These capacities are important performance characteristics which have to be investigated before the networks are built physically since it has to be guaranteed that the capacity provided at a given location is higher than the demand requested at this location. Otherwise, some LLC cannot be served. Thus, e.g. for strategic planning of telecommunication networks, the analysis of required capacities at given locations of the network is an important task.

We consider the SSLM as introduced in Chapter 5, i.e., T is a stationary random tessellation with length intensity γ, H is a stationary point process whose points are concentrated on $T^{(1)}$ almost surely and L is a Cox process on $T^{(1)}$ with linear intensity λ'_ℓ conditionally independent of H given T. Furthermore, we consider a random tessellation $T_H = \{(H_n, \Xi^o_{H,n})\}$ and a marked point process $H_S = \{(H_n, S^o_{H,n})\}$ representing the serving zones and the segment system inside the serving zones, respectively. A point L_n of L is then connected on the shortest path along $T^{(1)}$ to H_j if and only if $L_n \in S^o_{H,j} + H_j$. Recall that C^* denotes the shortest path length from the typical point of L to its associated point of H and that the density f_{C^*} of C^* does not depend on λ'_ℓ, see Theorem 5.7.

The capacity that is required at a given point x on the edge set $T^{(1)}$ is defined as the sum of all demands requested by those LLC which are located in the same serving zone as x and whose shortest paths cross x. More formally, we consider a sequence of independent and identically distributed random variables $K_1, K_2, \ldots$ which represent the demands of the LLC at the locations $L_1, L_2, \ldots$, respectively. Let $X = \{X_n\}$ be another stationary point process of random locations X_n on the edge set $T^{(1)}$ conditionally independent of L given $T^{(1)}$. The points of X are used in order to model the locations where we would like to analyze the required capacities. In the following, the (planar) intensity of the stationary point process $\{X_n\}$ is denoted by λ. Then, for each $n \geq 1$, we define the capacity $K(X_n)$ that is required at X_n as follows. If $X_n \in S_{H,j} = S^o_{H,j} + H_j$ for some $j \geq 1$, then we define

$$K(X_n) = \sum_{i=1}^{\infty} \mathbb{1}_{T_{sub}(X_n)}(L_i)\, K_i\,, \tag{8.1}$$

where we denote with $T_{sub}(X_n) = \{y \in S_{H,j} : X_n \in p(y, H_j)\}$ the subset of those points y on $S_{H,j}$ whose shortest path $p(y, H_j)$ from the location y to the associated HLC H_j along $T^{(1)}$ crosses X_n, see also Figure 8.1. Note that we then call $T_{sub}(X_n)$ the subtree rooted at X_n. Since $\{X_n\}$ is conditionally independent of L given the edge set $T^{(1)}$, formula (8.1) yields that $K(X_n) \stackrel{\mathrm{d}}{=} \sum_{i=1}^{J_n} K_i$, where

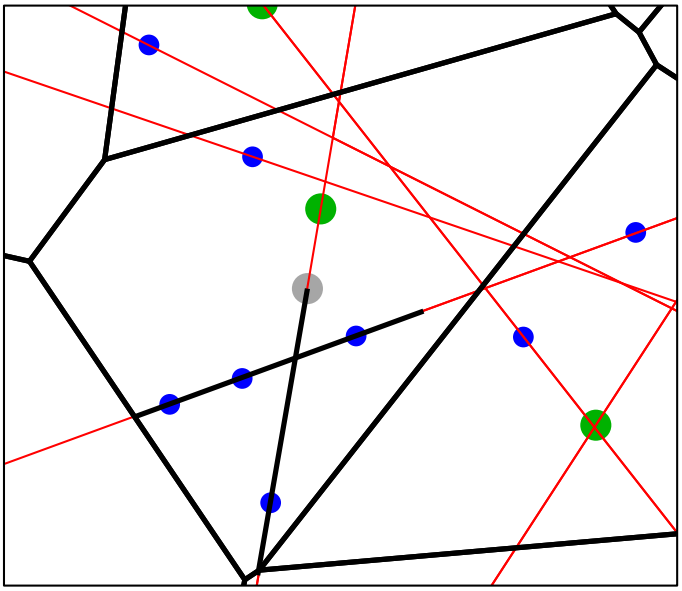

Figure 8.1: $T_{sub}(x)$ (black) at given location x (gray) with LLC (blue) on subtree.

$J_n \sim Poi(\lambda'_\ell \nu_1(T_{sub}(X_n)))$ given $\nu_1(T_{sub}(X_n))$. Hence, the distribution of $K(X_n)$ is fully specified by the distribution of K_1, λ'_ℓ and the subtree length $\nu_1(T_{sub}(X_n))$. Furthermore, it can be shown that a similar representation formula is valid for the *typical capacity* K^* (at the typical point of $\{X_n\}$), where we assume that the nonnegative random variable K^* is the typical mark of the stationary marked point process $\{(X_n, K(X_n))\}$, i.e., it is distributed according to the Palm mark distribution of $\{(X_n, K(X_n))\}$.

Theorem 8.1 *With the assumptions above, it holds that*

$$K^* = \sum_{i=1}^{J^*} K_i \,, \tag{8.2}$$

where $J^* \sim Poi(\lambda'_\ell \nu_1(T^*_{sub}))$ given $\nu_1(T^*_{sub})$ and the random variable $\nu_1(T^*_{sub})$ is distributed according to the Palm mark distribution of $X_{sub} = \{(X_n, \nu_1(T_{sub}(X_n)))\}$.

Proof Using equation (8.1) and the definition of the Palm mark distribution of $\{(X_n, K(X_n))\}$, we get that for each $h : \mathbb{R} \to [0, \infty)$

$$\begin{aligned} \mathbb{E}h(K^*) &= \frac{1}{\lambda}\, \mathbb{E}\Big(\sum_{X_i \in [0,1]^2} h\Big(\sum_{L_j \in T_{sub}(X_i)} K_j \Big)\Big) \\ &= \frac{1}{\lambda}\, \mathbb{E}\Big[\mathbb{E}\Big(\sum_{X_i \in [0,1]^2} h\Big(\sum_{L_j \in T_{sub}(X_i)} K_j \Big) \mid T^{(1)}, H \Big)\Big] \,, \end{aligned}$$

where

$$\begin{aligned}
&\mathbb{E}\Big(\sum_{i=1}^{\infty} h\Big(\sum_{j=1}^{J_i} K_j\Big) \mid T^{(1)}, H\Big) \\
&= \mathbb{E}\Big[\mathbb{E}\Big(\sum_{i=1}^{\infty} h\Big(\sum_{j=1}^{J_i} K_j\Big) \mid X\Big) \mid T^{(1)}, H\Big] \\
&= \mathbb{E}\Big[\sum_{i=1}^{\infty} \mathbb{E}\Big(h\Big(\sum_{j=1}^{J_i} K_j\Big) \mid X\Big) \mid T^{(1)}, H\Big] .
\end{aligned}$$

Furthermore, we have

$$\mathbb{E}\Big(h\Big(\sum_{j=1}^{K_i} K_j\Big) \mid X\Big) = \mathbb{E}\Big(h\Big(\sum_{j=1}^{K_i} K_j\Big) \mid \nu_1(T_{sub}(X_i)\Big)$$

with $J_i \sim Poi(\lambda'_\ell \nu_1(T_{sub}(X_i)))$ given $\nu_1(T_{sub}(X_i))$. Hence, the statement of the theorem is a consequence of the definition of the typical mark of the stationary marked point process $X_{sub} = \{(X_n, \nu_1(T_{sub}(X_n)))\}$. □

If λ'_ℓ and the distribution of K_1 are known, then, due to formula (8.2), it is sufficient to investigate only the distribution of the *typical subtree length* $\nu_1(T^*_{sub})$. Similar as for the typical Euclidean distance and the typical shortest path length it is possible to express the distribution of $\nu_1(T^*_{sub})$ as the expectation of some functional of the typical segment system S^*_H. The proof is again based on Neveu's exchange formula. Let λ_H denote the (planar) intensity of H and let $\widetilde{X}_{sub}$ be the Palm version of X_{sub} which is obtained under the Palm distribution with respect to $\{(H_n, S^o_{H,n})\}$, see Section 2.3.4 for details. Then, the following statement is true.

Theorem 8.2 *For any measurable* $h : [0, \infty) \to [0, \infty)$*,*

$$\mathbb{E}\, h(\nu_1(T^*_{sub})) = \frac{\lambda_H}{\lambda}\, \mathbb{E} \int_{S^*_H \times [0,\infty)} h(y)\, \widetilde{X}_{sub}(d(x, y)) . \tag{8.3}$$

Proof We consider the two jointly stationary marked point processes $H_S = \{(H_n, S^o_{H,n})\}$ and X_{sub}. Then we can regard (X_{sub}, H_S) as a random element of the space $\mathsf{N}_{[0,\infty),\mathcal{L}^o}$ of locally finite point sets with marks either in $[0, \infty)$ or in $\mathcal{L}^o$. Using the function $f : \mathbb{R}^2 \times [0, \infty) \times \mathcal{L}^o \times \mathsf{N}_{[0,\infty),\mathcal{L}^o} \to [0, \infty)$ defined by

$$f(x, y, \zeta, \psi) = \begin{cases} h(y) & \text{if } x \in \zeta\,, \\ 0 & \text{otherwise}\,, \end{cases} \tag{8.4}$$

we can apply Neveu's exchange formula for stationary marked point processes, see Theorem 2.9, which yields equation (8.3). □

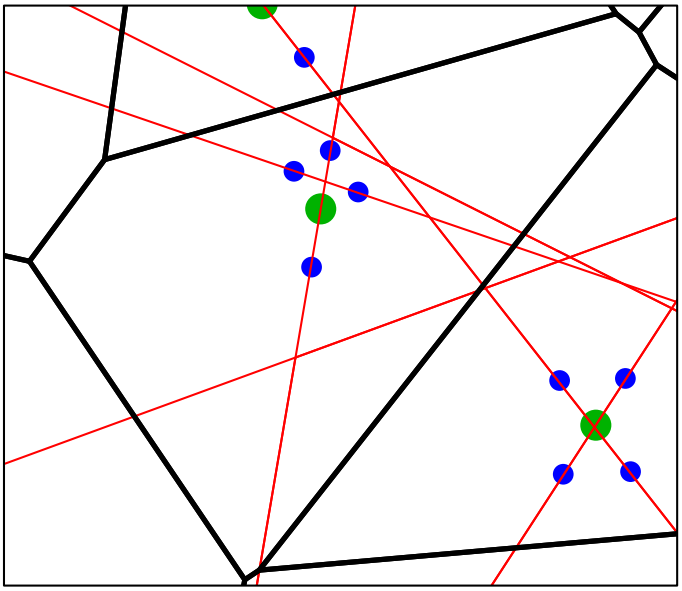

Figure 8.2: Points with fixed shortest path length to their associated HLC

In the rest of this chapter we concentrate on two special cases for the point process $\{X_n\}$ of locations at which we are interested in the required capacities. On the one hand, we consider the point process of locations on $T^{(1)}$ with a fixed shortest path length to the corresponding HLC and, on the other hand, we consider another Cox process on $T^{(1)}$. In both cases, we can construct estimators for the distribution function and density, respectively, see Sections 8.2 and 8.3.

8.2 Capacities at locations with fixed distance to HLC

8.2.1 Representation formula

Let $s > 0$ be fixed and let $X = \{X_n\}$ denote the point process which consists of all points of the locally finite set $\{x \in T^{(1)} : c(x) = s\}$, where we denote with $c(x)$ the shortest path length from x to H_n provided that $x \in S_{H,n}$. Thus, X is the point process of those points on the edge set $T^{(1)}$, whose shortest path lengths to their associated HLC is equal to s. This point process can be regarded as a cluster process, where the parents are the points of H and for each parent H_n the children are the points on $S_{H,n}$ with shortest path length s to H_n, see Figure 8.2. We can then specify the statement of Theorem 8.2 as follows.

Theorem 8.3 *For any measurable $h : [0,\infty) \to [0,\infty)$,*

$$\mathbb{E}h(\nu_1(T^*_{sub})) = \frac{\lambda_\ell}{f_{C^*}(s)}\,\mathbb{E}\sum_{i=1}^{\widetilde{J}} h(\nu_1(T_{sub}(\widetilde{X}_i)))\,, \tag{8.5}$$

where $(\widetilde{X}_1, T_{sub}(\widetilde{X}_1)), \dots, (\widetilde{X}_{\widetilde{J}}, T_{sub}(\widetilde{X}_{\widetilde{J}}))$ denote the marked points of $\widetilde{X}_{sub}$ on S^*_H and $\widetilde{J}$ is the random number of these points. In particular, the distribution function $F : \mathbb{R} \to [0,1]$ of $\nu_1(T^*_{sub})$ is given by

$$F(x) = \frac{\lambda_\ell}{f_{C^*}(s)}\,\mathbb{E}\sum_{i=1}^{\widetilde{J}} \mathbb{1}_{[0,x]}(\nu_1(T_{sub}(\widetilde{X}_i)))\,, \quad x \geq 0\,, \tag{8.6}$$

where f_{C^*} denotes the density of the typical shortest path length.

Proof Using formula (8.3) it is sufficient to show that

$$\frac{\lambda_H}{\lambda} = \frac{\lambda_\ell}{f_{C^*}(s)}\,.$$

Recall that $\lambda_H = \gamma\lambda_\ell$ with $\mathbb{E}\nu_1(S^*_H) = 1/\lambda_\ell$, thus we only have to show that $\lambda = \gamma f_{C^*}(s)$. It holds that

$$\begin{aligned}
\lambda &= \mathbb{E}\#\{n : X_n \in [0,1)^2\} \\
&= \mathbb{E}\sum_{i=1}^{\infty} \#\{n : X_n \in S_{H,i} \cap [0,1)^2\} \\
&= \lambda_H \int_{\mathbb{R}^2} \mathbb{E}\#\{n : \widetilde{X}_n \in S^*_H \cap ([0,1)^2 - x)\}\,dx\,,
\end{aligned}$$

where the latter equality is a consequence of the refined Campbell theorem for stationary marked point processes, see Theorem 2.7. Recall that S^*_H can be divided into segments $S_1, \dots, S_N$ with endpoints A_i and B_i for $i = 1, \dots, N$ such that $c(B_i) = c(A_i) + \nu_1(S_i)$, see Section 5.4.2. This means that each point $\widetilde{X}_i, i = 1, \dots, \widetilde{J}$ is located almost surely in exactly one segment of S^*_H and each of the segments contains 0 or 1 points of $\widetilde{X}_{sub}$, thus $\widetilde{J} \leq N$. Therefore we can assume without loss of generality that $\widetilde{X}_i \in S_i$ for $i = 1, \dots, \widetilde{J}$ and that there is no point with shortest path length s on all segments S_i with $i = \widetilde{J}+1, \dots, N$. This yields

$$\begin{aligned}
\lambda &= \lambda_H \int_{\mathbb{R}^2} \mathbb{E}\#\{n : \widetilde{X}_n \in S^*_H \cap ([0,1)^2 - x)\}\,dx \\
&= \gamma\lambda_\ell \mathbb{E}\sum_{j=1}^{N} \mathbb{1}_{[c(A_j),c(B_j))}(s) \int_{\mathbb{R}^2} \mathbb{1}_{[0,1)^2 - \widetilde{X}_j}(x)\,dx \\
&= \gamma\lambda_\ell \mathbb{E}\sum_{j=1}^{\widetilde{J}} \mathbb{1}_{[c(A_j),c(B_j))}(s) = \gamma f_{C^*}(s)\,,
\end{aligned}$$

where the latter equality is a consequence from Theorem 5.7. Thus, the proof is completed. □

Note that $f_{C^*}(s)$ is not known analytically. However, $f_{C^*}(s)$ can be estimated unbiasedly and consistently as described in Section 5.5.

8.2.2 Estimation of the distribution function

As mentioned above, $f_{C^*}(s)$ is not known analytically, but it can be estimated consistently and without bias e.g. by the estimator $\widehat{f}_{C^*}(s;n)$ given in (5.20). Thus, Theorem 8.3 directly leads to the natural estimator for $F(x)$ given by

$$\widehat{F}(x;n) = \frac{\lambda_\ell}{\widehat{f}_{C^*}(s;n)} \frac{1}{n} \sum_{j=1}^{n} \sum_{i=1}^{\widetilde{J}^{(j)}} \mathbb{I}_{[0,x]}(\nu_1(T_{sub}^{(j)}(\widetilde{X}_i^{(j)}))) \,, \tag{8.7}$$

where $\widetilde{J}^{(j)}$ and $\nu_1(T_{sub}(\widetilde{X}_1^{(j)})), \ldots, \nu_1(T_{sub}(\widetilde{X}_{\widetilde{J}^{(j)}}^{(j)}))$, $j = 1, \ldots, n$ are independent copies of $\widetilde{J}$ and $\nu_1(T_{sub}(\widetilde{X}_1)), \ldots, \nu_1(T_{sub}(\widetilde{X}_{\widetilde{J}}))$, respectively. It is easy to see that the estimator $\widehat{F}(x;n)$ is ratio–unbiased, i.e., it is the quotient of two unbiased estimators, and it is in addition strongly consistent for $F(x)$. Moreover, it is possible to prove the following result of Gliwenko-Cantelli type.

Theorem 8.4 *It holds that*

$$\mathbb{P}\big(\lim_{n\to\infty} \sup_{x\in\mathbb{R}} |\widehat{F}(x;n) - F(x)| = 0 \big) = 1 \,. \tag{8.8}$$

Proof Let $\varepsilon > 0$, then there exist $q_0 = 0 < q_1 < \cdots < q_m < q_{m+1} = \infty$ with

$$|F(q_{i+1}) - F(q_i)| < \frac{\varepsilon}{3}$$

for all $i = 0, \ldots, m$, where $F(q_{m+1}) = \widehat{F}(q_{m+1};n,\omega) = 1$. Now let $x \in [0,\infty)$, then $x \in [q_i, q_{i+1})$ for some $i = 0, \ldots, m$. Using the monotonicity of F and $\widehat{F}(\,\cdot\,;n)$ we get

$$\begin{aligned} &|\widehat{F}(x;n,\omega\,) - F(x)| \\ &\qquad \leq \; |\widehat{F}(x;n,\omega) - \widehat{F}(q_i;n,\omega)| + |\widehat{F}(q_i;n,\omega) - F(q_i)| + |F(q_i) - F(x)| \\ &\qquad \leq \; |\widehat{F}(q_{i+1};n,\omega) - \widehat{F}(q_i;n,\omega)| + |\widehat{F}(q_i;n,\omega) - F(q_i)| + |F(q_{i+1}) - F(q_i)| \,. \end{aligned}$$

Note that the latter term is smaller than $\varepsilon/3$ and

$$|\widehat{F}(q_i;n,\omega) - F(q_i)| \to 0$$

almost surely for $n \to \infty$ due to the law of large numbers. Furthermore, we have

$$\begin{aligned} |\widehat{F}(q_{i+1};n,\omega) - \widehat{F}(q_i;n,\omega)| &= \frac{\lambda_\ell}{f_{C^*}(s)} \frac{1}{n} \sum_{j=1}^{n} \sum_{k=1}^{\widetilde{J}^{(j)}} \mathbb{1}_{(q_i,q_{i+1}]}(\nu_1(T_{sub}(\widetilde{X}_i^{(j)}))) \\ &\to F(q_{i+1}) - F(q_i) < \frac{\varepsilon}{3} \end{aligned}$$

for $n \to \infty$ almost surely. Thus, there exists $N(\varepsilon,\omega)$ with

$$|\widehat{F}(q_{i+1};n,\omega) - \widehat{F}(q_i;n,\omega)| + |\widehat{F}(q_i;n,\omega) - F(q_i)| + |F(q_{i+1}) - F(q_i)| \leq \varepsilon$$

almost surely for $n > N(\varepsilon,\omega)$ and $i = 0,\ldots,m$ which completes the proof. □

8.3 Capacities at points of Cox processes

8.3.1 Representation formula

In this section we assume that the point process $X = \{X_n\}$ is a Cox process on T with linear intensity $\lambda_\ell'' = \lambda/\gamma$ which is conditionally independent of H and L given $T^{(1)}$. Recall that we can divide S_H^* into the segments $S_i, i = 1,\ldots,N$ with endpoints A_i, B_i such that $c(A_i) < c(B_i) = c(A_i) + \nu_1(S_i)$. Using this notation, the following representation formula for the density $f : \mathbb{R} \to [0,\infty)$ of the typical subtree length $\nu_1(T_{sub}^*)$ can be derived, which is similar to the representation formula for the density f_{C^*} of C^* stated in Theorem 5.7.

Theorem 8.5 *It holds that*

$$f(x) = \begin{cases} \lambda_\ell \, \mathbb{E}\left[\sum_{i=1}^{N} \mathbb{1}_{[l(B_i),l(A_i))}(x)\right] & \text{if } x \geq 0\,, \\ 0 & \text{otherwise,} \end{cases}$$

where $l(B_i)$ denotes the subtree length at B_i and $l(A_i) = \nu_1(S_i) + l(B_i)$.

Notice that Theorem 8.5 can be derived directly using Theorem 8.2 and the assumption that $\{X_n\}$ is a Cox process on T. Then similar arguments as in the proof of Theorem 5.7 can be used in order to prove the assertion. However, there is an alternative proof which makes use of the following relationship between the distribution of the typical subtree length $\nu_1(T_{sub}^*)$ at the points of the Cox process $\{X_n\}$ and the typical subtree length at the locations of the point process $\{X_{s,n}\}$ with fixed shortest path length s considered Section 8.2.

Lemma 8.6 *Let $s \in [0,\infty)$, then it holds that*

$$\mathbb{P}(\nu_1(T_{sub}^*) \leq x \mid C_X^* = s) = F_s(x)\,, \tag{8.9}$$

where C_X^* denotes the shortest path length at the typical point of X and F_s denotes the distribution function introduced in equation (8.6) for fixed shortest path length s.

Proof Let $\widetilde{J}_s$ and $\widetilde{X}_{s,1}, \ldots, \widetilde{X}_{s,\widetilde{J}_s}$ denote the random variables which have been defined in Theorem 8.3 for fixed $s \in [0,\infty)$, i.e., $c(\widetilde{X}_{s,i}) = s$ for $i = 1, \ldots, \widetilde{J}_s$, where $\widetilde{J}_s$ is the random number of points on S_H^* with shortest path length s to the origin. Furthermore, let $(\widetilde{X}, H_S^*)$ with $\widetilde{X} = \{\widetilde{X}_n\}$ be distributed according to the Palm distribution $P_{H_S}^*$ with respect to H_S. Note that the density $f_{C^*}(s)$ does not depend on the linear intensity λ_ℓ' of the Cox process $\{L_n\}$ of LLC, see e.g. Theorem 5.7. Thus, the equality $f_{C^*}(s) = f_{C_X^*}(s)$ holds almost everywhere and we have

$$\begin{aligned}
\mathbb{P}(\nu_1(T_{sub}^*) \le x \mid C_X^* = s) &= \lim_{\varepsilon \searrow 0} \mathbb{P}(\nu_1(T_{sub}^*) \le x \mid C_X^* \in [s, s+\varepsilon)) \\
&= \lim_{\varepsilon \searrow 0} \mathbb{E}\Big(\mathbb{1}_{[0,x]}(\nu_1(T_{sub}^*)) \frac{\mathbb{1}_{[s,s+\varepsilon)}(C_X^*)}{\int_s^{s+\varepsilon} f_{C_X^*}(u)\,du} \Big) \\
&= \lim_{\varepsilon \searrow 0} \frac{\lambda_\ell}{\lambda_\ell''} \mathbb{E} \sum_{\widetilde{X}_n \in S_H^*} \mathbb{1}_{[0,x]}(\nu_1(T_{sub}(\widetilde{X}_n))) \frac{\mathbb{1}_{[s,s+\varepsilon)}(c(\widetilde{X}_n))}{\int_s^{s+\varepsilon} f_{C^*}(u)\,du} \\
&= \lambda_\ell \lim_{\varepsilon \searrow 0} \mathbb{E} \int_{S_H^*} \mathbb{1}_{[0,x]}(\nu_1(T_{sub}(y))) \frac{\mathbb{1}_{[s,s+\varepsilon)}(c(y))}{\int_s^{s+\varepsilon} f_{C^*}(u)\,du}\, \nu_1(dy)\,,
\end{aligned}$$

where the last but one equality can be proven by a slight modification of Theorem 8.2 and the last equality is a consequence of the fact that the points $\{\widetilde{X}_n\}$ form a Cox process on S_H^* whose linear intensity is given by λ_ℓ'', see also Chapter 5. We can decompose S_H^* into the segments $S_1, \ldots, S_N$ as above and then get

$$\mathbb{P}(\nu_1(T_{sub}^*) \le x \mid C_X^* = s) = \lambda_\ell \lim_{\varepsilon \searrow 0} \mathbb{E} \sum_{i=1}^{N} \int_{S_i} \mathbb{1}_{[0,x]}(\nu_1(T_{sub}(y))) \frac{\mathbb{1}_{[s,s+\varepsilon)}(c(y))}{\int_s^{s+\varepsilon} f_{C^*}(u)\,du}\, \nu_1(dy).$$

Moreover, f_{C^*} is right-continuous, thus we get almost surely

$$\begin{aligned}
&\lim_{\varepsilon \searrow 0} \sum_{i=1}^{N} \int_{S_i} \mathbb{1}_{[0,x]}(\nu_1(T_{sub}(y))) \frac{\mathbb{1}_{[s,s+\varepsilon)}(c(y))}{\int_s^{s+\varepsilon} f_{C^*}(u)\,du}\ \nu_1(dy) \\
&\qquad = \frac{1}{f_{C^*}(s)} \sum_{i=1}^{\widetilde{J}_s} \mathbb{1}_{[0,x]}(\nu_1(T_{sub}(\widetilde{X}_{s,i})))\,.
\end{aligned}$$

Now

$$\begin{aligned}
\int_{S_i} \mathbb{1}_{[0,x]}(\nu_1(T_{sub}(y))) \frac{\mathbb{1}_{[s,s+\varepsilon)}(c(y))}{\int_s^{s+\varepsilon} f_{C^*}(u)\,du}\, \nu_1(dy) &\le \int_{S_i} \frac{\mathbb{1}_{[s,s+\varepsilon)}(c(y))}{\varepsilon \min\limits_{x \in [s,s+1)} f_{C^*}(x)}\, \nu_1(dy) \\
&\le \frac{1}{\min\limits_{x \in [s,s+1)} f_{C^*}(x)} < \infty\,,
\end{aligned}$$

hence we can apply the dominated convergence theorem in order to get

$$\mathbb{P}(\nu_1(T^*_{sub}) \le x \mid C^*_X = s) \;=\; \frac{\lambda_\ell}{f_{C^*}(s)} \mathbb{E} \sum_{i=1}^{\widetilde{J}_s} \mathbb{1}_{[0,x]}(T_{sub}(\widetilde{X}_{s,i})) = F_s(x)\,.$$

Thus, the proof is completed. □

Notice that Lemma 8.6 states that we can regard the distribution function F_s as the conditional distribution function of $\nu_1(T^*_{sub})$ given that $C^*_X = s$. This relationship is now used in order to prove Theorem 8.5.

Proof of Theorem 8.5 Let $x \ge 0$, then Lemma 8.6 yields

$$\begin{aligned} F(x) &= \mathbb{E}\left(\mathbb{P}(\nu_1(T^*_{sub}) \le x \mid C^*_X)\right) \\ &= \int_0^\infty \mathbb{P}(\nu_1(T^*_{sub}) \le x \mid C^*_X = s) f_{C^*_X}(s)\, ds \\ &= \int_0^\infty F_s(x) f_{C^*_X}(s)\, ds \\ &= \int_0^\infty \frac{\lambda_\ell}{f_{C^*}(s)} \mathbb{E} \sum_{i=1}^{\widetilde{J}_s} \mathbb{1}_{[0,x]}(T_{sub}(\widetilde{X}_{s,i}))\, f_{C^*_X}(s)\, ds\,, \end{aligned}$$

where the last equality follows from formula (8.6) and $\widetilde{J}_s, \widetilde{X}_{s,1}, \ldots, \widetilde{X}_{s,\widetilde{J}_s}$ are the random variables which have been introduced in the proof of Lemma 8.6. Since we have $f_{C^*}(s) = f_{C^*_X}(s)$ for almost all $s \in [0,\infty)$, we get

$$\begin{aligned} F(x) &= \lambda_\ell \mathbb{E} \int_0^\infty \sum_{i=1}^{\widetilde{J}_s} \mathbb{1}_{[0,x]}(T_{sub}(\widetilde{X}_{s,i}))\, ds \\ &= \lambda_\ell \mathbb{E} \sum_{i=1}^{N} \int_{l(B_i)}^{l(A_i)} \mathbb{1}_{[0,x]}(s)\, ds \\ &= \int_0^x \lambda_\ell \mathbb{E} \sum_{i=1}^{N} \mathbb{1}_{[l(B_i),l(A_i))}(s)\, ds\,, \end{aligned}$$

which completes the proof. □

8.3.2 Estimation of the density

For each $x \ge 0$, Theorem 8.5 can be used in order to construct the natural estimator

$$\widehat{f}(x;n) = \lambda_\ell \, \frac{1}{n} \sum_{j=1}^{n} \sum_{i=1}^{N_j} \mathbb{1}_{[l(B_i^{(j)}),l(A_i^{(j)}))}(x) \tag{8.10}$$

for $f(x)$ based on n independent and identically distributed copies of S^*_H. We now summarize some distributional results of the estimator $\widehat{f}(x;n)$.

Theorem 8.7 *Let $\widehat{f}(x;n)$ denote the estimator defined in (8.10). Then, for $x \in \mathbb{R}$,*

$$\mathbb{P}\big(\lim_{n\to\infty} \widehat{f}(x;n) = f(x)\big) = 1 \tag{8.11}$$

and

$$\mathbb{E}\widehat{f}(x;n) = f(x). \tag{8.12}$$

Let $h : \mathbb{R} \to [0,\infty)$ be a measurable function, then

$$\mathbb{E}\left[\int_{\mathbb{R}} h(x)\widehat{f}(x;n)\,dx\right] = \mathbb{E}h(\nu_1(T^*_{sub})) \tag{8.13}$$

and

$$\mathbb{P}\big(\lim_{n\to\infty} \int_{\mathbb{R}} h(x)\widehat{f}(x;n)\,dx = \mathbb{E}h(\nu_1(T^*_{sub}))\big) = 1\,. \tag{8.14}$$

Proof All statements easily follow from Theorem 8.5, see also the proof of Theorem 5.9. □

We can again show that the maximal error of the estimator $\widehat{f}(\,\cdot\,;n)$ converges to zero with probability 1.

Theorem 8.8 *It holds that*

$$\mathbb{P}\left(\lim_{n\to\infty} \sup_{x\in\mathbb{R}} |\widehat{f}(x;n,\omega) - f(x)| = 0\right) = 1\,.$$

Proof The statement can be proven in a similar way as Theorem 5.10. Let $q \in \mathbb{Q}$, then

$$\begin{aligned} |\widehat{f}(x;n,\omega) - f(x)| & \\ \leq\ & |\widehat{f}(x;n,\omega) - \widehat{f}(q;n,\omega)| + |\widehat{f}(q;n,\omega) - f(q)| + |f(q) - f(x)|\,. \end{aligned} \tag{8.15}$$

Now all three terms can be approximated as in Theorem 5.10 bearing in mind that f is bounded. □

8.4 Numerical results and possible extensions

In this section some numerical results are presented which were obtained using the estimators introduced above. Furthermore, we discuss some possible extensions and additional questions.

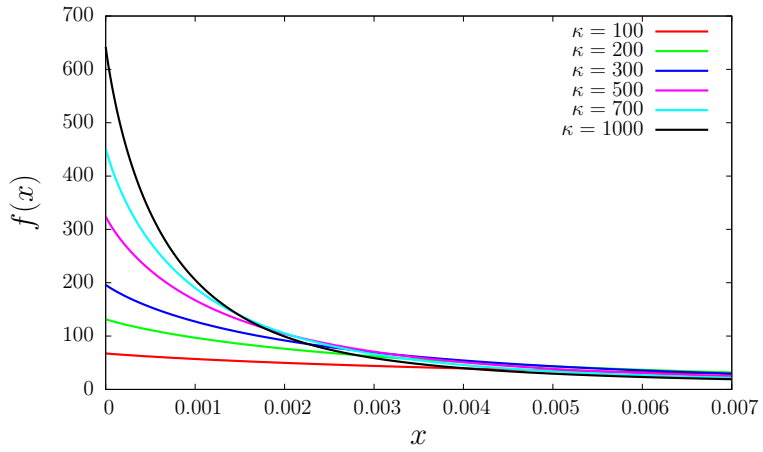

(a) PLT

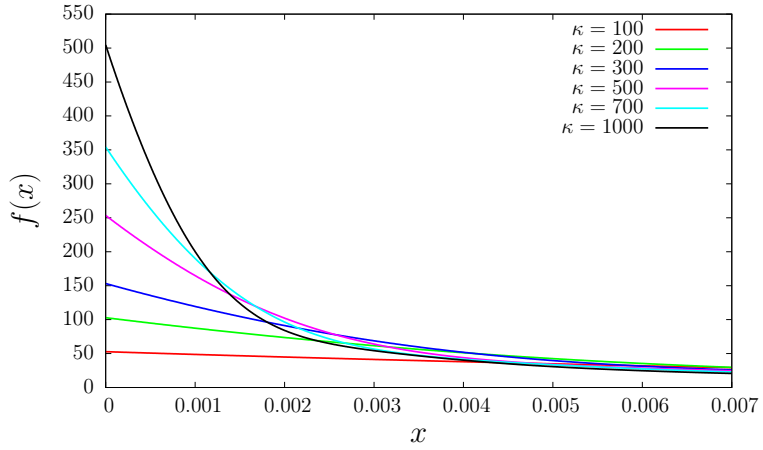

(b) PVT

Figure 8.3: Density f of $\nu_1(T^*_{sub})$ for Cox processes $\{X_n\}$

8.4.1 Numerical results

For the numerical results we focus on the cases that H is a Cox process on T, T is a PLT or PVT, respectively, and the serving zones are given by the Voronoi tessellation with respect to H. Then, the distribution function F of the typical subtree length $\nu_1(T^*_{sub})$ which is considered in (8.6) for network locations with fixed distance to their associated HLC, has a density. In order to see this, assume that the segment system S^*_H, the marked points $(\widetilde{X}_1, T_{sub}(\widetilde{X}_1)), \ldots, (\widetilde{X}_{\tilde{J}}, T_{sub}(\widetilde{X}_{\tilde{J}}))$ and the random tessellation T^* with respect to the Palm distribution of H are given. If we only condition on T^*, then the distribution of $\sum_{i=1}^{\tilde{J}} \mathbb{1}_B(\nu_1(T_{sub}(\widetilde{X}_i)))$ is not changed if we replace each HLC by a new HLC which is uniformly distributed on the same segment. Under this transformation all points with short-

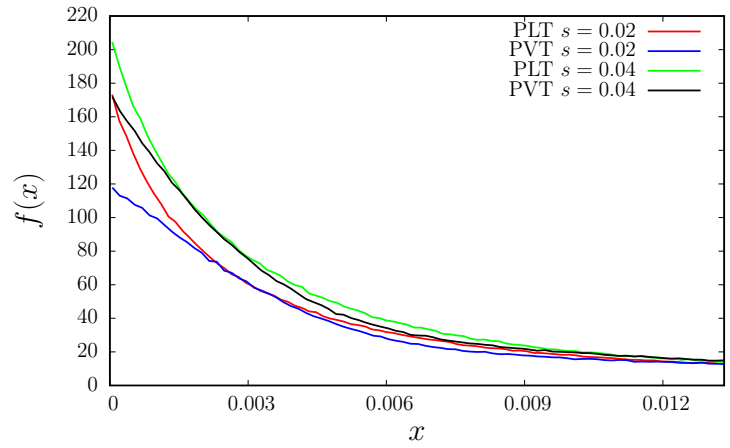

(a) $\kappa = 300$

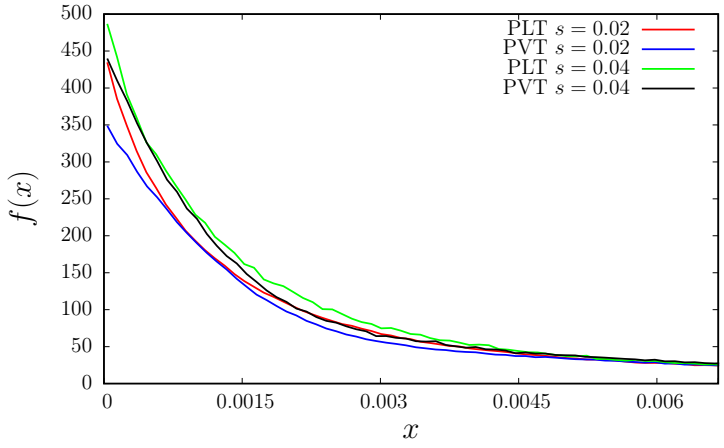

(b) $\kappa = 700$

Figure 8.4: Density f of $\nu_1(T^*_{sub})$ for fixed distance s to HLC

est path length s on T^* keep unchanged, but some new points may lie on the segments of S^*_H and some other points may not lie on S^*_H anymore. However, the subtree lengths $T_{sub}(\widetilde{X}_i), i = 1, 2, \ldots$ are transformed almost surely in a continuous and non-constant way if HLC are shifted along the segments. Hence $\sum_{i=1}^{\widetilde{K}} \mathbb{1}_B(\nu_1(T_{sub}(\widetilde{X}_i))) = 0$ almost surely for each set $B \in \mathcal{B}(\mathbb{R})$ with $\nu_1(B) = 0$ which yields that the distribution of $\nu_1(T^*_{sub})$ is absolutely continuous.

Furthermore, we can observe the same scaling invariance as e.g. for shortest path length if $\kappa = \gamma/\lambda_\ell$ is fixed. For different values of κ we used the estimators introduced in the preceding sections in order to determine the density $f(x)$ of the typical subtree length $\nu_1(T^*_{sub})$ based on i.i.d. samples of S^*_H.

For each realization of the typical segment system S^*_H we first compute the shortest path from o to all nodes of S^*_H using Dijkstra's algorithm ([22]). Then,

in a second step, all segments with distance peak are divided and thus S_H^* is transformed into a tree structure, the shortest path tree. Notice that the distance peaks are then the leaves of the tree. The shortest path tree is then used in order to compute the subtree length $l(B_i)$ and $l(A_i)$ at the endpoints $A_i, B_i, i = 1, \ldots, N$ of the segments. Based on these results the estimator $\widehat{f}(x;n)$ defined in equation (8.10) can then be computed directly. For the computation of the estimator $\widehat{F}_s(x;n)$ defined in equation (8.7) we first choose the segments $S_i, i = 1, \ldots, \widetilde{K}$ with $c(A_i) \leq s < c(B_i)$, i.e., the segments which contain the points $\widetilde{X}_1, \ldots, \widetilde{X}_{\widetilde{J}}$, and finally we compute $\nu_1(T_{sub}(\widetilde{X}_i)) = l(B_i) + c(B_i) - s$.

Some numerical results are shown in Figure 8.3 for a Cox processes $\{X_n\}$ on a PLT and PVT, respectively, for different values of κ. Here, the estimator introduced in (8.10) was used. Moreover, in Figure 8.4 the results are displayed which were obtained for network locations with a fixed distance s to their associated HLC. We computed for different values of s and κ the density of the typical subtree length $\nu_1(T_{sub}^*)$ as difference quotients of the empirical distribution function $\widehat{F}(x;n)$ defined in (8.7).

The shapes of all the densities shown in Figures 8.3 and 8.4 are quite similar to each other. Moreover, Figure 8.4 shows that the shape of the density $f(x)$ of the typical subtree length $\nu_1(T_{sub}^*)$ does not depend too much on the specific choice of the (fixed) distance s to the associated HLC. On the other hand, the density $f(x)$ changes considerably if the random tessellation T (PLT vs. PVT) or the scaling factor κ is modified, see Figures 8.3 and 8.4.

Finally, we remark that if we know the density $f(x)$ of the typical subtree length $\nu_1(T_{sub}^*)$, then we can use the representation formula (8.2) for the typical capacity K^* in order to compute e.g. the expectation $\mathbb{E}h(K^*)$ for various functionals $h : [0,\infty) \to [0,\infty)$ of K^* by

$$\begin{aligned}\mathbb{E}h(K^*) &= \mathbb{E}h(\sum_{i=1}^{J^*} K_i) \\ &= \sum_{k=0}^{\infty} \frac{1}{k!}\, \mathbb{E}h(\sum_{i=1}^{k} K_i) \int_0^{\infty} e^{-\lambda_\ell' x} (\lambda_\ell' x)^k \, f(x)\, dx\,,\end{aligned}$$

which follows from Theorem 8.1.

The numerical results presented here were obtained in cooperation with S. Müthing. Further numerical results can be found in his diploma thesis ([73]).

8.4.2 Possible extensions

The notion of required capacity in the SSLM has been introduced in this chapter. In particular, it has been shown that the distribution of the capacity is uniquely determined by the distribution of the so–called typical subtree length. Moreover, we have demonstrated how the distribution of the typical subtree length, and

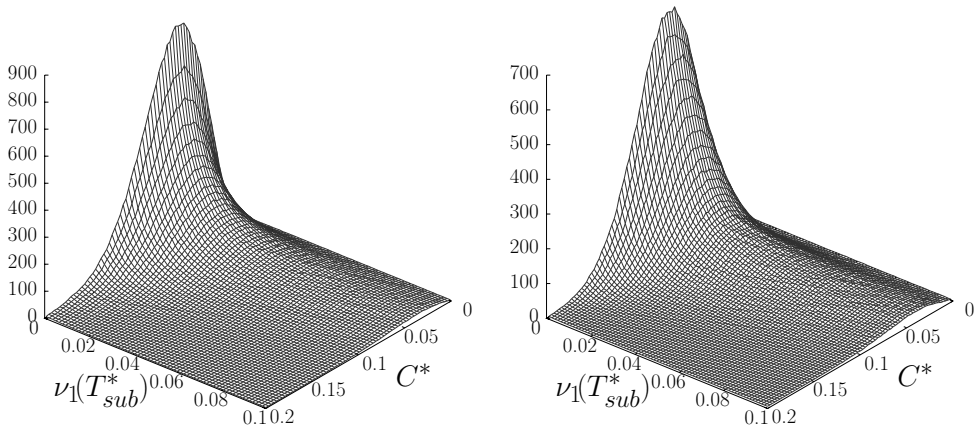

(a) PLT, $\kappa = 100$ (b) PVT, $\kappa = 100$

Figure 8.5: Joint density of $(C^*, \nu_1(T^*_{sub}))$

hence the typical capacity itself, can be computed for two specific models of network locations. These results can be extended in different ways, e.g. to typical capacities for further types of network locations like the thinned nodes of the underlying tessellation or subfamilies of these nodes obtained from conditioning on the number of nodes passed on the shortest path to HLC. Another subject for future research could be the investigation of scaling limits for the distribution of the typical capacity as the scaling factor κ tends to infinity. Recall that in Chapter 6 it has been shown that the distribution of the typical shortest path length C^* converges to known distributions for $\kappa \to \infty$. Such limit theorems are of great practical interest, see for instance Chapter 7. Moreover, it is possible to compute the joint density of C^* and $\nu_1(T^*_{sub})$ for Cox processes on T, see Figure 8.5. From this two-dimensional density we can then e.g. compute the density of $\nu_1(T^*_{sub})$ conditioned on $C^* = s$.

In summary, the ideas and techniques that have been developed in this chapter can be combined with the fitting techniques for optimal network models introduced in [32, 85] which provides an efficient tool in order to analyze the required capacities in real (planned or existing) telecommunication networks.

Chapter 9

Conclusion and outlook

The results elaborated in this thesis show that tools and methods from stochastic geometry can be used in order to efficiently analyze fixed telecommunication networks in urban areas. In the considered approach, parametric distributions of important cost functionals of telecommunication networks like connection lengths have been obtained using spatial stochastic models and a combination of Monte–Carlo and asymptotic methods. The parameters of the distributions computed in this manner can be linked to few characteristics which can be easily estimated from real data. It has been shown that these parametric distributions are excellent approximations of real distributions of connection lengths in the access network of Paris. Thus, the developed techniques provide powerful tools in order to analyze existing networks and to plan future networks based on new technologies.

In a first step, efficient simulation algorithms for the typical cell of various random tessellation models have been developed. These algorithms are of interest on their own since many important characteristics of random tessellations can be estimated based on the typical cell. Then, in a second step, it has been shown that samples generated with these algorithms can be used in order to estimate the distributions of important cost functionals like the typical Euclidean and shortest path connection lengths. In particular, estimators for the density and distribution function of these characteristics have been constructed which are based on samples of the typical cell and its inner structure. Moreover, scaling limits for both the typical Euclidean and shortest path length have been derived, i.e., it has been proven that the distributions of Euclidean and shortest path connection lengths converge to known parametric distributions if the underlying tessellation gets infinitely sparse and dense, respectively. Both results have been combined in order to obtain parametric distributions for connection lengths, where the parameters can be estimated easily and fast from real data. For real network data, it has been demonstrated that these parametric densities are extremely good approximations of the distributions of real connection lengths. In this way, the elaborated results have been validated for real data. Thus, the developed methods can be used in order to efficiently analyze telecommunication networks

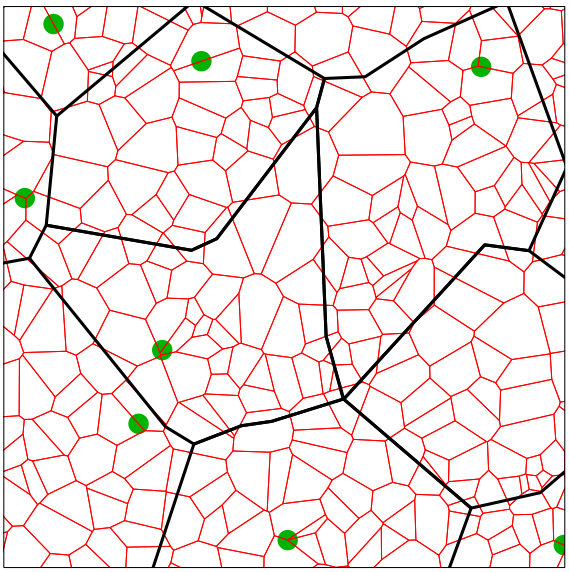

Figure 9.1: Serving zones generated as an aggregated Voronoi tessellation

in urban areas in the future.

There are different possibilities to continue the investigations of this thesis. So far, parametric densities have been only fitted to densities estimated for Cox processes on PDT, PLT or PVT. Using the simulation algorithms for the typical Voronoi cell of Cox processes on iterated tessellations, parametric densities for these more flexible models could be obtained. Furthermore, it is possible to model the serving zones with random tessellations different from Voronoi tessellations. For instance, Laguerre tessellations or aggregated Voronoi tessellations based on Cox processes could be considered. In Figure 9.1 a realization of a Cox process on PVT is shown together with (non-convex) serving zones generated by an aggregated Voronoi tessellation. Note that aggregated Voronoi tessellations arise naturally as serving zones if hierarchical networks with more than two hierarchy levels are considered. For these models, simulation algorithms for the typical cell could be developed and used to estimate the densities of shortest path connection lengths. In addition, as mentioned in Chapter 6, scaling limits for the typical shortest path length can also be derived for these models. Thus, this approach would lead to more flexible classes of parametric distance distributions. However, the models considered so far depend on one single parameter only, but all possible generalizations lead to many new models with more than one parameter. Thus, extensive simulation studies are necessary in order to determine new parametric families of distance distributions.

Finally, required capacities have been defined and it has been demonstrated how the distributions of such capacities can be estimated based on Monte-Carlo methods. These results are of interest for the analysis and strategic planning of telecommunication networks and can be generalized in different ways. For

instance, further point process models like thinned vertices can be considered in order to describe the locations, where required capacities are analyzed. Moreover, connection rules different from shortest path connections can be regarded like least nodes path. Another interesting question which arises here are scaling limits for required capacities. The results derived for shortest path lengths have been proven to be very useful e.g. in order to obtain parametric densities for distance distributions. Maybe the same approach is possible in order to construct parametric families of capacity distributions.

Appendix A

Mathematical background

The appendix provides a short overview of some definitions and results from measure theory, the theory of subadditive processes and geometric measure theory. In particular, convergence concepts and limit theorems from measure theory, the subadditive ergodic theorem and the generalized Blaschke-Petkantschin formula are reviewed.

A.1 Convergence concepts

This section provides some convergence concepts and limit theorems which are used in the thesis. It is assumed that the reader is familiar with fundamental notions of measure theory and probability theory; for details we refer to [11, 12, 37, 45].

A.1.1 Modes of convergence of measurable functions

Let $\{f_n\}$ be a sequence of real–valued measurable functions defined on a measure space $(\Omega, \mathcal{A}, \mu)$ and let $f : \Omega \to \mathbb{R}$ be another measurable function. Then we say that

- f_n converges μ-almost everywhere to f if

$$\mu(\{\omega \in \Omega : \lim_{n\to\infty} f_n(\omega) \neq f(\omega)\}) = 0\,,$$

  which is abbreviated by $f_n \overset{a.e.}{\to} f$.

- f_n converges in μ-measure to f if for any $A \in \mathcal{A}$ with $\mu(A) < \infty$ and $\varepsilon > 0$ it holds that

$$\lim_{n\to\infty} \mu(\{\omega \in \Omega : |f_n(\omega) - f(\omega)| > \varepsilon\} \cap A) = 0\,,$$

  which is abbreviated by $f_n \overset{\mu}{\to} f$.

- f_n converges in $L^p, p \geq 1$ or p-th mean to f if $f, f_1, f_2, \ldots$ are μ–integrable in the p-th power and

$$\lim_{n\to\infty} \left(\int_\Omega |f_n(\omega) - f(\omega)|^p \, \mu(d\omega) \right)^{\frac{1}{p}} = 0 \,,$$

  which is abbreviated by $f_n \xrightarrow{L^p} f$.

If μ is a probability measure and f_n converges to f in μ-measure resp. μ-almost everywhere, then we also say that f_n converges to f in probability resp. almost surely. Note that it is well-known that a sequence converges in μ-measure to f if it converges in L^p or μ-almost everywhere.

Theorem A.1 *If $f_n \xrightarrow{a.e.} f$ or $f_n \xrightarrow{L^p} f$, then $f_n \xrightarrow{\mu} f$.*

A proof of Theorem A.1 can be found e.g. in [11]. Now assume that $X, X_1, X_2, \ldots$ are real–valued random variables with distribution functions $F_X, F_{X_1}, F_{X_2}, \ldots$. We say that

- X_n converges in distribution to X if $\lim_{n\to\infty} F_{X_n}(x) = F(x)$ for all continuity points $x \in \mathbb{R}$ of F and we then write $X_n \xrightarrow{d} X$.

The connections to the other modes of convergence are summarized in the following theorem.

Theorem A.2 *Let $X, X_1, X_2, \ldots$ be real–valued random variables defined on the same probability space $(\Omega, \mathcal{A}, \mathbb{P})$. Then $X_n \xrightarrow{d} X$ if $X_n \xrightarrow{a.s.} X$, $X_n \xrightarrow{L^p} X$ or $X_n \xrightarrow{\mathbb{P}} X$.*

For a proof of Theorem A.2, see e.g. [11]. Let $P_X, P_{X_1}, P_{X_2}, \ldots$ denote the distributions of $X, X_1, X_2, \ldots$, then convergence in distribution can be characterized in the following way, see e.g. Chapter 1 in [15].

Theorem A.3 *Let $X, X_1, X_2, \ldots$ be real–valued random variables. Then $X_n \xrightarrow{d} X$ if and only if*

$$\lim_{n\to\infty} \int_{\mathbb{R}} f(x) \, P_{X_n}(dx) = \int_{\mathbb{R}} f(x) \, P_X(dx)$$

for every bounded and continuous function $f : \mathbb{R} \to \mathbb{R}$.

Now we consider two sequences $X_1, X_2, \ldots$ and $Y_1, Y_2, \ldots$ of real–valued random variables. Then the following result is true, see e.g. Theorem 3.1 of [15].

Theorem A.4 *Let $X_1, X_2, \ldots$ and $Y_1, Y_2, \ldots$ be two sequences of real–valued random variables defined on the same probability space $(\Omega, \mathcal{A}, \mathbb{P})$. If $X_n \xrightarrow{d} X$ for some random variable X and $X_n - Y_n \xrightarrow{\mathbb{P}} 0$, then $Y_n \xrightarrow{d} X$.*

A.1.2 Convergence theorems

In the preceding section we have summarized relationships between different modes of convergence. In particular, convergence almost everywhere as well as convergence in the p-th mean implies convergence in μ-measure, which in turn implies convergence in distribution if μ is a probability measure. However, the relationship between convergence in p-th mean and convergence almost everywhere is more complicated. We discuss this relationship in the present section.

To begin with, we summarize two classical limit theorems. The first one is the monotone convergence theorem of B. Levi ([11], Theorem 2.3.4).

Theorem A.5 (Monotone Convergence Theorem) *Let $(\Omega, \mathcal{A}, \mu)$ be a measure space and let $\{f_n\}$ be a non–decreasing sequence of measurable functions $f_n : \Omega \to [0, \infty]$, i.e.,*

$$0 \leq f_n(\omega) \leq f_{n+1}(\omega)$$

for all $n \in \mathbb{N}$ and $\omega \in \Omega$. Then $f : \Omega \to [0, \infty]$ defined by $f(\omega) = \lim_{n\to\infty} f_n(\omega)$ is measurable and

$$\lim_{n\to\infty} \int_\Omega f_n(\omega)\, \mu(d\omega) = \int_\Omega f(\omega)\, \mu(d\omega)\,.$$

Another important limit theorem is the famous dominated convergence theorem of H. Lebesgue ([11], Theorem 2.7.4).

Theorem A.6 (Dominated Convergence Theorem) *Let $\{f_n\}$ be a sequence of real–valued measurable functions on a measure space $(\Omega, \mathcal{A}, \mu)$ which converges μ-almost everywhere. Suppose that there is an integrable function $g : \Omega \to \mathbb{R}$ with*

$$|f_n(\omega)| \leq g(\omega)$$

for all $\omega \in \Omega$ and $n \in \mathbb{N}$. Then there is an integrable function $f : \Omega \to \mathbb{R}$ such that f_n converges μ-almost everywhere and in L^1 to f.

Note that a sequence $\{f_n\}$ converges in μ-measure if it converges μ-almost everywhere, but the converse statement is not true in general. However, the dominated convergence theorem can be refined for sequences which converge in μ-measure using the notion of uniform integrability. Let $\{f_n\}$ be a family of real–valued measurable functions defined on a measure space $(\Omega, \mathcal{A}, \mu)$. If for every $\varepsilon > 0$ there is a μ-integrable function $g : \Omega \to [0, \infty]$ such that

$$\int_{\{\omega\in\Omega:|f_n(\omega)|\geq g(\omega)\}} |f_n(\omega)|\, \mu(d\omega) \leq \varepsilon \quad \text{for all } n \in \mathbb{N}\,, \tag{A.1}$$

then $\{f_n\}$ is said to be uniformly μ-integrable. With this definition, convergence in L^1 can be characterized as follows, see e.g. Theorem 2.12.4 in [11].

Theorem A.7 *Let μ be a σ-finite measure on a measurable space $(\Omega, \mathcal{A})$. Then a sequence of μ-integrable functions $\{f_n\}$ on $(\Omega, \mathcal{A})$ converges in L^1 to a μ-integrable function $f : \Omega \to \mathbb{R}$ if and only if*

(i) f_n converges in μ-measure to f and

(ii) $\{f_n\}$ is uniformly μ-integrable.

An elementary but useful result in order to check a sequence for uniform integrability is given in the following lemma. It is a direct consequence of the definition of uniform integrability.

Lemma A.8 *Let $\{f_n\}$ and $\{g_n\}$ be two families of measurable functions on $(\Omega, \mathcal{A}, \mu)$ which satisfy that $|f_n| \leq |g_n|$ for all $n \geq 1$. Then $\{f_n\}$ is uniformly μ-integrable if $\{g_n\}$ is uniformly μ-integrable.*

A.1.3 Weak convergence of probability measures

In this thesis an additional convergence concept is considered. This is the concept of weak convergence of probability measures. Recall that a sequence of real–valued random variables $X_1, X_2, \ldots$ converges in distribution to the random variable X if and only if

$$\lim_{n\to\infty} \int_{\mathbb{R}} f(x)\, P_{X_n}(dx) = \int_{\mathbb{R}} f(x)\, P_X(dx)$$

for every bounded and continuous function $f : \mathbb{R} \to \mathbb{R}$, see Theorem A.3. Thus, convergence in distribution of X_n to X can be regarded as convergence of the probability measures P_{X_n} on $\mathcal{B}(\mathbb{R})$ to the probability measure P_X on $\mathcal{B}(\mathbb{R})$. This concept can be extended to sequences of probability measures P_n on more general measurable spaces $(\Omega, \mathcal{A})$.

Let Ω be a metric space and let $\mathcal{B}(\Omega)$ denote its Borel-σ-algebra. Then a sequence of probability measures $\{\mu_n\}$ on $\mathcal{B}(\Omega)$ is said to converge weakly to the probability measure μ if

$$\lim_{n\to\infty} \int_{\Omega} f(\omega)\, \mu_n(d\omega) = \int_{\Omega} f(\omega)\, \mu(d\omega)$$

for all continuous and bounded functions $f : \Omega \to \mathbb{R}$. Note that a sequence $\{X_n\}$ of random variables converges in distribution to the random variable X if and only if their distributions $\{P_{X_n}\}$ converge weakly to the distribution P_X of X. Therefore, we sometimes also say that a sequence of probability measures on $\mathcal{B}(\Omega)$ converges in distribution if it converges weakly.

Now suppose that $X^{(1)}, X^{(2)}, \ldots$ is a sequence of point processes and X another point process. We then say that $X^{(n)}$ converges weakly to X if the distribution $P_{X^{(n)}}$ of $X^{(n)}$ converges weakly to the distribution P_X of X. Weak convergence of point processes can be characterized in the following way, see [21], Theorem 11.1.VII.

Theorem A.9 *The sequence* $\{X^{(n)}\}$ *converges weakly to* X *if and only if*

$$\lim_{n\to\infty} \mathbb{P}(X^{(n)}(A_1) = k_1, \ldots, X^{(n)}(A_m) = k_m) = \mathbb{P}(X(A_1) = k_1, \ldots, X(A_m) = k_m)$$

for any family $A_1, \ldots, A_m$ *of bounded continuity sets of* X *and any* $k_1, \ldots, k_n \in \mathbb{N}$, *where a set* $A \in \mathcal{B}(\mathbb{R}^2)$ *is called continuity set of* X *if* $\mathbb{P}(X(\partial A) > 0) = 0$.

Theorem A.9 states that a sequence of point processes $\{X^{(n)}\}$ converges weakly to some point process X if the finite–dimensional distributions of $X^{(n)}$ converge to those of X. Thus, here we regard a point process as a stochastic process indexed by the Borel sets $\mathcal{B}(\mathbb{R}^2)$. Note that in general a sequence of stochastic processes does not converge weakly if the finite–dimensional distributions converge. The sequence has to fulfill in addition a so–called tightness condition, see e.g. [15]. However, for point processes (and random measures) this tightness condition is always fulfilled. Hence it is sufficient that the finite-dimensional distributions converge.

A.2 Kingman's subadditive ergodic theorem

Another tool used in this thesis is the notion of subadditivity. Let $\mathbf{Y} = \{Y_{ij}, i, j \geq 1, i < j\}$ denote a family of real-valued random variables which are defined on some probability space $(\Omega, \mathcal{A}, \mathbb{P})$. Note that we can regard the family $\mathbf{Y}$ as a random element of the measurable space $(\mathcal{S}, \mathcal{B}(\mathcal{S}))$, where $\mathcal{S}$ denotes the family of double–indexed sequences in $\mathbb{R}$ and $\mathcal{B}(\mathcal{S})$ is its Borel-σ-algebra. The family $\mathbf{Y}$ is called a subadditive process if

1. $Y_{ik} \leq Y_{ij} + Y_{jk}$ for all $i < j < k$,
2. $\mathbf{Y} = \{Y_{ij}\} \stackrel{\mathrm{d}}{=} \mathbf{Y}' = \{Y_{i+1,j+1}\}$,
3. $\mathbb{E}Y_{01}^+ < \infty$, where $Y_{01}^+ = \max\{0, Y_{01}\}$.

If a family of random variables is subadditive, then, under mild conditions, it can be shown that Y_{0j}/j converges almost surely and in L^1 to some constant ξ, see the following subadditive ergodic theorem which is due to Kingman ([46], Theorem 1). A slightly more general version of the subadditive ergodic theorem can be found in [45], Theorem 10.22.

Theorem A.10 *Let* $\mathbf{Y}$ *be a subadditive process. Then the limit*

$$\zeta = \lim_{j\to\infty} \frac{1}{j} Y_{0j} \tag{A.2}$$

exists and is finite with probability 1, where $\mathbb{E}\zeta = \inf_{j\in\mathbb{N}} \mathbb{E}Y_{0j}/j$. *If* $\mathbb{E}\zeta > -\infty$, *then the convergence in* (A.2) *also holds in the* L^1*-norm. Moreover, let* $\mathcal{I}_{\mathcal{S}} \subset \mathcal{B}(\mathcal{S})$

be the σ-algebra of subsets of $\mathcal{S}$ which are invariant under the shift $\mathbf{Y} \mapsto \mathbf{Y}'$, where $Y'_{ij} = Y_{i+1,j+1}$, and let $\mathcal{I} = \mathbf{Y}^{-1}\mathcal{I}_{\mathcal{S}} \subset \mathcal{A}$ be the corresponding sub-σ-algebra of events. Then,

$$\zeta = \lim_{j\to\infty} \frac{1}{j}\, \mathbb{E}\big(Y_{0j} \mid \mathcal{I}\big)\,. \tag{A.3}$$

In the same way as for (marked) point processes we define ergodic subadditive processes. A subadditive process $\mathbf{Y}$ is said to be ergodic if the σ–algebra $\mathcal{I}_{\mathcal{S}}$ is trivial, i.e., for each $A \in \mathcal{I}_{\mathcal{S}}$ it holds that $\mathbb{P}(\mathbf{Y} \in A) = 0$ or $\mathbb{P}(\mathbf{Y} \in A) = 1$. Thus, if $\mathbf{Y}$ is ergodic, the limit ζ considered in (A.2) is almost surely constant due to equation (A.3).

A.3 The Hausdorff measure and the generalized Blaschke–Petkantschin formula

In this thesis it is essential to measure lengths of segments and curves. This can be done using the 1-dimensional Hausdorff measure ν_1 which is defined for $B \subset \mathbb{R}^2$ by

$$\nu_1(B) = \sup_{\varepsilon>0}\, \inf\Big\{ \sum_{j\in\mathbb{N}} D(A_j) : B \subset \cup_{j\in\mathbb{N}} A_j, D(A_j) \le \varepsilon \Big\}\,,$$

where $D(A_j) = \sup\{\| x - y \| \colon x, y \in A_j\}$ is the diameter of the set A_j, see [43]. Note that for a differentiable curve C, the Hausdorff measure allows to integrate some function $f : C \to [0,\infty]$ along C with respect to the length measure ν_1 on C. However, ν_1 is not σ-finite and thus Fubini's Theorem ([11], Theorem 3.2.6) cannot be applied for integrals involving ν_1. This is one reason why it is often convenient to transform such integrals in order to obtain expressions which do not contain ν_1 anymore.

There are different possibilities to transform integrals with respect to the 1–dimensional Hausdorff measure in $\mathbb{R}^2$. A very general transform is the coarea formula which can be used to obtain the specific transformations used in this thesis. The following version of the coarea formula is a special case of Theorem 2.1 in [43] which is sufficient for our purposes. In order to formulate this result we use the notation $\mathrm{Tan}[C, x]$ for the tangent line of a differentiable curve C at $x \in C$.

Theorem A.11 (Coarea formula) *Let $D \subset \mathbb{R}^2$ be an open set, $C \subset D$ be a differentiable curve and $f : D \to \mathbb{R}$ be a differentiable mapping. Then, there is a function $Jf(\,\cdot\,; C) : C \to [0,\infty)$ which is called the Jacobian such that*

$$\int_C g(x)\; Jf(x; C)\, \nu_1(dx) = \int_0^\infty \sum_{x_i \in C \cap f^{-1}(y)} g(x_i)\, dy\,, \tag{A.4}$$

where $g : C \to [0, \infty)$ is a measurable function. Moreover, let $Df(x)$ be defined by

$$Df(x) = \Big(\frac{\partial f}{\partial x_1}(x), \frac{\partial f}{\partial x_2}(x) \Big) ,$$

and let $\ker Df(x) = \{y \in \mathbb{R}^2 : \langle y, Df(x) \rangle = 0\}$ be the kernel of the vector $Df(x)$, where $\langle \cdot \, , \cdot \rangle$ denotes the Euclidean scalar product on $\mathbb{R}^2$. Then $Jf(x; C) > 0$, if and only if the dimension of the subspace

$$\mathrm{Tan}[C, x] \cap (\ker Df(x) \cap \mathrm{Tan}[C, x])^{\perp}$$

is equal to 1 and then

$$Jf(x; C) = |\langle u, Df(x) \rangle| ,$$

where u is a unit vector with $\{tu : t \in \mathbb{R}\} = \mathrm{Tan}[C, x] \cap (\ker Df(x) \cap \mathrm{Tan}[C, x])^{\perp}$.

In the proofs of this thesis, the following decompositions of the Hausdorff measure ν_1 are used. First, we state a special case of the generalized Blaschke-Petkantschin formula ([43], Proposition 5.4).

Theorem A.12 (Generalized Blaschke–Petkantschin formula) *Let $C \subset \mathbb{R}^2$ be a differentiable curve and assume that*

$$\nu_1(\{x \in C : \, \mathrm{Tan}[C, x] = \mathrm{span}\{x\}\}) = 0 , \tag{A.5}$$

where $\mathrm{span}\{x\} = \{cx : c \in \mathbb{R}\}$ is the line which goes through the origin $o \in \mathbb{R}^2$ and the point $x \in C$. Then, for any measurable $g : C \to [0, \infty)$, it holds that

$$\int_C g(x) \, \nu_1(dx) = \int_0^{2\pi} \sum_{x_i \in C \cap \ell_\Phi^+} \frac{|x_i|}{\sin \alpha_i} \, g(x_i) \, d\Phi , \tag{A.6}$$

where ℓ_Φ^+ is the half line of direction $\Phi \in [0, 2\pi)$ emanating from the origin o and α_i is the angle between $\mathrm{Tan}[C, x_i]$ and $\mathrm{span}\{x_i\}$.

Furthermore, the Hausdorff measure ν_1 can be decomposed in the following way.

Lemma A.13 *Let C be a differentiable curve and let*

$$\nu_1(\{x \in C : dim(\mathrm{Tan}[C, x] \cap (\mathrm{span}\{x\}^{\perp} \cap \mathrm{Tan}[C, x])^{\perp}) = 0\}) = 0 .$$

Then we get for any measurable $g : C \to [0, \infty)$ that

$$\int_C g(x) \sin(\alpha(x)) \, \nu_1(dx) = \int_0^{\infty} \sum_{x_i \in C \cap \partial B(o,r)} g(x_i) \, dr , \tag{A.7}$$

where $\alpha(x)$ is the angle between x and $\mathrm{Tan}[C, x] \cap (\mathrm{span}\{x\}^{\perp} \cap \mathrm{Tan}[C, x])^{\perp}$.

Proof This decomposition of the Hausdorff measure ν_1 is an application of Theorem A.11. First we assume that $o \notin C$ and define $f : \mathbb{R}^2 \backslash \{o\} \to (0, \infty)$ by $f(x) = |x|$. Then $f^{-1}(r) = \partial B(o, r)$ and $Df(x) = x/|x|$, so we get $\ker Df(x) = \mathrm{span}\{x\}^\perp$. Now if the dimension of the subspace

$$\mathrm{Tan}[C, x] \cap (\mathrm{span}\{x\}^\perp \cap \mathrm{Tan}[C, x])^\perp$$

is equal to 1 and a basis is given by $\{u\}$, then the Jacobian $Jf(x; C)$ is given by

$$Jf(x; C) = |\langle u, \frac{1}{|x|} x \rangle| = \sin(\alpha(x)) \,.$$

Thus, we can apply Theorem A.11 and obtain equation (A.7). If $o \in C$, then we can divide the integral into integrals over $C \backslash \{o\}$ and $\{o\}$. For the first integral we can apply Theorem A.11 in the same way as before and the integral over $\{o\}$ is zero since $\nu_1(\{o\}) = 0$. This completes the proof. □

Lemma A.14 *With the notation and assumptions of Lemma A.13 it holds that*

$$\nu_1(C) = \int_0^\infty \sum_{x_i \in C \cap \partial B(o,r)} \frac{1}{\sin(\alpha(x_i))} \, dr \,, \tag{A.8}$$

Proof This is an direct application of Lemma A.13 for $g(x) = 1/\sin(\alpha(x))$. □

Bibliography

[1] D.J. Aldous and W.S. Kendall. Short-length routes in low-cost networks via Poisson line patterns. *Advances in Applied Probability*, 40:1–21, 2008.

[2] S. Asmussen and P. Glynn. *Stochastic simulation: Algorithms and Analysis*. Springer, New York, 2007.

[3] F. Baccelli and B. Błaszczyszyn. On a coverage process ranging from the Boolean model to the Poisson-Voronoi tessellation. *Advances in Applied Probability*, 33:293–323, 2001.

[4] F. Baccelli and B. Błaszczyszyn. *Stochastic Geometry and Wireless Networks*. NOW Publishers, Delft, 2009.

[5] F. Baccelli, C. Gloaguen, and S. Zuyev. Superposition of planar Voronoi tessellations. *Communications in Statistics, Series Stochastic Models*, 16:69–98, 2000.

[6] F. Baccelli, M. Klein, M. Lebourges, and S. Zuyev. Stochastic geometry and architecture of communication networks. *Telecommunication Systems*, 7:209–227, 1997.

[7] F. Baccelli, D. Kofman, and J. L. Rougier. Self organizing hierarchical multicast trees and their optimization. *Proceedings of IEEE Infocom '99*, pages 1081–1089, 1999.

[8] F. Baccelli, K. Tchoumatchenko, and S. Zuyev. Markov paths on the Poisson-Delaunay graph with applications to routeing in mobile networks. *Advances in Applied Probability*, 32:1–18, 2000.

[9] F. Baccelli and S. Zuyev. Poisson-Voronoi spanning trees with applications to the optimization of communication networks. *Operations Research*, 47:619–631, 1999.

[10] O.E. Barndorff-Nielsen, W.S. Kendall, and M.N.M. Van Lieshout. *Stochastic Geometry: Likelihood and Computation*. Chapman & Hall, London, 1999.

[11] H. Bauer. *Probability Theory and Elements of Measure Theory.* Academic Press, London, second edition, 1981.

[12] H. Bauer. *Maß-und Integrationstheorie.* Walter de Gruyter, Berlin, second edition, 1992.

[13] V. Baumstark and G. Last. Some distributional results for Poisson Voronoi tessellations. *Advances in Applied Probability*, 39:16–40, 2007.

[14] M. Beil, S. Eckel, F. Fleischer, H. Schmidt, V. Schmidt, and P. Walther. Fitting of random tessellation models to keratin filament networks. *Journal of Theoretical Biology*, 241:62–72, 2006.

[15] P. Billingsley. *Convergence of Probability Measures.* J. Wiley & Sons, New York, second edition, 1999.

[16] B. Błaszczyszyn and R. Schott. Approximate decomposition of some modulated Poisson–Voronoi tessellations. *Advances in Applied Probability*, 35:847–862, 2003.

[17] B. Błaszczyszyn and R. Schott. Approximationsof functionals of some modulated Poisson–Voronoi tessellations with applications to modeling of communication networks. *Japan Journal of Industrial and Applied Mathematics*, 22:179–204, 2005.

[18] P. Calka. The distributions of the smallest disks containing the Poisson-Voronoi typical cell and the Crofton cell in the plane. *Advances in Applied Probability*, 34:702–717, 2002.

[19] G. Casella and R.L. Berger. *Statistical inference.* Duxbury Press, Pacific Grove, second edition, 2002.

[20] R. Cowan. Properties of ergodic random mosaic processes. *Mathematische Nachrichten*, 97:89–102, 1980.

[21] D.J. Daley and D. Vere-Jones. *An Introduction to the Theory of Point Processes*, volume I and II. Springer, New York, 2005/2008.

[22] E. Dijkstra. A note on two problems in connexion with graphs. *Numerische Mathematik*, 1:269–271, 1959.

[23] S. Eckel, F. Fleischer, P. Grabarnik, M. Kazda, A. Särkkä, and V. Schmidt. Modelling tree roots in mixed forest stands by inhomogeneous marked Gibbs point processes. *Biometrical Journal*, 51:522–539, 2009.

[24] F. Fleischer. *Analysis and Fitting of Random Tessellation Models. Applications in Telecommunication and Cell Biology.* PhD thesis, Ulm University, 2007.

[25] F. Fleischer, R. Ananthakrishnan, S. Eckel, H. Schmidt, J. Kaes, T. Svitkina, V. Schmidt, and M. Beil. Actin network architecture and elasticity in lamellipodia of melanoma cells. *New Journal of Physics*, 9:420, 2007.

[26] F. Fleischer, C. Gloaguen, H. Schmidt, V. Schmidt, and F. Schweiggert. Simulation algorithm of typical modulated Poisson-Voronoi cells and application to telecommunication network modelling. *Japan Journal of Industrial and Applied Mathematics*, 25:305–330, 2008.

[27] F. Fleischer, C. Gloaguen, V. Schmidt, and F. Voss. Simulation of the typical Poisson-Voronoi-Cox-Voronoi cell. *Journal of Statistical Computation and Simulation*, 79:939–957, 2009.

[28] S.G. Foss and S.A. Zuyev. On a Voronoi aggregative process related to a bivariate Poisson process. *Advances in Applied Probability*, 28:965–981, 1996.

[29] J.E. Gentle. *Random Number Generation and Monte Carlo Methods*. Springer, Berlin, 2003.

[30] C. Gloaguen, P. Coupé, R. Maier, and V. Schmidt. Stochastic modelling of urban access networks. In *Proc. 10th Internat. Telecommun. Network Strategy Planning Symp.*, pages 99–104. (Munich, June 2002), VDE, Berlin, 2002.

[31] C. Gloaguen, F. Fleischer, H. Schmidt, and V. Schmidt. Simulation of typical Cox-Voronoi cells, with a special regard to implementation tests. *Mathematical Methods of Operations Research*, 62:357–373, 2005.

[32] C. Gloaguen, F. Fleischer, H. Schmidt, and V. Schmidt. Fitting of stochastic telecommunication network models, via distance measures and Monte-Carlo tests. *Telecommunication Systems*, 31:353–377, 2006.

[33] C. Gloaguen, F. Fleischer, H. Schmidt, and V. Schmidt. Modeling and simulation of telecommunication networks:analysis of mean shortest path lengths. In R. Lechnerova, I. Saxl, and V. Benes, editors, *Proceedings of the 6th International Conference on Stereology, Spatial Statistics and StochasticGeometry*, pages 25–36. Prague, 2006.

[34] C. Gloaguen, F. Fleischer, H. Schmidt, and V. Schmidt. Analysis of shortest paths and subscriber line lengths in telecommunication access networks. *Networks and Spatial Economics (to appear)*, DOI:10.1007/s11067-007-9021-z, 2008.

[35] C. Gloaguen, H. Schmidt, R. Thiedmann, J.-P. Lanquetin, and V. Schmidt. Comparison of network trees in deterministic and random settings using

different connection rules. *Proceedings of the 5th International Symposium on Modeling and Optimization in Mobile, Ad Hoc and Wireless Networks (WiOpt 2007)*, Limasol, April 2007.

[36] C. Gloaguen, F. Voss, and V. Schmidt. Parametric distance distributions for fixed access network analysis and planning. In *Proceedings of the 21st International Teletraffic Congress*, Paris, September 2009.

[37] G. Grimmett and D. Stirzaker. *Probability and Random Processes*. Oxford University Press, Oxford, 3rd edition, 2001.

[38] M. Haenggi. On distances in uniformly random networks. *IEEE Transactions on Information Theory*, 51:3584–3586, 2005.

[39] M. Haenggi, J.G. Andrews, F. Baccelli, O. Dousse, and M. Franceschetti. Stochastic geometry and random graphs for the analysis and design of wireless networks. *IEEE Journal on Selected Areas in Communications*, 27:1029–1046, 2009.

[40] L. Heinrich. On existence and mixing properties of germ-grain models. *Statistics*, 23:271–286, 1992.

[41] V. Icke and R. van de Weygaert. Fragmenting the universe. *Astronomy and Astrophysics*, 184:16–32, 1987.

[42] C. Ilg. *Simulation of the Typical Cell of Laguerre-Type Tessellations*. Diploma thesis, Ulm University, 2007.

[43] E. B. Vedel Jensen. *Local Stereology*. World Scientific Publ. Co., Singapore, 1998.

[44] O. Kallenberg. *Random Measures*. Akademie-Verlag, Berlin, 4th edition, 1986.

[45] O. Kallenberg. *Foundations of Modern Probability*. Springer, New York, second edition, 2002.

[46] J. F. C. Kingman. Subadditive ergodic theory. *Annals of Probability*, 1:883–909, 1973.

[47] J. F. C. Kingman. *Poisson Processes*. Oxford University Press, Oxford, 1993.

[48] D. König and V. Schmidt. *Zufällige Punktprozesse*. Teubner, Stuttgart, 1992.

[49] R. Lachieze-Rey. Strong mixing property for STIT tessellations. *Preprint*, 2009, arXiv:0905.1145v3 (math.PR).

[50] C. Lautensack. *Random Laguerre Tessellations.* PhD thesis, Karlsruhe Institute of Technology, 2007.

[51] C. Lautensack. Fitting three-dimensional Laguerre tessellations to foam structures. *Journal of Applied Statistics*, 35:985–995, 2008.

[52] C. Lautensack and S. Zuyev. Random Laguerre tessellations. *Advances in Applied Probability*, 40:630–650, 2008.

[53] R. Maier. *Iterated Random Tessellations with Applications in Spatial Modelling of Telecommunication Networks.* PhD thesis, Ulm University, 2003.

[54] R. Maier, J. Mayer, and V. Schmidt. Distributional properties of the typical cell of stationary iterated tessellations. *Mathematical Methods of Operations Research*, 59:287–302, 2004.

[55] R. Maier and V. Schmidt. Stationary iterated random tessellations. *Advances in Applied Probability*, 35:337–353, 2003.

[56] G. Matheron. *Random Sets and Integral Geometry.* J. Wiley & Sons, New York, 1975.

[57] T. Mattfeldt, S. Eckel, F. Fleischer, and V. Schmidt. Statistical analysis of reduced pair correlation functions of capillaries in the prostate gland. *Journal of Microscopy*, 223:107–119, 2006.

[58] K. Matthes, J. Kerstan, and J. Mecke. *Infinitely Divisible Point Processes.* J. Wiley & Sons, Chichester, 1978.

[59] J. Mayer. *On Quality Improvement of Scientific Software: Theory, Methods, and Application in the GeoStoch Development.* PhD thesis, Ulm University, 2003.

[60] J. Mayer and R. Guderlei. Test oracles of randomness. *Lecture Notes in Informatics*, P-58:179–189, 2004.

[61] J. Mayer, V. Schmidt, and F. Schweiggert. A unified simulation framework for spatial stochastic models. *Simulation Modelling Practice and Theory*, 12:307–326, 2004.

[62] J. Mecke. Stationäre zufällige Maße auf lokalkompakten Abelschen Gruppen. *Zeitschrift für Wahrscheinlichkeitstheorie und verwandte Gebiete*, 9:36–58, 1967.

[63] J. Mecke. Stereological formulas for manifold processes. *Probability and Mathematical Statistics*, 2:31–35, 1981.

[64] J. Mecke. Parametric representation of mean values for stationary random mosaics. *Mathematische Operationsforschung und Statistik*, 12:437–442, 1984.

[65] R. E. Miles. Random polygons determined by random lines in a plane. *Proceedings of the National Academy of Sciences of the United States of America*, 52:901–907, 1964.

[66] R. E. Miles. A synopsis of 'Poisson flats in Euclidean spaces'. In E. F. Harding and D. G. Kendall, editors, *Stochastic Geometry*, 202–227, J. Wiley & Sons, Chichester, 1974.

[67] R.E. Miles. A large class of random tessellations with the classic Poisson polygon distributions. *Advances in Applied Probability*, 30:285–285, 1998.

[68] R.E. Miles and M.S. Mackisack. Further random tessellations with the classic Poisson polygon distributions. *Advances in Applied Probability*, 28:338–339, 1996.

[69] I.S. Molchanov. *Statistics of the Boolean Models for Practitioners and Mathematicians*. J. Wiley & Sons, Chichester, 1996.

[70] I.S. Molchanov. *Theory of Random Sets*. Springer, London, 2005.

[71] J. Møller. Random tessellations in $\mathbb{R}^d$. *Advances in Applied Probability*, 21:37–73, 1989.

[72] J. Møller. *Lectures on Random Voronoi Tessellations*. Springer-Verlag, New York, 1994.

[73] S. Müthing. *Analysis of Capacity Functionals in Telecommunication Networks*. Diploma thesis, Ulm University, 2008.

[74] W. Nagel and V. Weiss. Limits of sequences of stationary planar tessellations. *Advances in Applied Probability*, 35:123–138, 2003.

[75] W. Nagel and V. Weiss. Crack STIT tessellations: Characterization of stationary random tessellations stable with respect to iteration. *Advances in Applied Probability*, 37:859–883, 2005.

[76] J. Neveu. Sur les mesures de palm de deux processus ponctuels stationnaires. *Zeitschrift für Wahrscheinlichkeitstheorie und verwandte Gebiete*, 34:199–203, 1976.

[77] J. Neyman and E.L. Scott. Statistical approach to problems of cosmology. *Journal of the Royal Statistical Society. Series B (Methodological)*, 20:1–43, 1958.

[78] X.X. Nguyen and H. Zessin. Ergodic theorems for spatial processes. *Zeitschrift für Wahrscheinlichkeitstheorie und verwandte Gebiete*, 48:133–158, 1979.

[79] A. Okabe, B. Boots, K. Sugihara, and S. N. Chiu. *Spatial Tessellations.* J. Wiley & Sons, Chichester, second edition, 2000.

[80] M. P. Quine and D. F. Watson. Radial generation of n-dimensional Poisson processes. *Journal of Applied Probability*, 21:548–557, 1984.

[81] B.D. Ripley. *Stochastic Simulation.* John Wiley & Sons, New York, 1987.

[82] M. Rösch. *Mean Subscriber Line Lengths and Expected Means of Shortest Path Lengths for Telecommunication Access Networks.* Diploma thesis, Ulm University, 2005.

[83] J. Rumpf, S. Pickel, S. Elspass, W. Koenig, and V. Schmidt. Structural analysis of dialect maps using methods from spatial statistics. *Zeitschrift für Dialektologie und Linguistik*, 2009 (to appear).

[84] P. Saffert. *Estimation of Cost Functionals for a Two–Level Hierarchical Model based on Voronoi Tessellations.* Diploma thesis, Ulm University, 2007.

[85] H. Schmidt. *Asymptotic Analysis of Stationary Random Tessellations with Applications to Telecommunication Network Modelling.* PhD thesis, Ulm University, 2006.

[86] R. Schneider and W. Weil. *Stochastische Geometrie.* Teubner, Stuttgart, 2000.

[87] R. Schneider and W. Weil. *Stochastic and Integral Geometry.* Springer, Berlin, 2008.

[88] I.M. Slivnyak. Some properties of stationary flows of homogeneous random events. *Theory of Probability and its Applications*, 7:336, 1962.

[89] S. Srinivasa and M. Haenggi. Distance distributions in finite uniformly random networks: Theory and applications. *IEEE Transactions on Vehicular Technology*, 2009 (to appear).

[90] D. Stoyan, W. S. Kendall, and J. Mecke. *Stochastic Geometry and its Applications.* J. Wiley & Sons, Chichester, second edition, 1995.

[91] K. Tchoumatchenko and S. Zuyev. Aggregated and fractal tessellations. *Probability Theory Related Fields*, 121:198–218, 2001.

[92] R. Thiedmann, F. Fleischer, C. Hartnig, W. Lehnert, and V. Schmidt. Stochastic 3D modeling of the GDL structure in PEMFCs based on thin section detection. *Journal of the Electrochemical Society*, 155:B391–B399, 2008.

[93] R. Thiedmann, C. Hartnig, I. Manke, V. Schmidt, and W. Lehnert. Local structural characteristics of pore space in GDLs of PEM fuel cells based on geometric 3D graphs. *Journal of the Electrochemical Society*, 156:B1339–1347, 2009.

[94] H. Thorisson. *Coupling, Stationarity and Regeneration.* Springer, New York, 2000.

[95] R. van de Weygaert and V. Icke. Fragmenting the universe. II - Voronoi vertices as Abell clusters. *Astronomy and Astrophysics*, 213:1–9, 1989.

[96] F. Voss, C. Gloaguen, F. Fleischer, and V. Schmidt. Density estimation of shortest path lengths in spatial stochastic networks. *Stochastic Models* (submitted), 2009.

[97] F. Voss, C. Gloaguen, F. Fleischer, and V. Schmidt. Distributional properties of Euclidean distances in wireless networks involving road systems. *IEEE Journal on Selected Areas in Communications*, 27:1047–1055, 2009.

[98] F. Voss, C. Gloaguen, and V. Schmidt. Capacity distributions in spatial stochastic models for telecommunication networks. *Image Analysis and Stereology*, 28:155–163, 2009.

[99] F. Voss, C. Gloaguen, and V. Schmidt. Scaling limits for shortest path lengths along the edges of stationary tessellations. *Advances in Applied Probability* (submitted), 2009.

[100] F. Voss, C. Gloaguen, and V. Schmidt. Palm calculus for stationary Cox processes on iterated random tessellations. In *Proceedings of 5th Workshop on Spatial Stochastic Models for Wireless Networks (SpaSWiN)*, Seoul, June 2009.

[101] M. P. Wand and M. C. Jones. *Kernel Smoothing.* Chapman & Hall, London, 1995.

[102] V. Weiss and W. Nagel. Interdependence of directional quantities of planar tessellations. *Advances in Applied Probability*, 31:664–678, 1999.

[103] J. G. Wendel. A problem in geometric probability. *Mathematica Scandinavica*, 11:109–111, 1962.

[104] D. Wolfmüller. *Cost Analysis for Telecommunication Networks.* Diploma thesis, Ulm University, 2006.

[105] S. Zuyev. Stopping sets: Gamma-type results and hitting properties. *Advances in Applied Probability*, 31:355–366, 1999.

[106] S. Zuyev. Stochastic geometry and telecommunications networks. In W. S. Kendall and I. Molchanov, editors, *New Perspectives in Stochastic Geometry.* Oxford University Press, Oxford, 2009.

List of Figures

List of Tables

Nomenclature

$(\Omega, \mathcal{A}, \mathbb{P})$	Probability space, page 13
$\mathcal{B}(\mathbb{R}^2)$	Borel σ–algebra on $\mathbb{R}^2$, page 12
$\mathcal{B}_0(\mathbb{R}^2)$	Family of bounded Borel sets on $\mathbb{R}^2$, page 12
$\mathcal{C}$	Family of compact sets in $\mathbb{R}^2$, page 23
$\mathcal{F}$	Family of closed sets in $\mathbb{R}^2$, page 23
$\mathcal{K}$	Family of convex bodies in $\mathbb{R}^2$, page 23
δ_x	Dirac measure, page 12
ℓ^+	$= \ell_0^+$, page 133
ℓ_Φ^+	Half line starting from o with direction Φ, page 133
γ	Length intensity, page 25
$\mathbb{1}_B$	Indicator function of B, page 12
Λ	Random measure, page 27
λ	Intensity of a (marked) point process, page 14
Λ^*	Palm version of the stationary random measure Λ, page 36
λ_ℓ	Intensity quotient λ/γ of a stationary point process on T; linear intensity of a Cox process on T, page 89
$\langle \cdot, \cdot \rangle$	Scalar product, page 11
$\mathbb{M}$	Mark space, page 18
$\mathcal{B}(\mathbb{M})$	Borel–σ–algebra on $\mathbb{M}$, page 19
$\mathcal{B}(\mathcal{F})$	Borel–σ–algebra on $\mathcal{F}$, page 23
$\mathcal{M}$	σ–algebra on M, page 27

$\mathcal{N}$ σ–algebra on N, page 13

$\mathcal{N}_{\mathbb{M}}$ σ–algebra on $\mathsf{N}_{\mathbb{M}}$, page 18

$Exp(\lambda)$ Exponential distribution with parameter λ, page 51

$Wei(\alpha, \beta)$ Weibull distribution with parameters α and β, i.e., the density f_Z of $Z \sim Wei\ (\alpha, \beta)$ is given by $f_Z(x) = \alpha\beta x^{\beta-1} e^{-\alpha x^{\beta}} \mathbb{1}_{[0,\infty)}(x)$, page 97

$\mathring{B}$ Interior of B, page 11

M Family of locally finite measures on $\mathcal{B}(\mathbb{R}^2)$, page 27

N Family of simple and locally finite counting measures on $\mathbb{R}^2$, page 13

$\mathsf{N}_{\mathbb{M}}$ Family of simple and locally finite counting measures on $\mathbb{R}^2 \times \mathbb{M}$, page 18

$\mathsf{N}_{\mathbb{M}_1,\mathbb{M}_2}$ $= \mathsf{N}_{\mathbb{M}_1} \times \mathsf{N}_{\mathbb{M}_2}$, page 22

$\mathbb{N}_0$ Set of non–negative integers, page 11

ν_1 Hausdorff measure on $\mathbb{R}^2$ of dimension 1, page 12

$\nu_1(T^*_{sub})$ Typical subtree length, i.e., typical mark of X_{sub}, page 167

ν_2 Lebesgue measure on $\mathbb{R}^2$, page 12

∂B Boundary of B, page 11

$\mathbb{R}$ Set of real numbers, page 11

$\widetilde{H}_0$ Closest point to o of point process $\widetilde{H}$, page 123

$\widetilde{T}$ Palm version of T with respect to $P^*_{T^{(1)}}$, page 36

Ξ Random closed set, page 23

Ξ^* Typical cell of a random tessellation, page 35

Ξ^*_H The typical serving zone, page 89

Ξ^*_X Typical Voronoi cell of X, page 47

$\Xi_{H,n}$ Serving zone of location H_n of H, page 89

$B(x, r)$ Closed ball around $x \in \mathbb{R}$ of radius $r > 0$, page 11

B^c Complement of B, page 11

$B^{\neq}(x,r)$	Open ball around $x \in \mathbb{R}$ of radius $r > 0$, page 11
$c(x,y)$	Shortest path length from x to y, page 132
$c(y)$	Shortest path lengths from o to y, page 107
C^*	Typical shortest path length, i.e., typical mark of L_C, page 106
D^*	Typical Euclidean distance, i.e., typical mark of L_D, page 92
E^*	Typical edge star of a random tessellation, page 35
H	Point process of points with high hierarchy, page 89
H_S	Point process H marked with the centered segment system inside the serving zone, page 89
K^*	Typical capacity, i.e., typical mark of $\{(X_n, K(X_n))\}$, page 167
L	Point process of points with low hierarchy, page 89
L_C	Point process $L = \{L_n\}$ marked with shortest path connection lengths, page 106
L_D	Point process $L = \{L_n\}$ marked with Euclidean connection lengths, page 91
M^*	Typical mark of the stationary marked point process X_M, page 20
o	Origin of $\mathbb{R}^2$, page 12
$P_Y^{(i)}$	Palm distribution of $Y = (X^{(1)}, X^{(2)})$ with respect to $X^{(i)}$, page 22
P_X	Distribution of the point process X, page 14
P_X^*	Palm distribution of the stationary point process X, page 17
P_Λ^*	Palm distribution of the stationary random measure Λ, page 28
$P_{T^{(1)}}^*$	Palm distribution of the random measure $\nu_1(\,\cdot \cap T^{(1)})$, page 36
P_{X_M}	Distribution of the marked point process X_M, page 19
$P_{X_M}^*$	Palm distribution of the stationary marked point process X_M, page 20
$P_{X_M}^o$	Palm mark distribution of the stationary marked point process X_M, page 20
$Poi(\lambda)$	Poisson distribution with parameter $\lambda > 0$, page 18

S^*	Typical edge of a random tessellation, page 36
S_H^*	Typical segment system, i.e., typical mark of H_S, page 90
S_X^*	Typical mark of X_S, page 48
$S_{H,n}^o$	Centered segment system inside the serving zone, page 89
T	Random tessellation, page 34
$T^{(0)}$	Point process of vertices of the random tessellation T, page 35
$T^{(1)}$	Edge set of the random tessellation T, page 36
T_γ	Random tessellation with length intensity γ, page 45
T_H	Serving zones of $H = \{H_n\}$, page 89
T_X	Random tessellation whose nuclei are given by X, page 47
t_x	Shift operator, page 12
$T_{sub}(X_n)$	Subtree rooted in X_n, page 166
V	Point process of vertices of a random tessellation, page 35
X	Random point process in $\mathbb{R}^2$, page 13
X^*	Palm version of the point process X, page 17
X_M	Random marked point process, page 19
X_S	Point process X on T marked with centered segment systems inside cells of T_X, page 48
X_{sub}	Point process $\{X_n\}$ marked with subtree length, page 167
cv	Coefficient of variation of a random variable X, i.e., $\mathrm{cv}X = 100 \cdot \sqrt{\mathrm{Var}X}/\mathbb{E}X$, page 80
HLC	High-level component(s), page 87
LLC	Low-level component(s), page 87
PDT	Poisson–Delaunay tessellation, page 39
PLT	Poisson line tessellation, page 40
PVT	Poisson–Voronoi tessellation, page 38
SSLM	Stochastic subscriber line model, page 3

Acknowledgment

First of all, I would like to thank Prof. Dr. Volker Schmidt for giving me the opportunity to write my PhD thesis about such an interesting subject, which comprises both theoretical and practical problems. In particular, I would like to thank him for his excellent guidance at every stage of the thesis as well as his availability and advice during the last years.

I also would like to thank Prof. Dr. Ulrich Stadtmüller for his kind agreement to act as a referee on this thesis and for his interest in my work.

Furthermore, I would like to express my gratitude to Dr. Catherine Gloaguen for continuously providing me with interesting and challenging questions related to stochastic modeling of telecommunication networks, for the good collaboration during the last years and for the interest in my work.

Another person I would like to thank is Prof. Dr. Eva Vedel Jensen for giving me the opportunity to stay at her department for 6 months at the beginning of my PhD–studies. This stay helped me substantially in order to complete parts of the thesis.

I also would like to thank all my colleagues at the Institute of Stochastics for the nice working atmosphere. In particular, I would like to thank Ralf Thiedmann for listening patiently to my (mathematical) problems, for proofreading of the thesis and for being a kind roommate in the office over the last years and Dr. Frank Fleischer for introducing me to the principles of stochastic modeling of telecommunication networks and for the good collaboration. Furthermore, I am grateful to Jonas Rumpf and Sebastian Lück for proofreading of the thesis and all other colleagues for their help and support during the last years.

Moreover, I would like to thank Peter Saffert, Steffen Müthing and Thomas Fricker for their help and collaboration in order to obtain some of the numerical results presented in this thesis.

Last but not least, I also would like to thank my family for their support during my studies and, finally, I would like to express my gratitude to Senta for her encouragement, support and, most of all, for sharing her life with me for so many years now.

Zusammenfassung

Die vorliegende Arbeit entstand im Rahmen eines gemeinsamen Forschungsprojekts des Instituts für Stochastik der Universität Ulm und Orange Labs in Issy les Moulineaux, Paris. In diesem Forschungsprojekt wurde das *Stochastic Subscriber Line Model* (SSLM) entwickelt, um Telekommunikationsnetzwerke zu modellieren und zu analysieren. Das SSLM ist ein zufälliges räumliches Netzwerkmodel, welches auf Methoden der stochastischen Geometrie beruht, und insbesondere für die Analyse von innerstädtischen Zugangsnetzwerken ausgelegt ist. In letzter Zeit haben sich Analysemethoden für große Telekommunikationsnetzwerke, die auf solchen stochastischen Netzwerkmodellen basieren, als Alternative zu traditionellen Ansätzen etabliert. Da sehr große und komplexe Datensätze nötig sind, um reale Telekommunikationsnetzwerke zu beschreiben, ist ihre direkte Analyse extrem schwierig oder gar unmöglich, falls z. B. nicht alle Daten zugänglich sind. Oftmals ist man jedoch nicht an lokalen Details des Netzwerks interessiert, sondern versucht vielmehr Aussagen über das globale Verhalten des Netzwerks treffen zu können. Vorteile bieten in diesem Zusammenhang stochastische Modelle, da sie die Variabilität und Größe der Netzwerke nützen, um das globale Verhalten des gesamten Netzwerks mit wenigen Parametern zu beschreiben. Dadurch können auch sehr große Netzwerke anhand des zugehörigen stochastischen Modells analysiert werden. So lassen sich beispielsweise durchschnittliche Verbindungslängen zwischen Netzwerkkomponenten und andere Kostenfunktionale anhand des SSLM berechnen.

Das SSLM ist speziell entwickelt worden, um zweistufige hierarchische Telekommunikationsnetzwerke in städtischen Ballungsgebieten abzubilden. Häufig sind geografische Daten zu den Kabelstränge des Netzwerkes nicht vorhanden. Daher wird im ersten Schritt nicht das Kabelsystem selbst, sondern die zugrundeliegende Infrastruktur des Netzwerks, d. h. das innerstädtische Straßennetz, modelliert. Hierfür werden die Kantensysteme von zufälligen Mosaiken verwendet. Im zweiten Schritt werden die Netzwerkkomponenten als zufällige räumliche Punktprozesse in der Ebene oder entlang des Straßensystems platziert. Als Modelle dienen dafür beispielsweise Cox–Prozesse entlang des Kantensystems. Schließlich müssen die Verbindungen zwischen den Netzwerkkomponenten im letzten Schritt beschrieben werden. Im SSLM wird zu diesem Zweck das Konzept der Einflusszonen verwendet. Jeder Netzwerkkomponente hoher Hierarchie wird ein

Bereich als Einflusszone zugeordnet, so dass die Einflusszonen der verschiedenen Komponenten die gesamte Ebene aufteilen. Eine Komponente niederer Hierarchie wird dann mit der Komponente hoher Hierarchie verbunden, in deren Einflusszone sie liegt. In dieser Arbeit werden zwei mögliche Verbindungswege unterschieden. Zum einen wird die direkte Verbindungslänge und andererseits die kürzeste Verbindung entlang des zugrundeliegenden Kantensystems betrachtet. Insbesondere interessiert uns die Verteilung der durchschnittlichen Verbindungslänge aller Netzwerkkomponenten im Netzwerk. Mathematisch lässt sich diese Verteilung durch die Palmsche Markenverteilung eines geeigneten markierte Punktprozesses definieren und wird als typische Verbindungslänge bezeichnet. Dies führt zum Begriff der typischen (direkten) Euklidischen Distanz bzw. der typischen kürzesten Weglänge. Das Ziel der vorliegenden Arbeit ist es, basierend auf dem SSLM, die Verteilungen von typischen Verbindungslängen zu analysieren. Hierfür werden sowohl Monte-Carlo Methoden als auch asymptotische Methoden betrachtet.

Die vorliegende Arbeit ist folgendermaßen gegliedert. Nach einer kurzen Einführung in Kapitel 1 werden in Kapitel 2 einige grundlegenden Begriffe und Ergebnisse der stochastischen Geometrie präsentiert. Da die betrachteten Netzwerkmodelle auf zufällige Mosaiken basieren, werden diese gesondert in Kapitel 3 eingeführt und Charakteristiken wie die typische Zelle von stationären zufälligen Mosaiken definiert.

Im ersten Teil der Arbeit werden Schätzer für die Verteilung der typischen Euklidischen Distanz und der typischen kürzesten Weglänge hergeleitet und analysiert. In Kapitel 5 wird insbesondere das SSLM als zufälliges hierarchisches Netzwerkmodell basierend auf zufälligen Mosaiken und markierten Punktprozessen eingeführt. Dabei wird das innerstädtische Straßensystem mit dem Kantensystems eines zugrundeliegenden zufälligen Mosaiks modelliert. Ferner werden sowohl Netzwerkkomponenten hoher Hierarchie als auch niederer Hierarchie mit zufälligen Punktprozessen beschrieben und die Einflusszonen der Komponenten hoher Hierarchie mit den Zellen von zufälligen Mosaiken dargestellt. Auf der Basis des so definierten Models lassen sich die typische Euklidische Distanz und die typische kürzeste Weglänge einführen. Für die Verteilungen der beiden typischen Verbindungslängen werden Darstellungsformeln hergeleitet, die nur von Funktionalen der typischen Einflusszone (oder Zelle) und des zugrundeliegenden Kantensystems abhängen, jedoch nicht von Komponenten niederer Hierarchie beeinflusst werden. Basierend auf diesen Darstellungsformeln lassen sich Schätzer für die Verteilung der typischen Euklidischen Distanz bzw. der typischen kürzesten Weglänge konstruieren, die anhand von Stichproben der typischen Einflusszone berechnet werden können. Es wird gezeigt, dass die entwickelten Schätzer sowohl erwartungstreu als auch gleichmäßig stark konsistent sind.

Um die entwickelten Schätzer berechnen zu können, werden effiziente Simulationsalgorithmen für die typische Voronoi Zelle von einer Vielzahl von Punktprozessmodellen entwickelt, die in Kapitel 4 beschrieben werden. In diesem Zusammenhang werden insbesondere Cox–Prozesse auf dem Kantensystem und un-

abhängige Ausdünnungen der Knoten von zufälligen Mosaikmodellen betrachtet. Mit diesen Ergebnissen lassen sich dann sowohl die Verteilung der typischen Euklidischen Distanz als auch die Verteilung der typischen kürzesten Weglänge für viele unterschiedliche Szenarien berechnen.

Der zweite Teil der Arbeit ist theoretischer Natur und beschäftigt sich mit sogenannten Skalierungsgrenzwertsätzen. In Kapitel 6 wird der Fall betrachtet, dass die Netzwerkkomponenten hoher Hierarchie mit Cox–Prozessen auf dem Kantensystem des zugrundeliegenden zufälligen Mosaiks modelliert werden und die Intensität dieses Kantensystem einerseits gegen 0 und andererseits gegen unendlich strebt. Um sicher zu stellen, dass die Grenzverteilung existiert, muss das Netzwerk passend skaliert und die Zahl der Netzwerkkomponenten geeignet erhöht bzw. ausgedünnt werden. In beiden Fällen wird in dieser Arbeit gezeigt, dass die Verteilung der typischen kürzesten Weglänge gegen eine bekannte parametrische Verteilung konvergiert.

Im ersten Ansatz wird der Fall betrachtet, dass die Intensität des Kantensystems immer mehr abnimmt. Für diesen Fall wird gezeigt, dass die typische kürzeste Weglänge in Verteilung gegen eine Exponentialverteilung konvergiert und die Grenzverteilung nicht vom Mosaikmodell für das Straßensystem abhängt.

Danach wird der Fall betrachtet, dass das Kantensystem unendlich dicht wird und die Netzwerkkomponenten geeignet ausgedünnt werden. Hier zeigt sich, dass die typische kürzeste Weglänge in Verteilung gegen ξZ konvergiert, wobei Z eine Weibull–verteilte Zufallsvariable und $\xi \geq 1$ eine Konstante ist. Der Faktor ξ hängt dabei wesentlich vom Modell für das Straßensystem ab und kann für Spezialfälle sogar explizit berechnet werden. Diese Aussage kann mit Hilfe von Methoden der schwachen Konvergenz von Punktprozessen, der geometrischen Maßtheorie sowie des subadditiven Ergodensatzes von Kingman bewiesen werden.

In Kapitel 7 werden dann die zuvor erzielten Resultate kombiniert, um parametrische Dichten für die typische kürzeste Weglänge zu bestimmen. Die Parameter dieser Dichten lassen sich für echte Daten leicht schätzen und es zeigt sich, dass die so bestimmten parametrischen Verteilungen sehr gut die realen Verteilungen von Verbindungslängen im Zugangsnetzwerk von Paris approximieren. Zusammenfassend wird dadurch gezeigt, dass die in dieser Arbeit entwickelte Techniken mächtige Werkzeuge für die Analyse und Planung von existierenden bzw. zukünftigen Netzwerken liefern.

Schließlich werden in Kapitel 8 die zuvor entwickelten Ansätze verallgemeinert, um sogenannte Kapazitäten im SSLM zu schätzen. Insbesondere wird gezeigt, wie sich die Verteilung der benötigten Kapazität mit Monte-Carlo Methoden schätzen lässt. Dies verdeutlicht, dass sich die entwickelte Methodik zur Analyse von Verbindungslängen auch leicht für die Analyse von komplexeren Kenngrößen anpassen lässt.

Vorträge

1. *Variance Paradoxes of Geometric Sampling: A Generalisation of the Jensen-Gundersen Paradox*, Frankfurter Stochastik–Tage, Frankfurt am Main, 14. März 2006

2. *Variance Paradoxes of Geometric Sampling: A Generalisation of the Jensen-Gundersen Paradox*, Workshop 'Spatial Stochastic Modelling of Telecommunication Systems', Hirschegg, Österreich, 27. März 2006

3. *Simulation of typical Poisson-Voronoi-Cox-Voronoi cells*, Winter School 'Geometric Measure Theory, Random Sets and Digital Stereology', Sandbjerg Estate, Sønderborg, 22. Januar 2007

4. *Anisotropic Sampling Grids for Length Estimation*, 12th International Congress for Stereology, St. Etienne, 5. September 2007

5. *Distributional properties of shortest path lengths in telecommunication networks*, 8th German Open Conference on Probability and Statistics, Aachen, 4. März 2008

6. *Distance distributions for stochastic network models*, 15th Workshop on Stochastic Geometry, Stereology and Image Analysis, Blaubeuren, Deutschland, 23. März 2009

7. *Capacity distributions in spatial stochastic models for telecommunication networks*, 10th European Congress of Stereology and Image Analysis, Mailand, 26. Juni 2009

8. *Capacity distributions in geometric network models*, Summer Academy on Stochastic Geometry, Spatial Statistics and Random Fields, Hirschegg, 25. September 2009

Publikationsliste

1. F. Voss, C. Gloaguen, and V. Schmidt. Palm calculus for stationary Cox processes on iterated random tessellations. In *Proceedings of 5th Workshop on Spatial Stochastic Models for Wireless Networks (SpaSWiN)*, Seoul, Juni 2009.

2. F. Voss, C. Gloaguen, and V. Schmidt. Scaling limits for shortest path lengths along the edges of stationary tessellations. *Advances in Applied Probability* (eingereicht), 2009.

3. F. Voss, C. Gloaguen, F. Fleischer, and V. Schmidt. Density estimation of shortest path lengths in spatial stochastic networks. *Stochastic Models* (eingereicht), 2009.

4. F. Voss, C. Gloaguen, and V. Schmidt. Capacity distributions in spatial stochastic models for telecommunication networks. *Image Analysis and Stereology*, 28:155–163, 2009.

5. C. Gloaguen, F. Voss, and V. Schmidt. Parametric distance distributions for fixed access network analysis and planning. In *Proceedings of the 21st International Teletraffic Congress*, Paris, September 2009.

6. E. Kokai, F. Voss, F. Fleischer, S. Kempe, D. Marinkovic, H. Wolburg, F. Leithaeuser, V. Schmidt, U. Deutsch, and T. Wirth. Myc regulates embryonic vascular permeability and remodeling. *Circulation Research*, 104:1151–1159, 2009.

7. F. Voss, C. Gloaguen, F. Fleischer, and V. Schmidt. Distributional properties of Euclidean distances in wireless networks involving road systems. *IEEE Journal on Selected Areas in Communications*, 27:1047–1055, 2009.

8. F. Voss, L. M. Cruz-Orive. Second moment formulae for geometric sampling with test probes. *Statistics*, 43:329–365, 2009.

9. F. Fleischer, C. Gloaguen, V. Schmidt, and F. Voss. Simulation of the typical Poisson-Voronoi-Cox-Voronoi cell. *Journal of Statistical Computation and Simulation*, 79:939–957, 2009.

10. F. Voss and T. L. Thorarinsdottir. Anisotropic sampling grids for length estimation. In *Proceedings of the 12th International Congress for Stereology*, St. Etienne, September 2007

11. F. Voss. First and Second Order Moment Measures in Geometric Sampling for Stereology. Diplomarbeit, Universität Ulm, 2005.

Erklärung

Hiermit erkläre ich, dass ich die vorliegende Arbeit selbstständig und nur mit den angegebenen Hilfsmitteln angefertigt habe. Alle Stellen, die anderen Werken entnommen sind, wurden durch Angaben der Quellen kenntlich gemacht.

Ulm, den 21.12.09